NOAA Colloquium on Operational Environmental Prediction

Program

June 6 - July 1, 1994
NOAA Science Center
Camp Springs, Maryland

NOAA COLLOQUIUM ON OPERATIONAL ENVIRONMENTAL PREDICTION

STUDENTS PARTICIPANTS

Elvira Brankov	State University of New York
David Burwell	University of South Florida
Christelle Escoffier	University of Paris
Paul Gaertner	University of South Australia
James A. Hansen	University of Oxford
Suzanne Hartley	University of Denver
Yimin Ji	University of Maryland
Samuel Levis	University of Wisconsin
Xiaofeng Li	North Carolina State University
Cheng-Hsuan Lu	State University of New York
Gregory S. Poulos	Colorado State University
Alec Richardson	University of South Florida
Axayacatl Rocha-Olivares	University of California, San Diego
Nancy Schmidt	University of South Florida
Yuval Shay-El	Tel Aviv University
Scott A. Stanley	University of California, San Diego
Zhaoqing Yang	Virginia Institute of Marine Science
Lihang Zhou	University of Maryland
Alan D. Ziegler	University of Hawaii

COLLOQUIUM ORGANIZING COMMITTEE

Dr. Vernon E. Kousky, Chairperson
NWS/NMC Climate Analysis Center

Dr. Wayman E. Baker
NWS/National Meteorological Center

Dr. Joseph Golden
OAR/Program Development and Coordination

Prof. Ferdinand Baer
Department of Meteorology
University of Maryland

Mr. J. Dane Clark
NESDIS/Office of Satellite Data Processing and Distribution

Dr. Danny L. Fread
NWS/Office of Hydrology

Mr. Walter G. Planet
NESDIS/Office of Research and Applications

OBJECTIVE OF THE COLLOQUIUM

This is the third in a series of NOAA Colloquia. The purpose is to encourage graduate students who have recently been accepted in a relevant doctoral program to pursue careers in the environmental sciences. Feedback from the participants and the lecturers on how to improve the program is appreciated.

SUMMARY OF THE COLLOQUIUM PROGRAM

June 6, 1994	Introduction
June 7-10, 1994	Weather Analysis and Prediction
June 10-15, 1994	Climate Monitoring and Prediction
June 16-20, 1994	Oceanographic Prediction
June 21-24, 1994	Hydrologic Prediction and Workshops
June 27-29, 1994	Prepare Lecture Notes and Visit Sterling Forecast Facility
June 30, 1994	Closing

AGENDA

MONDAY JUNE 6

9:00 - 9:15 am **INTRODUCTORY REMARKS**
Ronald D. McPherson, NOAA/National Weather Service/National Meterological Center

Richard H. Herman, Univeristy of Maryland, College Park, Maryland

9:15 - 10:30 am **ENVIRONMENTAL PREDICTION IN NOAA: WHAT'S NEW?**
Diana Josephson, Deputy Undersecretary NOAA

University of Maryland Adult Education Center, Firefighter Room, College Park, Maryland

11:00 am - 1:00 pm **LUNCH**

1:00-3:00 pm **VISIT TO AND OVERVIEW OF THE DEPARTMENT OF METEOROLOGY, UNIVERSITY OF MARYLAND**

WEATHER ANALYSIS AND PREDICTION

TUESDAY JUNE 7

9:00-10:30 am **OVERVIEW OF THE NMC FORECAST MODEL SUITE**
John Stackpole, NOAA/National Weather Service/National Meteorological Center, Camp Springs, Maryland

NOAA Science Center, Room 707
Camp Springs, Maryland

11:30-12:00 **NMC FORECAST DISCUSSION**

NOAA Science Center, Room 405
Camp Springs, Maryland

12:00-1:00 pm **LUNCH**

TUESDAY JUNE 7

1:00 -2.30 pm **OPERATIONAL NUMERICAL WEATHER PREDICTION AT THE NATIONAL METEOROLOGICAL CENTER**
Eugenia Kalnay, NOAA/National Weather Service/National Meteorological Center, Camp Springs, Maryland

NOAA Science Center, Room 707
Camp Springs, Maryland

WEDNESDAY JUNE 8

9:00-10:30 am **FORECASTING THE MARCH 1993 SUPERSTORM**
Louis Uccellini, NOAA/National Weather Service/National Meteorological Center, Camp Springs, Maryland

NOAA Science Center, Room 707
Camp Springs, Maryland

11:30-12:00 **NMC FORECAST DISCUSSION** (Optional)

NOAA Science Center, Room 405
Camp Springs, Maryland

12:00-1:00 pm **LUNCH**

1:00-2:30 pm **SATELLITE APPLICATIONS FOR NUMERICAL WEATHER PREDICTION**
James S. Lynch, NOAA/National Environmental Satellite, Data and Information Service, Camp Springs, Maryland

NOAA Science Center, Room 707
Camp Springs, Maryland

THURSDAY JUNE 9

9:00-10:30 am **TOPICS IN ANALYSIS TECHNIQUES**
Thomas Schlatter, NOAA/Office of Oceanic and Atmospheric Research/ERL/Forecast Systems Laboratory, Boulder, Colorado

NOAA Science Center, Room 707
Camp Springs, Maryland

THURSDAY JUNE 9

11:30-12:00 **NMC FORECAST DISCUSSION** (Optional)

NOAA Science Center, Room 405
Camp Springs, Maryland

12:00-1:00 pm **LUNCH**

1:00-2:30 pm **RESEARCH ON IMPROVING HURRICANE PREDICTION**
John Gamache, NOAA/Office of Oceanic and Atmospheric Research/Atlantic Oceanographic and Meteorological Laboratory, Miami, Florida

NOAA Science Center, Room 707
Camp Springs, Maryland

3:00-4:30 pm **MESOSCALE ANALYSIS TECHNIQUES**
Roger Wakimoto, University of California at Los Angeles, Los Angeles, California

NOAA Science Center, Room 707
Camp Springs, Maryland

FRIDAY JUNE 10

9:00 - 11:30 am **TOUR OF NMC**

11:30-12:00 **NMC FORECAST DISCUSSION** (Optional)

NOAA Science Center, Room 405
Camp Springs, Maryland

12:00-1:00 pm **LUNCH**

CLIMATE MONITORING AND PREDICTION

FRIDAY JUNE 10

1:00-2:30 pm **GREENHOUSE WARMING**
Anthony Broccoli, NOAA/Office of Oceanic and Atmospheric Research/Geophysical Fluid Dynamics Laboratory, Princeton, New Jersey

NOAA Science Center, Room 707
Camp Springs, Maryland

MONDAY JUNE 13

9:00-10:30 AM **STRATOSPHERIC OZONE DEPLETION: PREDICTIONS AND OBSERVATIONS**
A. James Miller, NOAA/National Weather Service/National Meteorological Center, Camp Springs, Maryland

NOAA Science Center, Room 707
Camp Springs, Maryland

11:30-12:00 **NMC FORECAST DISCUSSION** (Optional)

NOAA Science Center, Room 405
Camp Springs, Maryland

12:00-1:00 pm **LUNCH**

1:00-2:30 PM **STRATOSPHERIC MONITORING USING OPERATIONAL SATELLITES**
Walter Planet, NOAA/National Environmental Satellite, Data and Information Service/Office of Research and Applications, Camp Springs, Maryland

NOAA Science Center, Room 707
Camp Springs, Maryland

MONDAY JUNE 13

3:00-4:30 PM **SATELLITE MONITORING OF CLIMATE VARIABLES**
George Ohring, NOAA/National Environmental Satellite, Data and Information Service/Office of Research and Applications, Camp Springs, Maryland

NOAA Science Center, Room 707
Camp Springs, Maryland

TUESDAY JUNE 14

9:00-10:30 am **ENSEMBLE FORECASTING**
Steven Tracton, NOAA/National Weather Service/National Meteorological Center, Camp Springs, Maryland

NOAA Science Center, Room 707
Camp Springs, Maryland

11:30-12:00 **NMC FORECAST DISCUSSION** (Optional)

NOAA Science Center, Room 405
Camp Springs, Maryland

12:00-1:00 pm **LUNCH**

1:00-2:30 pm **PREDICTION OF LOW-FREQUENCY PHENOMENA**
Kingste Mo, NOAA/National Weather Service/National Meteorological Center, Camp Springs, Maryland

NOAA Science Center, Room 707
Camp Springs, Maryland

3:00-4:30 pm **OPERATIONAL 6-10 DAY, MONTHLY AND SEASONAL FORECASTS**
Edward O'Lenic, NOAA/National Weather Service/National Meteorological Center, Camp Springs, Maryland

NOAA Science Center, Room 707
Camp Springs, Maryland

WEDNESDAY JUNE 15

9:00-10:30 am **MONITORING AND PREDICTION OF INTERANNUAL VARIABILITY**
Chester Ropelewski, NOAA/National Weather Service/National Meteorological Center, Camp Springs, Maryland

NOAA Science Center, Room 707
Camp Springs, Maryland

10:30 - 11:30 am **NMC SSI ANALYSIS SYSTEM**
John C. Derber, NOAA/National Weather Service/National Meteorological Center, Camp Springs, Maryland

NOAA Science Center, Room 707
Camp Springs, Maryland

11:30-12:00 **NMC FORECAST DISCUSSION** (Optional)

NOAA Science Center, Room 405
Camp Springs, Maryland

12:00-1:00 pm **LUNCH**

1:00-2:30 pm **OBSERVATIONS FOR SHORT-TERM CLIMATE ANALYSIS AND PREDICTION**
Michael J. McPhaden, NOAA/Office of Oceanic and Atmospheric Research/Pacific Marine Environmental Research Laboratory, Seattle, Washington

NOAA Science Center, Room 707
Camp Springs, Maryland

3:00-4:30 pm **COUPLED MODEL OCEAN-ATMOSPHERE FORECAST SYSTEM**
Ming Ji, NOAA/National Weather Service/National Meteorological Center, Camp Springs, Maryland

NOAA Science Center, Room 707
Camp Springs, Maryland

OCEANOGRAPHIC PREDICTION

THURSDAY JUNE 16

9:00-10:30 am **GLOBAL SEA SURFACE TEMPERATURE ANALYSIS TECHNIQUES**
Richard W. Reynolds, NOAA/National Weather Service/National Meteorological Center, Camp Springs, Maryland

NOAA Science Center, Room 707
Camp Springs, Maryland

THURSDAY JUNE 16

11:30-12:00 **NMC FORECAST DISCUSSION** (Optional)

NOAA Science Center, Room 405
Camp Springs, Maryland

12:00-1:00 pm **LUNCH**

1:00 - 2:30 pm **COASTAL PREDICTION AND DATA ASSIMILATION IN OCEANOGRAPHY**
Tal Ezer, Princeton University, Princeton, New Jersey

NOAA Science Center, Room 707
Camp Springs, Maryland

3:00-4:30 pm **GOES-NEXT PRODUCTS AND APPLICATIONS**
Christopher Hayden, University of Wisconsin, Madison, Wisconsin

NOAA Science Center, Room 707
Camp Springs, Maryland

FRIDAY JUNE 17

9:00 - 10:30 am **A COASTAL FORECAST SYSTEM**
Frank Aikman, NOAA/National Ocean Service/Ocean and Earth Sciences, Silver Spring, Maryland

NOAA Science Center, Room 707
Camp Springs, Maryland

FRIDAY JUNE 17

11:30-12:00 **NMC FORECAST DISCUSSION** (Optional)

NOAA Science Center, Room 405
Camp Springs, Maryland

12:00-1:00 pm **LUNCH**

1:00 - 2:30 pm **WAVE INTERACTION WITH COASTAL STRUCTURES AND SHORELINES**
John Ahrens, NOAA/Office of Oceanic and Atmospheric Research, Silver Spring, Maryland

NOAA Science Center, Room 707
Camp Springs, Maryland

3:00 - 4:30 pm **MARINE FORECASTING FOR THE GREAT LAKES**
David Schwab, NOAA/Office of Oceanic and Atmospheric Research/Great Lakes Environmental Research laboratory, Ann Arbor, Michigan

NOAA Science Center, Room 707
Camp Springs, Maryland

MONDAY JUNE 20

9:00 - 10:30 am **NUTRIENT ENHANCED COASTAL OCEAN PRODUCTIVITY (NECOP): PREDICTING HYPOXIA AND EFFECTS ON BENTHIC POPULATIONS**
Nancy Rabalais, Louisiana University Marine Consortium, Chauvin, Louisiana

NOAA Science Center, Room 707
Camp Springs, Maryland

11:30-12:00 **NMC FORECAST DISCUSSION** (Optional)

NOAA Science Center, Room 405
Camp Springs, Maryland

12:00-1:00 pm **LUNCH**

MONDAY JUNE 20

1:00 - 2:30 pm **PRIMARY PRODUCTION AND NUTRIENTS (NECOP) - PROCESSES**
Steve Lohrenz, University of Southern Mississippi, Center for Marine Science, Stennis, Mississippi

NOAA Science Center, Room 707
Camp Springs, Maryland

3:00-4:30 am **OVERVIEW OF OCEAN OBSERVING AND PREDICTIONS: A LOOK AHEAD AT OPERATIONAL PROGRAMS, GLOBAL SCALE TO COASTAL SCALE**
William E. Woodward, NOAA/National Ocean Service, Silver Spring, Maryland

NOAA Science Center, Room 707
Camp Springs, Maryland

HYDROLOGIC PREDICTION AND WORKSHOPS

TUESDAY JUNE 21

9:00-10:30 am **PRECIPITATION ESTIMATION FOR CLIMATE**
Phillip A. Arkin, NOAA/National Weather Service/National Meteorological Center, Camp Springs, Maryland

NOAA Science Center, Room 707
Camp Springs, Maryland

10:30 - 11:30 am **REVIEW OF 1993 EXTREME WEATHER EVENTS**
Joe Golden, NOAA/Office of Oceanic and Atmospheric Research/Program Development and Coordination, Silver Spring, Maryland

NOAA Science Center, Room 707
Camp Springs, Maryland

11:30-12:00 am **NMC FORECAST DISCUSSION** (Optional)

NOAA Science Center, Room 405
Camp Springs, Maryland

TUESDAY JUNE 21

12:00-1:00 pm **LUNCH**

1:00-2:30 PM **RAINFALL ESTIMATION (NOWCASTING)**
Roderick Scofield, NOAA/National Environmental Satellite, Data and Information Service/Office of Research and Applications, Camp Springs, Maryland

NOAA Science Center, Room 707
Camp Springs, Maryland

WEDNESDAY JUNE 22

9:00-9:45 am **RAINFALL ESTIMATION USING RADAR**
David Kitzmiller, NOAA/National Weather Service/Office of Systems Development, Silver Spring, Maryland

NOAA Science Center, Room 707
Camp Springs, Maryland

10:00-10:45 am **QUANTITATIVE PRECIPITATION FORECASTING**
Norman W. Junker, NOAA/National Weather Service/National Meteorological Center, Camp Springs, Maryland

NOAA Science Center, Room 707
Camp Springs, Maryland

11:30-12:00 **NMC FORECAST DISCUSSION** (Optional)

NOAA Science Center, Room 405
Camp Springs, Maryland

12:00-1:00 pm **LUNCH**

1:00 - 3:00 pm **RAINFALL ESTIMATES FROM NEXRAD**
Robert C. Shedd, NOAA/National Weather Service/Office of Hydrology, Silver Spring, Maryland and *James Smith*, Princeton University, Department of Civil Engineering, Princeton, New Jersey

NOAA Science Center, Room 707
Camp Springs, Maryland

WEDNESDAY JUNE 22

3:30-4:30 pm **LARGE-SCALE APPLICATIONS WITH AN EMPHASIS ON THE 1993 MIDWEST FLOOD**
Lee W. Larson, NOAA/National Weather Service Central Region, Kansas City, Missouri

NOAA Science Center, Room 707
Camp Springs, Maryland

THURSDAY JUNE 23

9:00 - 10:00 am **SNOW DATA**
Thomas Carroll, NOAA/National Weather Service/Office of Hydrology, Minneapolis, Minnesota

Silver Spring Metro Center 2, Room 8246
Silver Spring, Maryland

10:30 - 12:00 **SOIL MOISTURE/RUNOFF MODELING**
Eric A. Anderson, NOAA/National Weather Service/Office of Hydrology, Silver Spring, Maryland

Silver Spring Metro Center 2, Room 8246
Silver Spring, Maryland

12:00-1:00 pm **LUNCH**

1:00 - 2:30 pm **INTERACTIVE HYDROLOGIC FORECASTING DEMONSTRATION**
George F. Smith, NOAA/National Weather Service/Office of Hydrology, Silver Spring, Maryland

Silver Spring Metro Center 2, Room 8246
Silver Spring, Maryland

3:00-4:30 pm **HYDROLOGIC FORECASTING IN THE NWS**
Michael D. Hudlow, NOAA/National Weather Service/Office of Hydrology, Silver Spring, Maryland

NOAA Science Center, Room 707
Camp Springs, Maryland

FRIDAY JUNE 24

9:00 - 10:15 pm **HYDRODYNAMIC MODELING OF RIVERS AND ESTUARIES**
Danny L. Fread, NOAA/National Weather Service/Office of Hydrology, Silver Spring, Maryland

Silver Spring Metro Center 2, Room 8246
Silver Spring, Maryland

10:30 - 12:00 **HYDRODYNAMIC MODELING DEMONSTRATION**
Danny L. Fread and *Janice Lewis*, NOAA/National Weather Service/Office of Hydrology, Silver Spring, Maryland

Silver Spring Metro Center 2, Room 8246
Silver Spring, Maryland

12:00-1:00 pm **LUNCH**

1:00 - 3:00 pm **LONG-RANGE HYDROLOGIC FORECASTING**
Ann McManamon, NOAA/National Weather Service/Office of Hydrology, Silver Spring, Maryland and *Gerald Day*, Riverside Technology, Inc., Columbia, Maryland

Silver Spring Metro Center 2, Room 8246
Silver Spring, Maryland

TUESDAY JUNE 28

9:00 am-2:00 pm Visit forecast office in Sterling, Virginia

THURSDAY JUNE 30

10:00 -11:00 am **CONCLUDING REMARKS**
Elbert W. Friday, NOAA/National Weather Service

Silver Spring Metro Center 3, Room 4427
1325 East-West Highway
Silver Spring, Maryland

Overview of the NMC Forecast Model Suite

Lecturer: John Stackpole
Date: June 7, 1994
Notes by: Scott Stanley
Gregory Poulos

The National Meteorological Center (NMC) provides a variety of weather analysis and forecast data to private and public organizations throughout the world on a set schedule. This data is utilized by the Federal Aviation Administration, the Department of Defense, private airlines, as well as by the media for presenting to the public. These weather forecasts are based on observations of the state of the weather throughout the world, as well as on a variety of forecasting models which are used to forecast the future weather conditions. All forecasts are completed within 3 hours of the receipt of the data.

Observations of the world weather conditions are received from a variety of sources. This includes National Weather Service (NWS) observations, aircraft observations, satellite soundings from the National Environmental Satellite, Data, and Information Service (NESDIS), as well as international observations received through the World Meteorological Organization (WMO). This data is collected using balloon carried radiosondes, land surface observations, ship observations, drifting buoys, aircraft reports, satellites , and cloud tracking. **Table 1** gives a basic breakdown of the number of observations points available on the planet's surface and aloft. Data is obtained from these sources a minimum of twice daily, at 00Z and 12Z (midnight and noon GMT). However, data is available from some sources more frequently. Aside from satellite information, data is sparse over the oceans.

TABLE 1

Obs. Type	Num. Obs.	Comments
Surface observations	8000 - 10000	includes land and ocean observations, many are available hourly
Balloon Radiosondes	800 - 1000	
Satellite	Global Coverage	
Aircraft	~10000 the common flight	available as streaks of data along routes

These data are passed through the National Weather Service Telecommunications Gateway (NWSTG) to the NMC computational facilities. These facilities consist of two IBM based front end machines used for data manipulation and verification, and two UNIX based Cray computers (YMP, C-90) on which the majority of the numerical forecasting models are run.

There are five and sometimes six computer runs which are made twice daily (once in the 00Z cycle, and once in the 12Z cycle) for use in the weather forecasting process. A time line demonstrating one 24 hour period is shown in **Fig. 1**. Also, **Table 2** provides information regarding the forecast period and prediction model utilized for each run. The Early run is intended to provide a quick look at the regional forecast, but it utilizes a limited period of data. The Regional run provides a more detailed look at the U.S. region forecast using a larger set of

observational data and is the primary short-range model at NMC. The Eta model will eventually replace the Nested Grid Model or be run simultaneous with it. This run provides 1-2 day forecasts for the entire U.S. and will eventually provide 3 day outlooks. The Aviation run provides a longer range global forecast and also provides upper level winds for use by the aviation community. The Hurricane run is only executed when necessary and provides hurricane tracking data. The Medium-Range-Forecast run, using the same model as that for the Aviation run, provides a more extended global forecast using a larger set of observational data and ensemble forecasting techniques. Finally, the Final Analysis run is used to assimilate all observed data into the best possible analysis and short range forecast which will be utilized in the next cycle's operational analysis. The Regional (RGL) run has its own Regional Data Assimilation System (RDAS) performing the same function as the Final Analysis. All the short-term forecasts are completed in less than 3 hours from the observation times (00Z and 12Z).

TABLE 2

Run	00Z Data Cutoff Time	Model	Forecast Period (hr)	Geometrical Range
Early (ERL)	1:10	LFM	48	U.S. Region
	1:10	Eta	48	U.S. Region
Regional (RGL)	2:00	NGM	48	U.S. Region
Aviation (AVN)	2:45	SGM	72	Global
Hurricane (HCN)	2:45	QLM	72	Global
Medium-Range-Forecast (MRF)	6:00	SGM	240	Global
Final Analysis (FNL)	6:00 (00Z)	SGM	6	Global
	9:30 (06Z)	SGM	6	Global
	9:00 (12Z)	SGM	6	Global
	10:00 (18Z)	SGM	6	Global

There are five numerical forecasting models utilized in these operational forecasting runs. A few details of these models are presented in **Table 3** below. Each of these models iterates time dependent equations of fluid motion (known as the primitive equations) at a certain level of approximation. To be solved over a gridded domain the derivatives in the equations are represented with finite difference forms; those models that are 'spectral' solve the phase-space transformed equations for a limited number of wavenumbers. NMC also receives model output from the European Center (ECMWF), the United Kingdom Meteorological Office (UK Met), Japan and Canada to supplement its data to help forecasters. In addition to these forecasting models, a number of analysis routines are utilized. These analysis tools are outlined in **Table 4**. Model Output Statistics (MOS) are of great importance to everyday forecasters since they allow model estimates of maximum and minimum temperature and accumulated 6 hour precipitation forecasts out to 48 hours among other useful meteorological variables. MOS uses statistical regression techniques based on previous model history to generate these variables.

TABLE 3

Model	Horizontal Resolution	Vertical Layers	Notes
Limited range Forecast Model (LFM)	90	7	Being phased out
Eta coordinate direction	80	38	Utilizes eta in vertical
MESO Eta implemented in	29	50	To be ~October, 1994
Nested Grid Model (NGM) range	80	16	Primary short- model until Eta
Spectral Global Model (SGM) with truncation	< 1 degree	28	Spectral model triangular 126
Quasi Lagrangian Model (QLM) predicting tropical			Used for tracks of storms

TABLE 4

Routine	Notes
OI ANL	Optimal Interpolation Analysis
SSI	Spectral Statistical Interpolation
MOS	Model output statistics (from NGM)
FOG	Predicts the presence of surface fog
GMW	Gulf of Mexico Model (oceanic surges)
NOW	NOAA Ocean Wave Model
SST	Sea Surface Temperature analysis

NMC PRODUCTION SUITE

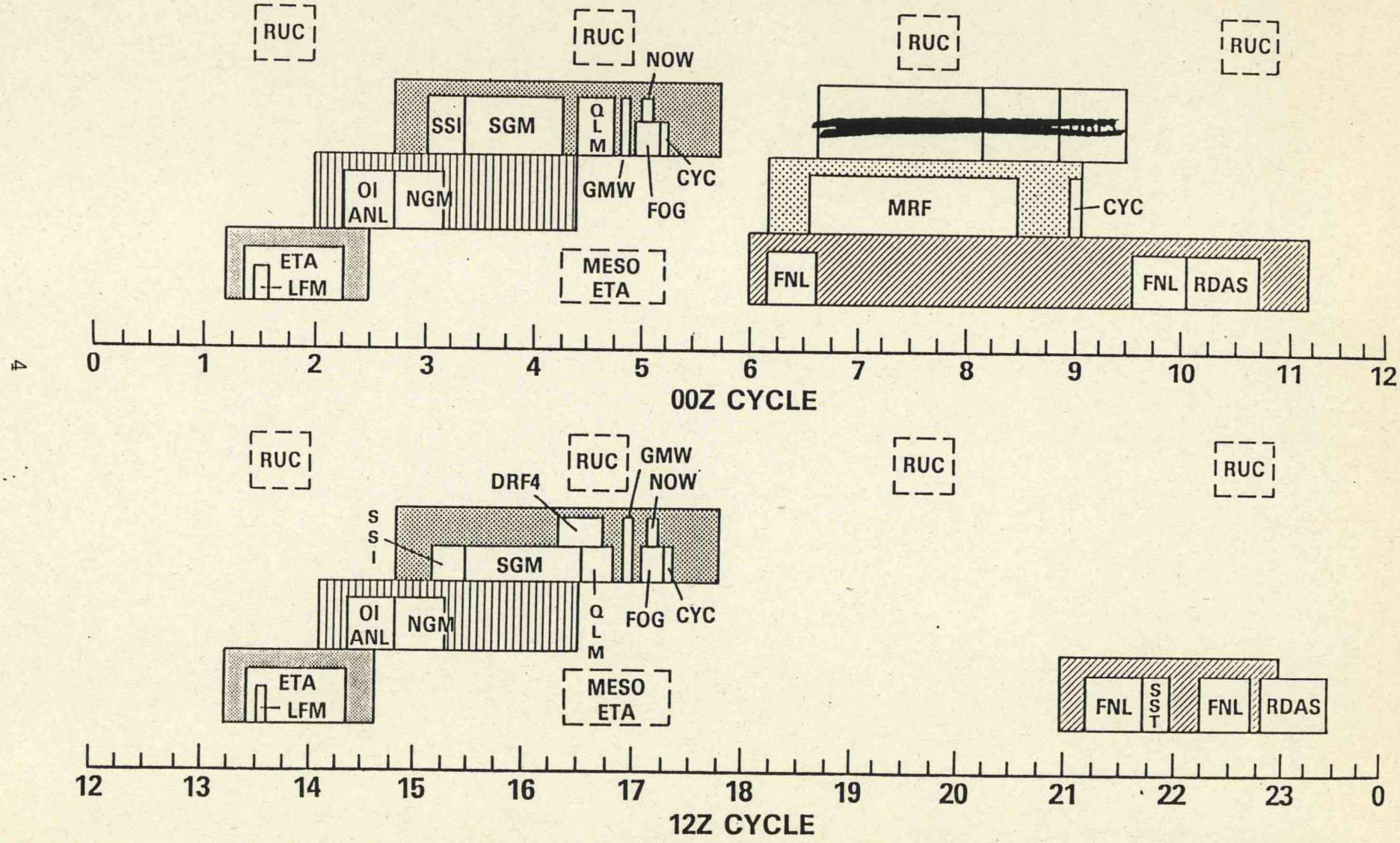

FIGURE 1

Ensemble runs all day long

Operational Numerical Weather Prediction at the National Meteorological Center

Lecturer: Eugenia Kalnay
Notes by: Gregory Poulos
Elvira Brankov
Date: June 7, 1994

The operational numerical models are continually in need of improvement to make better forecasts. Operational forecasts for both the atmosphere and the ocean have improved very much in the last decade. One measure for this improvement is "forecasting skill" shown in **Fig. 1**. This figure shows that NMC operational 36 hour forecast skill for 500-mb height above sea level over North America have been steadily increasing with time over last 30 years. Indeed, within the bounds of the accuracy of the observational data (which is incorporated into the skill score) these forecasts cannot improve much more. These high skill scores are not found for other atmospheric variables such as precipitation, temperature, surface pressure etc. so that improvement is still necessary.

Dr. Kalnay summarized the following:

1. Structure of National Meteorological Center (NMC)
2. Regional modeling
3. Global modeling
4. Data assimilation and quality control
5. Ensemble forecasting

Structure of NMC

NMC will soon change its name to National Center for Environmental Prediction (NCEP), which consists of six centers located in various regions around the United States:

a) hydrometeorological prediction center
b) storm prediction center
c) aviation weather center
d) tropical prediction center
e) marine prediction center
f) climate prediction center

The role of each of these branches is summarized in **Fig. 2**.

Regional Modeling

For regional short range atmospheric modeling NMC uses twice-daily (00 UTC and 12 UTC) runs of the Eta model (see Janjic 1994) in conjunction with the Nested Grid Model (NGM) and the Limited-area Fine Mesh model (LFM, being phased out). The current

operational Eta model has horizontal grid spacing of 80 x 80 km over 70 degrees of latitude and 50 degrees of longitude, and 38 eta layers in vertical. An even finer resolution Eta version called 'meso-Eta' will soon be implemented operationally with 29 x 29 km horizontal grid spacing and 50 vertical layers. The primary feature of the Eta model is the "eta coordinate" which by its definition requires underlying terrain to be represented in steps (see **Fig. 3**; p is current pressure at the calculated level, p(ref) is standard pressure at that level, p(sfc) is pressure at the underlying surface, and P(oo) is pressure at 1000-mb level). This method was developed by Fedor Mesinger (Black 1994) to eliminate the undesirable pressure gradient calculation in the sigma (terrain-following) coordinate system.

Global Model

The global model at NMC is spectral. Global models, due to their spherical nature, need not be concerned with lateral boundary conditions (unlike limited-area models). 4-dimensional data assimilation (4DDA) is used to continuously improve the model's initial condition prior to each forecast. Because of lack of the data over the Pacific Ocean, forecasts over the western U.S. are of somewhat lower accuracy than those over the eastern U.S. Satellite data are of great importance in the Southern Hemisphere (70% improvement in forecast), while in the Northern Hemisphere their assimilation has only a marginal effect on forecasts (about 3-4% improvement). Some of the global spectral model's uses are:

1. GDAS (Global Data Assimilation System) - a 6 hour forecast (4-times daily) that provides a first guess for the observational analysis system.
2. AVN (Aviation)- a 72-hour forecast (twice daily) that provides short-range U.S. guidance and a global aviation forecast.
3. MRF (Medium Range Forecast) - 10-day forecast (once daily) to provide medium (3-5 day) and extended range (5-10 day) guidance. Twice monthly, a low resolution (T62, triangular truncation at equator wavenumber 62) 30-day forecast is made for monthly outlook and beyond. Multi-runs with T62 resolution are currently made for ensemble prediction guidance.
4. Coupled model project is interested in 1 month to 3 season prediction using MRF as the atmospheric branch of the coupled model.
5. Multi-year runs using T40 resolution are done for the atmospheric model intercomparison project (AMIP).

Implementation of the new Pan-Grell cumulus parameterization into the NMC global model (in August 1993) has been shown to improve the precipitation forecasts compared to using the Kuo cumulus parameteriztion. This new cumulus parameterization has the benefit of interacting to a greater extent with atmospheric dynamics and is a modification of the original Arakawa-Schubert scheme. **Figure 4** shows that the 30-day mean precipitation estimates obtained with this new parameterization compare better to satellite estimates than the same model run with the Kuo parameterization. Also, the vertical resolution in the model has been increased from 18 to 28 levels and the model top has been raised to 3 hPa (well into the stratosphere). This model was very successful at forecasting the "snow storm of the century" (still 6 years left in the century, however) in March 1993, 5 days in advance.

Data Assimilation and Quality Control

Data Assimilation

The typical analysis cycle of data assimilation is shown schematically in **Fig. 5**. Two analysis schemes are currently used in this cycle:

1) Optimal Interpolation (OI) - which generates an analysis field from observed and forecasted values (within a specified radius) multiplied by a weighting factors which minimize the root mean square (RMS) error, or
2) Spectral Statistical Interpolation (SSI) - which uses every observation over the entire globe to determine the meteorological field at every grid point. This method also minimizes the RMS error of approximation (Derber et al. 1994; Parrish and Derber 1992).

Figure 6 shows the sudden improvement in jet-stream level (250 hPa) wind speed forecast at 24 hours upon SSI implementation.

Complex Quality Control (CQC, implemented October, 1991)

Complex QC of rawinsondes temperatures and heights (Collins and Gandin 1990; Gandin 1988):

* currently the most advanced meteorological artificial intelligence-based quality control
* many independent checks (hydrostatic, horizontal, vertical...)
* single decision making algorithm:
  - accept
  - reject
  - correct
* human monitoring of CQC decisions
* finds errors in 7-10% of rawinsondes and corrects 70% of the errors

Ensemble forecasting

An ensemble forecast can be defined as an array of forecasts whose forecasts are a function of small alterations to initial conditions. These techniques were developed in response to chaos theory which showed that non-linear systems, such as the equations of fluid motion used in numerical forecast models, are subject to a sensitivity to initial conditions.

GOALS:

* Improve average forecast by filtering out unpredictable components
* Predict forecast skill based on agreement between ensemble member individual solutions (high agreement => high skill?, low agreement => low skill?)

* Probability forecasting (If,say, 40% of forecasts show one result, and 60% of them show another, does this mean that the second result is 60% more probable to happen?)

The ensemble is composed of individual predictions that are 12 days long, so that with time lagging of up to 2 days the net result is 14 forecasts available through 10 days every day (Toth and Kalnay 1993). Since high resolution in model has been shown not to have significant effect on the long term forecast, the model runs with high resolution (T126) for the first 6 days, and at low resolution (T62) for the ensuing 6 days. Perturbations to the model's initial conditions are created using the 'breeding method', which iteratively finds the fastest-growing perturbations. If these perturbations are superimposed upon a sensitive point of analysis in the model, the perturbations will grow dramatically. Current plans are to increase the number of forecast included in the ensemble to 46.

References

Black, T.L., 1994: The new NMC mesoscale ETA model: Description and forecast examples. *Weather and Forecasting* (to be published in September).

Collins, W.G. and L.S. Gandin, 1990: Comprehensive hydrostatic quality control at the National Meteorological Center. *Mon. Wea. Rev.*, **118**, 2752-2767.

Derber, J.C., D.F. Parrish and S.J. Lord, 1994: The new global operational analysis system at the National Meteorological Center. *Weather and Forecasting*, **6**, 538-547.

Gandin, L., 1988: Complex quality control of meteorological observations. *Mon. Wea. Rev.*, **116**, 1137-1156.

Parrish, D.F. and J.C. Derber, 1992: The National Meteorological Center's spectral statistical interpolation analysis system. *Mon. Wea. Rev.*, **120**, 1747-1763.

Toth, Z. and E. Kalnay, 1993: Ensemble forecasting at NMC: The generation of perturbations. *Bull. Amer. Met. Soc.*, **74**, 2317-2330.

Janjic, Z.I., 1994: The Step-Mountain Eta Coordinate Model: Further Developments of the Convection, Viscous Sublayer, and Turbulence Closure Schemes. *Mon. Wea. Rev.*, **122**, No. 5.

NATIONAL CENTERS for ENVIRONMENTAL PREDICTION

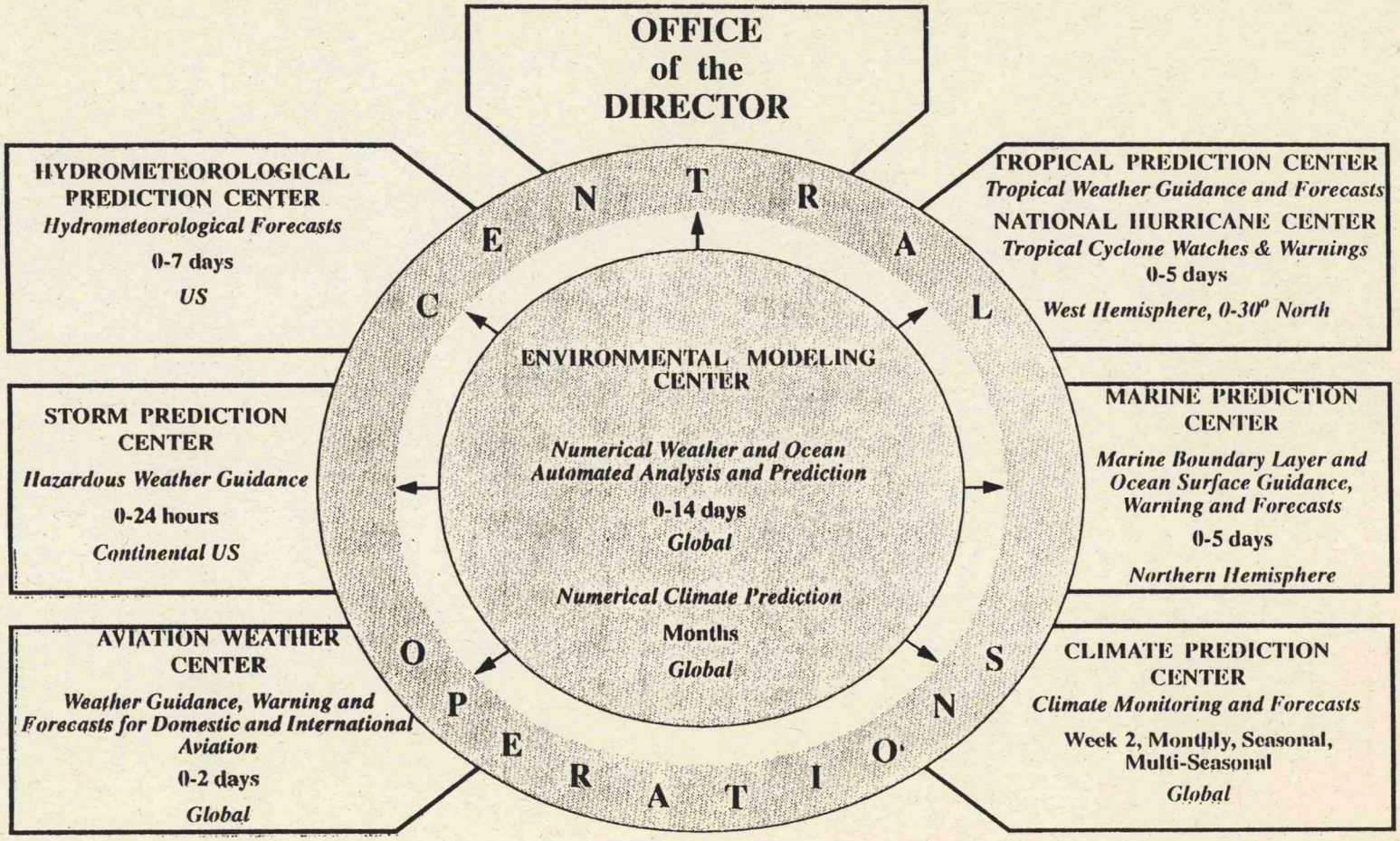

FIGURE 1

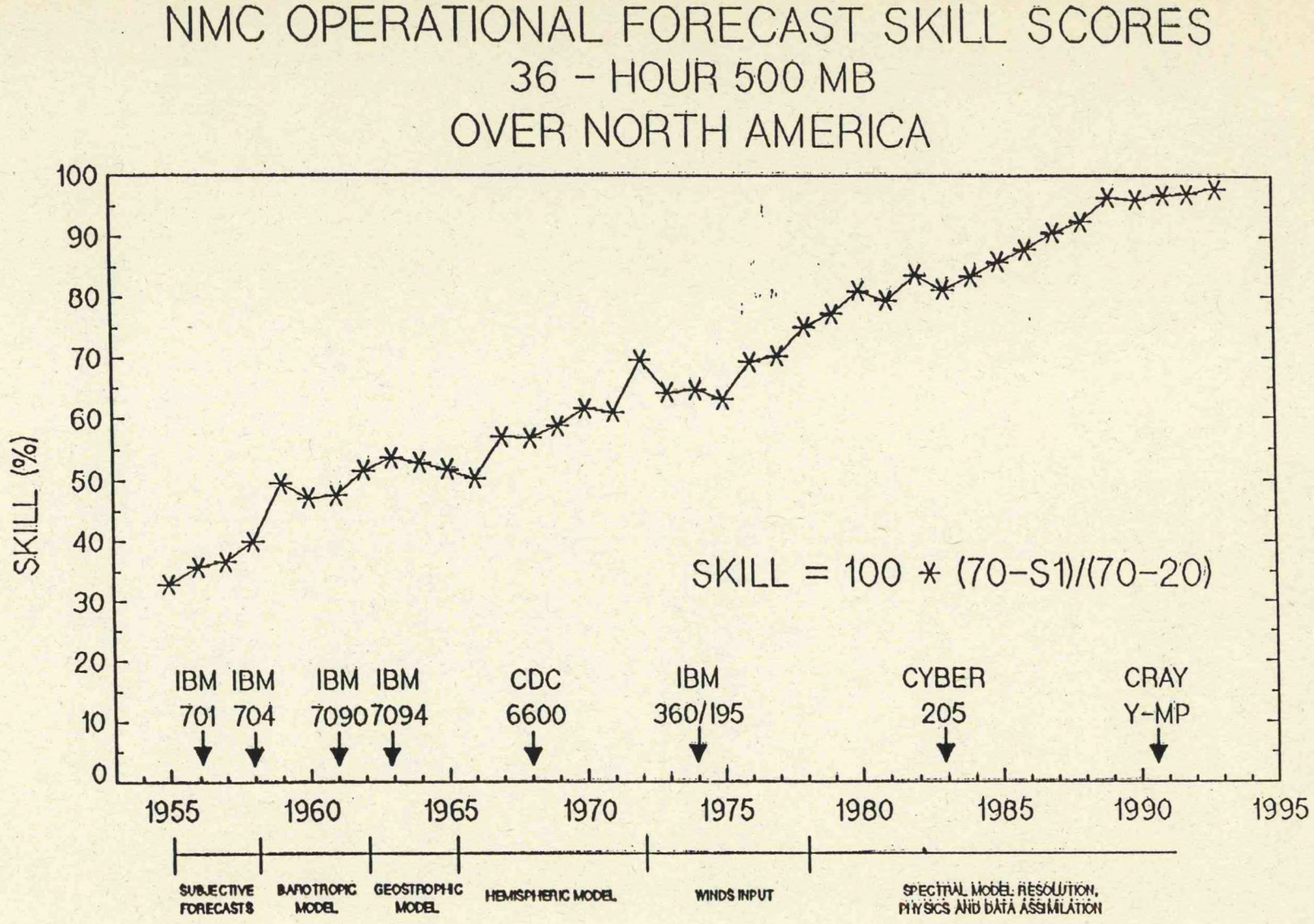
NMC OPERATIONAL FORECAST SKILL SCORES
36 - HOUR 500 MB
OVER NORTH AMERICA
SKILL (%)
100
90
80
70
60
50
40
30
20
10
0
SKILL = 100 * (70-S1)/(70-20)
IBM 701
IBM 704
IBM 7090
IBM 7094
CDC 6600
IBM 360/195
CYBER 205
CRAY Y-MP
1955
1960
1965
1970
1975
1980
1985
1990
1995
SUBJECTIVE FORECASTS
BAROTROPIC MODEL
GEOSTROPHIC MODEL
HEMISPHERIC MODEL
WINDS INPUT
SPECTRAL MODEL: RESOLUTION, PHYSICS AND DATA ASSIMILATION

FIGURE 2

ETA model

Every day at 80 km

Experimentally at 30 km / 40 km

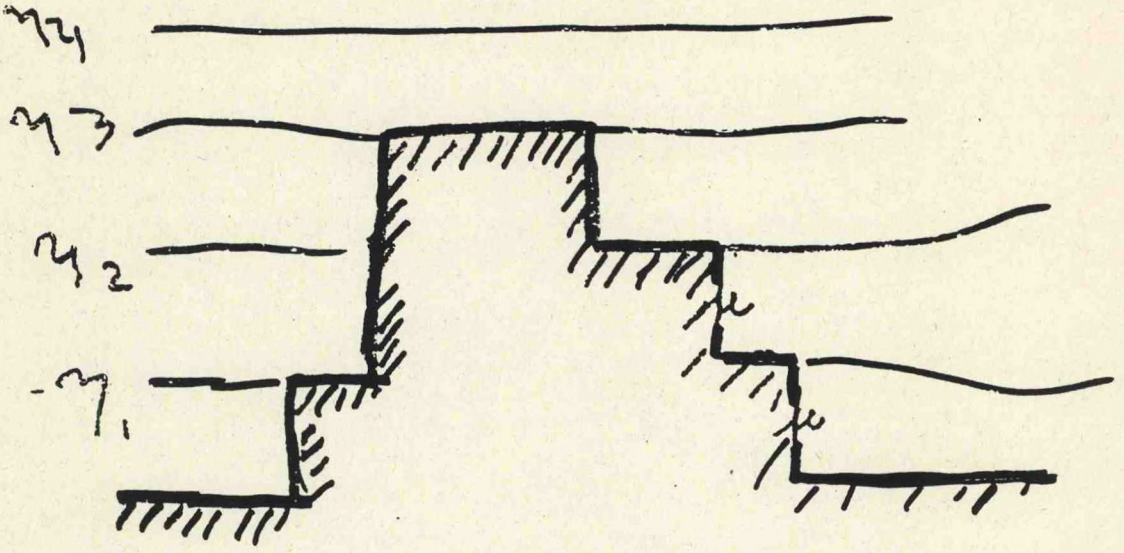

$$\eta = \frac{p}{p_{sfc}} \cdot \frac{p_{ref}(z_{sfc})}{p_{oo}}$$

FIGURE 3

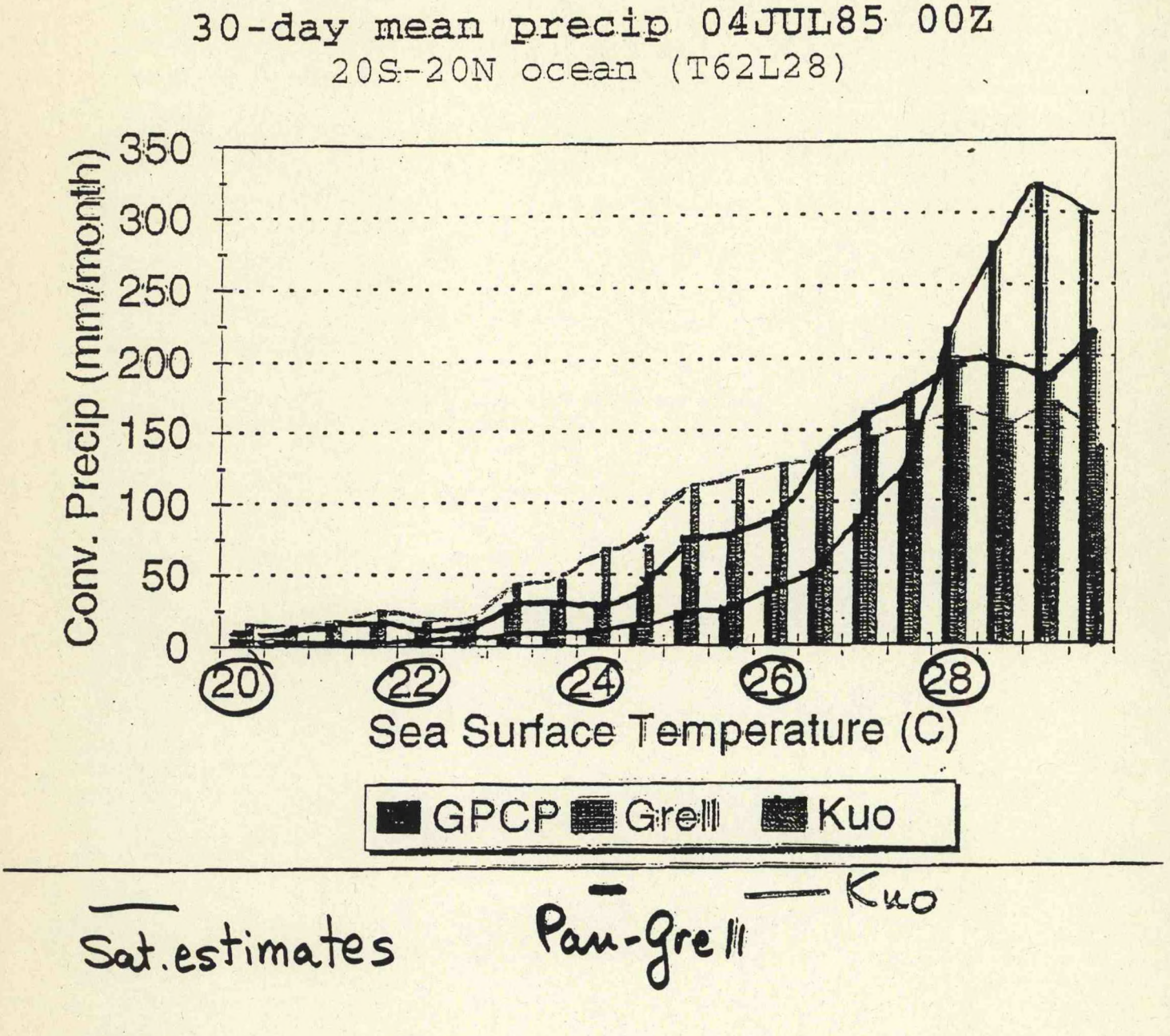
30-day mean precip 04JUL85 00Z
20S-20N ocean (T62L28)
Conv. Precip (mm/month)
350
300
250
200
150
100
50
0
20
22
24
26
28
Sea Surface Temperature (C)
GPCP
Grell
Kuo
Sat. estimates
Pan-Grell
Kuo

FIGURE 4

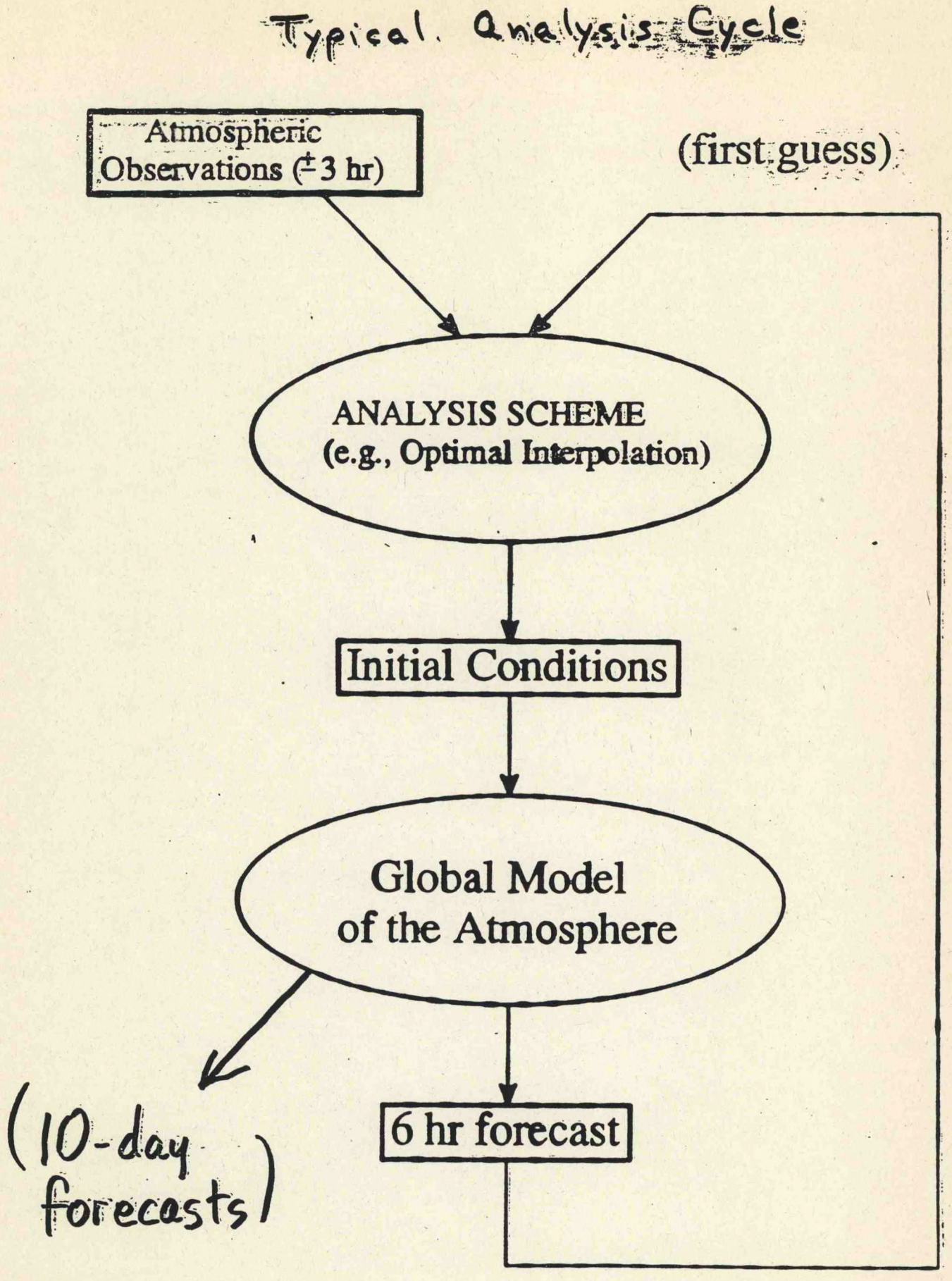
Typical Analysis Cycle
Atmospheric Observations (±3 hr)
(first guess)
ANALYSIS SCHEME
(e.g., Optimal Interpolation)
Initial Conditions
Global Model of the Atmosphere
6 hr forecast
(10-day forecasts)

FIGURE 5

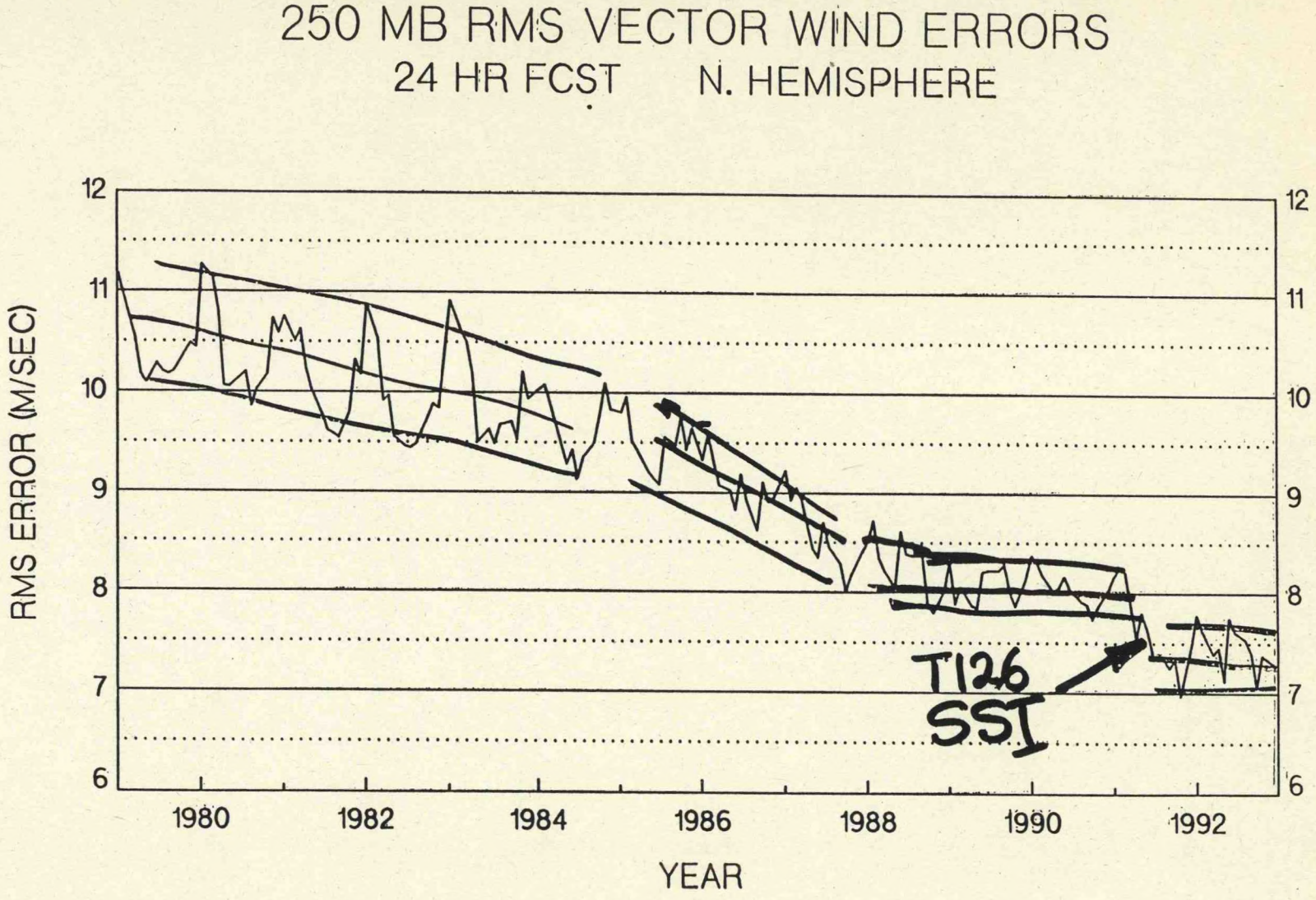
250 MB RMS VECTOR WIND ERRORS
24 HR FCST N. HEMISPHERE
RMS ERROR (M/SEC)
12
11
10
9
8
7
6
1980
1982
1984
1986
1988
1990
1992
YEAR
T126
SSI

FIGURE 6

Forecasting the Superstorm of March 1993

Lecturer: Louis Uccellini
Date: June 8, 1994
Notes by: Suzanne Hartley
Yuval Shay-El

Introduction

During the period 12-14 March 1993, one of the most intense extratropical cyclones in years, dubbed by some the "Storm of the Century", paralyzed much of the eastern United States (Kocin et al. 1994). The Superstorm, with unprecedented snowfall, record-low sea-level pressures, and record low temperatures resulted in dozens of fatalities, hundreds of injuries, damage estimated to exceed $2 billion and the most widespread disruption of air travel in the history of U.S. aviation (**Fig. 1**).

In contrast to many of the previous major storm events, the overall forecast for this particular storm was very successful (Uccellini et al. 1994). That this storm was able to be predicted as much as 5-6 days in advance is testimony to the advances in weather forecasting over the last few decades. The failure of forecasters to anticipate several of the major storms of the last century had lead to the general public perception that "forecasters are usually wrong and don't know what they are doing"!

However, the last 40 years have seen radical changes in the "forecast process". Now, forecasters have access to extensive networks of observations, including remotely-sensed data. Data assimilation systems provide efficient analysis of these observations for input to numerical models which can provide single forecasts or ensemble forecasts as far ahead as 10 days. Model Output Statistics (MOS) allow many meteorological parameters to be inferred from model outputs and coordination with local forecast offices produces detailed local forecasts. Finally, coordination with government officials has permitted necessary warnings to be conveyed to the general public in a timely manner.

Overview of the Storm

The evolution of the storm is depicted in the sequence of surface charts in **Fig. 2**. The cyclone developed in the western Gulf of Mexico and intensified as it moved eastward and then northeastward toward to Florida panhandle. Development of the surface storm was enhanced by upper level jet-streak dynamics and a feedback between latent heat release and upper level potential vorticity maxima. As the low moved into southeastern Georgia, blizzard conditions and heavy snows were occurring to the north and west, severe convective storms were occurring to the south and east, and a 3-4 m storm surge was inundating the northwest Florida coast. Over the next 24 hours, the storm moved rapidly to the northeast, tracking just inland of the coastline, and continued to deepen, achieving its minimum sea-level pressure of 960 mb over the DelMarVa peninsula. The major urban centers of the northeast received snowfall accumulations of 10-12 inches, but the heaviest snowfall occurred inland.

MRF Forecasts

The possibility of a major storm was suggested as early as days 6 and 5, but the results were interpreted cautiously. Model output for days 4 and 3 continued to suggest a major storm and the storm track remained consistent for days 2 and 1.

The UKMET and ECMWF models also gave early indications of the potential for a major storm, but MRF was the first model to show the amplification of the upper level trough and was the most consistent during the forecast period. On day 4 (Wednesday), MRF placed the storm off the east coast, the European model placed the storm well off the coast, while the UKMET model predicted the storm to track well inland. On day 3 (Thursday), the ECMWF model placed the storm west of the Appalachians while the UKMET model had the storm tracking off the east coast.

The consistency of the MRF prediction (the ensemble prediction at day 4 also suggested an east coast low) lead the forecasters to stick to a track just inland of the east coast. The Atlantic coast sequence suggests that the model performed very well. However, it failed to forecast the cyclogenesis in the Gulf of Mexico and tended to delay the period of most rapid cyclogenesis.

Conditional probabilities of snow were first issued at 96 hours and updates continued to suggest a high potential for a large area of snowfall centered on the Appalachian Mountains. The combination of high snow probabilities (as high as 85%) and model-predicted precipitation water-equivalent amounts exceeding 2 inches strongly suggested that this might indeed be a storm of historic proportions.

Regional models

Regional model forecasts started to converge at around 36 hours, but did not predict a deep enough storm over the Gulf. The models continued to underdevelop the storm until 12 UTC on 13 March when the models predicted the maximum development to be farther northeast than the Gulf. By 00 UTC on 14 March, all the regional models were overdeveloping the storm and predicting a mountain storm rather than a coastal storm. However, the forecasters made the decision (based in part on guidance provided by the aviation model (AVN)) not to revise the earlier guidance which had suggested a stormtrack just inland of the coastline. This was to be one of the key factors in the success of the forecast. The 1-2 day forecasts confirmed the earlier predictions. Forecasts of 12-hr snowfall accumulations were consistent and matched the analysis well.

Although the storm was underpredicted in the Gulf, both the Eta and LFM models performed well. Throughout the forecast period, manual adjustments were made to model predictions and the corrections turned out to be in the right direction with regard to earlier storm development, consistency of track and slower rate of movement, and forecasts of precipitation occurrences and quantities. The amount of snow forecast by the NMC/MOD was unprecedented as was the typical lead time for winter storm watches (2 days) and winter storm warnings (1 day). The impact of the storm was substantially reduced due to the advanced prediction.

At the local level, high wind warnings were prompted by radar wind profiles showing high winds moving down toward the surface. In the Washington D.C. area, location of bands of precipitation by NEXRAD facilitated excellent nowcasting of precipitation, with regard to

both form and amount.

Summary

This was not the only major storm in recent years to have been predicted 4-5 days in advance. However, there were several key factors that contributed to the success of the forecast: the relatively consistent guidance provided by the models; the increasing confidence of the forecasters to make predictions; consistent forecast decisions; and an unprecedented effort to coordinate and interact with emergency management. Forecaster modification of model guidance was essential in providing sufficient lead time for action and in providing consistency of forecasts distributed to the public.

References

Caplan, P., 1994: The Superstorm of 12-14 March 1993. Performance of the NMC Global Medium Range Model. *Bull. Amer. Meteor. Soc.,* (in press).

Kocin, P.J., P.N. Schumacher, R.F. Morales Jr., and L. Uccellini, 1994: Overview of the 12-14 March 1993 Superstorm. *Bull. Amer. Meteor. Soc.,* (in press).

Uccellini, L.W., P.J. Kocin, R.S. Schneider, P.M. Stokols, and R.A. Dorr, 1994: Forecasting the 12-14 March 1993 Superstorm. *Bull. Amer. Meteor. Soc.,* (in press).

"The Blizzard of '93"

12-15 March 1993

At Least 219 Fatalities (Cuba to Canada)

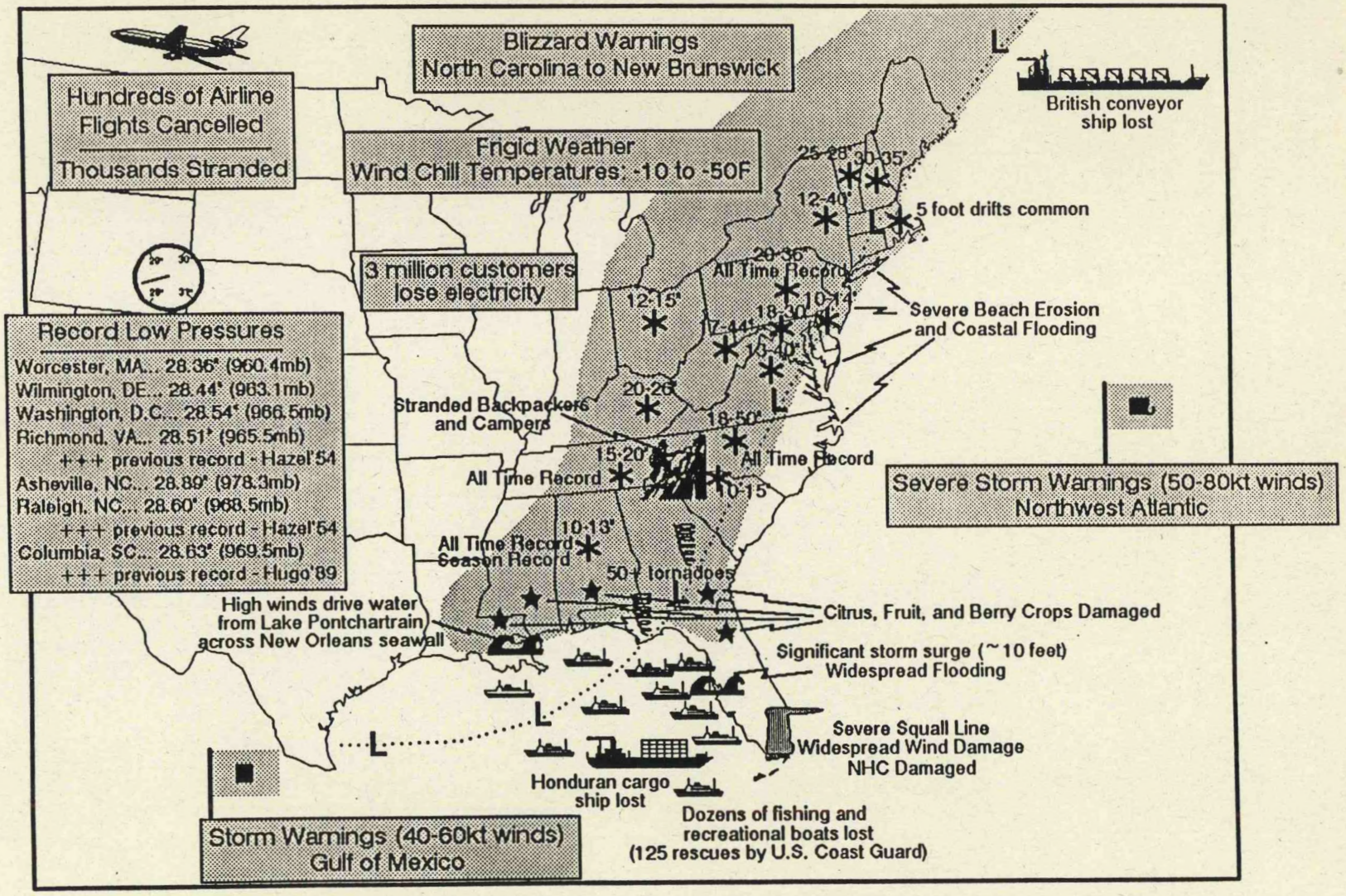

Total snowfall was estimated at 44 million acre-feet of water (one acre-foot is the amount of water that would stand one foot deep over one acre of land). More water fell as snow than flows past the mouth of the Mississippi River in 40 days.

FIGURE 1

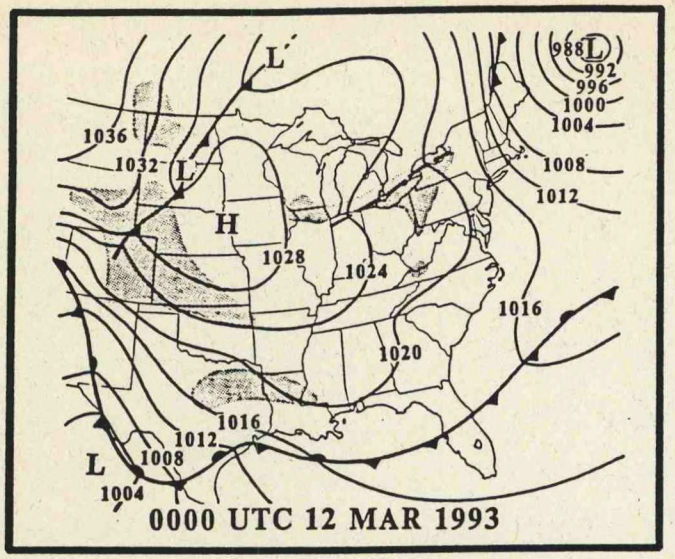
0000 UTC 12 MAR 1993

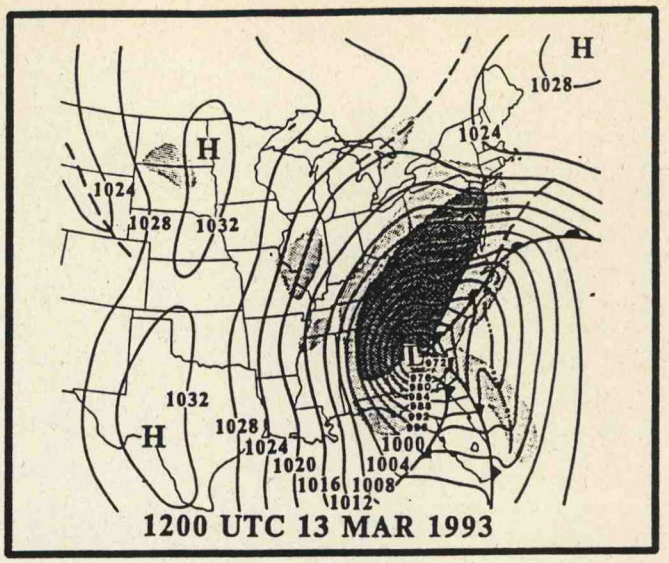
1200 UTC 13 MAR 1993

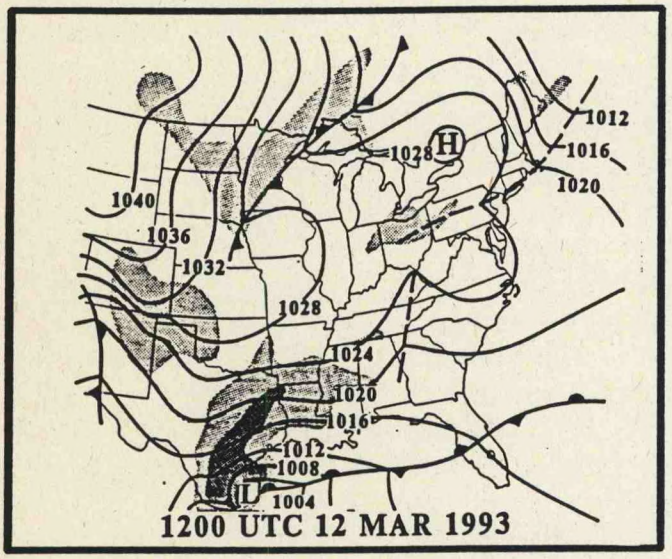
1200 UTC 12 MAR 1993

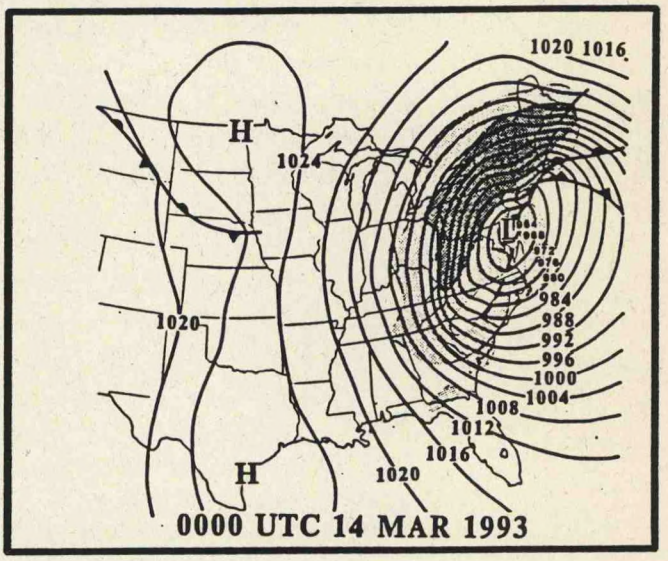
0000 UTC 14 MAR 1993

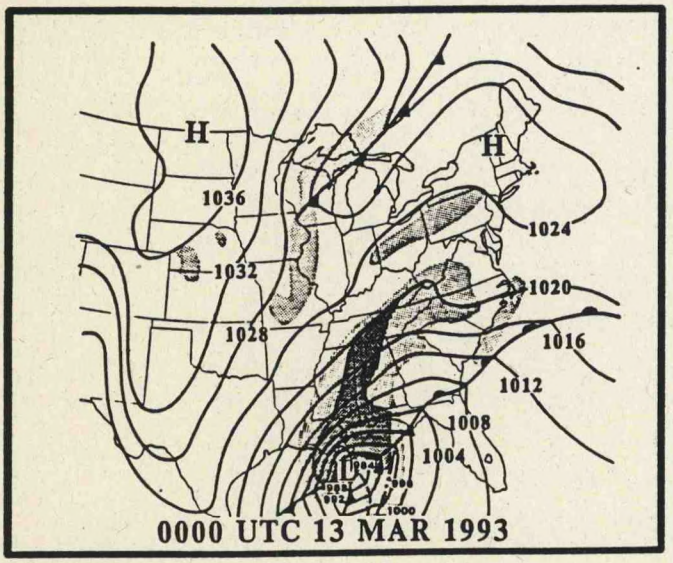
0000 UTC 13 MAR 1993

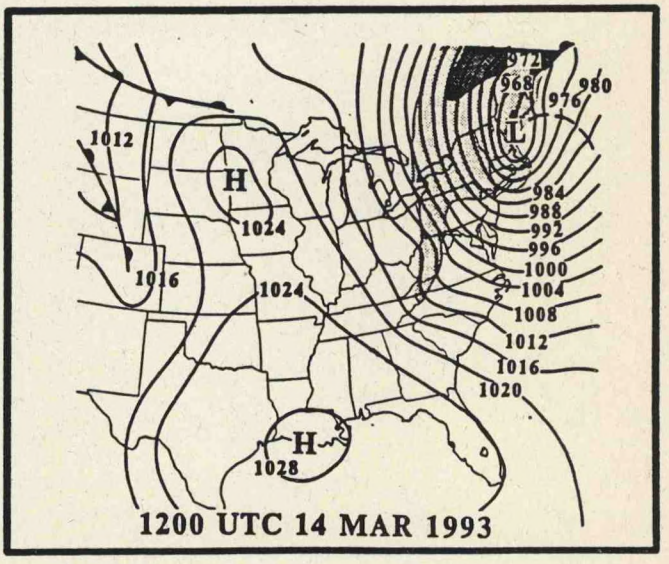
1200 UTC 14 MAR 1993

FIGURE 2

Satellite Applications for Numerical Weather Prediction

Lecturer: James S. Lynch
Date: June 8, 1994
Notes by: Xiaofeng Li
David C. Burwell

There are two types of operational satellites up now. They are the low earth orbit satellites (NOAA 11/12, DMSP 10/11), and the geostationary satellites (GOES 7/8). NOAA 11/12 have a nearly circular orbit that is only 833 to 870 km high. Their orbits are inclined by 98.89 degrees which allows for almost total earth coverage, and since the NOAA satellites are sun-synchronous satellites they pass over the equator at approximately the same local time twice daily, once ascending and once descending. They each carry an imager like the Advanced Very High Resolution Radiometer (AVHRR) aboard the NOAA series. Which has a spatial resolution of 1.1 km at nadir and operates in the infrared (IR) and visible band. They also carry a microwave sounder like the Microwave Sounding Unit (MSU) aboard the NOAA series which has a resolution of 105 km and 4 bands between 50 and 60 GHz. The NOAA-11/12 also carry an ARGOS data collection system that allows them to link remote stations to local ground stations when in range. DMSP-10/11 also carry a microwave imager but the information from DMSP satellites is time delayed and sometimes corrupted to protect the security of the United States.

The GOES series have an orbit that is 35800 km high, which allows them to orbit once daily thus they remain in the same location relative to the ground. GOES 7 is currently at 112 degrees west longitude until the GOES-8 comes on line in the very near future. The GOES-7 can recover an image from its Visible and Infrared Spin Scan Radiometer (VISSR) once every 30 minutes. This capability allows for a series of images to be recovered and played back to show the motion of weather systems. It has a resolution of 1 km in the visible and 7 or 14 km in the infrared, depending upon the band that the IR detector uses. It also carries a data collection system. The GOES-7 together with various other operational geosynchronous satellites that are run by various other countries in cooperation with NOAA provide world wide coverage between 50 degrees north and 50 degrees south latitude, with some loss of resolution near the edge of individual satellite coverage areas.

The traditional satellite products that are used in numerical weather prediction are winds, moisture, and thermal soundings. Geostationary satellite data are utilized to determine cloud movement that is wind driven. By coupling these data with surface observations and cloud top temperatures, winds at many heights can be determined. There is an empirical multi-channel algorithm for use with the GOES-7 data that allows for accurate retrieval of cloud top data. These data together with inferred wind, temperature, and height fields give the human operator a picture of the structure of the atmosphere. The NOAA series AVHRR provides data used in producing a global sea surface temperature (SST) analysis and used for many ancillary products,such as the analyses of the vegetation index, sea-ice and snow-cover.

Satellite products are also utilized in numerical weather forecasting (e.g., hurricane tracking, severe weather outbreaks), in estimating precipitation, and in determining the outgoing long wave radiation (OLR), which is extremely useful in determining areas of deep convection within the Tropics. For data sparse areas, such as over the oceans, satellites serve as an important source of information that allows for accurate global meteorological analyses, which in turn are used as initial conditions in numerical weather prediction models.

Topics in Analysis Techniques

Lecturer: Thomas W. Schlatter
Notes by: Scott Stanley
Alan Zeigler
Date: June 9, 1994

Incorporating weather observations into numerical weather forecast models is difficult because reality is a chaotic, dynamic, continuous, nonlinear system, and models are finite, discrete representations of this reality. Techniques for generating initial conditions from observation data have evolved from simple objective analysis schemes of the 1950's and 1960's to current sophisticated data assimilation schemes. Objective analysis techniques estimate small-scale meteorological parameters from observations unevenly distributed both in time and space. Data assimilation is a more sophisticated form of objective analysis which combines a numerical model with observations to give a 4-dimensional estimate of parameters that is consistent with the constraints of the forecast model.

The inclusion of numerical prediction model in the generation of an initial field creates dynamic consistency between the mass and wind fields and allows the advection of information into data-sparse regions. This is an improvement over climatology and persistence and supports temporal continuity. Although data assimilation includes a numerical model (other objective analysis schemes may or may not), there are a number of inherent problems:

1) Calculated initial conditions do not always match realizable model states;
2) The distribution of observations is highly non-uniform;
3) Observed variables don't always match variables predicted by the model;
4) Observations are subject to errors; thus one must determine how closely to fit the observations.

Popular objective analysis schemes include surface fitting, empirical linear interpolation, and optimum interpolation. Surface fitting (e.g. ordinary least squares and weighted least squares) is no longer used with meteorological data, but does work well for a small fixed network of observations. Surface fitting requires no first guess and allows accountability of observational error. However, there are several disadvantages to surface fitting:

1) Hazards of underfitting, overfitting, and using the wrong set of functions;
2) In data sparse areas or outside the domain of the observations, functional values can be "off the wall";
3) Computationally expensive when large numbers of observations are considered (in some cases, problem is ill-conditioned);
4) Ignores meteorological knowledge about the situation except when variational constraints are imposed.

Empirical linear interpolation schemes (e.g. Cressman analysis, Barnes analysis) are simple, quick, and produce results which are smooth and generally pleasing. However, these techniques are not well-suited for diverse observations because observation errors are not accounted for. They also do not account for the distribution of observations relative to one another. Other drawbacks include no obvious extension to multivariate applications, variation

of "scale" of the result with observation density, as well as the need to determine an optimum scan radii using trial and error.

Optimum Interpolation is a widely used statistical approach that allows differentiation among observing systems and the incorporation of error information specific to each. Optimum interpolation has the ability to estimate one variable from the observation of another (so long as they are correlated). This technique weights observations consistent with their past atmospheric behavior. It also allows for quality control of observations, and generates an analysis error as a function of the distribution and accuracy of the data. The disadvantages of optimal interpolation are that it is computationally expensive, and isn't designed for good performance during extreme events. Also, in general scale-dependent correlation models require a long history of numerical forecasts for accurate determination of the empirical coefficients.

Bayesian schemes and nudging are recent trends in data assimilation. The Bayesian approach, given a numerical forecast and a set of observations, finds the most probable state by maximizing the probability density function. Nudging is an economical approach to data assimilation that pushes the model towards an observed state, eliminating computational noise. Although nudging may lack a solid foundation, it maintains approximate balance in the model, incorporates model physics, easily accommodates asynoptic data, and avoid exciting rapidly varying modes in the model.

More information

Schlatter (1988) provides a detailed review (with extensive bibliography) of objective analysis techniques used in environmental prediction. Much of his review is taken from Thiebaux and Pedder (1987). A partial bibliography of current publications involving objective analysis and data assimilation follows:

Daly, R., 1991: *Atmospheric Data Analysis*. New York: Cambridge University Press. 457 pp.

Davies, J. C., and R. E. Turner, 1977: Updating prediction models by dynamical relaxation: an examination of the technique. *Quart. J. Roy. Meteor. Soc.*, **103**, 225-245.

Derber, J. C., D. Parrish, and S. J. Lord, 1991: The new global operational analysis system at the National Meteorological Center. *Wea. and Forecast.*, **6**, 538-547.

Harville, D. A., and A. L. Carriquiry, 1992: Classical and Bayesian prediction as applied to an unbalanced mixed linear-model. *Biometrics*, **48**, 987-1003.

Innocente, V., and L. Lista, 1994: Evaluation of the upper limit to rare processes in the presence of background, and comparison between the Bayesian and classical approaches. *Nuclear Instruments & methods in Physics Research Section A-Accelerators Spectrometers Detectors and Associated Equipment*, **340**, 396-399.

Lorenc, A.C., R. S. Bell, and B. MacPherson, 1991: The Meteorological Office Analysis Correction Data Scheme. *Quart. J. Roy. Meteor. Soc.*, **117**, 59-81.

Malanotterizzoli, P., and R. E. Young. 1992: How useful are localized clusters of traditional oceanographic measurements for data assimilation. *Dyn. Atmos. and Oceans*, **17**, 23-61.

Mitchell, H. L., C. Carat, and C. Chouinard, 1990: Revised interpolation statistics for the Canadian data assimilation procedure: their derivations and application. *Mon. Wea. Rev.*, **118**, 1591-614.

Parrish, D. F., and Derber, J. C., 1992: The National Meteorological Center's Spectral Statistical Interpolation Analysis System. *Mon. Wea. Rev.*, **120**, 1747-1763.

Phoebus, P. A., and J. S. Goerss, 1992: The assimilation of marine surface data into the Navy operational global atmospheric prediction system. *Mar. Tech. Soc. Journal*, **26**, 63-77.

Stauffer, D. R., N. L. Seaman, and F. S. Binkowski, 1991: Use of four-dimensional data assimilation in a limited-area mesoscale model part II: effects of data assimilation within the planetary boundary layer. *Mon. Wea. Rev.*, **119**, 734-754.

Stensrud, D. J., and J. W. Bao, 1992: Behaviors of variational and nudging assimilation techniques with a chaotic low-order model. *Mon. Wea. Rev.*, **120**, 3016-3028.

Stern, W. F., and J. J. Ploshay, 1992: A scheme for continuous data assimilation. *Mon. Wea. Rev.*, **120**, 1417-1432.

Wu, X., and W. L. Smith. 1992. Assimilation of ERBE data with a nonlinear programming technique to improve cloud-cover diagnosis. *Mon. Wea. Rev.*, **120**, 2009-2024.

Zupanski, M. 1993. Regional 4-dimensional variational data assimilation in a quasi-operational forecasting environment. *Mon. Wea. Rev.*, **121**, 2396-2408.

References

Schlatter, T. W. 1988. Past and present trends in the objective analysis of meteorological data for nowcasting and numerical forecasting. Paper presented at the Eighth Conference on Numerical Weather Prediction, 22-26 Feb., 1988, Baltimore, Maryland. Proceedings published by the American Meteorological Society, Boston, Massachusetts.

Thiebaux, H. J., and M. A. Pedder, 1987: *Spatial Objective Analysis with Applications in Atmospheric Science*. New York: Academic Press. 299 pp.

Research on Improving Hurricane Prediction

Lecturer: John F. Gamache
Date: June 9, 1994
Notes by: Alec Richardson
Alan Zeigler

Tropical cyclones and hurricanes are subjects of continuous ongoing atmospheric and oceanographic research by the National Meteorological Center (NMC). The goal of this research is to improve the accuracies in the numerical modeling and forecasts of tropical storms and hurricanes, with respect to their location of origin over the sea, travel path, intensity profile, time and location of impact of the storm with a coastline, and potential damage assessment inflicted by the storm. The NMC desires to improve the accuracy of their storm predictions, so that the forecast data and storm warnings can be disseminated to emergency personnel, media, and the public sufficiently early so that the necessary precautions and evacuation procedures can be implemented, resulting in a potentially significant reduction in the loss of lives and in property damage.

In August 1992, the National Hurricane Center in Coral Gables, FL, tracked Hurricane Andrew as it migrated along its travel path through the Caribbean Sea, striking the east coast of Florida at Homestead (south of Miami), traveling across Florida and the Gulf of Mexico, striking Louisiana, and eventually dissipating inland. The hurricane inflicted over $20 billion in damage across south Florida (particularly mobile home parks) and Louisiana, establishing itself as the largest natural disaster in U.S. history in terms of property damage costs. Hurricane Andrew exhibited an atmospheric pressure minimum of 922 mb (located in the eye), and originated in the Caribbean Sea via intensification brought about by an interaction between the developing tropical storm and a low pressure system north of the storm. This interaction intensified the winds of the (then) tropical storm, upgrading the storm to a hurricane.

A cyclone is defined as a low pressure atmospheric center with winds circulating counterclockwise in the Northern Hemisphere (clockwise in the Southern Hemisphere). A tropical cyclone is classified into three categories according to wind speed:

1) Tropical depression: sustained winds of speeds less than 18 m/sec with at least one closed isobar (i.e. closed circulation).
2) Tropical storm: sustained winds of speeds 18-32 m/sec.
3) Hurricane: sustained winds of speeds greater than 32 m/sec.

Hurricanes are further classified into 5 categories based on maximum sustained wind speed (SWS) and storm surge (SS), according to the Saffir/Simpson Hurricane Scale:

1) Category 1: SWS = 74-95 mi/hr or SS = 4-5 ft above normal.
2) Category 2: SWS = 96-110 mi/hr or SS = 6-8 ft above normal.
3) Category 3: SWS = 111-130 mi/hr or SS = 9-12 ft above normal.
4) Category 4: SWS = 131-155 mi/hr or SS = 13-18 ft above normal.
5) Category 5: SWS > 155 mi/hr or SS > 18 ft above normal.

Hurricane observational data include:

1) Aircraft measurements, such as EVTD Doppler radar via the PBL model, SFMR surface wind speed, and C-SCAT wind speed and direction.
2) Ocean platform measurements, such as wind speed at the air-sea interface, sea surface temperature (SST), and sea surface pressure.

Composites of the hurricane's wind field were constructed via the adjustment of flight level data, land-based data, and mooring data to the 10 m level, and the subsequent composition of these data into an analysis package which measures streamlines and isotachs.

Radar color images of a hurricane reports various atmospheric parameters (such as pressure, temperature, and precipitation), and identifies cyclonic storm features such as the eye, inner and outer eyewalls, the principle band, and secondary bands.

Physical processes associated with the development, sustenance, and dissipation of hurricanes include: Conservation of mass; conservation of angular momentum; conservation of energy; surface friction; condensation and freezing, advection; atmosphere-ocean transport fluxes; oceanic mixing processes; and heat-engine features of the ocean.

A hurricane's physical structure is characterized by:

1) An eye, which is a low pressure center located near the middle of the hurricane, and is characterized by calm winds.
2) Outer and inner eyewalls, which are bands encircling the eye and which are characterized by high local tangential velocity.
3) Principle band and secondary bands, which are located on the outer periphery (edges) of the hurricane and in which the winds associated with the hurricane have dissipated to speeds of the order of the surrounding environmental winds.

Within a vertical cross section of the hurricane exist mesoscale updrafts, downdrafts, and rainshafts (**Fig. 1**). The downdrafts of air meet with an inflow path of air toward the center of the hurricane. As this air flows toward the storm's interior, air pressure decreases and the air begins to rise (i.e. updraft) in both the outer eyewall and inner eyewall. As the air is updrafted, the moisture content of the air begins to condense, causing stratiform precipitation (called rainshafts) away from the hurricane's center. The air may rise to heights of 10-15 km and then either flow either away from (outflow) or toward (inflow) the storm's center. As the inflow stream of air approaches the eye, this air is forced to descend due to conservation of mass.

Anthes (1982) illustrates a typical state of the lower troposphere in a hurricane. As evaporation occurs at the sea surface, air at the air-sea interface typically has a high humidity and energy content. The resultant increased buoyancy causes the air to rise through the atmospheric boundary layer into the free atmosphere through cumulus cloud bases. These clouds entrain additional air from above the boundary layer, and heavy precipitation falls from the convective clouds, some of which entrain unsaturated air. This air undergoes evaporative cooling and descends toward the sea surface, where it undergoes an increase in temperature (via sensible heat gain) and humidity (via evaporation of seawater). Precipitation may also result from mesoscale lifting of stable air in the troposphere, and subsidence occurs

between convective clouds. Caused by strong vertical wind shear, turbulent eddies entrain dry air into the boundary layer, where it undergoes an increase in humidity via evaporation of seawater.

Emanuel (1986) illustrates the minimum attainable surface central pressure (P_{min}) as a function of surface air temperature (T_s) and weighted mean outflow temperature (T_{out}) for the Atlantic, Pacific, and Indian Oceans for Sept. 1986. For example, for T_{out} = -50 °C and T_s = 26 °C, the minimum possible storm eye pressure is P_{min} = 970 mb. Minimum attainable surface central pressures have been measured over the Atlantic, Pacific, and Indian Oceans in Sept. 1986 (**Fig. 2**). These measurements indicate pressure lows of 895 mb in the Bay of Bengal, 880 mb in the central Gulf of Mexico, and 870 mb in the SW Pacific north of Australia and east of Indonesia.

Tropical cyclones and hurricanes form under favorable environmental conditions such as a warm sea surface temperature (SST) and weak wind shear stresses. In the presence of high wind stress at the air-sea interface, converging air masses are broken up before they have a chance to accumulate forces typical of cyclones or hurricanes. Tropical cyclone statistics show that:

1) Tropical cyclones do not typically occur in the South Atlantic or eastern South Pacific Oceans because of the relatively low SSTs in these regions during most of the year. Low SSTs are not conducive conditions for hurricane formation.
2) Tropical cyclones are twice as frequent in the Northern, compared to the Southern, Hemisphere.
3) Approximately 80 cyclones with maximum sustained winds greater than 20 m/sec occur annually worldwide.
4) Because the SSTs are sufficiently warm in this region all year round, tropical cyclones may form in the western North Pacific any time of the year.
5) Approximately 25 tropical cyclones occur annually in the eastern North Pacific (west of Mexico and Central America), the most favorable region for hurricane formation during the early summer.
6) Because of short warning times, coastline topography, and large human coastal populations, the Bay of Bengal coasts are the sites of the worst death tolls inflicted by tropical cyclones and hurricanes, with perhaps 100,000 deaths from a single storm.

Gray (1979) conducted measurements of annual cyclone origin locations over the past 20 years, showing that most of the recent cyclones originate in the tropical Atlantic, Gulf of Mexico, southeast tropical Pacific, tropical South Pacific, Bay of Bengal, and the south Indian Ocean. The frequency of annual occurrence of tropical cyclones has been measured as a function of: average SST; thermal energy of the upper 60 m of the water column; mean relative humidity of the atmosphere at the 500-700 mb altitude range; atmospheric buoyancy forces; relative vorticity at the 950 mb altitude; and wind shear stress.

Landsea and Gray (1992) and Landsea (1993) measured the intense hurricane track climatology by monthly periods for the period 1944-91 (**Fig. 3**). Climatology shows that tropical cyclones and hurricanes most frequently occur during September of a given year.

Studies of interannual variability of North Atlantic tropical cyclones have been conducted in order to correlate tropical cyclone activity to large scale climate parameters such

as SST, air temperature, surface pressure, humidity, and wind speed. General relationships have been determined between hurricane climatic fluctuations and: El Niño-Southern Oscillation (ENSO); SST; horizontal wind shear stress; and the quasi-biennial oscillation of equatorial winds.

A strong connection has also been established between interannual variability of major Atlantic hurricanes and the western Sahelian (Africa) rainfall. Attempts have been made to predict the hurricane season activity in the North Atlantic prior to the peak of the season or as much as 6-11 months in advance. Landsea and Gray's (1992) study of the effect of Sahelian rainfall activity on intense hurricane tracks in the Atlantic Ocean shows that the tropical storm occurrence frequency increases as the amount of annual precipitation in the Sahelian region increases. Goldenberg and Shapiro (1994) examined the effects of Sahelian rainfall and wind shear stress on tropical storm activity, and concluded that storm activity increases with an increase in Sahelian rainfall and with a decrease in wind shear stress.

Hurricane motion prediction is based on:

1) Persistence (short term), which states that the hurricane will continue along its present path.
2) Climatology (longer term), which states that, at a given location on a given date, the hurricane will follow the path which exhibits the maximum degree of correlation with all previously experimentally observed paths for that specific date, location, and storm motion.
3) CLIPER (Climatology and Persistence): Forecasting relies on persistence in the short run, and on climatology in the long run.

The deterministic prediction of hurricane motion is based on the environmental flow field, storm structure, and intensity. Computer simulations predict the future location of the hurricane with respect to both large scale flow, and movement relative to the large scale flow.

Satellite observations of hurricane motion can identify the location to within 100 km of the storm center, with an improved spatial accuracy for cases of more intense, well organized storms, and can also provide estimates of upper-troposphere and lower-troposphere winds by tracking the motions of clouds and variations in water vapor. Thus, sufficient data is available to draw a correlation between hurricane location/activity and wind shear stress, a correlation which has been found by numerous researchers to be negative.

A standard rawinsonde network provides high quality winds for inclusion in large scale prediction models. Commercial craft observations enhance the measurement accuracy of upper-troposphere wind speed and direction. Land-based radar are used to track storms as they approach or pass by landmasses.

Aircraft observations are obtained on a regular basis only over the Atlantic Ocean, because of the scarcity of landmasses over the other world oceans. Fundamental information such as minimum central pressure and maximum flight level winds are obtained by NOAA and Air Force observations. Regular center observations provide information on storm motion (such as storm wind speed and direction), which is a significant initial condition for many model simulations of storm motion. The Hurricane Research Division (HRD) has conducted synoptic flow experiments in which 40-50 dropsondes are dropped from aircraft flying in the periphery of the storm. Dropsondes measure features of the near-storm environmental flow (such as temperature, pressure, humidity, and wind speed) as they fall through the atmosphere, reach the sea surface, sink to the seafloor, never to be recovered. The purpose of omega dropwindsonde (ODW) experiments is to obtain a correlation between storm motion

and mean wind flow, for a given altitude and distance away from the storm center. Relatively few middle tropospheric observations have been conducted over the ocean, but were used operationally in Hurricanes Andrew and Emily in order to improve and increase the confidence in storm track forecasts.

Observational research has been conducted in the form of a vortex motion experiment, in which the winds are measured out to 300 km from the storm center, concurrently during observations of the flow field in the center of the storm. Generally, the storm's motion is most highly correlated to the average wind motion in a band 100-300 km from the storm center.

Hurricane intensity predictions have been conducted using both statistical model and satellite methods. Statistical methods include the Statistical Hurricane Intensity Forecasts (SHIFOR) and the Statistical Hurricane Intensity Prediction System (SHIPS). Satellite methods are used to assess the amount and structure of upper-level outflow, in order to determine the likelihood of storm intensification. These methods are used to determine both the storm intensity change over time, and the present intensity.

As a result of condensation heating, the outer eyewall contracts, moves toward the storm's inner core center, and removes a significant amount of available energy from the air flowing in at the lower boundary. The subsidence associated with the outer eyewall starts to suppress and dissipate the inner eyewall, resulting in a temporary increase in the central pressure and hence a decrease in the velocity of the most intense winds.

In the upper troposphere, a trough associated with the storm generally approaches to the northwest of the developing tropical cyclone. Air interactions occur where the air in the outflow sectors has a relatively lower angular momentum, and the air in the inflow sectors possess a higher angular momentum. These interactions are characterized by eddy transports of angular momentum, and produce an increase in the angular momentum of the storm's inner core. The tangential wind consequently increases, resulting in a deepening of pressure at the storm center. The response to these contracting rings of outflow is the production of a secondary eyewall which then propagates inward. Hurricanes are most stable inertially in the lowest level in the atmosphere. As altitude increases, storm instability generally increases.

Extensive research has been conducted over the past several years concerning the physical processes associated with tropical cyclone and hurricane activity. DeMaria et. al. (1993) conducted studies of the time evolution of maximum wind, maximum expected wind, vertical wind shear stress, and eddy angular momentum flux convergence as functions of time and radius away from the storm center. Molinari and Vollero (1989) conducted model forecasting of the eddy angular momentum flux convergence as a function of time and radius away from the storm center. Willoughby (1990) carried out aircraft flight measurements of tangential wind as a function of radius away from the storm center, and concluded that the maximum wind speeds occur between 20 and 30 km from the storm center.

Finally, McAdie and Lawrence (1993) conducted studies of forecast error trends over the past 20 years for both short term (i.e. 24-hour) and longer term (i.e. 48- and 72-hour) forecasting. The error reductions have been measured in the unadjusted cases, in the adjusted cases using CLIPER (Climatology and Persistence) errors only, and in the adjusted cases using both CLIPER errors and average longitude. Because of improvements in remote sensing technology, the forecast errors for both short- and long-term forecasts have generally decreased over the last 20 years, with a more dramatic improvement in the long-range than in the short-range forecasts.

References

Anthes, R. A., 1982: *Tropical Cyclones: Their Evolution, Structure, and Effects.* American Meteorological Society.

DeMaria, M., J. J. Baik, and J. Kaplan, 1993: Upper-Level Eddy Angular Momentum Fluxes and Tropical Cyclone Intensity Change. *J. Atmos. Sci.*, **50**, 1133-1147.

DeMaria, M., and J. Kaplan, 1994: A Statistical Hurricane Intensity Prediction Scheme (SHIPS) for the Atlantic Basin. *Wea. and Forecast.*

Gray, W. M., 1979: Hurricanes: Their Formation, Structure, and Likely Role in the Tropical Circulation. Meteorology Over the Tropical Oceans (ed. D.B. Shaw), Royal Meteorological Society.

Landsea, C. W., and W. M. Gray, 1992: The Strong Association Between Western Sahelian Monsoon Rainfall and Intense Atlantic Hurricanes. *J. Climate*, **5**, 435-453.

Landsea, C. W., 1993: A Climatology of Intense (or Major) Hurricanes. *Mon. Wea. Rev.*, **121**, 1703-1713.

McAdie, C., and M. Lawrence, 1993: AMS Conference on Hurricanes and Tropical Meteorology, San Antonio.

Molinari, J., and D. Vollaro, 1989: External Influences on Hurricane Intensity. Part I: Outflow Layer Eddy Angular Momentum Fluxes. *J. Atmos. Sci.*, **46**, 1093-1105.

Shapiro, L., and S. Goldenberg,: To be submitted (1994).

Willoughby, H. E., 1990: Temporal Changes in the Primary Circulation of Tropical Cyclones. *J. Atmos. Sci.*, **47**, 242-264.

FIGURE 1 Vertical Cross-Section of a Hurricane, Illustrating the Eye, Eyewall, Outer Eyewall, Mesoscale Updrafts, Downdrafts, and Rainshafts.

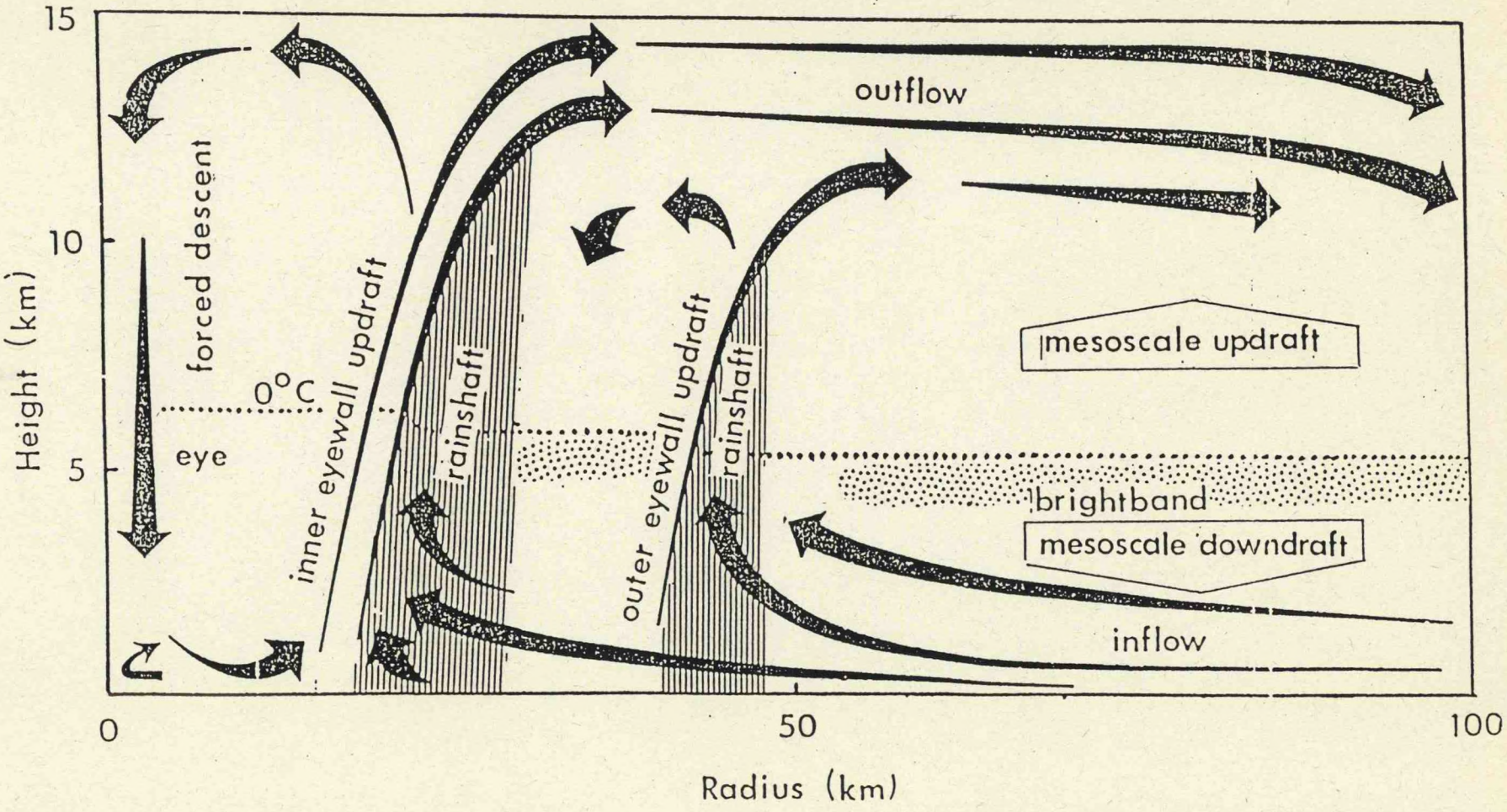

FIGURE 2 Minimum Attainable Surface Central Pressure (mbar) for Sept. 1986 for the Atlantic, Indian, and Pacific Oceans (Emanuel, 1986).

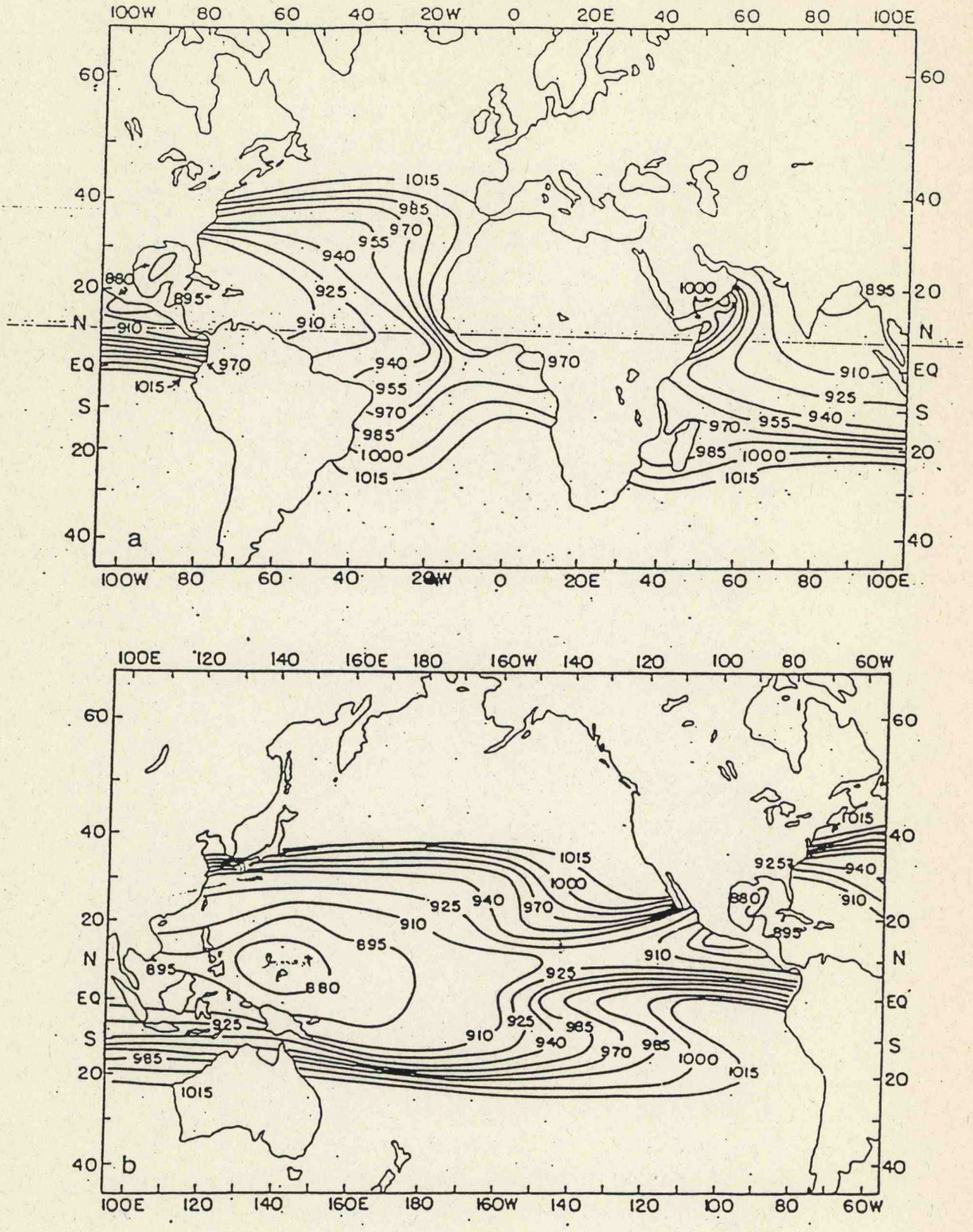

FIGURE 3 Intense Hurricane Track Climatology by Monthly Periods for the Years 1944-91. June Tracks are labeled "6", and November Tracks are Labeled "11" (Landsea and Gray, 1992).

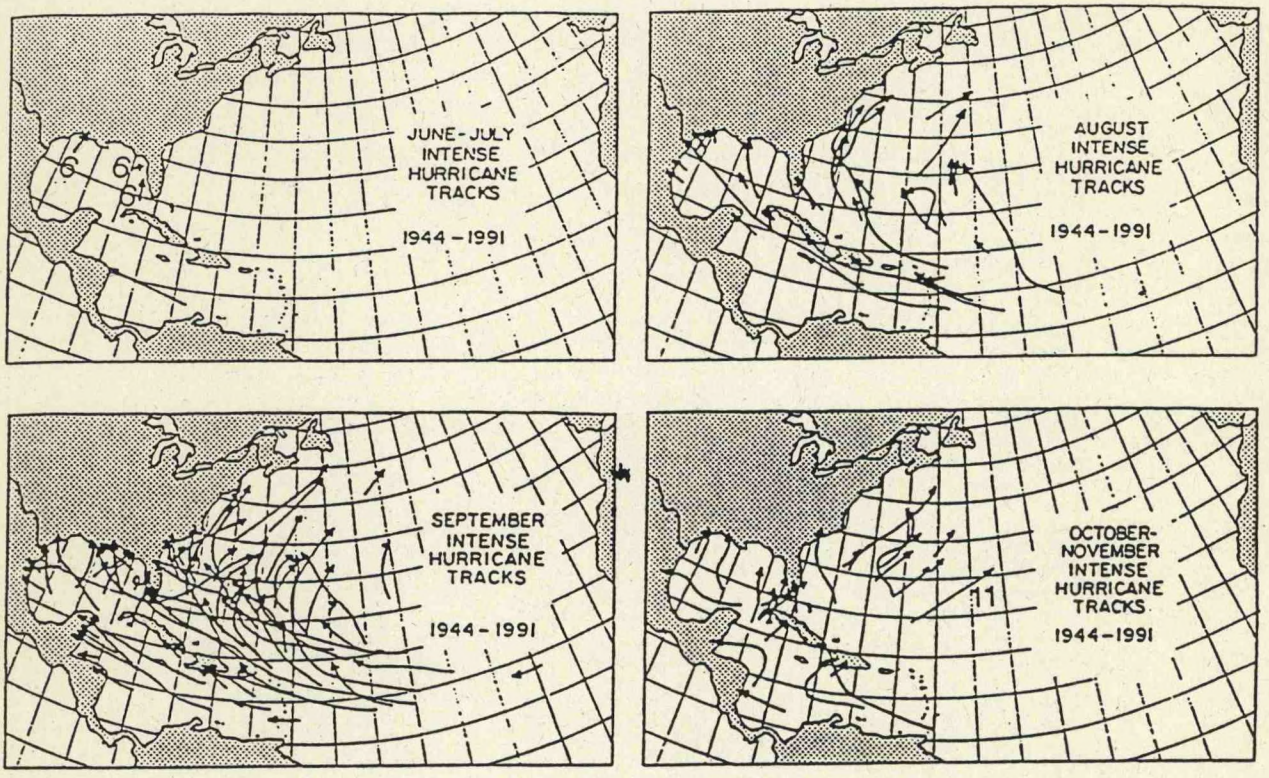

Mesoscale Analysis Techniques

Lecturer: Roger Wakimoto
Date: June 8, 1994
Notes by: Scott Stanley
Yuval Shay-El

Mesoscale analysis suffers from the problem of lack of data. Two major developments enabled closing the gap of missing information: 1. The use of innovative techniques which derive the most information from limited data. 2. The increase in remote sensing and in-situ measurement techniques, such as satellites and radars.

The first analysis of mesoscale data was done by Fujita et al. (1955). In a detailed analysis of meteorological data Fujita showed that a meso-high can be found below thunderstorms, within a larger scale front. This small scale data was earlier ignored. In order to enhance the mesoscale data he used a method called time-space conversion (Fujita 1963). Knowing the propagation speed of a phenomena, observations in a single station, expressed as time-series, can be converted by advection to a spatial distribution. Since the phenomena being observed is not truly steady, this advection process must be done very carefully.

Mesoscale analysis was enhanced by combining sounding data with data from aircraft penetrations in crisscrossing patterns. **Figure 1**, for example, shows an upper-level front analysis, obtained from rawinsonde observations supplemented with aircraft data (Shapiro and Keyser 1990). These investigators used dropsondes to obtain wind, temperature and humidity profiles and flew penetration patterns to obtain samples in the upper-level front. Some analyses used a quasi-steady composite analysis techniques to study mesoscale phenomena using sounding data. In this technique, soundings are taken at a range of positions relative to the phenomena being observed. These soundings at slightly different times are then combined to give a quasi-steady image of the phenomena. Carr and Millard (1985), for example, have examined the structure of comma clouds with this technique.

Two additional techniques introduced by Fujita (1957), in an analysis of the Fargo tornadoes of June 20, 1957, are **photogrammetry** and **ground damage surveys.** Photogrammetry is the use of photographs for qualitative analysis. By tracing the ground damage done by the tornado, Fujita was able to describe the three dimensional structure of the tornado. He defined terms such as collar cloud, wall cloud, and tail cloud related with the small scale structure of the tornado. In another damage survey Fujita found that a tornado can break down into multi-funnels which he called "suction" vortices. Fujita defined an F scale, based on degree of damage, to classify tornadoes by intensity. Fujita (1985) also used this technique to investigate microbursts, strong downdrafts accompanied by outflows.

Another device which has been useful on collecting data in mesoscale phenomena is Doppler radar. The book by Atlas is an excellent reference on the use of radar. A number of studies of mesoscale phenomena have been made utilizing Doppler radar. Forbes (1981) used radar to examine the reliability of using hook echoes as an indicator of tornado activity and Bluestein and Unruh (1989) used Doppler radar to take measurements inside tornadoes. Doppler radar has also been used to identify convergence zones, cold fronts, and intense squall lines (Wilson et al. 1980.) Kropfli and Miller (1976) also showed that by using dual Doppler radar, the kinematic flow field within a phenomena could be reconstructed. Gal-Chen (1978) also showed that this kinematic flow field could then be used to determine the pressure and buoyancy fields. Multi-parameter radar, such as the CP-2 radar built by NCAR,

can be used to distinguish between rainfall and hail in storm. When raindrops get large, they become oblique spheroids; hail on the other hand is spherical. Using multi-parameter radar, the size and shape of the precipitation can be determined indicating whether it is hail or rain.

Another sensing tool which has been very useful in mesoscale analysis is satellite data. Purdom (1982) used satellite imagery to determine the effects of morning cloud cover on afternoon thunderstorm development in Alabama. He also showed that 93% of the 9850 convective storms he observed were a result of mergers and intersections of arc clouds. Maddox (1980) defined a mesoscale phenomena called a Mesoscale Convective Complex (MCC) based solely on satellite imagery. It has been shown that MCCs can cause flash floods and are responsible for most of the rain during the growing season.

Dr. Wakimoto has used a number of the techniques described above to study different phenomena. For instance a pollution study of the Los Angeles area was performed utilizing surface data, balloon soundings, aircraft, and lidar measurements. This data was used to derive information about the aerosols in the area. Also, as part of the Convective Initiation and Downburst Experiment (CINDE) a single Doppler radar combined with cloud photogrammetry was used to stud the relationship between the hook echo and the visual features of tornadoes (Wakimoto and Martner 1992). Results from this study are shown in **Fig. 2.**

References

Atlas, D., 1990: *Radar in Meteorology.* Amer. Meteor. Soc., Boston, MA, 806 pp.

Bluestein, H. B., and Unruh, W. P., 1989: Observations of the wind field in tornadoes, funnel clouds, and wall clouds with a portable Doppler radar. *Bull. Amer. Meteor. Soc.*, **70**, 1514-1525.

Carr, F. H. and J. P. Millard, 1985: A composite study of comma clouds and their association with severe weather over the Great Plains. *Mon. Wea, Rev.*, **113**, 370-387.

Forbes, G. S., 1981: On the reliability of hook echoes as tornado indicators. *Mon. Wea. Rev.* **109**, 1457-1466.

Fujita, T., H. Newstein, and M. Tepper, 1955: Mesoanalysis - An important scale in the analysis of weather data. U.S. Dept. of Commerce, Weather Bureau, Research Paper No. 39, 83 pp.

Fujita, T., 1963: Analytical mesometeorology: A review. *Meteor. Mono.*, **5**, 77-125.

Fujita, T., 1957: Detailed Analysis of the Fargo Tornadoes of June 20, 1957. The University of Chicago, Severe Local Storms Project, Technical Report No. 5, 29 pp.

Fujita, T., 1985: The downdraft. Satellite and Mesometeorology Research Project Research Paper No. 210, Dept. of the Geophysical Sciences, The University of Chicago, 122 pp.

Gal-Chen, T., 1978: A method for the initialization of anelastic equations: Implications for matching models with observations. *Mon. Wea. Rev.*, **106**, 587-606.

Kropfli, R. A., and L. J. Miller, 1976: Kinematic structure and flux quantities in a convective storm from dual-Doppler radar observations. *J. Atmos. Sci.*, **33**, 520-529.

Maddox, R. A., 1980: Mesoscale convective systems. *Bull. Amer. Meteor. Soc.*, **61**, 1374-1387.

Purdom, J. F. W., 1982: Subjective interpretation of geostationary satellite data from nowcasting. *Nowcasting*, K. Browning, ed., Academic Press, 149-166.

Shapiro, M. A. and D. Keyser, 1990: Fronts , jet streams and the tropopause. *The Erik Palmen Memorial Volume*, Newton and Holopainen, eds. Amer. Met. Soc., 167-191.

Wakimoto, R. M., and B. E. Martner, 1992: Observations of a Colorado tornado. Part II: Combined photogrammetric and Doppler radar analysis. *Mon. Wea. Rev.*, **120**, 522-543.

Wilson, J., R. Carbone, H. Baynton, and R. Serafin, 1980: Operational application of meteorological Doppler radar. *Bull. Amer. Meteor. Soc.* **61**, 1154-1168.

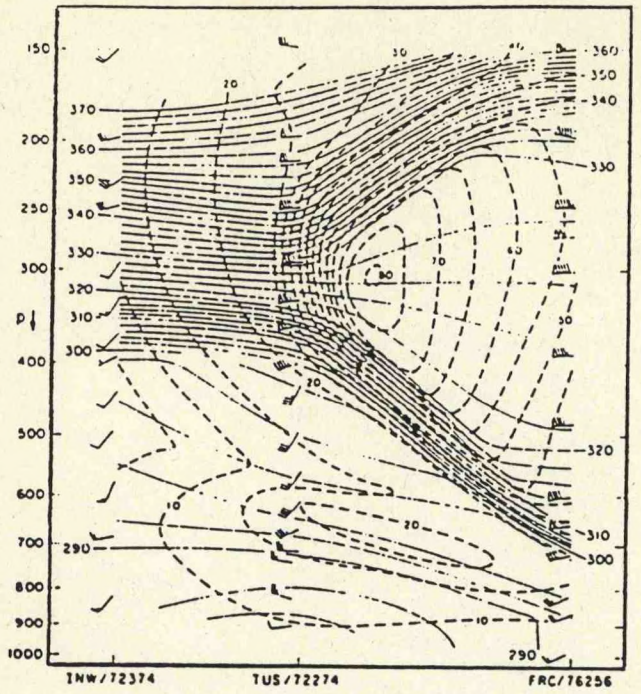

(a)

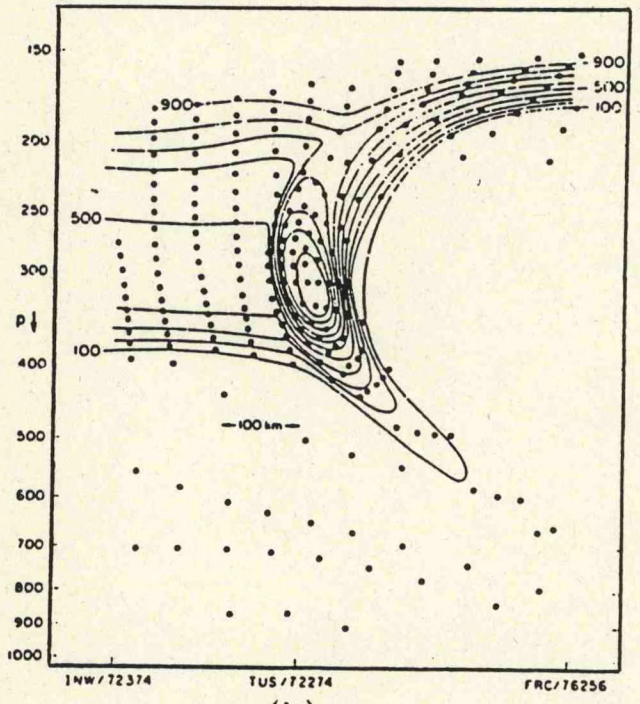

(b)

FIGURE 1 Example of upper-level front analysis obtained from rawinsonde observations supplemented with aircraft data (Shapiro and Keyser, 1990).

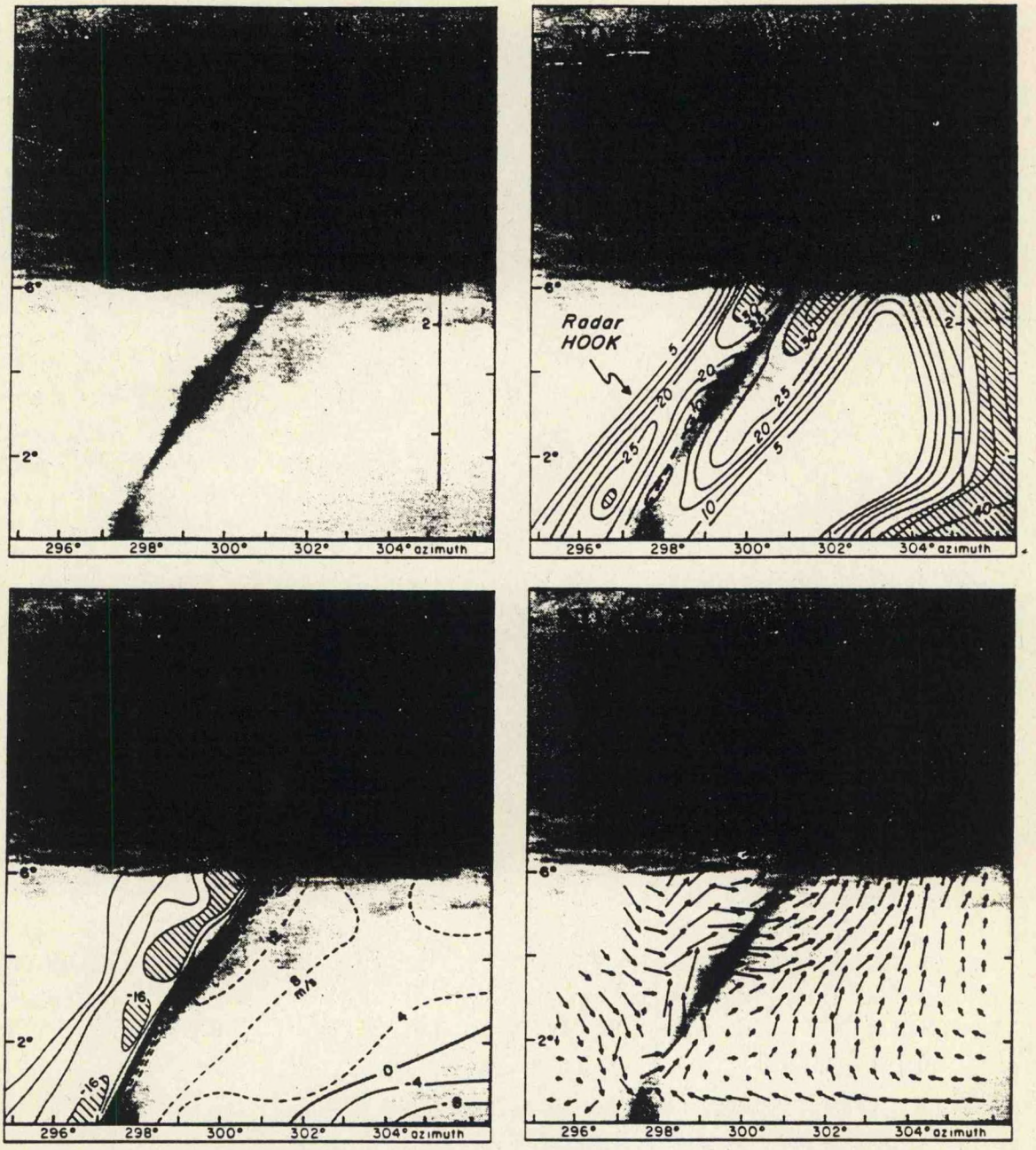

FIGURE 2 *Photograph of the 2 July 1987 tornado at 1435 MST superimposed on vertical cross sections through the center of the hook echo/misocyclone of radar reflectivity (upper right), single-Doppler velocities (lower left) from the NOAA-C radar, and dual-Doppler winds (lower right) from the NOAA-C and NOAA-D. Radar reflectivities greater that 35 dBZ are hatched. Solid and dashed contours represent Doppler velocities out of and into the photograph, respectively. Heights are in kilometers (AGL).*

Greenhouse Warming

Lecturer: Anthony Broccoli
Date: June 10, 1994
Notes by: Elvira Brankov
Paul Gaertner

Physics of the Greenhouse Effect

Without atmosphere the earth surface would be at a radiative equilibrium temperature of 255K. Since the atmosphere contains a variety of gases which are transparent to solar radiation but absorb terrestrial radiation, the effective radiating temperature is higher, about 288K.

In what is called an "Atmospheric Window" the atmosphere is almost transparent to infrared radiation. Most of the radiative cooling of the earths surface will be due to wavelengths in this region. Gases such as carbon dioxide and water vapor (greenhouse gases) have some absorption in the atmospheric window region. Carbon dioxide contains several absorption bands in the region, particularly towards longer wavelengths. Water vapor, however, has significant absorption at the borders of this region. Thus increases in the concentration of greenhouse gasses in the atmosphere make the atmosphere more opaque to infrared radiation, producing what is now know as the *greenhouse effect.* While carbon dioxide and water vapor are important greenhouse gases other greenhouse gases such as methane, nitrous oxide and CFCs though exist in minute quantities, molecule for molecule they absorb more radiation than carbon dioxide or water vapor, thus must be given similar importance.

Evidence for greenhouse effect

Annual estimated global (land only) surface temperature anomalies from 1855 to the present have been computed using the period 1951-1980 as a base reference. The anomalies indicate a sharp rise in temperature from the turn of the century up into the 1940s followed by a period of relatively flat anomalies and a fairly rapid warming trend from mid 70s to the present. Although these anomalies do fall within the bounds of natural variability they also seem to indicate an upward trend in global temperature anomalies occurring since the later half of the 19th century.

Modeling climate effects

In order to address the problem of greenhouse warming, climate models must contain an atmospheric component, an oceanic component, and must also address interactions between the atmosphere and the continental surface, particularly if the surface is covered with snow. **Figure 1** is shows some of the important physical processes present within a climate model.

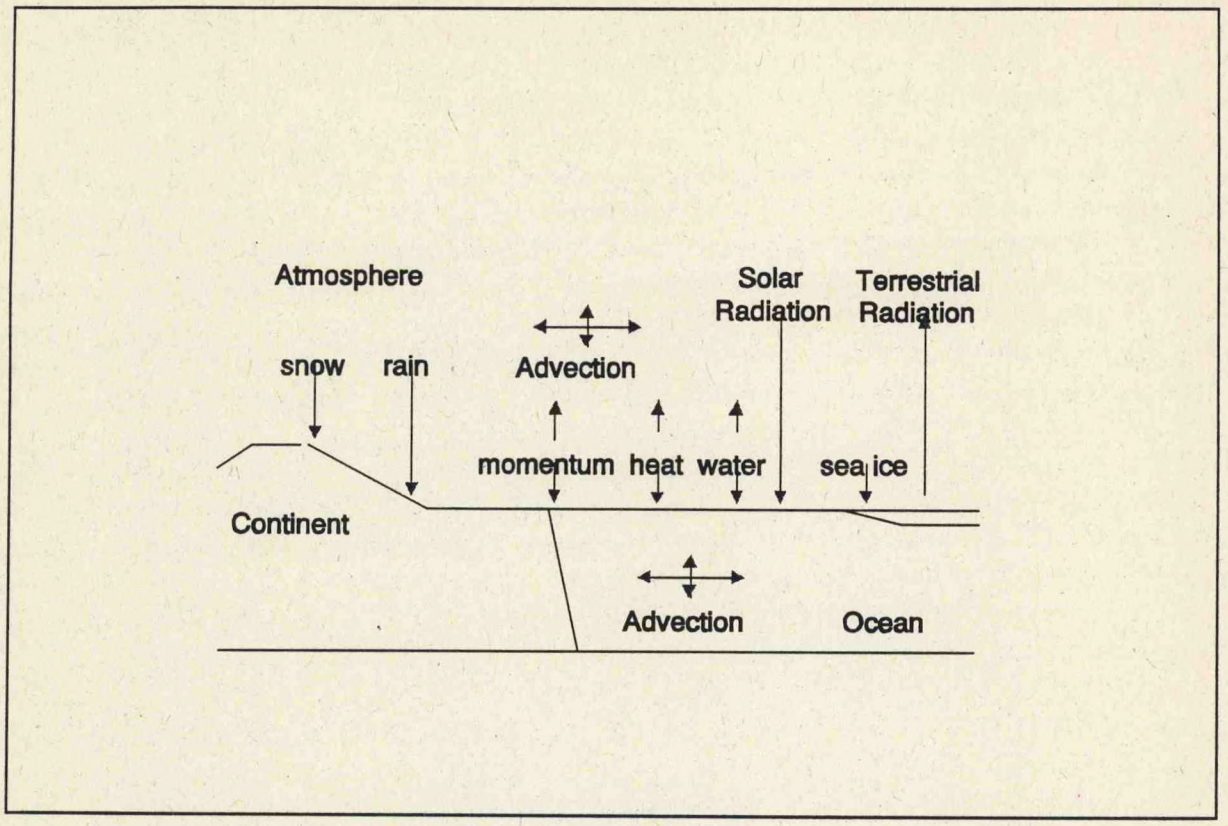

Figure 1.

Climate models will never be able to predict the temperature or precipitation on a certain day. The idea instead is to give an indication of what the climate conditions will be at some point in the future. Climate models can be considered as grid point models where the atmosphere is divided into discrete grid cells, with a set of coupled nonlinear differential equations that are solved numerically by being discretized into finite differences.

Climate models have been used to perform two types of experiments for investigating the greenhouse effect. *Equilibrium experiments* (**Fig. 2**) compare an atmosphere containing the present day CO_2 concentration with one that has a doubling of CO_2 concentration. With this type of experiment we are only interested in discovering how different the two climate states will be. There is no need to know how heat is flowing through the deep ocean because the assumption is that these climatic states are at equilibrium after some period of time. The model runs long enough so that the climate settles to a point where we can compare the climate states.

Key results from equilibrium experiments

CO_2 doubling in the troposphere would result in:

* warming of the surface and the lower atmosphere
* cooling of the stratosphere
* increase in global mean precipitation
* area and snow cover and sea decrease
* "polar amplification" of the surface warming at high latitudes during the cold season
* soil moisture decreases over northern midlatitude continents in summer

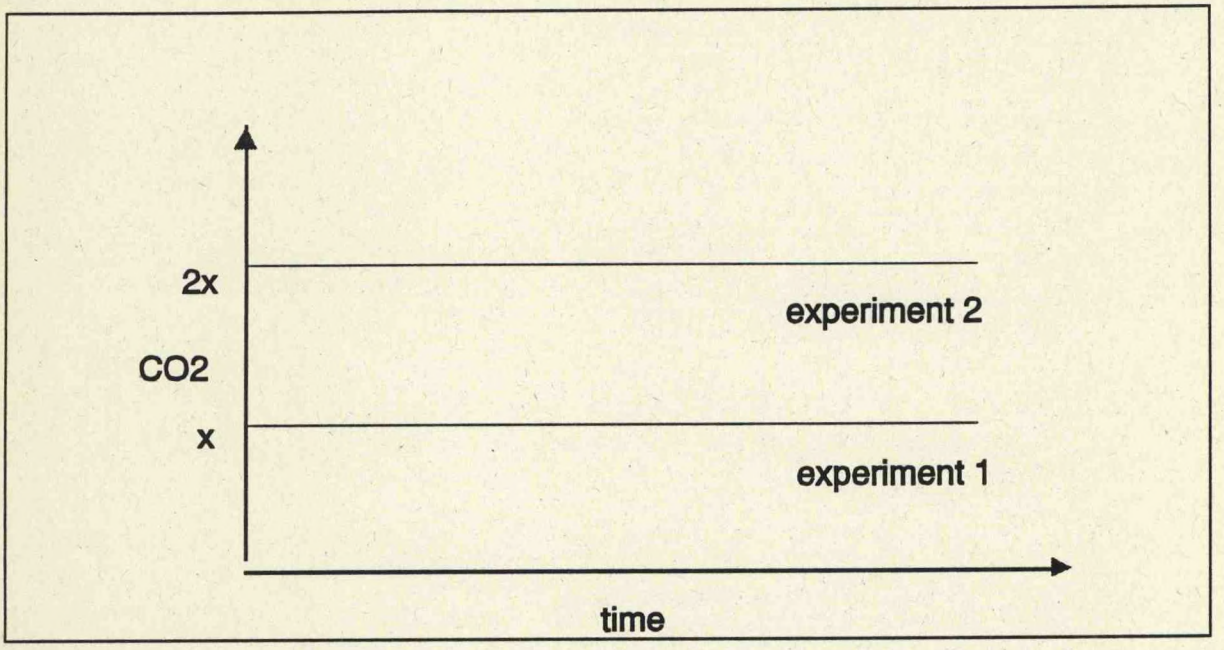

Figure 2

Transient experiments (**Fig. 3**) are experiments in which the CO_2 concentration is changing gradually. Unlike equilibrium experiments, it is necessary to couple the model with an ocean model that takes into account the flow of heat into the deep ocean. In both experiments the CO_2 concentration is given as input, and they do not attempt to calculate the carbon cycle. Also the fact that the differences in climate are themselves a function of time must be dealt with.

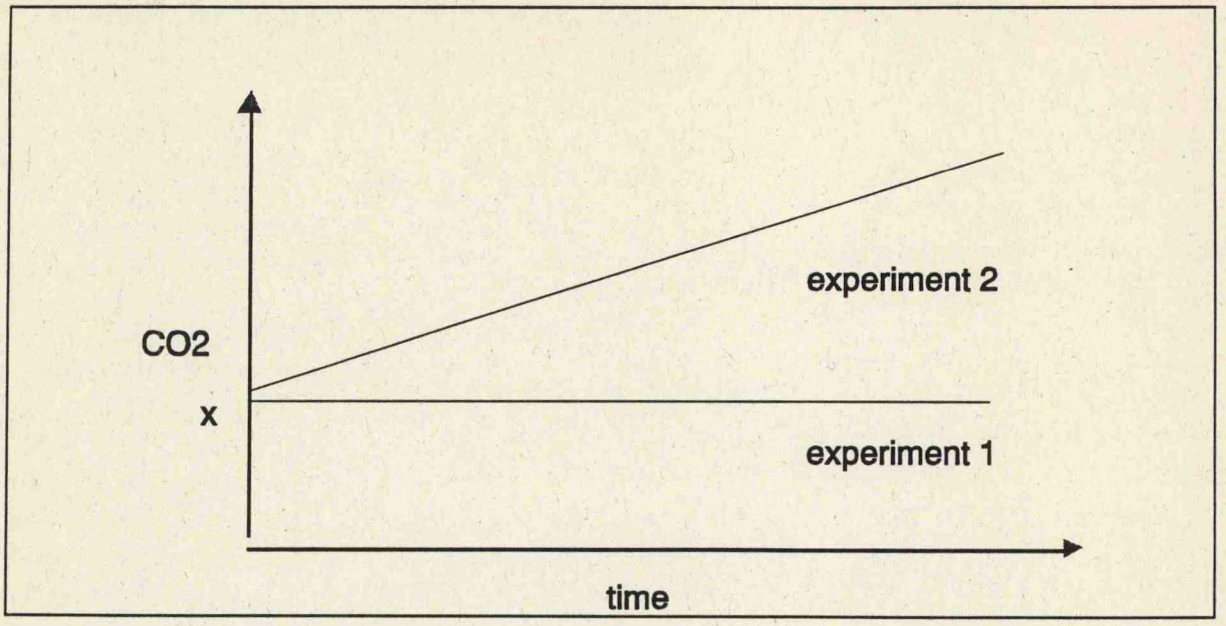

Figure 3

Key results from transient experiments:
Time-dependent studies show that large scale patterns of climate changes are similar to those obtained in comparable "equilibrium" experiments, except over the circumpolar and the North Atlantic oceans, where mixing with the deep ocean sharply reduces the rate of warming over the circumpolar and North Atlantic ocean relative to the global average. A raise in global mean sea level (associated with the thermal expansion of ocean waters) will accompany global warming, even without accounting for possible melting of glaciers and ice sheet.

Forecasting Future Climate

In order to make a hindcast (forecast) of climate it is necessary to fulfil two conditions: (IPCC 1990). Firstly, all major natural and anthropogenic factors known to influence climate must be included, and secondly, a record (prediction) of the past (future) variation in the "forcing factors" must exist. Sources of forcing factors include greenhouse gases, sulphate aerosols (industrial), volcanic aerosols (stratospheric injections) and variations in solar variability.

Conclusions

Feedbacks are a key area of uncertainty in climate models. For example, an increase in temperature causes an decrease in snow and ice, causing a decrease of surface reflectivity. An increase in the absorbed sunlight would then lead to an increase in temperature, producing a positive feedback. On the other hand, an increase in temperature causes an increase of moisture in the atmosphere, which will increase the cloud cover. Clouds reflect sunlight decreasing the solar radiation absorbed by earth's surface and therefore decreasing its temperature, a negative feedback. However, very little is known about clouds, thus an

increase in cloud cover could increase the infrared opacity of the atmosphere and thus the height of the effective radiating level, increasing the temperature.

References

IPCC, 1990: Intergovernmental Panel on Climate Change, Climate Change: The IPCC Scientific Assessment, J.T. Houghton, G.J. Jenkins, and J.J. Ephraums, eds., New York, Cambridge University Press.

Jones, P. D., T. M. L. Wigley, and P. B. Wright, 1990: Global and Hemispheric Annual Temperature Variations between 1861 and 1988, NDP-022/R1, Carbon Dioxide Information Center, Oak Ridge National Laboratory, Oak Ridge, TE.

Lashof, Danial A. and Dilip R. Ahuja, 1990: Relative Contributions of Greenhouse Gas Emissions to Global Warming. *Nature*, **344**, 529-531.

Machta, L., 1972: The Role of the Oceans and Biosphere in the Carbon Dioxide Cycle. *Nobel Symposium*, **20**, 121-145.

Wuebbles, D. J. and J. Edmonds, 1988: A Primer on Greenhouse Gases, prepared for the Department of Energy, DOE/NBB-0083.

Stratospheric Ozone Depletion

Lecturer: A. James Miller
Notes by: Alec Richardson
Date: June 13, 1994
Sam Levis

Ozone (O_3) is an important atmospheric trace gas. In the troposphere it acts as a greenhouse gas and a localized atmospheric pollutant, while in the stratosphere it forms a protective shield for life on earth from the harmful solar ultraviolet (UV) radiation. If it were not for the stratospheric ozone layer, life on earth would probably not exist.

NOAA monitors atmospheric ozone in order to determine the variability of O_3 on different temporal and spatial scales. This lecture focused on the available data related to the recent anthropogenic depletion of stratospheric O_3.

An average global distribution of total O_3 around the world for the period 1957-67 (pre-depletion) shows O_3 minima straddling the equator, with a significant increase in O_3 concentration with an increase in latitude. O_3 concentrations are generally higher in the Northern than in the Southern Hemispheres, and O_3 maxima are found in central Canada (400 Dobson units), Europe (380 DUs), and eastern Asia (380 DUs). A typical pre-depletion O_3 profile in the vertical exhibits a relative constant O_3 concentration through the troposphere, an increase to a maximum at about 25 km altitude (in the stratosphere), followed by a continuous decrease in O_3 with a further increase in altitude.

Through a series of complex photochemical catalytic atmospheric reactions, UV radiation is responsible for both the formation and degradation of O_3 in the stratosphere. In the presence of gaseous nitrous oxides (NO_x), hydroxides (HO_x), chloroxides (ClO_x), and/or bromoxides (BrO_x) (which may be injected into the atmosphere via pollutant sources and volcanic emissions), incoming solar UV radiation acts to photo-dissociate these chemical species into free radicals, which then attack O_3 to dissociate it into free oxygen (O_2) and an oxygen radical. For example:

$$ClO + h\nu \text{ ---> } Cl + O$$
$$O_3 + Cl \text{ ---> } ClO + O_2$$
$$ClO + O \text{ ---> } Cl + O_2$$

The net O_3 degradation mechanism, which is the result of the above series of reactions, is:

$$O + O_3 \text{ ---> } 2\ O_2$$

Alternative mechanisms describing the specific involvement of chloroxides and bromoxides in the O_3 degradation are described by Molina and Molina (1987) and McElroy et. al. (1986b).

The Montreal Protocol mandated a gradual reduction in global chlorofluorocarbon (CFC) emissions by the year 2000, because CFCs are known to efficiently contribute to the degradation of O_3 to O_2. CFCs are highly inert, so once they are injected into the atmosphere, they will remain there for a long time. Eventually, the CFCs ascend into the stratosphere, where they participate in the UV-catalyzed photo-dissociation reactions that degrade O_3 to O_2.

ALE/GAGE network data of $CFCl_3$ concentration over different regions of the world

show a definite increase in the $CFCl_3$ mixing ratio between 1978 and 1984. A total ozone (O_3) numerical model predicts that, between 1980 and 2060, the percent change in local ozone concentration (at an altitude of 45 km) will decrease by as much as 40% in the Northern Hemisphere, and by 20% in the Southern Hemisphere, based on chemistry alone and not including atmospheric dynamics.

Data measurements of total ozone and the vertical O_3 profile in the atmosphere are obtained on various spatial (i.e. local, regional, global) and temporal (i.e. diurnal, seasonal, annual, interannual) resolutions. The types of O_3 data currently available include:

1) Ground-based total O_3 (Dobson, Brewer, M-134).
2) Ground-based vertical O_3 profiles (Umkehr, balloonsondes).
3) Satellite total O_3 (TOMS, SBUV, SBUV/2, TOVS).
4) Satellite vertical profiles (SBUV, SBUV/2, Sage I and II, UARS).

In the (ground-based) Dobson total O_3 measurement method, the ground-based instrument looks at the sun directly overhead and calculates the relative intensity ratio of the incoming solar UV radiation at two different times, corresponding to two different positions of the sun in the sky (i.e. two different zenith angles). These two different positions possess characteristic O_3 optical path lengths. Comparison of the two measurements of solar UV intensity thus allows total O_3 in the stratosphere to be estimated.

In the (ground-based vertical O_3) Umkehr method, the instrument looks directly upward into the zenith sky and calculates the relative intensity ratios during sunrise and sunset from the reflected UV radiation by atmospheric constituents. From measurements over 3-hour periods, corresponding to different sun elevation angles in the atmosphere, information is obtained on the O_3 profile. The typical vertical resolution of the Umkehr method is 5-7 km.

Another ground-based vertical O_3 method is the balloonsonde, which measures O_3 based on a calibration between O_3 consumed and iodine (I_2) produced, according to the reaction:

$$O_3 + 2\ KI + H_2O \text{ ---> } 2\ KOH + O_2 + I_2$$

Air is bubbled through a solution of potassium iodide (KI), and an electric current is generated, whose magnitude is proportional to the rate of the above chemical reaction. One mole of iodine (I_2) is produced for every mole of O_3 consumed. The O_3 concentration in the stratosphere is simply proportional to the measured I_2 concentration, according to a pre-determined calibration factor. The balloonsonde method exhibits a relatively high degree of vertical resolution (100 m) compared to the Umkehr method (5-7 km).

It should be noted that, although the ground-based data coverage for total O_3 is sufficient around the world, the corresponding ground-based data for O_3 changes and trends in the stratosphere is sparse.

There is particular concern about the development and growth of an "O_3 hole" (first detected in 1985 over Halley Bay by British scientists) over Antarctica. According to time-series analyses, total O_3 over Antarctica exhibits a seasonal variability, with O_3 maxima occurring during austral autumn (March-April) and O_3 minima occurring during austral spring (September-October). Between 1960 and 1980, the measured O_3 concentration in the O_3 hole during austral spring has decreased from 300 DUs to under 200 DUs. As of 1992, the lowest

reported O_3 concentration in the O_3 hole was less than 100 DUs. Furthermore, databases for 1978-93 show that the areal coverage of this intensifying O_3 hole is maximum during austral spring and has increased steadily over time. The year 1988 was characterized by higher O_3 concentrations compared to other years, due to the fact that 1988 was a relatively warm year. There exists a positive correlation between temperature and O_3 concentration for the measured period 1986-93. Ballonsonde measurements of total O_3 at the South Pole show that the O_3 concentration decreased from 276 DUs in August 1993, to 91 DUs in October 1993.

The O_3 hole is attributed to a unique to Antarctica deep and intense vortex of frigid temperatures near -90 °C at 50 mb (i.e. 20 km altitude). At such low temperatures, polar stratospheric clouds form. In those, chlorine can exist free in radical form. These clouds also remove nitrogen from the atmosphere that would otherwise tie up the free chlorine. As a result, the chlorine efficiently degrades the O_3 to O_2. The Northern Hemisphere exhibits the same effect only locally. Because of the lack of land-ocean contrasts in the Southern Hemisphere, the variability in the circulation is low and the O_3 hole remains intact. However, in the Northern Hemisphere, due to the transport patterns of O_3 and temperature, the O_3 hole breaks down before it has a chance to develop.

Validation, calibration, and correlation between the numerical model predictions and the measured experimental total O_3 and vertical profiles are conducted using a statistical time series analysis, involving linear least squares regression analysis. The objective of this analysis is to reduce the sum of squares deviation error between the numerical and experimental data, either by increasing the number of data points, or by decreasing the mean square value between the individual data point value and the relative mean value summed over all data points (Madden 1979), assuming all the data points are completely independent (i.e. no autocorrelation). The effects of autocorrelation are not negligible, and are discussed by Taio et. al. (1990).

In order to obtain accurate estimates of total O_3 and the O_3 vertical profile, as many forms of natural variability as can be physically detected must be included in the analysis. To reduce the sum of squares error, all the various forms of natural variability need to be filtered out of the analysis. An example of such natural variability is the 11-year sunspot cycle. Variation in solar output results in variation both in the amount of solar UV radiation reaching the earth's surface, and in O_3 concentration in the stratosphere.

Analysis of total O_3 involves a comparison between satellite data and ground-based data. Data for the period 1989-93 shows that the SBUV/2 data exhibits a drift of -2.1% per decade; SBUV exhibits a drift of -1.233% per decade; and TOMS shows a drift of -1.639% per decade (all relative to the Dobson), due to degradation of the satellite remote sensors over time. Satellite data are drifting over time, relative to ground-based data.

Figure 1 shows a strong positive correlation between temperature and O_3 concentration for the period 1978-93, except for the years 1982 (El Chichon eruption) and 1991 (Pinatubo eruption). This correlation gives credibility to both data bases (i.e. satellite and ground-based). In periods of volcanic activity, the emitted aerosols absorb outgoing terrestrial radiation and thus cause an increase in stratospheric temperature, which then does not remain correlated with O_3 concentration.

Examination of the long-term (i.e. 1968-1991) and short-term (i.e. 1977-1991) ground-based total O_3 data shows an increasing rate of decrease in O_3 concentration.

Further data comparisons are made between the balloonsonde and Umkehr data sets (Miller et. al. 1993). Because of its specific method of measuring O_3, the Umkehr

measurements are affected by atmospheric aerosols, an additional source of scatter and attenuation of solar radiation which is not included in the present predictive model's algorithm for O_3 profile retrieval.

Figure 2 shows an overlap of profiles of balloon ozonesonde data (which become invalid for altitudes greater than 20 km) and Umkehr data (which become invalid for altitudes less than 20 km). Throughout the stratosphere, a general decrease in O_3 concentration is observed for the period 1968-91.

In summary, in order to accurately simulate total O_3 and the O_3 vertical profile, modelers need to consider data autocorrelation within the trend analysis. When the various data quality issues are incorporated, reasonable agreement is observed among the trend results. Specifically, within the mid-latitude Northern Hemisphere, the satellite and ground-based data show that the general total O_3 trend is -2 to -4% change per decade. Both ozonesonde data (collected at 15 km altitude) and Umkehr data (collected in the 35-40 km altitude range) illustrate a -6% change in O_3 per decade.

In conclusion, the general science objective of the Upper Atmosphere Research Satellite (UARS) is to understand the coupled, chemistry, dynamics, and energy inputs that control the upper atmosphere structure. Because of the complex interactions and chemical reaction processes occurring among all the atmospheric constituents with each other and with the incoming solar radiation, this objective will not easily be met, and will require continuous research into the development of improved data measurement/ collection systems, refined physical theories of atmospheric phenomena, and more reliable statistical methods of data analysis. In this way, specific trends in the data, and contributions of specific processes to the overall observed data trend, can be more accurately detected and confidently assessed.

References

Madden, R.A., 1979: Simple Approximation for the Variance of Meteorological Time Averages. *J. Applied Met.*, **18**, 703-706.

Molina and Molina, 1987: Production of Cl_2O_2 from the self-reaction of the ClO radical. *J. Phys. Chem.*, **91**, 433.

McElroy, M. B., R. J. Salawitch, and S. C. Wofsy, 1986: Antarctic O_3: Chemical mechanisms for the spring decrease. *Geophys. Res. Let.*, **13**, 1296.

Miller, A.J. et al., 1994: Comparisons of Observed Ozone Trends in the Stratosphere Through Examination of Umkehr and Balloon Ozonesonde Data. Submitted for publication to the *Journal of Geophysical Research.*

Taio, et al., 1990: Effects of Autocorrelation and Temporal Sampling Schemes on Estimates of Trend and Spatial Correlation. *J. Geophys. Res.*, **95**, 20 507-20 517.

FIGURE 1 Comparison of Total Ozone and Temperature Anomalies

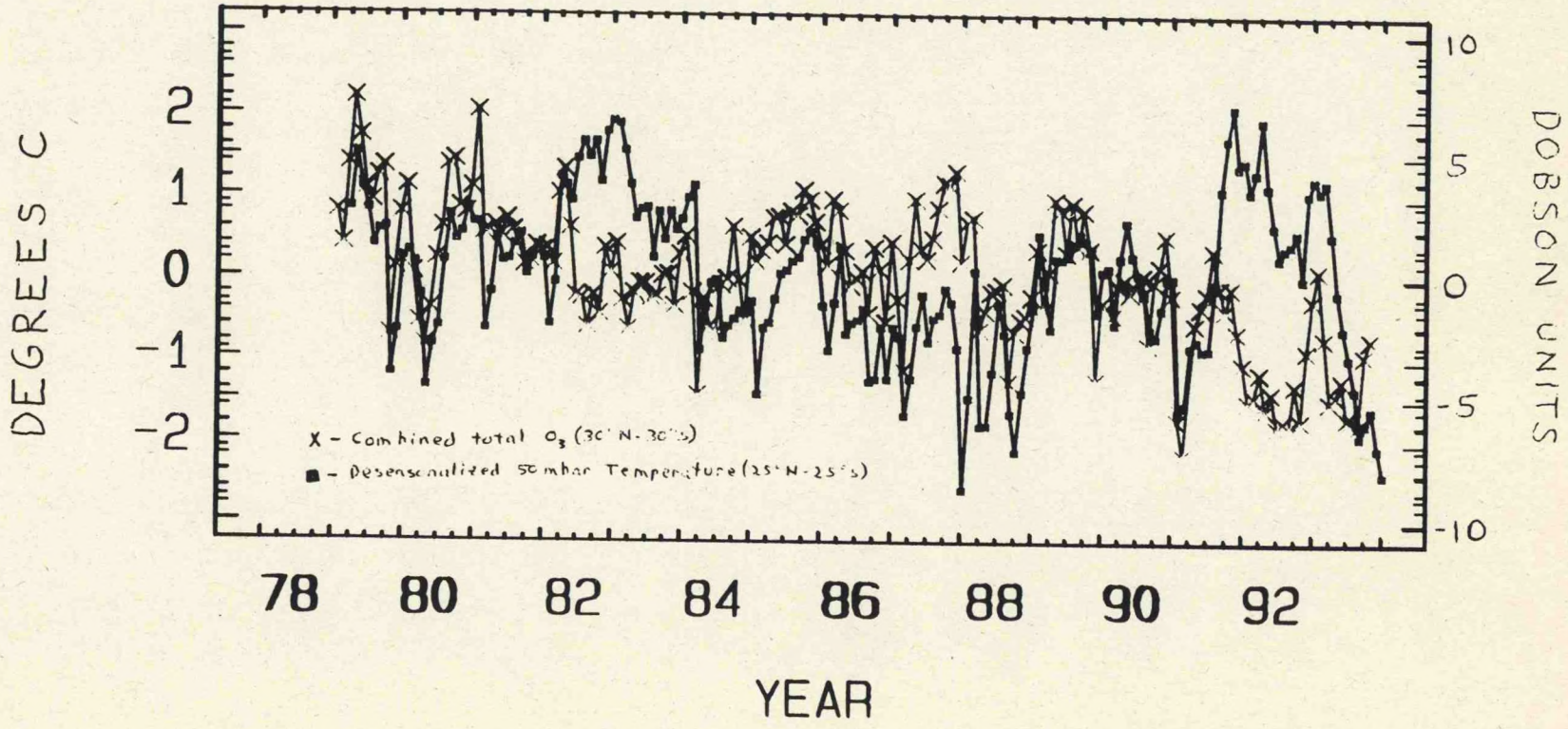

FIGURE 2 Comparison of Balloonsonde and Umkehr Data on Vertical O_3 Profile (Global Average)

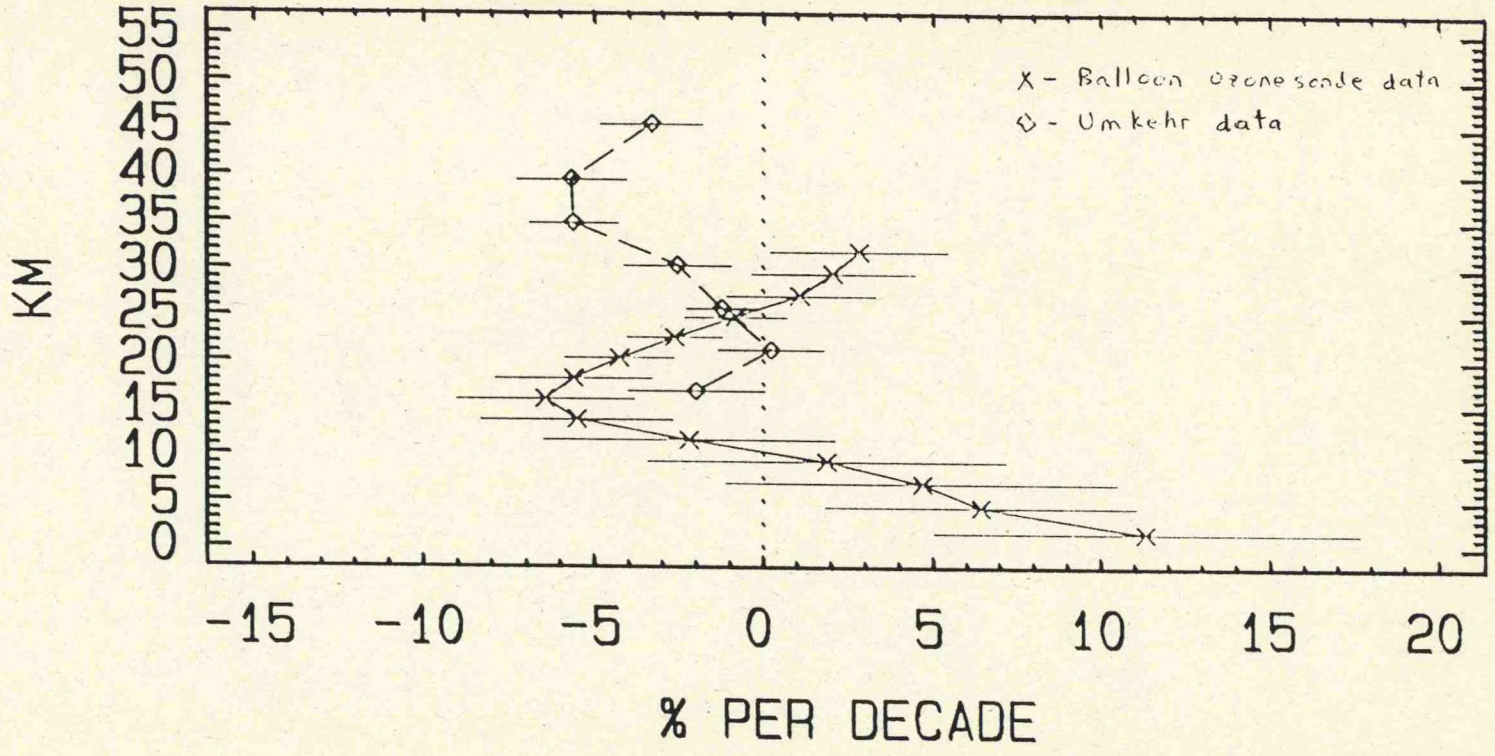

Stratospheric Monitoring Using Operational Satellites

Lecturer: Walter Planet
Date: June 13, 1994
Notes by: Christelle Escoffier
Paul Gaertner

Introduction

Satellite observations of the stratosphere commenced around the end of 1978. These measurements are now required in response to a congressional program for stratospheric monitoring of ozone trends, and other factors for understanding the greenhouse effects and global warming. Although satellites give relatively accurate data for long periods of time with the same instrumentation, in-orbit changes, orbit drifts and episodic artifacts (volcanoes) can cause serious problems in the analysis of the data obtained.

Techniques of measurements

Ozone observations by satellites are performed using ultraviolet and infrared techniques. Ultraviolet observation are gathered using a Solar Backscatter ultraviolet (SBUV) instrument on NOAA-9. A newer version the SBUV/2 is operational on NOAA-11. These instruments provide ozone profiles for a 25 - 55 km range. Infrared observations are made using the TIROS Operational Vertical Sounder (TOVS), which drives vertical profiles of temperature and moisture. Both instruments measure ozone quantities in the atmosphere. Eventually all satellite data will be merged to construct a data set from 1979 into the next decade.

As mentioned accuracy in measurements is an important issue so it should be noted that currently sensitivity drift on NOAA-11 lead to ~0.5% uncertainty in total ozone over 4 years, (Ahmad et. al. 1993) and the validation with Dobson data sets shows difference of 0.13%.

Data Validation

The objective is to provide a credible ozone data set from SBUV/2 and demonstrate it's utilization. While SBUV and SBUV/2 provide a good cover of global ozone data with the daily total ozone measurements between 50N-50S for SBUV and SBUV/2, there is a shift of almost 6%, about 20 Dobson between the curves, **Fig. 1**.

TOVS ozone anomalies show the level of decrease in ozone is greater in southern hemisphere than in the northern and thus each year the ozone hole in the southern hemisphere grows larger. The largest hole thus far was recorded in October 1993. Two sources of data validation is available, the World Ozone Data Center (WODC) in Toronto and the Climate Monitoring and Diagnostic Laboratory (CMDL) at NOAA. Satellite data is re-evaluated with data from WODC and CMDL. **Figure 2** shows the comparison between the annual means of total ozone for the original and the re-evaluated data.

Comparisons have been made between SBUV/2 data and data from microwave, lidar, Umkher, balloonsonde, SBUV, TOMS, DOBSON. For example, comparisons with microwave show that between the ~50 hPa and 1 hPa pressure levels a 5% difference is observed. At

lower and higher pressure levels a difference between 10 and 15% is observed. However, over more than 20% is observed for low pressure levels (Planet 1994).

Figure 3 shows decadal trends of total ozone from SBUV + SBUV/2, TOMS and Dobson measurements. Notice that the % per decade trend is minimum at the equator and increases with latitude with the maximum appearing in the southern higher latitudes.

References

Ahmad, 1993: Accuracy of total ozone retrievable from NOAA SBUV/2 measurements: Impact of instrument performance. Submitted to *Journal Geophysical Research.*

Planet, W., 1993: Northern Hemisphere total ozone values from 1989-1993 determined with the NOAA-11 SBUV/2 instrument. Submitted to *Geophysical Research Letters.*

Planet, W., 1994: Stratospheric Monitoring using Operational Satellites, NESDIS Satellite Research Laboratory, NOAA, Camp Springs, Maryland.

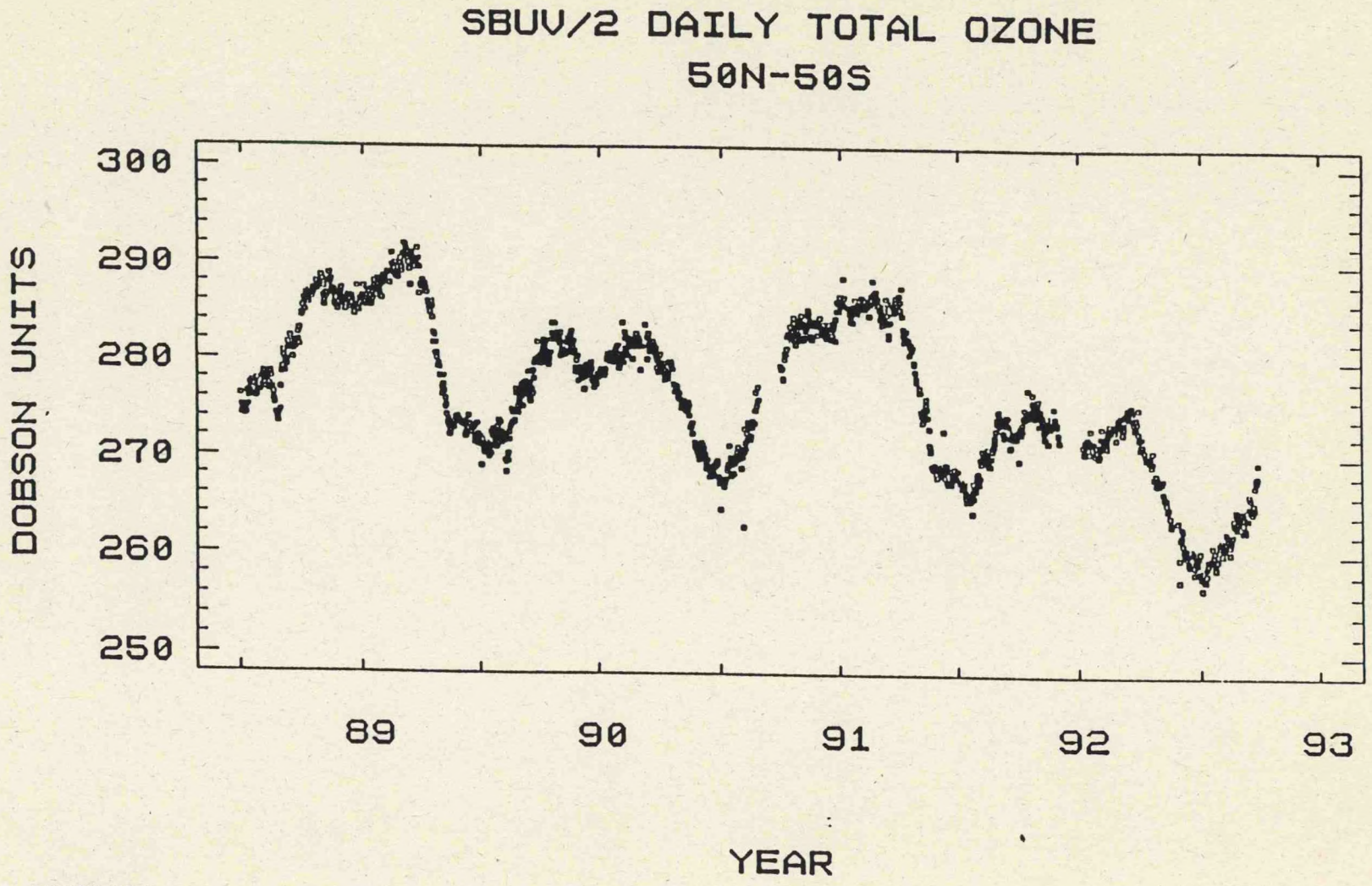
SBUV/2 DAILY TOTAL OZONE
50N-50S
DOBSON UNITS
300
290
280
270
260
250
89
90
91
92
93
YEAR

FIGURE 1

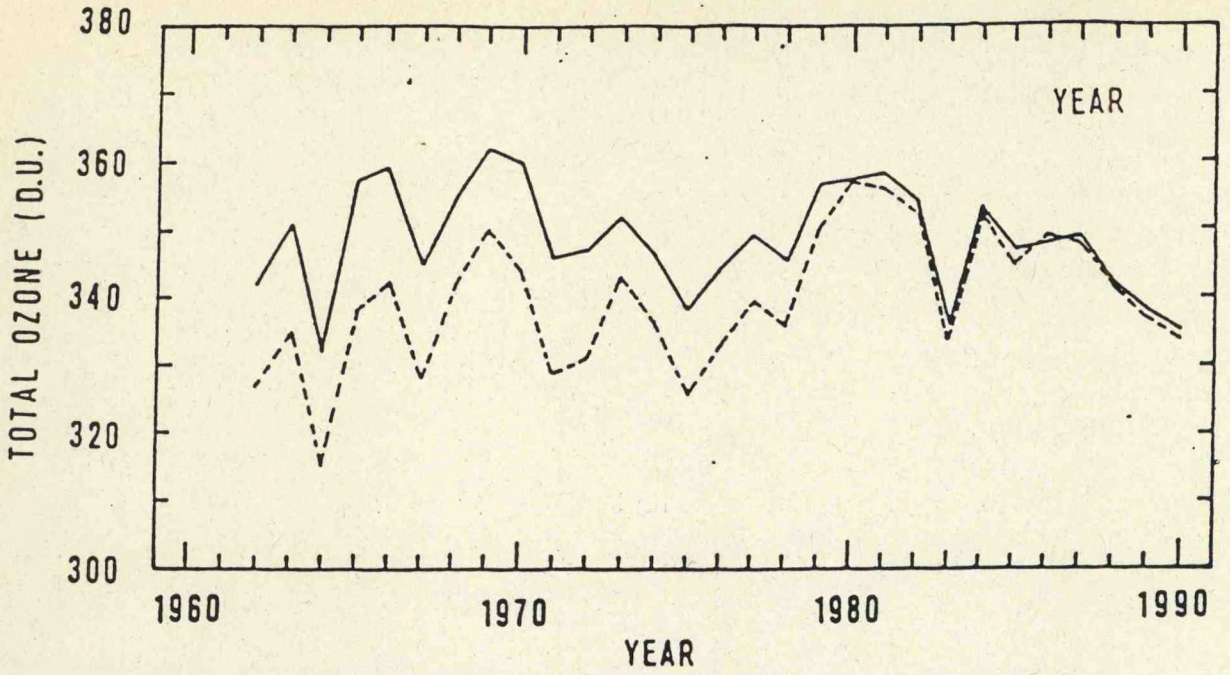

FIGURE 2 Annual means of total ozone (--- original, —— re-evaluated), Hradec Kralove, 1962-1990.

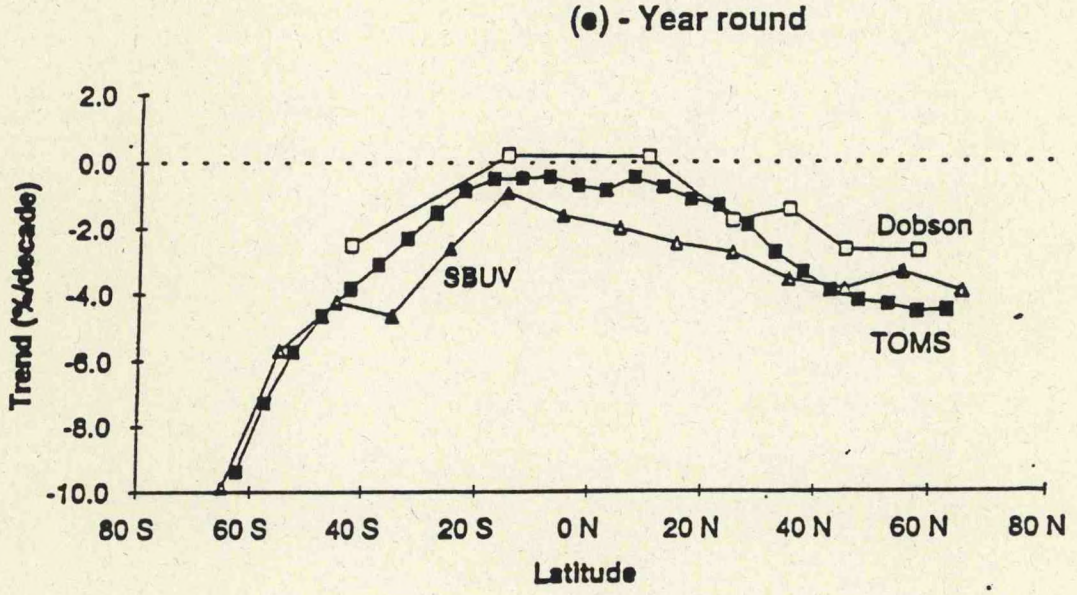

FIGURE 3 Decadal Trend of Total Ozone from SBUV + SBUV/2, TOMS and Dobson measurements from Nov. 1978 through December 1991

Satellite Monitoring of Climate Variables

Lecturer: George Ohring
Date: June 13, 1994
Notes by: Yuval Shay-El
Lihang Zhou

Overview of operational satellites, instruments and products

The operational environmental satellites are either geostationary (GOES=Geostationary Operational Environmental Satellite), or polar-orbiting (POES). The geostationary satellites are synchronized with the earth rotation, thus staying at a fixed longitude, 27,000 miles above the equator. Since their viewpoint is constant they are ideal for image animation. GOES-E and GOES-W are geostationary satellites operated by NOAA. Other ones are the European METEOSAT, the Indian INSAT, and the Japanese GMS. Polar-orbiting satellites cycle the earth in an orbit which crosses the equator at a constant local time. For example, the so-called "afternoon" NOAA satellite crosses the equator at 2PM (and at 2AM at the 'opposite' equatorial point), while the "morning" satellite crosses at 7:30AM (7:30PM). Therefore, each polar orbit satellite provide a picture of every point on earth twice a day. The polar orbit satellites rotate the earth at a height of 800 miles, thus can have a better resolution than the geostationary. They are not good for animation, however, since their viewpoint varies. Other POES are the two morning satellites operated by the Defense Meteorological Satellite Program (DMPS).

Table 1 presents the characteristics of the instruments installed on the satellites. AVHRR, TOVS and SBUV installed on the POES, while VAS on the GOES. Satellites have the advantage of giving a global atmospheric coverage from a single sensor. They provide data over oceans, deserts and other unpopulated areas, while ground-based observations are confined largely to populated areas. Remote sensing has, however, the disadvantage of providing only indirect measurement of variables, which rely on ground-based measurements for calibration. **Table 2** is a list of the climate variables accessible from operational satellites. The importance (three stars the highest), and the present knowledge of the global distribution of each variable (F the lowest) is also shown (ESSC, 1988).

Theory, validation and results of each product

Temperature Profile: The satellite observed radiance can be expressed as a sum of a surface contribution, and an atmospheric contribution, both depend on the temperature through the Planck function, and on the transmittance. For each wavelength the transmittance can be expressed as a weighting function (**Fig. 1**). As absorption increases the peak gets higher altitude. Thus, using the measured radiance in a specific channel (i.e., specific wavelength), the temperature of the corresponding height can be retrieved. As long as there are no clouds the error is about 2-3 degrees, compared to about 1 degree of radiosonde measurement.

Water Vapor Profile: With temperature profile known, B(z) (Planck function, expressed as function of height) is known and one can integrate by parts the radiation transfer equation, to receive the transmittance profile for a specific wavelength. While for retrieving the temperature one use the CO_2 bands, for retrieving water vapor profile one use the water vapor bands, i.e. the wavelengths in which water vapor is the major absorption gas. Thus

knowing the transmittance profile in these bands, one can know the water vapor profile.

Microwave Sounding Unit (MSU): By taking a linear combination of channel 2 and channel 4, one can create another weighting function which has less sensitivity to the stratosphere than the original weighting functions. The new weighting function can represent the temperature of the troposphere. It is useful for monitoring the long-range change of the troposphere, such as global warming. A comparison of the 850-300 mb average temperature, between the MSU and radiosondes (GFDL), shows good agreement over the years 1979-91 (Oort and Liu 1993). Passive microwave is useful for obtaining the column water vapor and liquid. Total precipitable water from microwave measurement agree to within 10% with radiosonde measurements. Various other fields, such as sea ice, and snow cover, are accessible from SSM/I microwave measurements.

Ozone Profile from Solar Backscatter Ultraviolet (SBUV) Measurements: Ultraviolet radiation back-scattered from the atmosphere is strongly affected by O_3 absorption. Each wavelength scattered back at different height, therefore vertical distributions can be retrieved. Some of the major analyses of the ozone "hole" over the last few years were based on SBUV measurements.

Sea Surface Temperature from AVHRR: Theoretically, SST can be retrieved from two channels that are nearly transparent. Random error of the operational SST product is about 0.5 °C. Mount Pinatubo's eruption in 1991, however, created a large bias on the order of -1 °C.

Other Products: Sea Surface Wind Speeds retrieved from satellites agree well with buoy winds, with standard deviation of about 2 ms^{-1}. Different soils got different typical reflectance dependence on wavelength. A *vegetation index*, defined as the difference between the near infra red reflectivity and the visible reflectivity, can be calculated from AVHRR. The Solar radiation reaching the ground, from GOES visible channels, is used as a measure for *cloud coverage*. SSM/I measurements provide a measure of *floods,* or more generally a *soil moisture index,* based on the different dependence of the brightness temperature on frequency, between dry land, flooded land, and a lake. Outgoing Longwave Radiation (OLR), as well as Short Wave Radiation (SWR) are available from AVHRR. The Earth Radiation Budget Experiment (ERBE) diagnosed the annual average radiation budget. AVHRR provides measures of cloud coverage, as well as aerosol optical thickness over the oceans.

While satellites are very useful for monitoring climate variables, there is still a need for improvement, in order to get to better accuracy for long-term monitoring.

References

ESSC, 1988: Earth System Science: A closer View. Report of the Earth System Sciences Committee, NASA, 208 pp.

Houghton, J. T., 1977: *The Physics of Atmospheres.* Cambridge University Press, 202 pp.

Janssen, M. A., 1993: *Atmospheric Remote Sensing by Microwave Radiometry.* Wiley, 572 pp.

Ohring George, et al., 1994: Satellite Monitoring of Climate Variables-Extended Abstract. NESDIS.

Rao, P. K. et al., 1990: *Weather Satellites: Systems. Data, and Environmental Applications.* American Meteorological Society, 503 pp.

TABLE 1

OPERATIONAL INSTRUMENT CHARACTERISTICS

Instrument	No. of Channels	Spectral Range (μm)	Resolution (km)	Swath Width (km)
AVHRR	2 solar	0.58- 1.1	4*	2700
	3 infrared	3.55-12.5	4*	2700
TOVS	20 infrared	3.8 -15.0	17.4	2240
	3 infrared	14.7 (centered)	147	736
	4 microwave	50.3 -57.05 GHz	109	2347
SBUV	12 ultraviolet	252 - 339.8 nm	169	Nadir viewing
GOES VAS				
Imaging	1 visible	0.55- 0.7	1	Limb to Limb
	4 infrared	3.90-14.7	8	Limb to Limb
Sounding	12 infrared	3.90-14.7	7-14	Limb to Limb
SSM/I	7 microwave	19.3 -85.5 GHz	15-55	1400

* Resolution cited is for Global Area Coverage (GAC) data; original resolution is 1 km.

TABLE 2

GLOBAL CHANGE PARAMETERS ACCESSIBLE FROM OPERATIONAL SATELLITES

Variable	Importance (Based on ESSC Report, 1988)	Quality
Atmosphere		
Temperature	***	B
Water vapor	**	D
Winds		
tropical	**	C
extratropical	*	B
Clouds	**	D
Aerosols		
tropospheric	*	C
stratospheric	**	B
Precipitation	***	C
Ozone	***	C
Ocean Surface		
Sea surface temperature	***	C
Surface wind	***	C
Land Surface		
Vegetation Index	***	D
Albedo	*	C
Insolation	*	C/D
Downward longwave flux	---	---
Surface temperature	*	F
Soil moisture	***	F
Cryosphere		
Snow	*	C
Sea ice	**	B
Earth Radiation Budget		
Longwave radiation	**	B
Planetary albedo	**	B

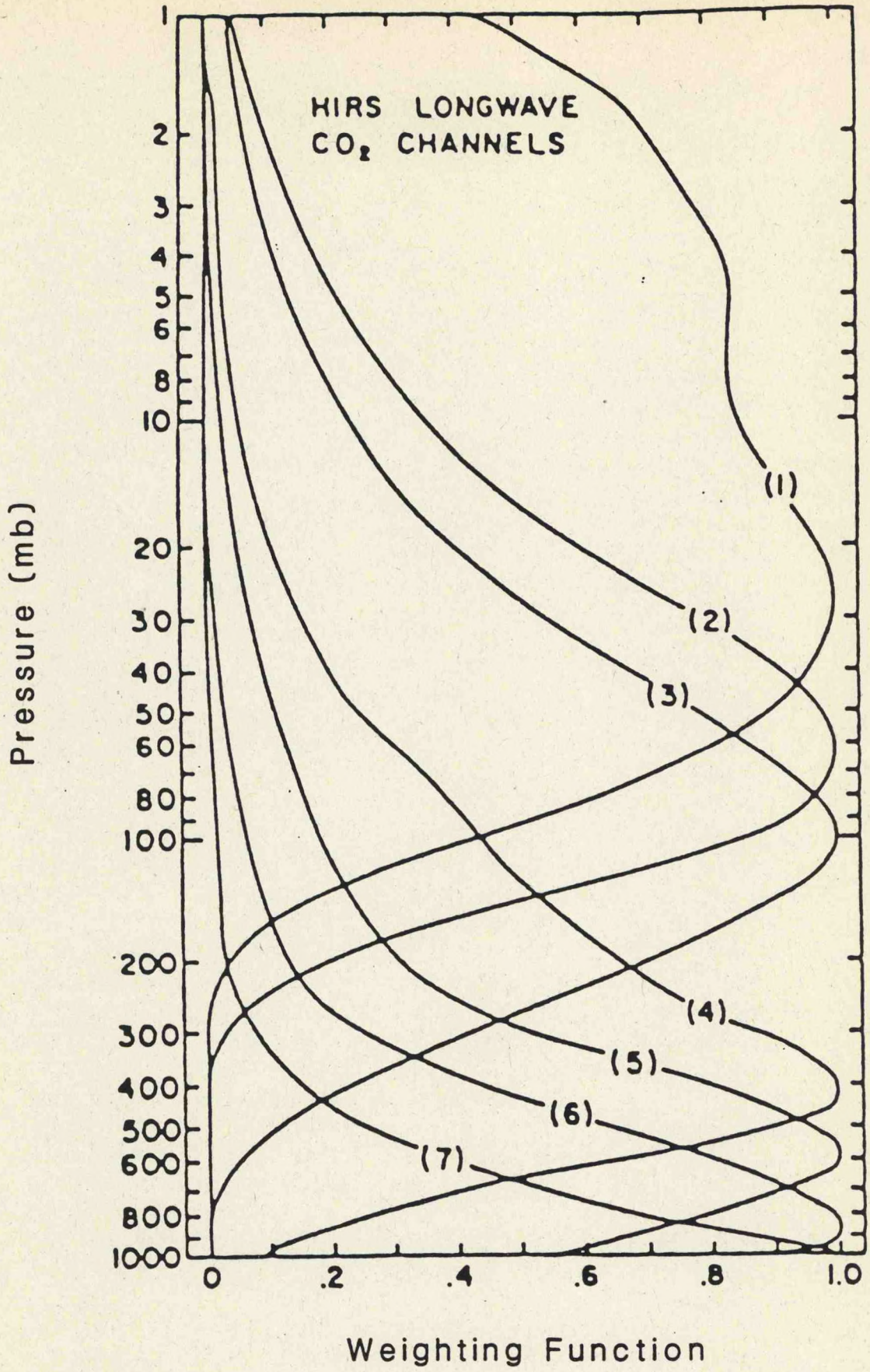
HIRS LONGWAVE
CO_2 CHANNELS
(1)
(2)
(3)
(4)
(5)
(6)
(7)
Pressure (mb)
1
2
3
4
5
6
8
10
20
30
40
50
60
80
100
200
300
400
500
600
800
1000
0
.2
.4
.6
.8
1.0
Weighting Function

FIGURE 1

OPERATIONAL 6-10 DAY, MONTHLY AND SEASONAL FORECASTS

Lecturer: Edward O'Lenic
Date: June 14, 1994
Notes by: Yimin Ji
Paul Gaertner

Introduction

It is difficult to predict weather beyond one or two weeks. At longer time ranges, averages of the weather can be usefully predicted only to the extent that the variations of the averages exceed the "noise" produced by the omnipresent but unpredictable transient weather. This margin of potential predictability is not large, but parts of it are being exploited in routinely issued monthly and seasonal forecasts. The idea of Long Range Forecasting (LRF) concerns the prediction of the general behavior of the larger scales of atmospheric circulation and weather over a month or season. The lower bound of LRF is currently provided by the practical limit of about 1-2 weeks to the predictability of individual synoptic-scale daily weather system. Thus LRF is used for the prediction of the means of variables and possibly, their variability. Hence long range forecasts concern population values. At present the accuracy in predicting long range forecasts is low because they are forecasts of values of a population, while they are verified against a single event, which includes the noise associated with the unpredictable synoptic disturbances which actually occur.

Skill measures used in model validation are Heidke skill score, root mean square error, anomalies and anomaly correlation. The Heidke skill score is given as S = (C-E)/(T-E), where C is the number of stations that forecast correct, T defines the total number of stations, and E the number of stations that forecast correct by chance.

Multivariate linear statistical models

Empirical forecast techniques are used where other techniques, such as dynamical forecasts, fail. Forecasts of this type involve established predictor-predictand relationships where the predictor often involves the lower boundary, eg., SST, soil moisture, etc., which serve as the lower limit of skill, or standard, which is required of future NWP models. The choice to use an empirical approach reflects the fact that both simple and complex general circulation models can not adequately reproduce the real atmospheric processes at the lead time and averaging periods concerned.

Three most common linear statistical models are Canonical Correlation Analysis (CCA), Singular Value Decomposition (SVD) and Principle Oscillation Pattern (POP) analysis. Of the models CCA seems the most useful as it is a specialized version of EOF analysis which reflects a linear combination of predictors that corresponds, in a least squares error sense, to a linear combination of predictands (i.e., multiple regression for a multivariate predictand). A typical application of CCA is to use near-global SST (60°N - 40°S), Northern Hemisphere 700-mb height, and U.S. surface temperature (prior values of the predictand field itself) to predict U.S. surface temperature.

The CCA technique relies heavily upon global SST and has useful correlation skill in forecasting seasonal mean U.S. surface temperature at leads of up to 1 year. **Figure 1** is a structure diagram showing how CCA is used for making predictions.

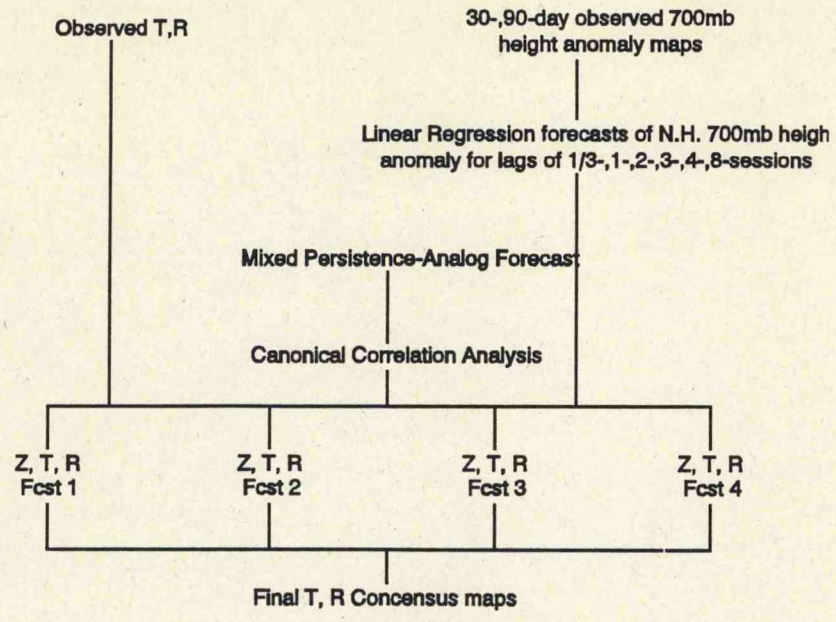

Figure 1

Ensemble forecasting is used to create a distribution of forecasts by running one or several NWP models from slightly perturbed initial conditions to make forecasts. Under ideal conditions this allows the determination of the most and least likely solutions for a given forecast. Ensembles are a principal input to the 6-10 day forecasts. These forecasts should be presented is a probabilistic format, since such a format permits a very accurate portrayal of both the known skill and the confidence the forecaster has a reliable tool to help the construction of the forecast.

The Future of LRF

The current 6-10 day forecast needs to be upgraded to include Alaska and Hawaii. Current seasonal forecasts should be converted to a seasonal long lead forecast with leads from 1/6 to 4 seasons. NMC hope to provide a lead of two weeks for monthly forecasts using CCA for months *abc* with data through the middle of month *a*. The central month, i.e., *b*, then becomes the target month. Finally, the 6-10 day forecast should be changed to a two week forecast, for example, a forecast of 7-day mean 500-mb height, surface T and precipitation at one week lead. For further information on LRF consult the following references.

References

Epstein, E. S., 1988: Long-range weather prediction: Limits of predictability and beyond. *Wea. and Forecast.*, **3**, 69-75.

Farmer, J. D., and J. J. Sidorowich, 1987: Predicting chaotic time series. *Phys. Rev. Letters*, **59**.

Madden, R. A., 1976: Estimates of the natural variability of time average sea level pressure. *Mon. Wea. Rev.*, **104**, 942-952.

Madden, R. A., and D. J. Shea, 1978: Estimates of the natural variability of time averaged temperatures over the United States. *Mon. Wea. Rev.*, **106**, 1695-1703.

World Meteorological Society, 1984: Report of the session of the commission for atmospheric sciences working group on long-range weather forecasting research. *Long-Range Forecasting Research Publications Series*, No. 4, WMD, Geneva.

Prediction of Low-Frequency Phenomena

Lecturer: Kingste Mo
Date: June 14, 1994
Notes by: Elvira Brankov
Yimin Ji

Overview

It is believed that beyond ten days or so we are unable to predict high-frequency or small scale weather events, such as hurricanes. Fortunately, we are able to predict low-frequency Methods of forecasting low frequency or large-scale events beyond that time limit because these events have relatively longer memory. The methods of forecasting low-frequency (10 days and beyond) events are:

* Statistical methods - based on historical data: extrapolate past conditions to the present. An example of this method is using observed sea surface temperatures to predict ENSO events.

* Dynamical Extended Range Forecast (DERF) - based on post-processed General Circulation Model (GCM) outputs. **Figure 1** shows some results from 108 contiguous 30-day GCM runs (Tracton et al. 1989). The high anomaly correlation (AC) values from mean GCM forecasts show that the GCM results are better than persistence. The AC is defined as the pattern correlation between the forecast anomalies and the observed anomalies. The DERF experiment also indicated that for some initial conditions the forecast for days 21-30 still contained skill. The GCMs, however, are far from perfect: there are systematic errors and the skill varies from one run to the next depending on the initial and boundary conditions.

The major scientific problems are :

* how to post-process the model output
* can the forecast skill be predicted

Systematic error

Systematic error is defined here as the difference between the models climatology and the observed climatology. The model is not perfect and it can produce errors in calculations due to:

a) initial conditions in the model
b) model physics
c) boundary conditions in the model
d) resolution
e) clouds parameterization
f) radiative scheme

Some common systematic errors are:

- cold biases in the stratosphere and in the lower troposphere
- weaker convection in the tropics
- easterly bias in the tropical zonal winds
- most GCMs are not able to forecast blocking situation
- at 500-mb model is not as vigorous as the observed atmosphere

Postprocessing

To postprocess the model output, we could use statistics or empirical adjustment to correct systematic errors. **Figure 2** shows the anomaly correlations, as a function of time, for persistence, unadjusted and adjusted model predictions of 500-mb height. The forecast skill is enhanced after empirical adjustment. However, at the moment the ensemble average is the best way to correct the forecasts.

EXAMPLE: 10-day forecast
T = training period, (30-60 days). Here we use 40 days.
To correct the forecast starting form day D:

1. From D-50 to D-10, each day we run 10 day forecast
2. calculate the forecast error for each day
3. compute the average (systematic) error
4. remove error from the forecast

Forecast the forecast skill

The forecast skill varies both in space and time. Ensemble forecasting provides the means for forecasting forecast skill. Methods to forecast the forecast skill are:

- agreement: do the forecast skills agree with each other?
- persistence: are the forecasts consistent?
- forecast regimes: what is the response of the model to regime transitions?

Figure 3 shows the Northern Hemisphere 500-mb height skill and agreement. For a 10-day run both the AC and agreement are high and consistent. **Figures 4** and **5** show the ACs and RMSE (root mean square error) for the daily 200-mb stream function in two cases (observed daily updated SST and climatological SST). It is evident that the anomalous SSTs have an impact on the atmospheric circulation over the North Pacific and North American regions. The impact on the daily mean is smaller than on the 15-day running mean. Within 15 forecast days, the impact is small.

Teleconnections

Teleconnections show the relationship between anomalies in one region and other distant regions. They are often used to evaluate model predictions. **Figure 6** shows the principal teleconnection patterns for the Pacific - North American region.

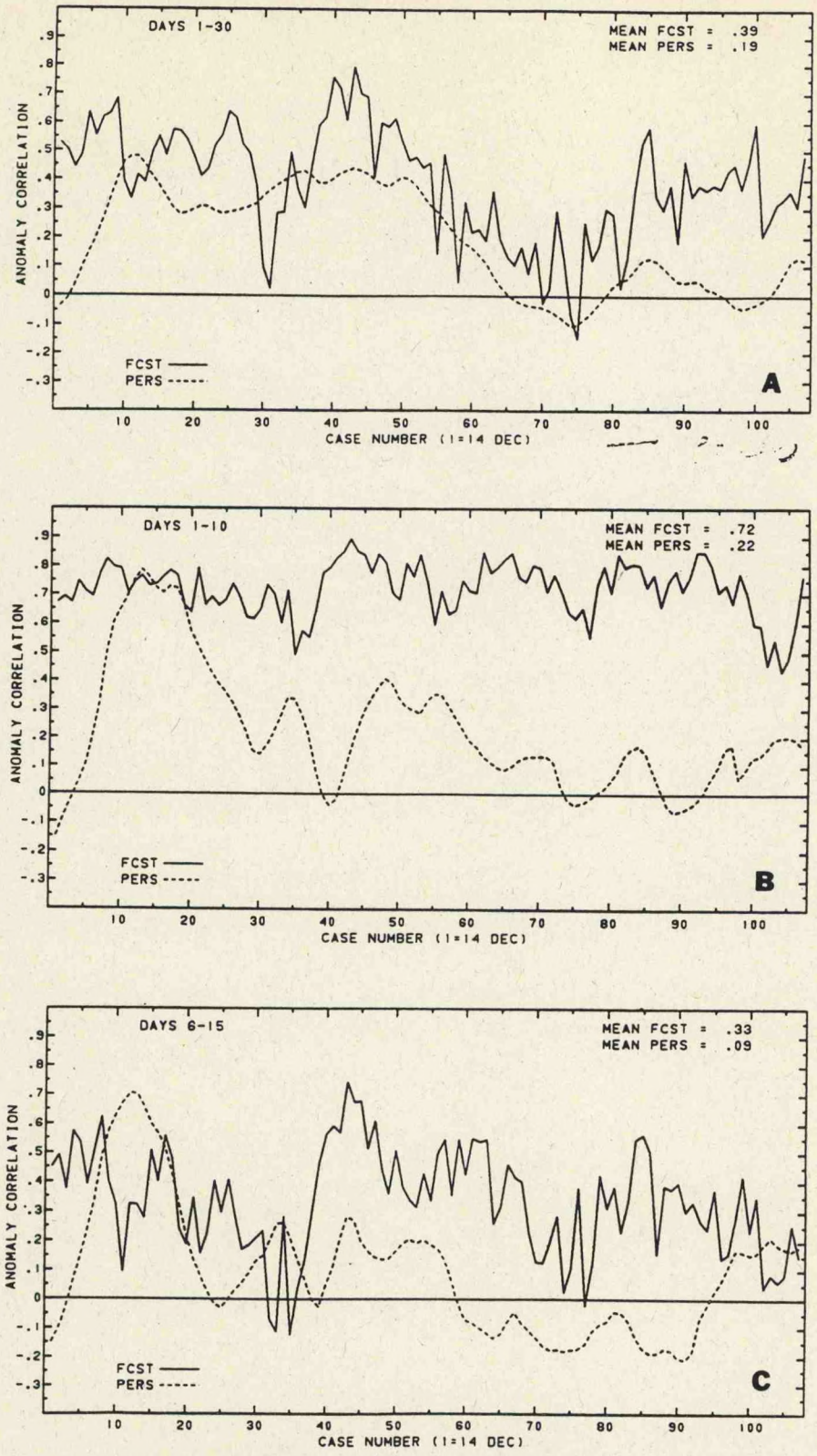

FIG. 1. Anomaly Correlation (AC) of Northern Hemisphere (20°–80°N) 500 mb height for the contiguous series of 108 cases (case 1, 14 December 1986 initial conditions): (a) 1–30, (b) 1–10, (c) 6–15, (d) 11–20, (e) 16–25, (f) 21–30 day means.

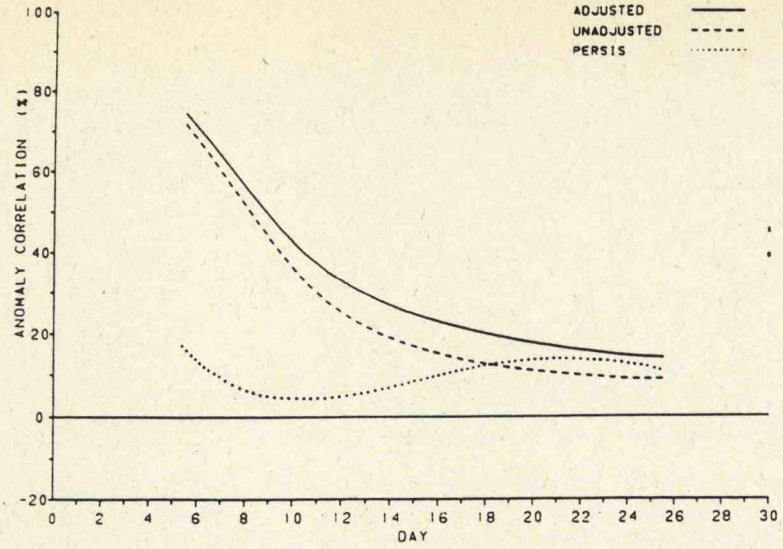

FIG. 2.. AC (108-case average) of NH 500 mb height for with and without "empirical adjustment" (10-day means). Adjusted (X) and unadjusted (O) scores for 30-day means plotted at day 30.

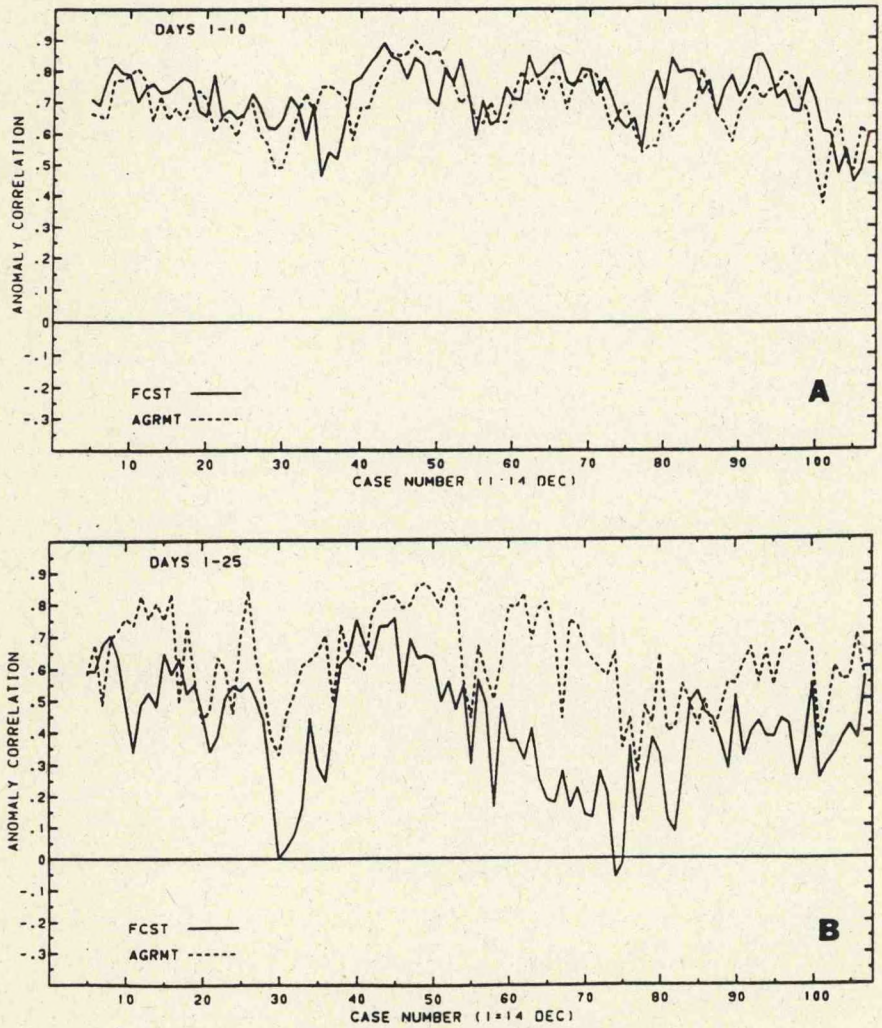

FIG. 3. Northern Hemisphere 500 mb skill and agreement for (a) 1–10 and (b) 1–25 day means.

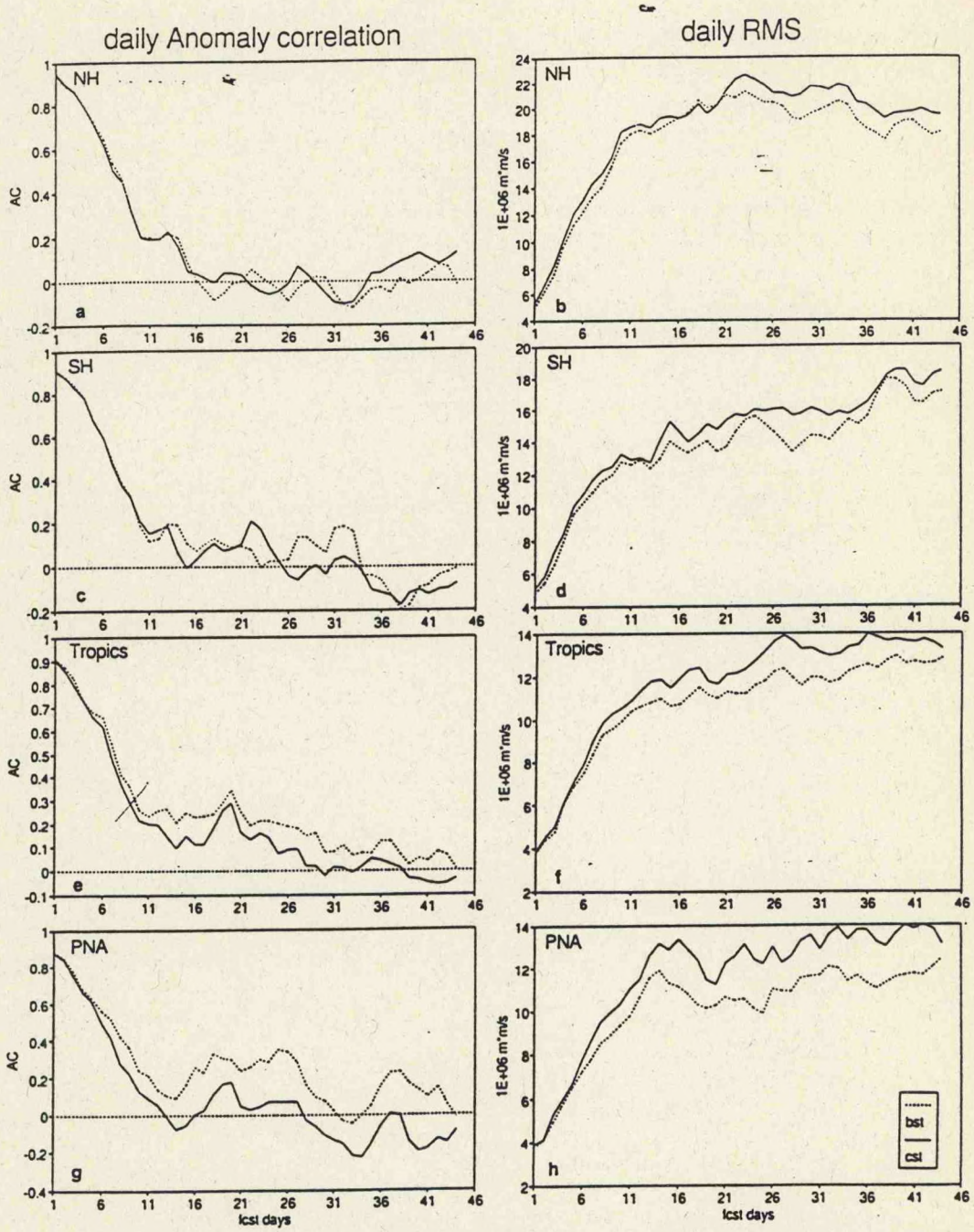

FIG. 4. (a) Anomaly correlation and (b) rms error in units of 1.0×10^6 m^2 s^{-1} for the daily 250-mb streamfunction averaged over the BST (dashed line) and the CST (solid line) cases over the Northern Hemisphere; (c) same as (a) but for the Southern Hemisphere; (d) same as (b) but for the Southern Hemisphere; (e) same as (a) but for tropics; (f) same as (b) but for tropics; (g) same as (a) but for the PNA region; and (h) same as (b) but for the PNA region.

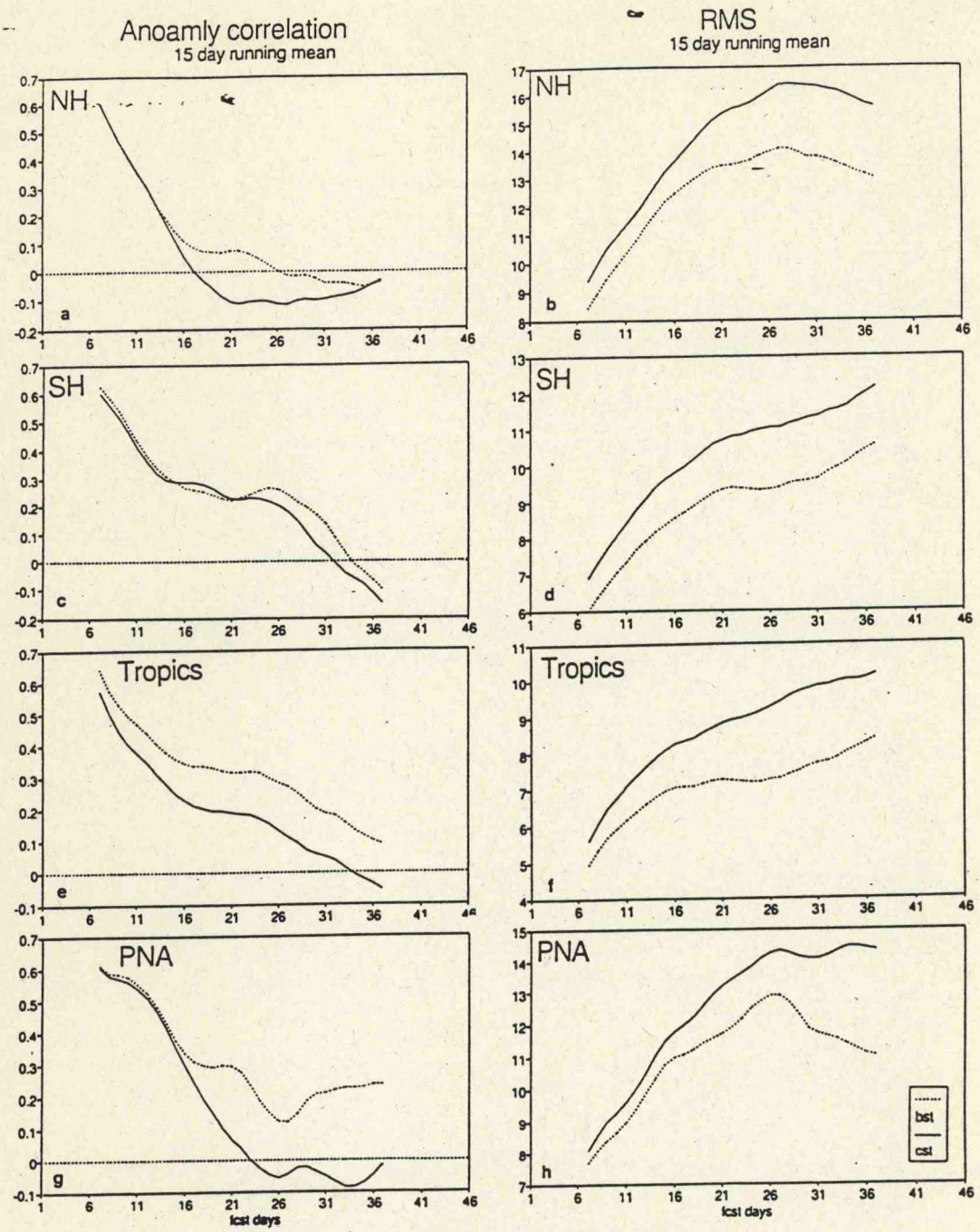

FIG. 5. Same as Fig. 4 but for 15-day running means.

Teleconnection patterns related to the Pacific and North America

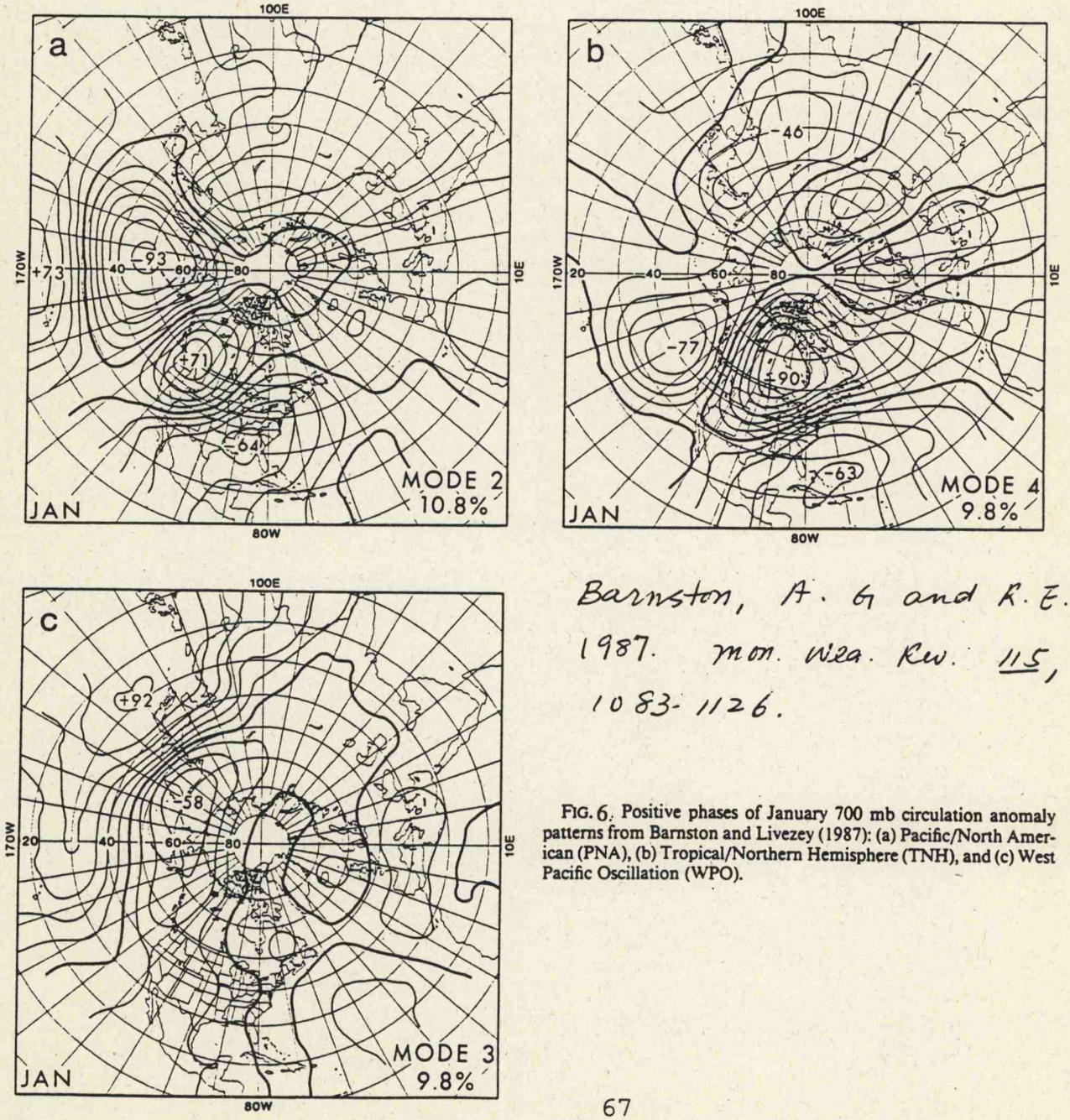

Barnston, A. G and R. E. Livezey 1987. Mon. Wea. Rw. 115, 1083-1126.

FIG. 6. Positive phases of January 700 mb circulation anomaly patterns from Barnston and Livezey (1987): (a) Pacific/North American (PNA), (b) Tropical/Northern Hemisphere (TNH), and (c) West Pacific Oscillation (WPO).

ENSEMBLE FORECASTING

Lecturer: M. Steven Tracton
Date: June 14, 1994
Notes by: David C. Burwell
Yimin Ji

Since weather is a stochastic process and is inherently unstable, the ability to predict it is inherently uncertain. Once we admit this fact, the important question becomes how best to express this uncertainty. Ensemble forecasting produces an array of forecasts as a function of the uncertainties in the initial conditions of the system. This array, or ensemble, of possible future states of the weather is produced by a slight perturbation of the initial conditions of the Medium Range Forecast (MRF) model. Since the weather is stochastic any perturbation of the initial conditions should produce a different weather pattern, and thus so would a "perfect" model of the weather system. The ensemble of different states produced is thus a look at many possible future states of the dynamic weather system in an attempt to enhance the ability of forecasters by giving them an idea of the probability of future weather patterns. The ensemble thus allows one to get a reliable estimate of the range of future weather states, in such a way so as to increase the accuracy of the forecast.

Some key considerations in building the ensemble include the strategies involved in choosing the initial perturbations, clearly a random choice of initial conditions is not necessarily the best. The scheme used at the CAC is a combination of time lagging (**Fig. 1**) and a procedure to force a divergence of solutions by choosing only those solutions that trend away from the MRF run which is called Breeding of Growing Modes (BGM). In this way it is hoped that an end member set of realizations will be generated to give greater utility to the forecasters. Other considerations are model resolution and physical sophistication which tend to take up more time which translates into less members in any given ensemble, there should be an optimal scheme of give and take between these considerations for any given computer system but to date it seems that with the T126/T62 the more members the better.

The ensemble products can range from individual forecasts, to clusters of smaller groups of forecasts that demonstrate "similar" traits and provide information on the probability (confidence) of a given event and the range of possible intermediate events. It is important to note in regards to the range of intermediate events that skill is measured as:

$$\frac{\text{(number correct) - (number correct at random)}}{\text{(total number) - (number correct at random)}}$$

Then on the average the ensemble mean has a better skill score than any individual model run. To put it another way the ensemble mean is better than the mean of scores of the individual runs. **Figure 2** shows this improvement to be significant after five days or so. This improvement in fact is similar to the expected model improvement of several years.

Realizing that the weather is stochastic and modeling it as such, to provide an array of possible forecasts, enhances the reliability (**Fig. 3**) of the forecast. The utility is also improved as many products, like cluster size (**Fig. 4**), are available so that the forecaster will get a better idea of the size of the uncertainty of the evolving state of the weather. This knowledge coupled with the forecasters skill and experience in evaluating the developing

system has improved forecast skill.

References

Toth, Z., and E. Kalnay, 1993: Ensemble forecasting at NMC: the generation of perturbations. *Bull. Amer. Met. Soc.*, **116**, 2522-2526

Tracton, M. S., and E. Kalnay, 1993: Operational ensemble prediction at the National Meteorological Center: Practical aspects. *Wea. Forecast.*, **8**, 379-398.

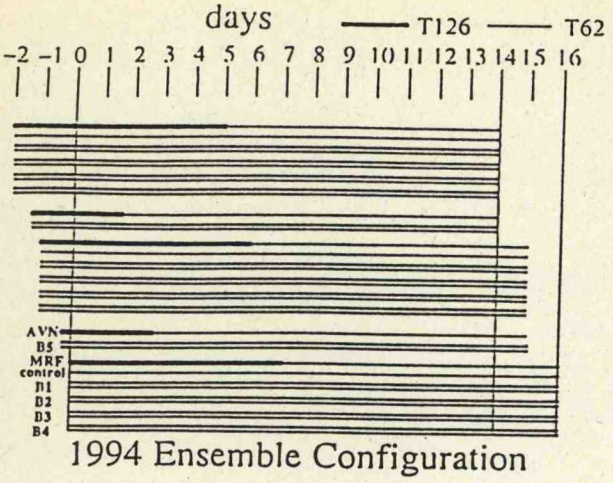

Fig. 1. Currently operational configuration of ensemble configuration. See Toth and Kalnay (1994) for construction of multiple "breeding" cycles.

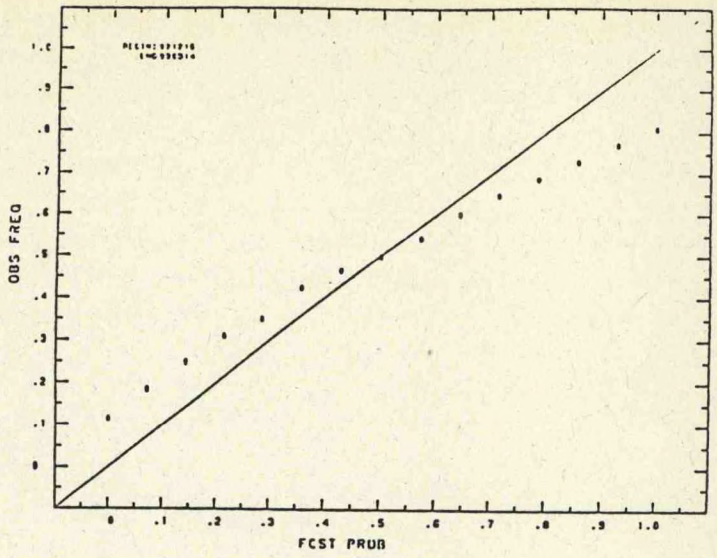

Fig. 3. "Reliability diagram" of the forecast probability versus observed frequency of occurrence for the sign of the D+8 500-hPa height anomaly over the same period as in Fig. 2.

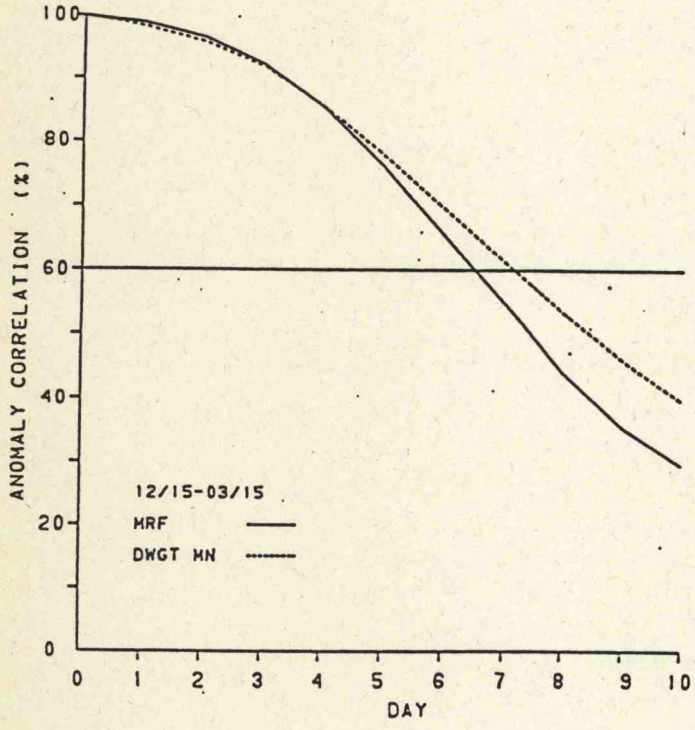

Fig. 2. Northern Hemisphere anomaly correlation (AC) skill scores of MRF and "optimally weighted" ensemble mean 500-hPa height forecasts averaged over period 15 Dec 1992 - 15 March 1993.

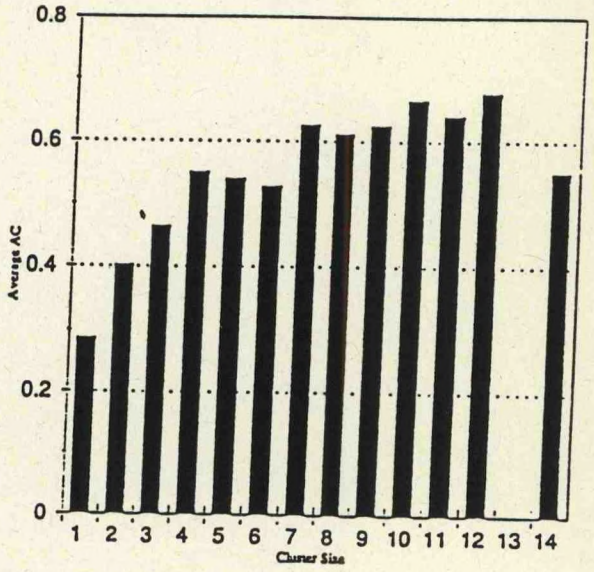

Fig. 4. Northern Hemisphere anomaly correlation (AC) skill scores for 500-hPa heights as a function of cluster size for same winter period as above.

Monitoring and Prediction of Interannual Variability

Lecturer: Chester Ropelewski
Date: June 15, 1994
Notes by: Sam Levis
Suzanne Hartley

Introduction

Until 20-30 years ago, climatology was a rather descriptive, static science which considered mainly statistical averages and annual cycles. More recently, with the increasing efforts to understand the El Niño-Southern Oscillation (ENSO), climatologists have come to appreciate the importance of interactions between the ocean circulation and the atmospheric circulation, and have gained greater insight into interannual variability.

Description of El Niño

Annual mean SSTs for the tropical Pacific show an area of temperatures as high as 28-29°C in the far western Pacific and a tongue of cold water intruding along the equator from the eastern Pacific. SSTs in the mid-to-high latitudes in the Northern Hemisphere are higher in July and lower in January (as might be expected). However, in the eastern equatorial Pacific, the highest SSTs occur in the northern spring while the lowest SSTs occur in the northern fall. The relative warmth observed in the spring begins to develop around Christmas - hence the name "El Niño" (Christ child) given to this feature of the annual cycle by Peruvian fishermen. With time the fishermen noted that during certain years the warming was stronger and longer lasting than in other years. Gradually the term El Niño became associated with the periods of abnormal warmth.

Figure 1(a) shows normal conditions for December. Convective rainfall occurs over the warm waters of the western Pacific, in the ascending limb of a Walker circulation cell. Easterly trade winds blow toward this area of convection and are balanced by a westerly return flow aloft. The response of the ocean is reflected in the depth of the thermocline - deep in the far western Pacific, and shallow in the eastern Pacific associated with coastal upwelling.

Figure 1(b) shows El Niño (warm episode) conditions for December. The Walker circulation and area of convection is displaced eastward accompanying the area of higher SSTs. The easterly trades are diminished in strength and in the far western Pacific westerly winds may be observed at the surface. The E-W thermocline gradient is less steep. The deeper thermocline in the east is associated with reduced upwelling and the eastward progression of a series of oceanic Kelvin waves. The time for development of these conditions is around 2-3 months and warm episodes usually last 1-2 years. The return interval is anywhere from 2-7 years. The opposite phase of the cycle, i.e. cold episode, is sometimes referred to as La Niña. This phase is associated with lower SSTs at the equator, stronger easterlies in the central and western Pacific and a stronger Walker circulation.

El Niño and the Southern Oscillation

Correlations of annual mean sea-level pressure (MSLP) anomalies at Darwin with points elsewhere on the globe show a pressure see-saw across the Pacific, i.e. abnormally high SLP in the west and abnormally low SLP in the east. The pressure see-saw is reasonably well documented and is related to the pressure gradient associated with ENSO. The Southern Oscillation Index (SOI) is based on the difference between the SLP anomalies at Tahiti and Darwin. The warm phase of the ENSO is indicated by a low value of the SOI, i.e. positive pressure anomaly at Darwin and negative anomaly at Tahiti. Annual SST anomalies are maximally correlated (positively) with the SOI in the western Pacific, suggesting the link between El Niño and the Southern Oscillation. Eastern Pacific SSTs are also linked with the SOI, but the correlation is negative.

Teleconnections

Although the forcing occurs in the tropical Pacific, the effects are also felt in the mid-latitudes through various teleconnections. Anomalously wet/dry or warm/cold conditions form a fairly consistent pattern (in a statistical sense) (**Figure 2**), despite the variations within ENSO itself. We can take advantage of this as a predictive scheme e.g. for temperatures in NW North America, but there are cases where subtle changes in the global circulation may not produce a consistent response from one episode to another. For example, due to the uncertainty in the position of the subtropical westerly jet, conditions in California may be either wet or dry (there is evidence that energy from convection at the equator feeds the mid-latitude jets).

During La Niña episodes, the patterns are similar but the signs of the anomalies are reversed.

Monitoring

Currently, there is no operational system to monitor the atmospheric climate in real-time. Data come primarily from operational weather services. Data currently available include satellite measurements of sea ice, snow cover, outgoing radiation etc., historical station records, and analyses from global operational models. The latter is useful in describing and diagnosing the global atmosphere.

For the oceans, SSTs are monitored by "ships of opportunity" and moored and drifting buoys. An array of moored buoys in the Pacific monitors variations in the thermocline depth. As a result of improved monitoring, it is now possible to do basin-scale analyses for oceans.

Problems remaining to be resolved!

Lots of them! There was only time to mention the need to understand more about the interaction between interannual variability and the annual cycle.

(a)

DECEMBER
NORMAL CONDITIONS

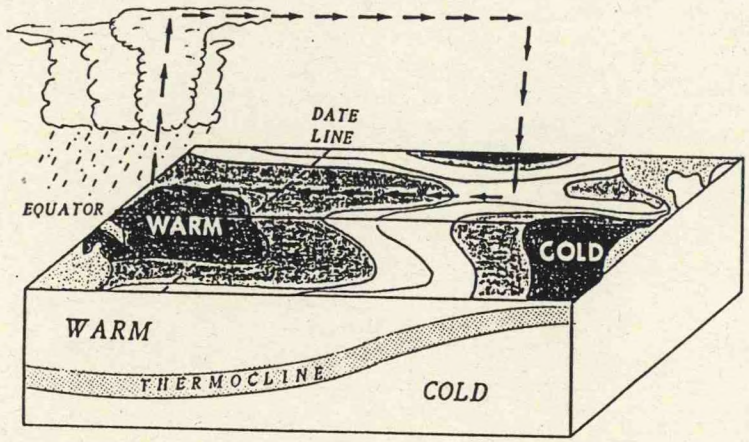

(b)

DECEMBER
EL NIÑO CONDITIONS

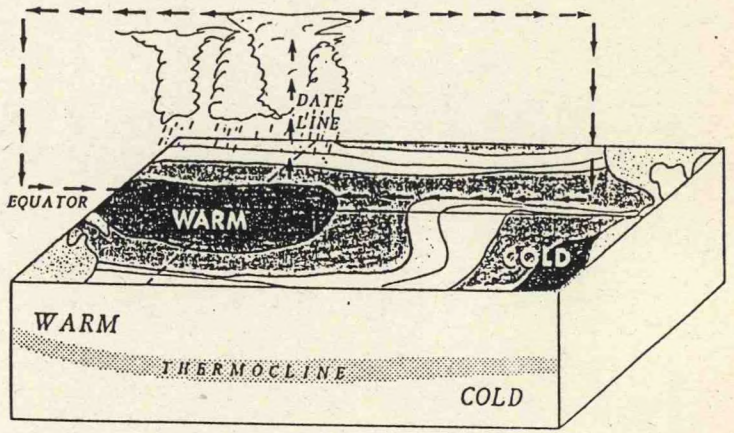

FIGURE 1

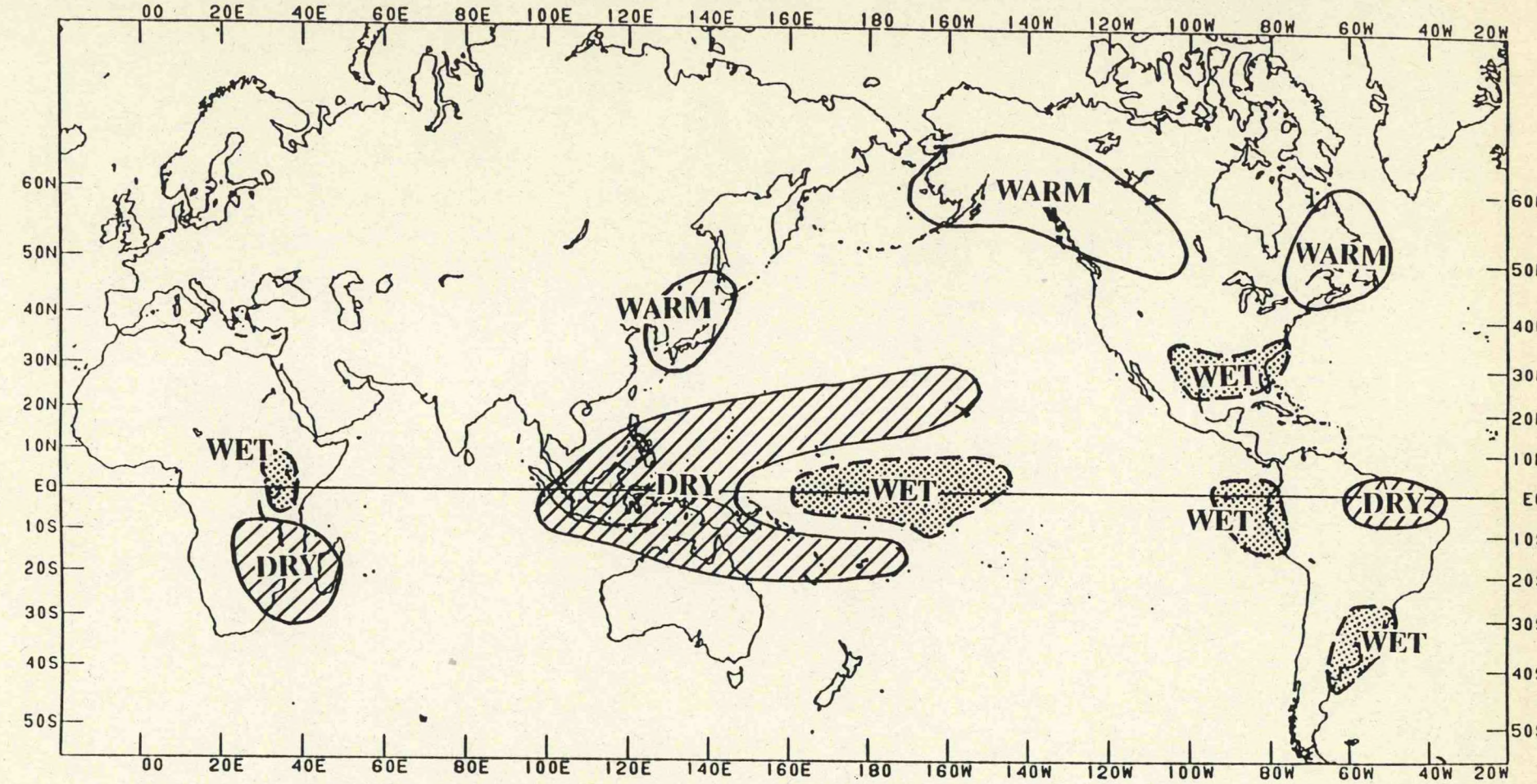

FIGURE 2 Temperature and precipitation anomaly patterns generally found during November - March in warm (ENSO) episodes.

Spectral Statistical Interpolation (SSI)

Lecturer: John Derber
Date: June 15, 1994
Notes by: David C. Burwell
Jim Hansen

The National Meteorological Center is currently utilizing a unique method of data assimilation for their Global Data Assimilation System (GDAS). Spectral statistical interpolation (SSI) takes the Bayesian approach of optimal interpolation (OI) and applies it to the the case of a spectral model. An objective function is defined that allows one to optimize a model fit with respect to many different variables. In this case, a combination is made from the deviations between a desired analysis and forecast and observational data. These deviations are then multiplied by the inverse of their respective forecast or observational error covariance matrices to weight the confidence of those values.

The objective function is:

$$J = (x - x_b)^t E^{-1}(x - x_b) + (K(x) - O)^t F^{-1}(K(x) - O)$$

where:

x is the result of the analysis
x_b is the background field from model prediction
E is the background error covariance matrix
O are the observations
F is the observation error covariance matrix
K is the transfer operator from analysis variables to types and locations of observations

The first part of the equation is the optimum interpolation fit to the background prediction information, and the second part of the equation is the optimum interpolation fit to the observations.

K is a linear (although it need not be) operator that allows one to go from the spectral coordinate system with its specially chosen variables to the grid coordinate system and variables of the observations. The observation variables are simply dictated by those that are readily available and consist of: temperature, winds, specific humidity and surface pressure. The analysis variables were chosen to take advantage of the spectral nature of the technique and simply certain matrices, but also in order to insure that mass and momentum are balanced at all times. These variables are the streamfunction, velocity potential, specific humidity, and something called the unbalanced height which combines geostrophic winds and heights into a single variable. It should be noted that the analysis variables are not the same variables that will be fed into the Eta model once the data assimilation is complete. The SSI variables will go through another transformation to make them compatible with the forecasting model.

The background error and observation error covariance matrices reflect the confidence one has and the weighting that goes into the various data sets that are being assimilated. One must take into account not only the accuracy of a given data point, but also the way in which a point of data effects the surrounding area.

To determine the analysis variables, the objective function is minimized by differentiating with respect to the analysis variables and setting it equal to zero:

$$E^{-1} (x - x_b) + K^t F^{-1} (K(x) - O) = 0$$

for the case when K is linear.
This equation is then solved for the analysis variables:

$$x = x_b + (E^{-1} + K^t F^{-1} K)^{-1} K^t F^{-1} O$$

This gives the analytical solution for the analysis variables, but the matrices involved are so large as to make the analytic solution to the problem computationally too expensive to solve. So, instead of solving for x directly, a preconditioned conjugate gradient method is employed to slip along the surface of the objective function in search of a global minimum. With this method, convergence on a minimum will occur within 100 iterations. This is computationally less expensive than the analytical solution as one need only concern themselves with K and K^t instead of having to try to determine something looking like:

$$(E^{-1} + K^t F^{-1} K)^{-1}$$

Preconditioning can be thought of as providing the system with a wisely chosen first guess that will place one near the global minimum of the objective function. It is actually a scaling that which attempts to align the gradients in the objective function towards the global minimum. Imagine in 2D an objective function who's contours project into the shape of an ellipse. In this case, with an unfortunate starting location, the gradients will send one in a direction that is not towards the global minimum. Usually, the shallow valley near the minimum is reached and a long time is spent following the small gradient to the target. However, with preconditioning, the projection of the contours are scaled towards a circular shape so that the gradients at the starting location send one much closer towards the global minimum. Perfect preconditioning would scale the projection of the contours into perfect circles, and the minimum would be found in one step. This is the equivalent of solving the analytical solution.

In the case of SSI, the perfect preconditioning matrix would be C such that:

$$C = (E^{-1} + K^t F^{-1} K)^{-1/2}$$

but as in the analytical solution, this involves prohibitive computations. It turns out that the background term in the above expression is dominant, so excellent results can be achieved using

$$C = E^{1/2}$$

which is the square-root of the background error covariance matrix.

It should be pointed out that due to the spectral nature of this technique, the background error covariance matrix is made up of simply the difference between 24-hour and 48-hour forecasts for a given day. The result of this differencing produces a diagonal matrix that is far more computationally efficient than the full matrix necessary for gridpoint OI analysis. It is not fully understood why this differencing produces such a useful background error, and there are certainly methods that would produce a full matrix with more reasonable errors. But, the fact is, this method works well and is quite efficient.

This spectral optimal interpolation gives superior results over standard, gridpoint optimal interpolation since the entire problem is solved at once. There are none of the discontinuities that exist between gridpoints and can cause noisy analysis. Problems such as these translate into the necessity of initializing the analysis before implementing it in the predictive model, a step that is not necessary for SSI.

Improvements to be made to SSI in the future include a condition to minimize the effects of gravity waves, the inclusion of precipitation, a nonlinear K matrix, the assimilation of surface wind speed, the direct inclusion of radiances, ERS-1 scatterometer data and perhaps even the complete inclusion of the MRF model into the K operator for the capability of 4D analysis.

References

Derber, J.C., Parrish, D.F. and Lord, S.J., 1991, The New Global Operational Analysis System at the National Meteorological Center. *Wea. and Forecast.*, **6**, 538-547.

Parrish, D.F. and Derber, J.C., 1991, The National Meteorological Center's Spectral Statistical-Interpolation Analysis System. *Mon. Wea. Rev.*, **120**, 1747-1763.

Observations for Short-Term Climate Analysis and Prediction

Lecturer: Michael McPhaden
Date: June 15, 1994
Notes by: Cheng-Hsuan Lu
Jim Hansen

The El Niño/Southern Oscillation (ENSO) phenomenon is the most significant signal for the study of short-term climate analysis and prediction. To the first order, ENSO can be described as an oscillation between a cold and a warm state in the tropical Pacific. The cold state is referred to as La Niña, and the warm state as El Niño. The El Niño phase is identified by anomalously warm SSTs throughout the tropical Pacific, especially in the east. The results of this warming effect not only the local weather patterns, but also such things as global circulation and global rainfall distribution. Coupled with the climactic impact, there are economic results that make the study and reliable prediction of El Niño of great interest beyond that of theoretical understanding.

ENSO

The prevailing conceptual model of ENSO is that of the delayed action oscillator (Schopf and Suarez 1989). The basic idea is that SST anomalies in the center of the tropical Pacific (usually in a cold, La Niña phase) create wind stress anomalies that result in a Kelvin wave propagating to the east, and at the same time, a Rossby wave propagating to the west. This Kelvin wave features upwelling, and as a result of the shallow thermocline typical of the eastern Pacific, creates cold sea surface temperatures which provide positive feedback to the anomalous easterly winds in the central Pacific.

However, the Rossby wave propagating to the west reflects off of the western boundary and returns a signal of downwelling Kelvin waves to the east. This results in a deepening of the thermocline in the east (effectively tilting the thermocline) and providing negative feedback to the easterly winds in the central Pacific. Eventually, the change in sea surface temperature distribution will result in a weakening, and on occasion a change in sign of the winds in the central Pacific. Anomalous westerlies will trigger downwelling Kelvin waves that propagate to the east, which deepen the thermocline, and raise the SSTs in the eastern Pacific, thus providing positive feedback to the anomalous westerly winds (**Fig. 1**). But once again, a Rossby wave will propagate westward, reflect off the western boundary and send Kelvin waves to the east. However, this time they will be upwelling Kelvin waves and will provide negative feedback to the winds in the central Pacific, and therefore eventually the anomaly pattern will reverse. In this model, ENSO is simply a low-frequency oscillation in the tropical Pacific complete with positive and negative feedback.

Of course, the delayed action oscillator is an idealized model. In reality, it is difficult to pick out all of these phenomena from the real data, and ENSO is anything but a steady state oscillator. An ENSO episode generally lasts for about one year, and the time between episodes tends to be on the order of four to seven years. So, instead of constantly oscillating between warm and cold, the true state of the tropical Pacific is generally "normal" conditions with quasi-periodic warm or cold deviations. Some feel that there is little evidence to support the theory that the reflected Rossby waves eventually result in significant changes in the central Pacific winds (Li and Clarke 1994). Others maintain that the ENSO cycle may simply

be non-periodic. That is, on occasion, the delayed action oscillator is damped out and the signal is lost, only to be randomly re-initiated at some later time. However, during the ENSO episodes themselves, delayed action oscillator signals can be observed. Another popular theory is that ENSO episodes are triggered by high-frequency forcing of the unstable pool of warm water in the western, tropical Pacific, and the time between ENSOs is simply the time it takes for that reservoir to replenish.

The effects of ENSO include climactic impacts of temperature and precipitation around the globe as well as direct ecosystem impacts in the tropical Pacific. Ostensibly, an El Niño event only effects SSTs in the tropical Pacific. However, these SST anomalies are capable of disrupting atmospheric circulation world-wide. This alteration to global circulation has been correlated to anomalously warm, cold, wet and dry periods around the world (**Fig. 2**). For more detailed information, the reader is referred to papers by Ropelewski and Halpert (1987, 1989 and 1992). On the economic side, a strong warm phase of ENSO will deepen the thermocline in the eastern Pacific to such an extent as to seriously inhibit the upwelling of nutrient rich cold water that is necessary to support the large populations of anchovies, sardines, mackerel and other fish in that area.

TOGA

The Tropical Ocean-Global Atmosphere (TOGA) program was developed in 1985 as a ten-year program to focus on short-term (100-1000 day) climate variability. It was initiated shortly after the 1982-83 "El Niño of the Century" that successfully eluded detection by the scientific community until well into its mature phase. Once the global consequences of that episode were realized, scientists decided to implement a program designed to try to understand the mechanisms involved with ENSO, determine the predictability of events, and develop both in situ and satellite observing systems for data collection and monitoring purposes.

The motivation of expanded in situ, real time measurements in the tropical Pacific includes the detection and monitoring of ocean climate anomalies. While it may seem that this is unnecessarily redundant given the capabilities of satellites, satellites are in constant need of calibration and validation from surface observations. Also, satellites are not capable of providing data concerning the subsurface structure of the ocean, and their measurements can be adversely affected by extreme events such as volcanic eruptions The combination of in situ and satellite data can be assimilated into operational ocean/atmosphere models for improved analysis, and these data are absolutely essential for the correct initialization and validation of ENSO forecasts. The key variables measured by these in situ instruments are sea surface temperature (SST), sea surface winds, subsurface temperature, sea level height, upper ocean currents, local salinity, surface heat flux, and others.

TOGA/TAO

To achieve these ends, TOGA initiated the Ocean Observing System. This is a multinational effort to install and maintain an array of instrumentation to observe the Pacific ocean. The instruments used are a system of moored buoys, numerous tide gauge stations, satellites, drifting buoys and volunteer observing ships (VOS). A schematic is shown in **Fig. 3**.

The moored buoys are known as the Tropical Atmosphere-Ocean (TAO) array, and there are currently 66 of them deployed throughout the equatorial Pacific. Along their tether lines are instruments to give temperature in the upper 500 m of the ocean, and onboard the buoys are instruments to record such things as SST, humidity, air temperature, and winds. Of course, there is the potential of loading much more instrumentation onto an individual buoy, and there are some that do many other things, but the high costs associated with the production, upkeep and retrieval of the basic buoy tends to keep extra instrumentation at a minimum. All of the data collected by the buoys, and all the other components of TAO, are telemetered in real time to receiving stations that make the data collected readily available.

There are approximately 60 tide gauge stations spread throughout the tropical Pacific, typically being located in sheltered harbors. These instruments are inexpensive and easy to maintain and allow you to observe the low-frequency changes in sea level height. Unfortunately, they do not have as wide a distribution as would be optimal due to the simple lack of islands in the eastern Pacific.

The drifting buoys are the global Lagrangian drifter type. They consist of a float attached to a long drogue that pulls them through the water at about the speed of the currents at 15 meters. There are approximately 840 of them currently deployed and their main task is to determine SSTs and 15 m current speeds. Some are equipped with a barometer and irradiance meter, but they tend not to work very well. Drifting buoys can be deployed throughout an area of interest, but by their very nature, one generally ends up oversampling a convergent zone of the ocean, and undersampling a divergent one.

The VOSs provide a valuable, though temporally infrequent data set. Commercial ships agree to periodically drop expendable bathythermographs (XBTs) into the ocean at a rate of about twice a day. The XBTs measure the temperature profile of the top 500 meters of the ocean by sensing the temperature at a known rate of decent. This information is passed up a thin copper wire to the ship and is automatically telemetered to a collection center. Although an average of 3400 XBT drops are made a month, they are taken only along designated shipping lanes and it is unlikely to get XBT drops with enough spatial and temporal resolution to directly observe any small scale oceanographic events.

The TOGA mission officially ends in December 1994, and there are many questions regarding any post-TOGA missions. It looks as though the TOGA operations will be maintained in a transition to the Global Ocean Observing System (GOOS) and the Global Climate Observing System (GCOS). The entire program will be expanded through the research of the Global Ocean/Atmosphere Land System (GOALS) and the Climate Variability (CLIVAR) programs that will run from 1995-2010. The role in prediction will be expanded with the work of the International Research Institute for Climate Prediction (IRICP).

References

Halpert, M. S., and C. F. Ropelewski, 1992: Surface Temperature Patterns Associated with the Southern Oscillation. *J. Climate*, **5**, 577-593.

Li, B., and A. J. Clarke, 1994: An Examination of Some ENSO Mechanisms Using Interannual Sea Level at the Eastern and Western Equatorial Boundaries and the Zonally Averaged Equatorial Wind. *J. Phys. Oceanog.*, **24**, 681-690.

Ropelewski, C. F., and M. S. Halpert, 1987: Global and regional scale precipitation patterns associated with the El Niño/Southern Oscillation. *Mon. Wea. Rev.*, **115**, 1606-1626.

Ropelewski, C.F., and M. S. Halpert, 1989: Precipitation Patterns Associated with the High Index Phase of the Southern Oscillation. *J. Climate*, **2**, 268-284.

Schopf, P. S., and M. J. Suarez, 1990: Ocean Wave Dynamics and the Time Scale of ENSO. *J. Phys. Oceanog.*, **20**, 629-645.

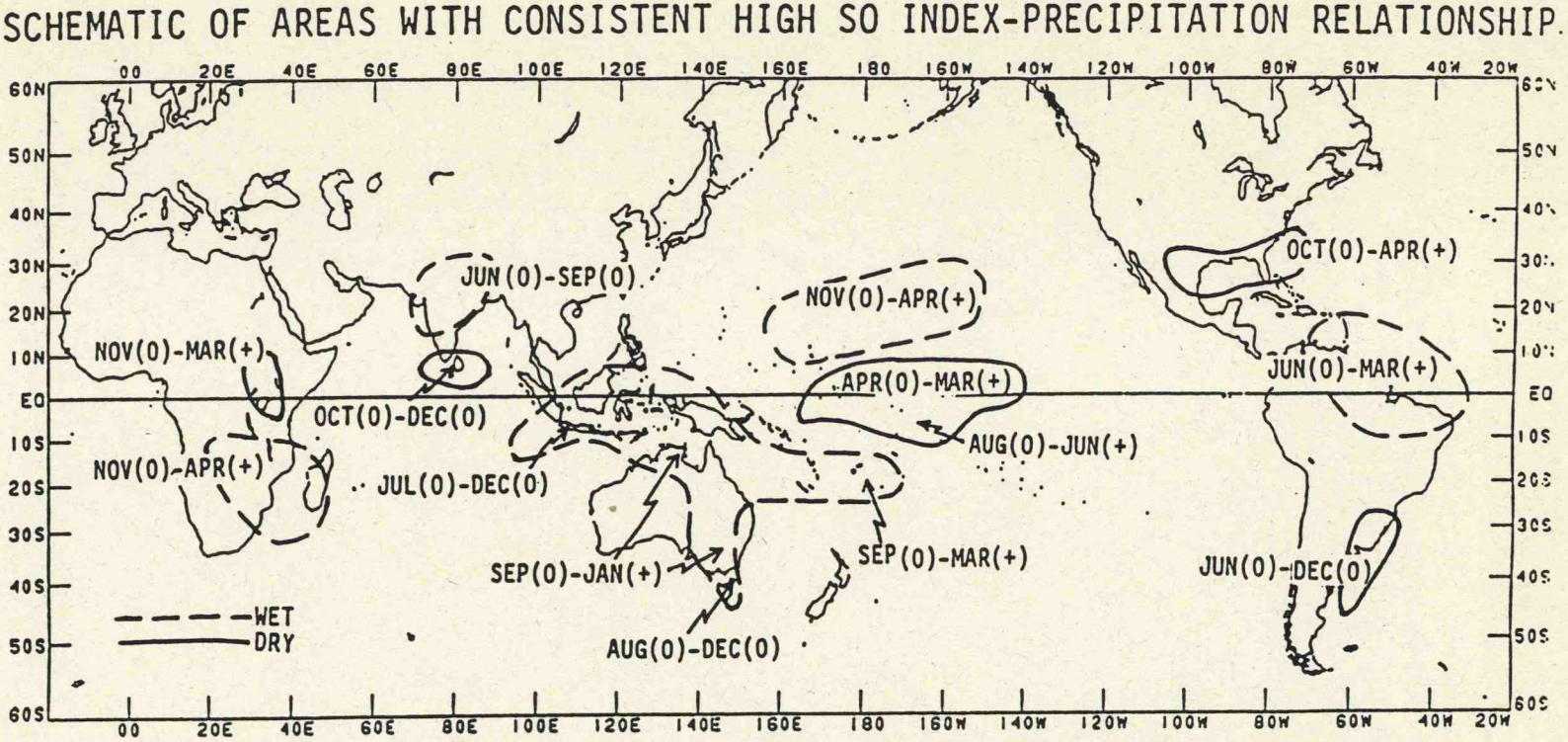

FIGURE 1 Schematic representation of the principal areas of high-SO index related precipitation based on the analysis of precipitation composites and time series. Regional maps should be consulted for details.

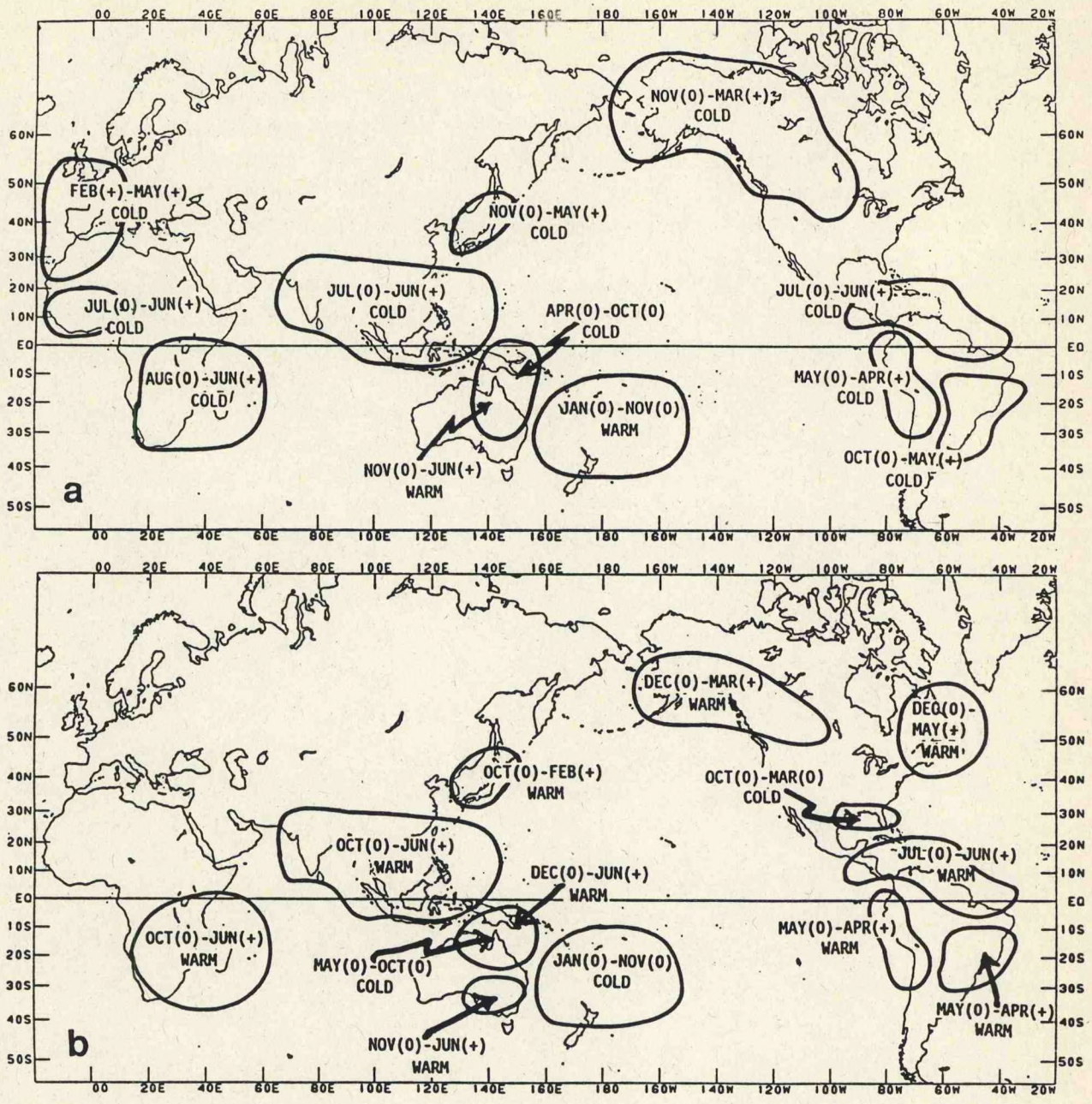
NOV(0)-MAR(+)
COLD
FEB(+)-MAY(+)
COLD
NOV(0)-MAY(+)
COLD
JUL(0)-JUN(+)
COLD
JUL(0)-JUN(+)
COLD
APR(0)-OCT(0)
COLD
JUL(0)-JUN(+)
COLD
AUG(0)-JUN(+)
COLD
MAY(0)-APR(+)
COLD
JAN(0)-NOV(0)
WARM
NOV(0)-JUN(+)
WARM
OCT(0)-MAY(+)
COLD
a
DEC(0)-MAR(+)
WARM
DEC(0)-
MAY(+)
WARM
OCT(0)-FEB(+)
WARM
OCT(0)-MAR(0)
COLD
OCT(0)-JUN(+)
WARM
JUL(0)-JUN(+)
WARM
DEC(0)-JUN(+)
WARM
OCT(0)-JUN(+)
WARM
MAY(0)-APR(+)
WARM
MAY(0)-OCT(0)
COLD
JAN(0)-NOV(0)
COLD
MAY(0)-APR(+)
WARM
NOV(0)-JUN(+)
WARM
b

FIGURE 2

Tropical Pacific Ocean Observing System

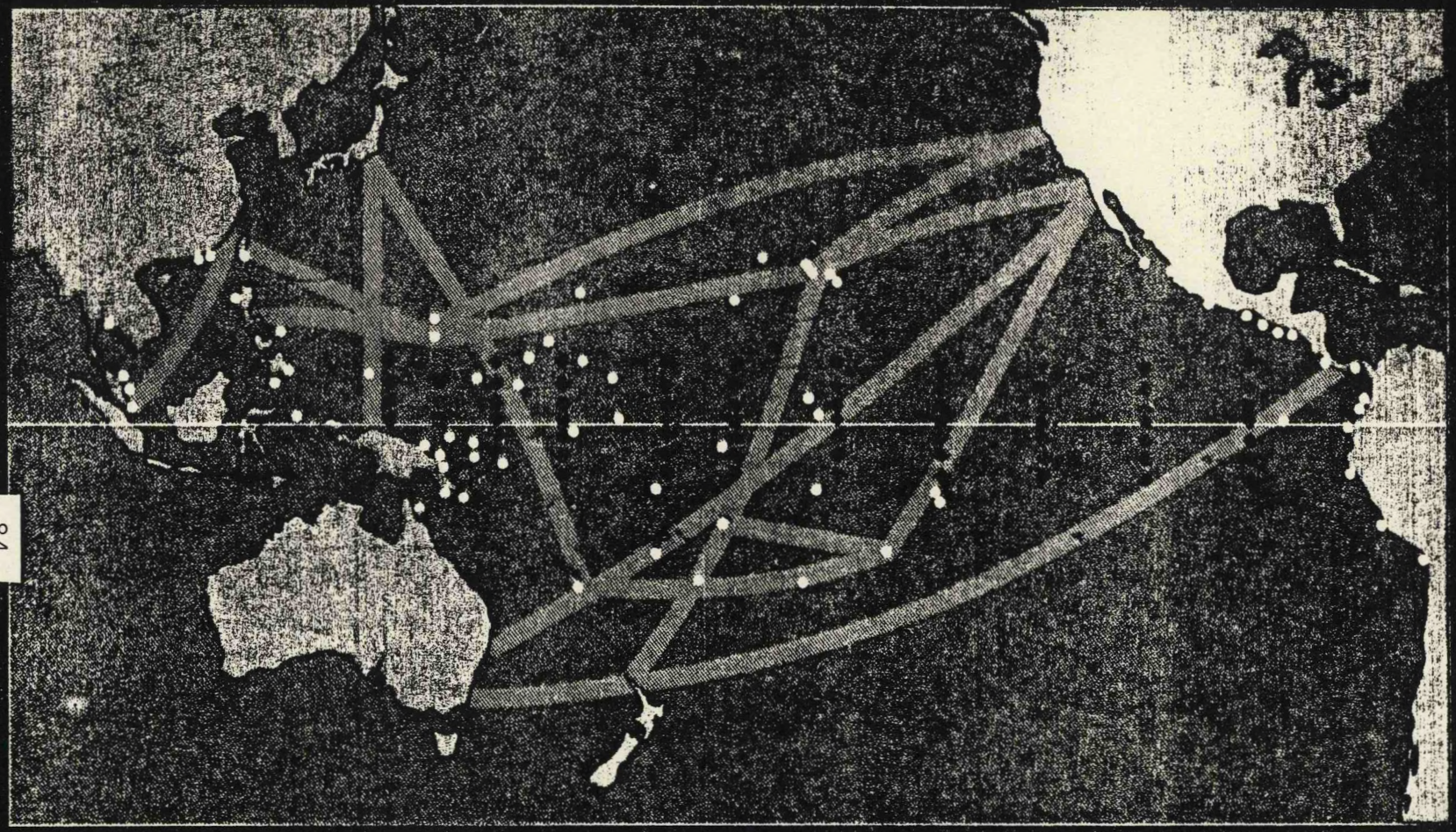

moored buoys

tide gage stations

satellite data relay

drifting buoys

volunteer observing ships

NOAA

FIGURE 3

Coupled Model Ocean-Atmosphere Forecast System

Lecturer: Ming Ji
Notes by: Christelle Escoffier
Jim Hansen
Date: June 15, 1994

The objective of the Climate Analysis Program/Coupled Model Project is the forecast of interseasonal to interannual time scale climate variability such as the El Niño/Souther Oscillation (ENSO). ENSO events typically last on the order of a year (with notable exceptions), and have a recurrence time of four to seven years.

It may seem like an unreasonable desire to forecast anything longer than the limit of predictability (LOP) proposed by Lorenz. He stated that the theoretical limit to weather prediction would be on the order of two-three weeks, or roughly the period of cyclic weather events. But of course, Lorenz was only talking about the internal variability of weather systems. When something is strongly effected by external forcing, an entire new time scale is defined. In general, processes that are driven by such things as the earth's distance from the sun, the oceans, volcanoes, the quasi-biennial oscillation (QBO), ice caps, and more tend to have intrinsic periods of much longer than Lorenz's two-three weeks, and their predictability can be pushed to new limits.

To the first order, ENSO can be described as an oscillation between a cold and a warm state in the tropical Pacific. The cold state is referred to as La Niña, and the warm state as El Niño. The El Niño phase is identified by anomalously warm SSTs throughout the tropical Pacific, especially in the east. The results of this warming effect not only the local weather patterns, but also such things as global circulation and major changes in global rainfall distribution. coupled with the climactic impact, there are economic results that make the study and reliable prediction of El Niño of great interest. For a description of the a conceptual model of ENSO known as the delayed action oscillator, see the report on the lecture given by Michael McPhaden.

The delayed action oscillator highlights the importance of sub-surface activity in the ENSO cycle. Although sea surface temperatures are a convenient tracer and can be an index of sub-surface dynamics, they cannot reflect the physics and memory below the surface of the ocean. Therefore, any model designed for ENSO prediction should incorporate sub-surface information. The state of the art in ENSO forecasting seems to support this statement. Latif et al. (1994) have produced a review of ENSO prediction studies.

There are four different types of coupled models. The first is the statistical model, where past history of oceanic and atmospheric variables are manipulated with statistical techniques in a effort to predict future events. Next in complexity come the intermediate models, where "simple" atmospheric and "simple" oceanic models are coupled so that the results of one can drive the other and vise versa. The hybrid models follow the intermediate models in complexity by coupling a statistical atmosphere with a physical ocean. Finally, the most complex of them all is the coupled general circulation models (GCMs), which couple a full primitive equation atmosphere with a full primitive equation ocean. Each of these techniques has its own set of strengths and weaknesses, and after considering them all, the scientists in the Coupled Model Project have decided to use the coupled GCM in the attempt to model the ENSO cycle.

They take the two-tiered approach of coupled modeling. The process starts out with

an optimum interpolation assimilation of ocean data to develop the initial conditions for the coupled model. In this way, there is no need for the traditional spin-up of the ocean model with a history of real winds. With assimilation, the model starts at the best guess of the current state of the ocean. The coupled model itself is an anomaly model that only calculates the deviations from some prescribed climatology. The ocean model is run for a time step, the calculated coupling fields are fed to the atmospheric model which in turn is run for a time step. Coupling fields from the atmosphere are fed back to the ocean, and the entire process repeats until the desired prediction length is reached. The prediction process is done in an ensemble method in such a way that one takes the average of three runs, each starting with a lag of one month. For example, this month's run will produce a prediction that will include the prediction for next month. That prediction is compared with the second month prediction that was as part of last month's prediction, and the third month prediction that was run two months ago. The anomalies generated with the coupled model are added to the observed SST climatology for the Pacific basin, and serve as bottom boundary conditions for an atmospheric GCM (AGCM). The AGCM is then run nine times in an ensemble manner without the direct influence of any climatology. A schematic of this process is shown in **Fig. 1**. Perturbations are developed by taking the atmospheric conditions after seven days of run time (the typical period of weather events) and using them as the initial conditions along with the original oceanic fields.

The reason that the coupled model output is not used as the working prediction is because ocean GCMs (OGCMs) tend to produce their own climatology. That is, since it is impossible to get all of the physics perfectly correct when designing a model of this complexity, instead of representing the real world, the model will represent the world as it thinks it should be.

Under certain conditions, the ensemble of the AGCM forced with the SST anomalies derived from the coupled GCM (CGCM) is able to produce useful predictions with lead times of up to 11 months. However, like many other ENSO models, the prediction skills suffer from a "spring barrier". Skill tends to drop off rapidly when a prediction enters the spring months, and then recover once its made it through. There are numerous explanations for this phenomenon, including the idea that since SST gradients are relatively weak during the spring in the central and eastern Pacific, there is the opportunity for increased variability in the different fields forcing the ocean (wind stress, heat flux). Therefore, small errors in these potentially variable fields could result in relatively large errors in SST. It should be noted that predictions initiated in the spring do not suffer from this problem, and it is most likely a result of the four dimensional assimilation scheme used to initialize the ocean. In comparison to other CGCMs, the NMC model has significantly better skill in the first few months of the prediction, however, after 6-10 months, the skill of other models will generally be higher than that of the NMC model (see **Fig. 2**). The reason for this is not yet fully understood. It could very well be that the same data assimilation technique that is providing the superior skill at the beginning of forecasts is somehow degrading the skill near the end of forecasts.

The ultimate goal of any work produced at the NMC is to eventually improve the reliability of climactic and weather forecasts. The AGCM attempts to do this by capturing the mid-latitude response to the CGCM produced tropical SSTs. It turns out that they show a strong correlation in the Pacific/North America (PNA) region during the winter of ENSO years, which would suggest a level of skill at certain times for predicting surface temperature

patterns that might be affected by these tropical Pacific SSTs. In fact, **Fig. 3** shows that the SSTs produced by the CGCM are at least as skillful in this respect as is persistence and the use of "true" SST fields produced from observations.

References

Ji M., A. Kumar, and A. Leetmaa A., 1994: A Multiseason Climate Forecast System at the National Meteorological Center. *Bull. Amer. Meteor. Soc.*, **75**, 569-577.

Latif M., T. P. Barnett, M. A. Cane, M. Flugel, N. E. Graham, H. von Storch, J. S. Xu, and S. E. Zebiak, 1994: A review of ENSO prediction studies. *Clim. Dyn.*, **9**, 167-179.

CLIMATE PREDICTION SYSTEM

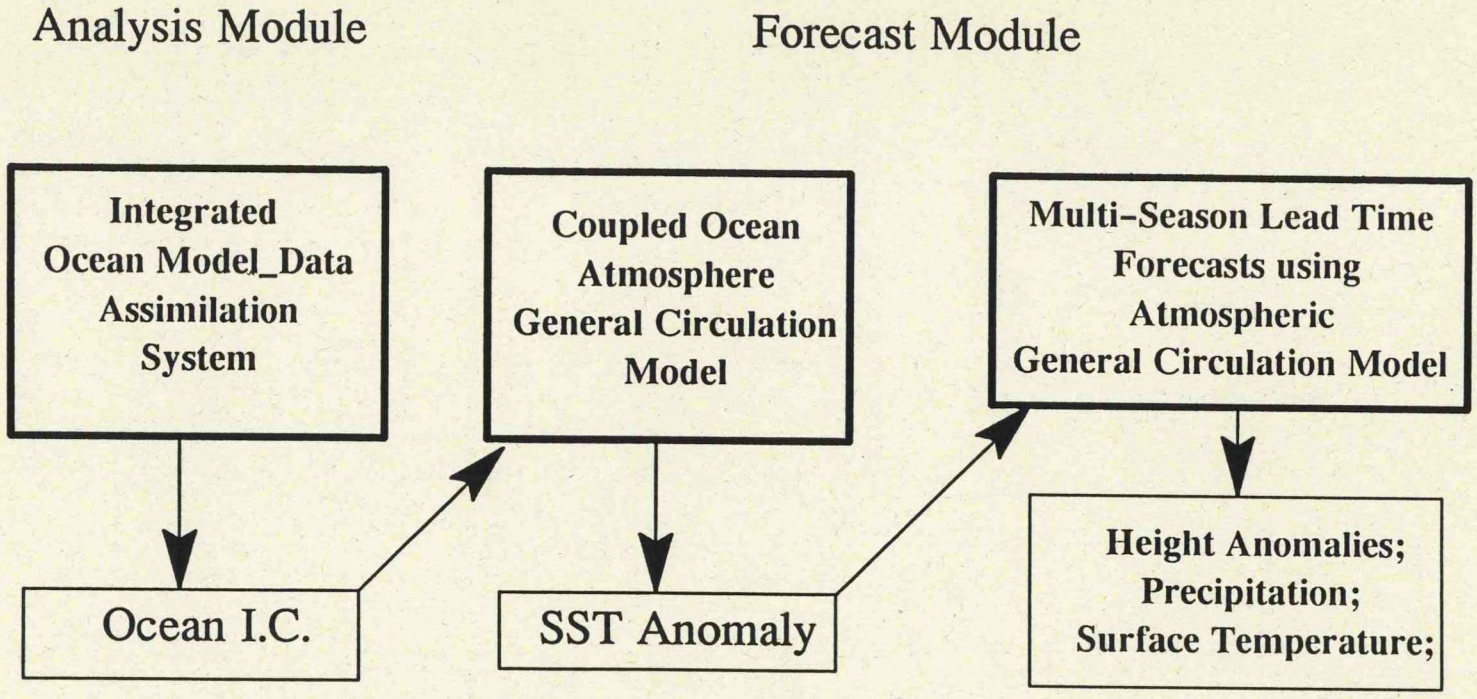

FIGURE 1

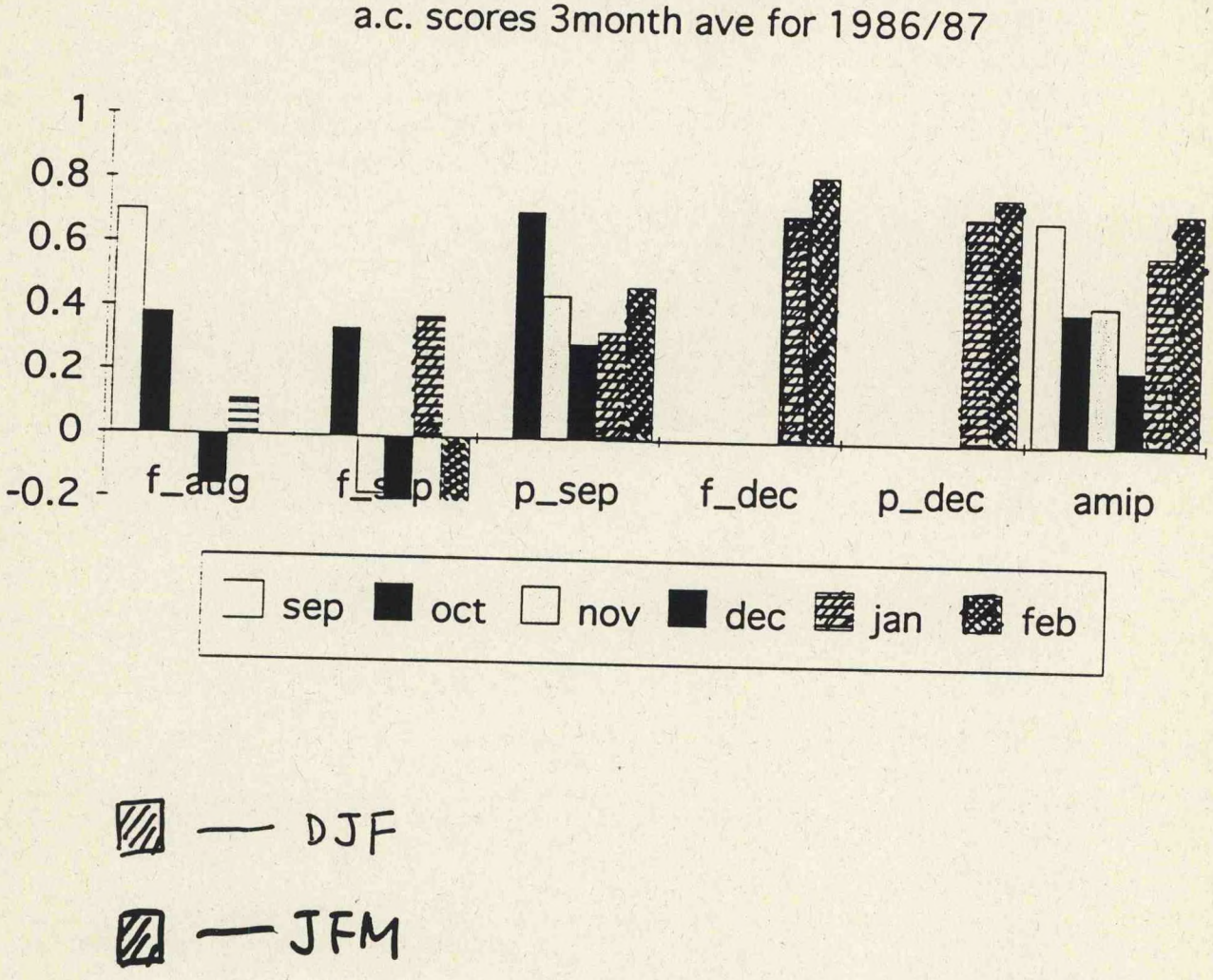
a.c. scores 3month ave for 1986/87
1
0.8
0.6
0.4
0.2
0
-0.2
f_aug
p_sep
f_dec
p_dec
amip
sep
oct
nov
dec
jan
feb
DJF
JFM

FIGURE 2

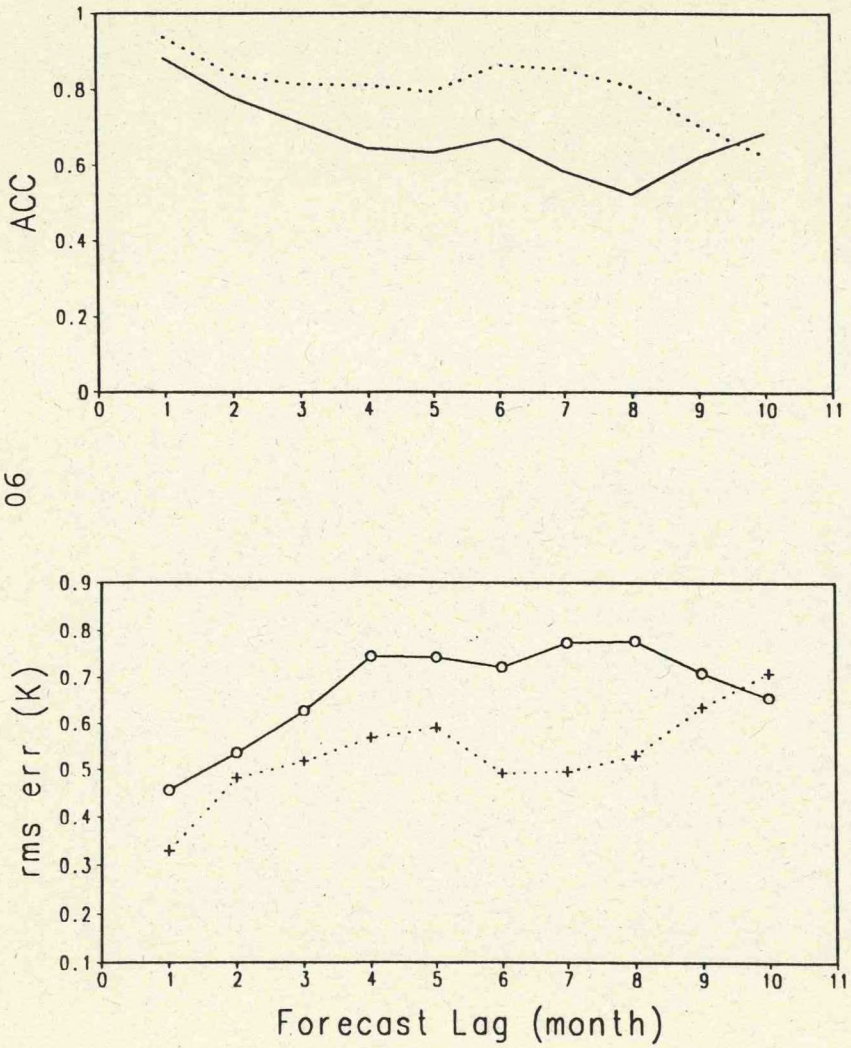

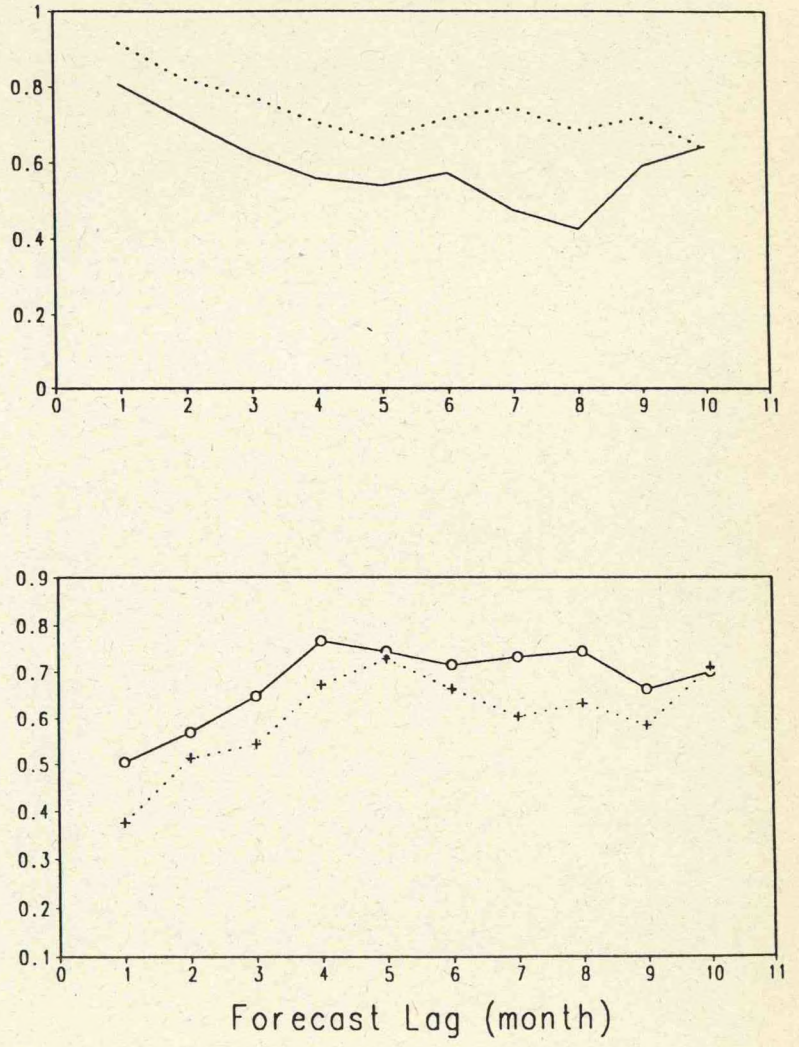

06

FIGURE 3

solid-fsu, dash-ra2

solid-fsu, dash-ra2

GLOBAL SEA SURFACE TEMPERATURE ANALYSIS TECHNIQUES

Lecturer: Richard W. Reynolds
Notes by: Zhaoqing Yang
Date: June 16, 1994
Paul Gaertner

Global sea surface temperature (SST) fields are useful for monitoring climate change as an oceanic boundary condition for atmospheric models. As SSTs can be estimated by satellites, the SST field may be the best-known ocean parameter on global scales. Here we discuss three SST analysis techniques used by NMC: in situ analysis, blended (Poisson) analysis and optimal interpolation (OI) analysis. Data for the analysis is obtained from sources such as ships, drifter and mooring buoys and AVHRR on the NOAA polar orbiting satellites.

The in situ analysis uses quality-controlled ship/buoy SST observations obtained monthly from GTS. The monthly distribution of in situ observations is adequate to describe the SST patterns between 30°S 60°N except in the central and eastern tropical and South Pacific areas. The individual observations are subject to large errors in both temperature and position, thus in situ analysis is accompanied by further analysis. The in situ analysis is used as ground truth, thus providing "benchmark" temperatures in regions of frequent in situ observations; satellite analysis is used to define the shape of the final field between the benchmarks. The data is averaged onto a 2-degree grid and smoothed using a nonlinear filter (Reynolds 1988).

Blended analysis uses the two preliminary monthly analysis, in situ and satellite analysis, as input. This method uses the in situ analysis to define the blended field in regions of sufficient in situ observations. Satellite analysis is used to define the shape of the field in regions with little or no in situ data. The procedure is carried out by requiring that the SST field satisfy Poisson's equation. This equation is subject to internal boundary conditions imposed by the in situ benchmark values and the external boundary conditions which can be specified by initially defining the poleward limits of all SST measurements. The solution to the Poisson equation adjusts any large-scale biases and gradients in the satellite field relative to the in situ internal boundary conditions. Because global satellite coverage is superior to the in situ coverage, the satellite field has potentially better accuracy. Comparing in situ analysis with blended analysis it can be shown that blended analysis has a vast improvement over in situ analysis, especially where the in situ data is sparse, e.g., the southern ocean. With Optimal Interpolation analysis, satellite data bias are corrected using in situ observations. Before SST data can be used in the OI it must pass quality control procedures. These procedures include the use of programs that track ships and buoys by their identification codes and eliminate observations with unlikely position changes. All in situ observations that pass the tracking tests and all satellite retrievals are tested for accuracy of the SST. Observations are discarded if the SST is less than -2°C or greater than 35°C or if the SST anomaly lies outside ±3.5 times the climatological standard deviation.

These tests are necessary because OI assumes no systematic biases and satellite data has biases, thus the tests are designed to eliminate some of the worst data. OI uses a weekly one-degree global grid, with the previous analysis being used as a first guess. **Figure 1** shows a schematic of the OI technique. The OI with the satellite bias correction is superior to the blended analysis because of its higher spatial and temporal resolution.

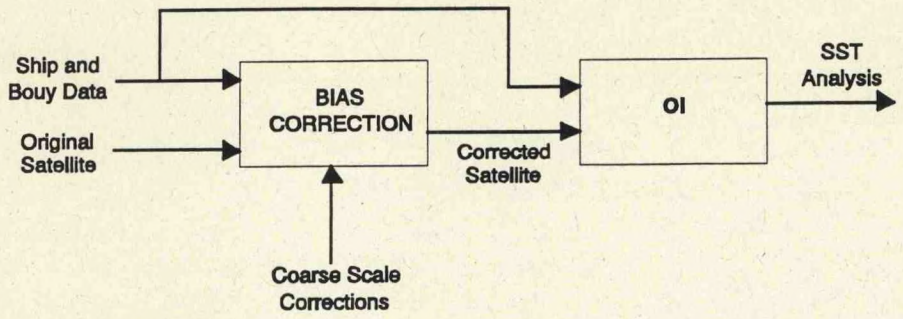

Figure 1. Flow chart of the OI technique

References

Clancy, R. M., P. A. Phoebus, and K. D. Pollak, 1990: An operational global-scale ocean thermal analysis system. *J. Atmos. Ocean. Technol.*, **7**, 233-254.

Lorenc, A. C., 1981: A global three-dimensional multivariate statistical interpolation scheme. *Mon. Wea. Rev.*, **109**, 701-721.

Reynolds, R. W., 1978: Sea surface temperature anomalies in the North Pacific. *Tellus*, **30**, 97-103.

Reynolds, R. W., 1988: A real-time global sea surface temperature analysis. *J. Climate*, **1**, 75-86.

Reynolds, R. W., and D. C. Marsico, 1993: An improved real-time global sea surface temperature analysis. *J. Climate*, **6**, 114-119.

Reynolds, R. W., and T. M. Smith, 1994: Improved global sea surface temperature Analyses using optimum interpolation. *J. Climate.*, **7**, 929-948.

COASTAL PREDICTION AND DATA ASSIMILATION IN OCEANOGRAPHY

Lecturer: Tal Ezer
Notes by: Zhaoqing Yang
Christelle Escoffier
Date: June 16, 1994

This lecture covers three areas:

1) a description of the Princeton Ocean Model (POM) and some of its applications;
2) the problem of assimilating satellite data into an ocean model with an example of the prediction of the Gulf Stream and its eddies;
3) the discussion of preliminary results from an operational coastal forecast system aimed at forecasting oceanic fields on an regular basis.

The Princeton Ocean Model (POM)

The Princeton Ocean Model is a three dimensional coastal model, which was developed by Blumberg and Mellor (1987). It has a free surface primitive equation, a bottom-following sigma vertical coordinate system and a coastal-following curvilinear, orthogonal horizontal coordinate system. It contains an embedded, second moment turbulence closure sub-model to provide vertical mixing coefficients. The dependent variables are temperature, salinity (and other scalars), surface heights, current and turbulent kinetic energy and length scale.

This model has been successfully applied in many regions around the world for dynamic process studies (Ezer and Mellor 1992) and modeling of circulations in estuaries, coastal seas and oceans, such as Long Island Sound, Delaware Bay, Great Lakes, California Coast, Gulf stream, Gulf of Mexico, Norwegian Sea, Mediterranean Sea, Red sea, Arctic Ocean, etc..

Continuous Assimilating Satellite Data into an Ocean Model

Although data assimilation has been used in numerical weather prediction models for a long time, this technique is in an early developmental stage in ocean modeling due to the limited observing network. Satellite-derived altimeter data on a global ocean coverage, such as obtained from Geosat, make it possible to continuously assimilate these data into ocean models. However, there are still some problems in oceanic data assimilation, such as

1) Errors from Geoid, tides, atmospheric corrections;
2) Altimetry and temperature data on a global coverage are only available at the sea surface;
3) SST data are missing in areas with cloud coverage;
4) The distance between tracks is greater than mesoscale features;
5) Repeat cycle is only every ~ 17 days (Geosat);

Also, a continuous assimilation ocean model is required in order to be eddy-resolving, to have fast adjustment of model fields to data updating and to have more efficient computa-

tion. Therefore, the data assimilation scheme must be sophisticated enough to fill the holes in space and time but simple enough to be efficient.

A three-dimensional data assimilation scheme is developed and tested using Geosat altimeter data and POM model in Gulf Stream region. The assimilation scheme is based on an optimal interpolation approach in which data along satellite tracks are continuously interpolated three dimensionally into the model grid and assimilated with model prognostic fields. The three-dimensional problem is divided into two steps:

1) Solving a two-dimensional problem horizontally by assimilating surface elevation from data along satellite tracks and interpolated the data into the model grid;

2) Solving a one-dimensional problem vertically by using the analysis elevation fields and correlation factors that relate surface elevation anomalies and subsurface temperature and salinity anomalies. A schematic diagram of the data assimilation scheme is shown in **Fig.1.**

Synoptic analysis fields of temperature and salinity are obtained from the Optimal Thermal Interpolation System (OTIS). The skill of the assimilation scheme is evaluated for two periods in which OTIS analysis fields are available. The first OTIS analysis field is used as in initial condition. An application of the model on the Gulf Stream show that for the first 14 days, the difference between the assimilated and unassimilated fields is relatively small due to the poor accumulation of altimeter data and not enough measurements to constrain the model (**Fig. 2a**). However, 74 days after initialization, the model calculations depart from each other; meanders and general location of the stream are more realistic than the unassimilated field (**Fig. 2b**). Experiments also showed that assimilation of SST data only can give good location of the Gulf Stream and assimilation of SST data only can generate similar meanders of the Gulf Stream compared to the OTIS analysis field. In **Fig. 3**, at the sea surface, the rms error of temperature anomalies is greatly reduced due to the assimilation of SST (sea surface temperature). And, deeper than 100 m, the error is reduced due to the assimilation of SSH (sea surface height). Apparently, the data assimilation in the ocean model is very useful for nowcasting/forecasting meso-scale ocean variabilities.

Coastal Forecast System (CFS)

The Coastal Forecast System is a joint project of Princeton University, Geophysical Fluid Dynamics Laboratory (GFDL/NOAA), National Meteorological Center (NMC/NOAA) and National Ocean Service (NOS/NOAA). The system has currently been in operation less than a year. The goal of this system is using the daily forecasts of an atmospheric model for data assimilation scheme every 3 hours to drive the ocean model and provide hourly output of currents, temperatures, salinities and elevations to the public and provide information for evaluation of the forecast skill and for understanding the sensitivity of the different parameters.

The first results which can be looked at are the coastal sea level prediction. The important parameters to predict coastal sea level are the mean circulation, the basin-scale variability, the meso-scale variability, the wind stress, the surface atmospheric pressure, tides and the thermal expansion of water. For example, the wind, even for a short period like a storm can increase the sea level for a short time. An annual cycle is also observed in sea level due to thermal expansion.

The future implementations in coastal forecast system are to assimilate SST, altimetry and other data. Also important are the inclusion of more effects like tidal forcing, atmospheric

pressure, thermal expansion, river runoffs and an improvement in the boundary conditions. The resolution in ocean and atmospheric models has to be improved too. Then, the estuary and bay models have to be connected to the CFS. Finally, data distribution and common visualization have to be developed between the different participants of CFS.

References

Blumberg, A. F., and G. L. Mellor, 1987: A description of a three-dimensional coastal ocean circulation model. *Three-dimensional Coastal Ocean Models*, **4**, N Heaps, Ed., Amer. Geophys. Union, 208 pp.

Ezer, T., 1993: On the interaction between the gulf Stream and the New England seamount chain, *J. Phys. Oceanogr.*, **24**, 191-204.

Ezer, T., and G. L. Mellor, 1992: A numerical study of the variability and the separation of the Gulf stream induced by surface atmospheric forcing and lateral boundary flows, *J. Phys. Oceanogr.*, **22**, 660-682.

Ezer, T., D. -S. Ko, and G. L. Mellor, 1992: Modelling and forecasting the Gulf Stream, In: *Oceanic and Atmospheric Nowcasting and Forecasting*, D. L. Durham and J. K. Lewis (Eds.), *Mar. Tech. Soc. Journal*, **26**, 5-14.

Ezer, T. G. Mellor, D. -S. Ko, and Z. Sirkes, 1993: A comparison of Gulf Stream sea surface height fields derived from Geosat altimeter and those derived from sea surface temperature data, *J. Atmos. Ocean. Tech.*, **10**, 76-87.

Mellor, G. L., 1991: An equation of state of Numerical Models of Oceans and Estuaries, *J. Atmos. Oceanic. Tech.* **8**, 609-611.

Mellor, G. L., 1992: User's guide for a three-dimensional, primitive equation, numerical ocean model, prog. in Atmos. and Ocean. Sci., Princeton University, 35pp.

Mellor, G. L., and A. F. Blumberg, 1985: Modeling vertical and horizontal diffusivities with the sigma coordinate system, *Mon. Wea. Rev.*, **113**, 1380-1383.

Mellor, G. L., and A. F. Blumberg, 1991: A Gulf Stream model and an altimetry assimilation scheme, *J. Geophys. Res.*, **96**, 8779-8795.

Mellor, G. L., T. Ezer, and L.-Y. Oey, 1993: On the pressure gradient conundrum of sigma coordinate ocean models, *J. Atmos. Ocean Tech.*, Submitted.

Mellor, G. L., and T. Yamada, 1982: Development of a turbulence closure model for geophysical fluid problems, *Rev. Geophys. Space Phys.*, **20**, 851-875.

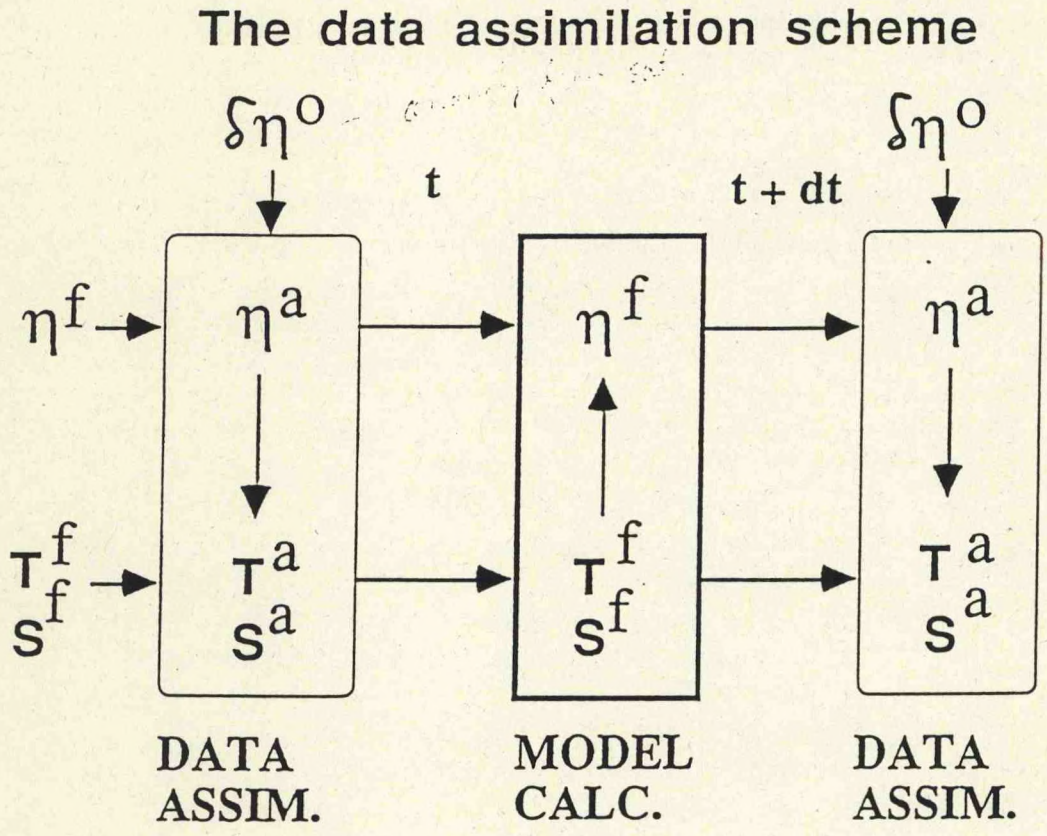
The data assimilation scheme
δη°
t
t + dt
δη°
η^f
η^a
η^f
η^a
T^f
S^f
T^a
S^a
T^f
S^f
T^a
S^a
DATA ASSIM.
MODEL CALC.
DATA ASSIM.

FIGURE 1

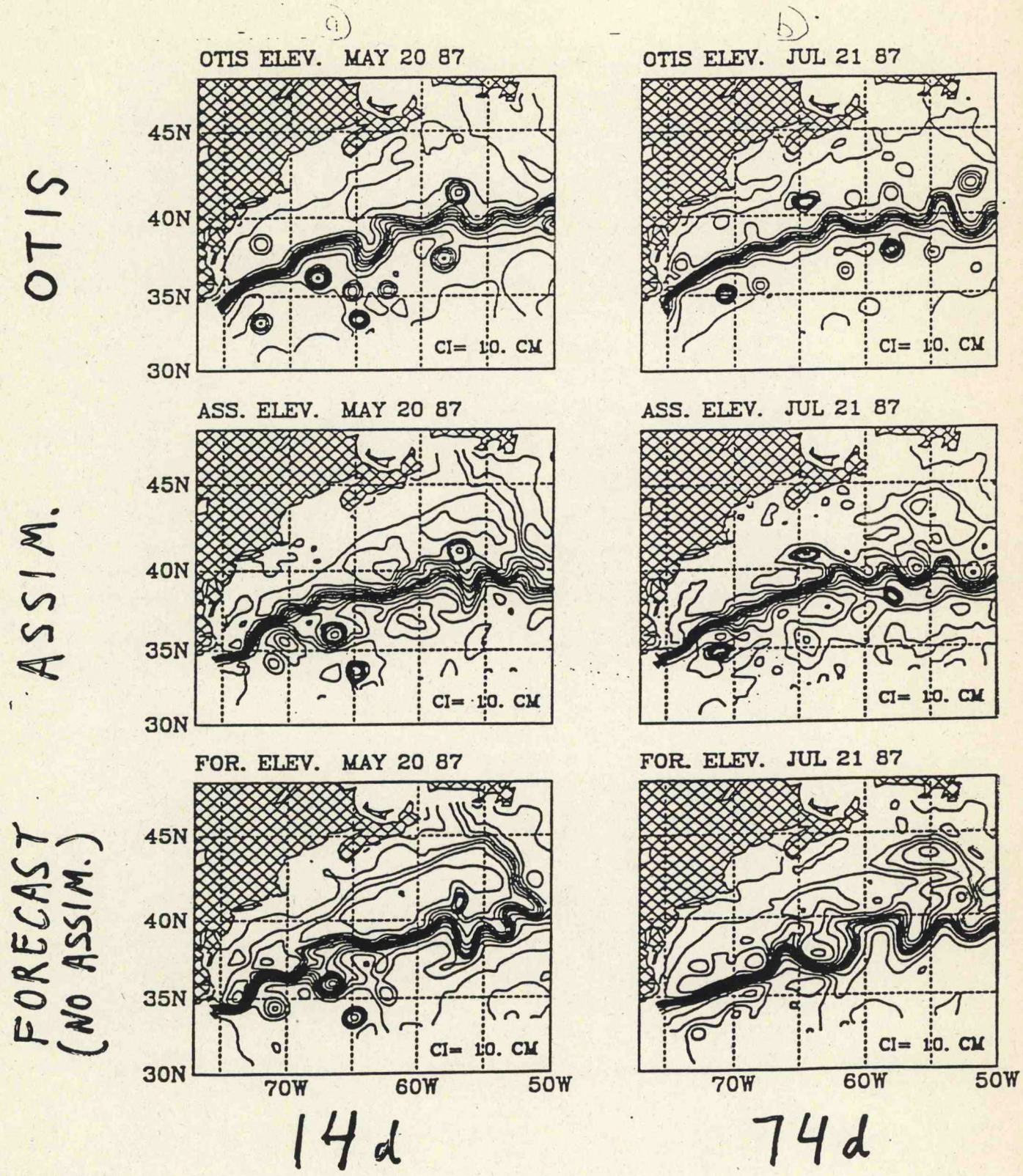
a)
b)
OTIS ELEV. MAY 20 87
OTIS ELEV. JUL 21 87
ASS. ELEV. MAY 20 87
ASS. ELEV. JUL 21 87
FOR. ELEV. MAY 20 87
FOR. ELEV. JUL 21 87
45N
40N
35N
30N
CI= 10. CM
70W
60W
50W
OTIS
ASSIM.
FORECAST
(NO ASSIM.)
14d
74d

FIGURE 2

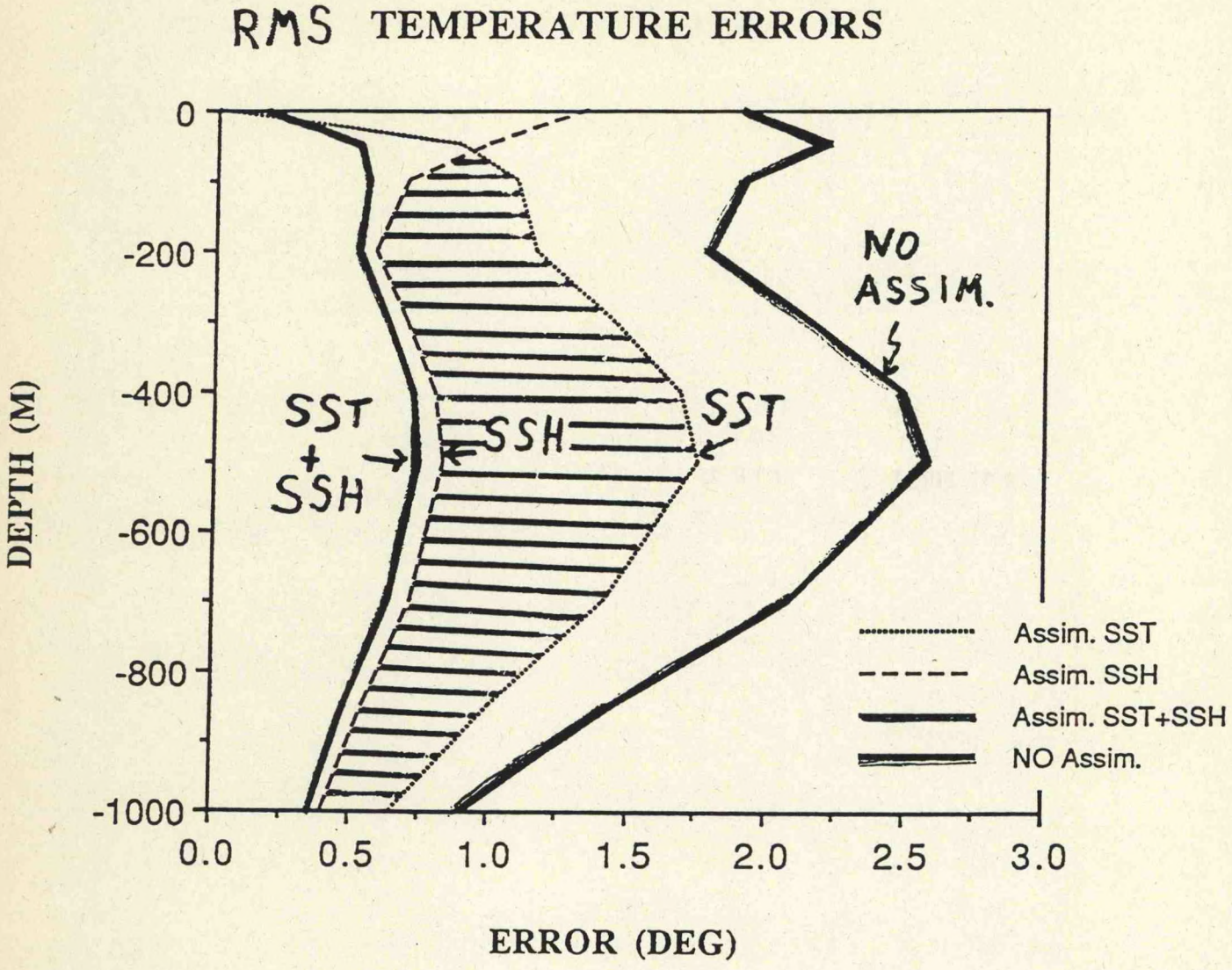
RMS TEMPERATURE ERRORS
0
-200
-400
-600
-800
-1000
DEPTH (M)
0.0
0.5
1.0
1.5
2.0
2.5
3.0
ERROR (DEG)
NO ASSIM.
SST + SSH
SSH
SST
Assim. SST
Assim. SSH
Assim. SST+SSH
NO Assim.

FIGURE 3

Geostationary Satellite Meteorological Instrumentation and Applications

Lecturer: Christopher Hayden
Notes by: Gregory Poulos
David C. Burwell
Date: June 16, 1994

The following topics were addressed in this lecture.

1) Basic radiative transfer
2) Geostationary satellites and their instrumentation
3) Products available from GOES-8 and their application

Radiative Transfer

All life forms rely on the sun to provide energy. The energy is delivered in the form of radiation. Radiation is the only way energy can be transmitted through a vacuum (i.e. outer space). According to the conservation of energy principle, then, the Earth must return the energy it absorbs back to space also in the form of radiation, or else it would continuously heat up. Satellites can measure the various wavelengths of radiation and make inferences about the Earth/atmosphere system.

Radiant energy is created by the motion of molecules (vibration, rotation or translation) and the amount of radiation emitted or absorbed is dependent on wavelength and temperature. The energy is given off in discrete quanta, as described by the Planck relationship (**Fig. 1**) which relates temperature and wavelength to the quanta. In **Fig. 1**, T is temperature, v is frequency, $B_{v,T}$ is energy and C_1 and C_2 are constants composed of various other constants (such as the speed of light and Planck's constant). This equation can be approximated in three useful ways:

1) The Stefan-Boltzmann Law which is found through an integration over all wavelengths of the Planck relationship. This law states that the radiation emitted in Watts/meter^2 is proportional to σT^4, where σ is Boltzmann's constant (5.67×10^{-8} $Wm^{-2}K^{-4}$). The hotter the body the more radiation emitted for a given emissivity.

2) Wein and the Rayleigh-Jeans distributions which consider the high and low limits of frequency in the Planck relation. As frequency approaches infinity Wein's distribution states the radiation is proportional to $\exp(-C_0T)$; in other words, at very short wavelengths the Planck's relationship becomes approximately exponential. For long wavelengths the Rayleigh-Jeans distribution states that radiative emission becomes approximately linear with respect to temperature. The exponential character of high frequency radiation is non-linear such that compared to low frequency radiation the interpretation of its satellite returns is more difficult.

3) Wein's displacement law, which is found by setting the derivative of the Planck relation with respect to wavelength to zero (finding its maximum in this case). This relation reveals that temperature times wavelength is a constant. For hotter objects the wavelength of maximum emission is shorter. **Figure 2** shows the radiance distribution generated by the Planck function for various blackbody (emissivity = 1) temperatures versus wavelength (dashed lines) and the actual measured distribution measured for the Earth (solid line, to be

considered later). Note that the wavelength of maximum emission decreases with increasing temperature in accordance with Wein's displacement law.

Since the Earth is in radiative equilibrium, the incoming solar radiation (termed 'shortwave') is balanced by outgoing terrestrial (termed 'longwave') radiation. The obviously hotter Sun emits primarily in wavelengths shorter than that emitted by Earth. Emission from the Sun is a maximum in a range of wavelengths (near 0.45 micrometers) called the visible spectrum, whereas the maximum radiance from Earth is in the infrared spectrum (near 10.0 micrometers) in the 'atmospheric window'. The total incident radiation from the Sun averages about 1370 Wm^{-2}. If this were to be balanced by only the longwave outgoing radiation at the surface of the Earth the temperature at the surface would be about 280 Kelvin (K). However, as shown in **Figure 3**, the Earth and its atmosphere combine to reflect about 30% of the incoming solar radiation (known as albedo, much due to clouds); the resulting equilibrium temperature considering this reflection is a cold 255K (-18°C). Fortunately, atmospheric absorption and emission raises the surface temperature of the Earth. The atmosphere selectively absorbs and transmits radiation according to its composition (the well-known greenhouse effect) and, as also shown in **Figure 3**, produces an average equilibrium temperature near 286K (+13°C). E is the solar irradiance absorbed by the Earth/atmosphere system (about 241 Wm^{-2}), Y is the irradiance emitted by the surface and atmosphere and a is the absorptivity for solar and terrestrial radiation. **Figure 2** (solid line) shows the absorption by the atmosphere for the region of maximum emittance from the Earth where various absorbing constituents are noted. The atmospheric window is that region of poor absorption near 10 microns as noted in the figure.

Figure 4 introduces Beer's Law which states that transmittance decays exponentially with path length. Thus, for a particular absorbing frequency, the greater the distance through the atmosphere containing the absorbing constituent the less the irradiance at the absorbed frequency. The long Ozone path length in the stratosphere depletes a large portion of incoming harmful ultraviolet radiation in the Ozone layer essentially shielding the Earth's surface. Radiative transfer to a satellite sensor is expressed as the emission from the surface transmitted throughout the atmosphere and the emittance of the atmospheric layers, modulated by the intervening atmosphere. This gives rise to radiative transfer equation shown in simple form in **Figure 2** and again on the bottom of **Figure 4**. The kernel modulating the Planck function (the derivative with respect to pressure term) is usually called a 'weighting' function and describes per frequency the contribution of the atmosphere to the total outgoing radiation as a function of pressure. An example of the weighting functions for the GOES-8 sounder is given in **Figure 5**. Frequencies of observation are chosen such that the atmosphere is sampled by the weighting function (longwave, midwave and shortwave channels near 15, 10-12 and 4 microns, respectively). For a given amount of detected radiation in a spectral channel, the radiative transfer equation is then inverted to estimate the radiance as a function of pressure. A profile of temperature can then be derived with 2-3 km resolution for a significant portion of the atmosphere.

The GOES-8 Satellite

The GOES-8 satellite weighs about two tons and carries half of that in fuel. It is 90 feet long with its solar sail deployed. The primary meteorological instruments it carries are the imager and the atmospheric sounder. These are very similar in operation except for the

filter and detector arrays they utilize. The imager scans continuously right-to-left then left-to-right at 20 degrees of arc per second for its multiple channels (radiation bands it samples). Each scan is split into 1 km resolution for 8 visible spectrum detectors, 4 km resolution for channels 2, 4 and 5, and 8 km resolution for channel 3. The sounder instrument steps through its scan in 0.1 second increments and uses a filter of three concentric bands. The surface resolution of the sounder is about 9 km for the soundings it measures.

3. GOES-8 Products

The most important product of GOES-8 is the imagery. Imagery is used primarily to monitor severe weather and a full disk image can be obtained in 20 minutes. During particularly severe weather events the imager can be trained on a storm over as small as a 1000 x 1000 km area to produce images as often as every minute. The power of this tool is in its animation. The development, direction and intensity of weather can be subjectively determined. Because of the sampling at different frequencies, a number of products too numerous to discuss in detail here can be obtained. A specific application is the detection of supercooled liquid water which is a danger to flying aircraft because it can induce wing icing. Because the emissivity at 3.7 microns is very different for water and ice the satellite can sense the temperature and phase of a cloud to determine where there is supercooled liquid water. Spectral differencing can also detect fog. We may use the split window to create imagery of total moisture, water vapor and atmospheric instability. The animated imagery can also be used to estimate winds at cloud level, by tracking the clouds.

The sounder is used for sounding the atmosphere, obtaining temperature and moisture profiles which may be used in the initialization of numerical models. We have already discussed the fundamentals of remote sounding in Part I, demonstrating that weighting functions allow you to sample the vertical structure of the atmosphere by inverting the radiative transfer equation. The actual retrieval is complicated by variations in vertical concentration of the constituent that is weighted. Whereas uniformly mixed CO_2 creates a relatively unambiguous transmittance profile, water vapor is so unevenly distributed that no such simplification is possible. For this reason a first guess is often used to simplify the sounding retrieval when H_2O vapor values are used. Iteration procedures are used for water vapor channels to adjust the initial guess toward the measured profile and invert the radiative transfer equation toward the integrated radiance in that channel. Large errors can be made because of the widely varying vapor concentration and measurement contamination. The actual resolution of temperature profiles is about 2-3 km.

Reference

NASA/NOAA, 1994: Mission Overview - Geostationary Operational Environmental Satellite (GOES). NOAA/NESDIS, FB-4, Room 0124, Washington D.C. 20233; (301)763-2560.

PLANCK'S LAW

$$B_{\nu,T} = \frac{C_1 \nu^3}{e^{C_2 \nu / T} - 1}$$

R.T.E.

$$R_\nu = \int_0^{p_s} \tau_{\nu,p} dB_\nu\left(T_p\right)$$

$$R_\nu = B_\nu\left(T_s\right)\tau_{\nu,s} + \int_{\tau_s}^{1} B_\nu\left(T_p\right) d\tau_{\nu,p}$$

FIGURE 1

Earth- Atmosphere emitted IR radiation shows Planck emission and molecular absorption spectra

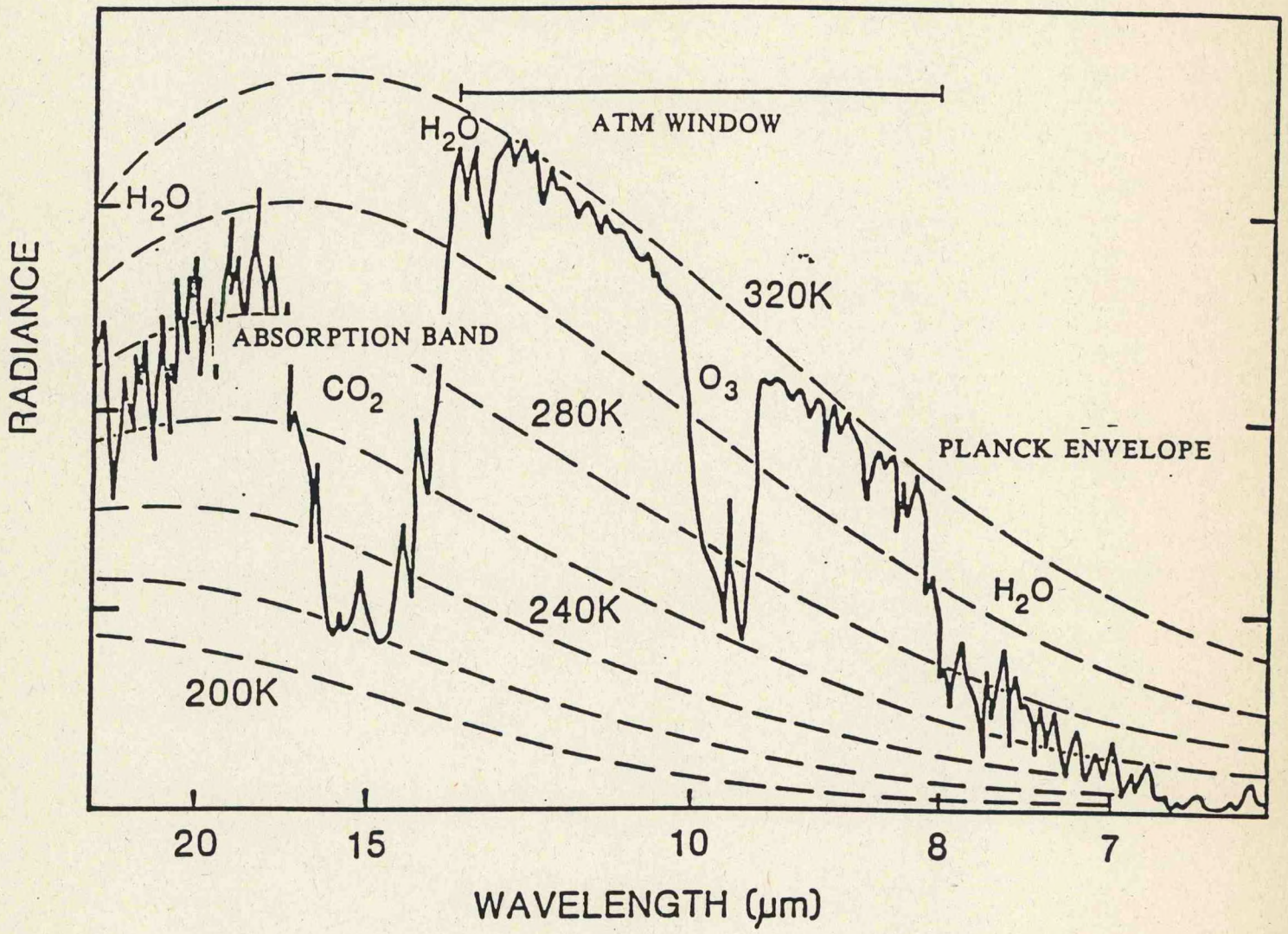

CO_2 is uniformly mixed in the atmosphere, while H_2O varies with time and space

FIGURE 2

Effect of Selective Absorption and Emission

without

effective blackbody temperature of the earth
(assuming .3 of incident radiation is reflected)

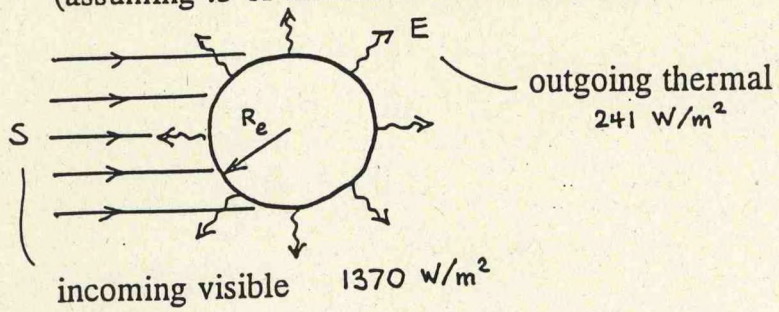

flux in = $S \pi R_e^2 (1-r)$

flux out = $E\, 4\pi R_e^2$

thermal equilibrium implies $E = (1-r)S/4 = \sigma T_s^4$;
$T_s = 255°K$

with

effective blackbody temperature of the earth
(assuming .3 of incident radiation is reflected, and
$a_{IR} = .8$ and $a_{VIS} = .2$)

radiative equilibrium implies

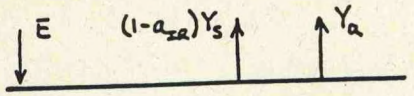

top of the atmosphere

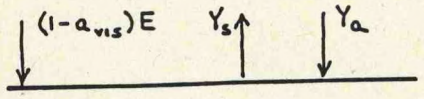

surface of the earth

solving

$$Y_s = \frac{(2 - a_{VIS})}{(2 - a_{IR})} E = \sigma T_s^4 \; ; \quad T_s = 286°K$$

FIGURE 3

Radiative transfer to the satellite sensor is governed by (a) emission from the earth surface transmitted through the atmosphere and (b) emission from the atmosphere layers transmitted through the outer layers of the atmosphere. Transmittance decays exponentially with increasing path length (Beer's Law).

$$\hat{\tau} = e^{-k_\lambda u}$$

k_λ: absorbing power

u: path length

Surface contribution

$$R_\lambda^{sfc} = \epsilon_\lambda^{sfc} B_\lambda(T_{sfc}) \hat{\tau}_\lambda(sfc \rightarrow top)$$

Atmospheric contribution

$$R_\lambda^{atm} = \sum_{layers} \epsilon_\lambda^{\ell} B_\lambda(T_\ell) \hat{\tau}_\lambda(layer \rightarrow top)$$

Together

$$R_\lambda = \epsilon_\lambda^{sfc} B_\lambda(T_{sfc}) \hat{\tau}_\lambda(sfc) - \int_0^{P_{sfc}} B_\lambda(T(p)) \frac{d\hat{\tau}_\lambda(p)}{dp} dp$$

FIGURE 4

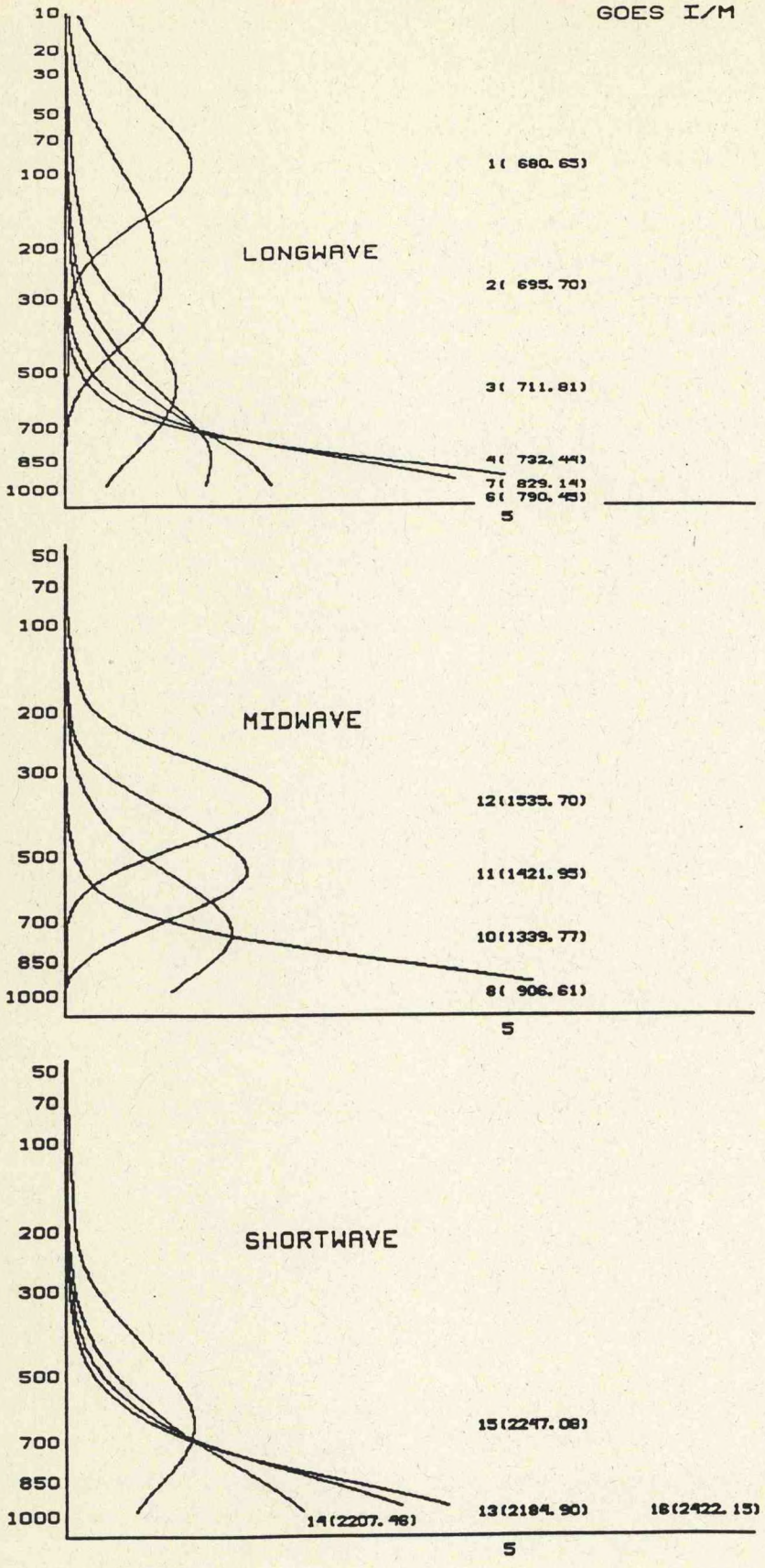
GOES I/M
10
20
30
50
70
100
200
300
500
700
850
1000
LONGWAVE
1(680.65)
2(695.70)
3(711.81)
4(732.44)
7(829.14)
6(790.45)
5
50
70
100
200
300
500
700
850
1000
MIDWAVE
12(1535.70)
11(1421.95)
10(1339.77)
8(906.61)
5
50
70
100
200
300
500
700
850
1000
SHORTWAVE
15(2247.08)
14(2207.46)
13(2184.90)
16(2422.15)
5

FIGURE 5

On the Development of a NOAA Coastal Forecast System

Lecturer: Frank Aikman III
Date: June 17, 1994
Notes by: Nan Schmidt
Xiaofeng Li

Introduction

In the United States, coastal areas are socioeconomically important, comparable in size to the agriculture, forestry, communications, mining, and transportation sectors. Fifty percent of the U.S. population lives in coastal areas, they are commercial hubs, and they are important in terms of fisheries, recreational activities, and sanctuaries for protected habitats and species. In response to the increase in property values, development, and demand for resources in coastal areas, NOAA plans to implement a coastal forecast system (CFS) to help manage coastal areas.

In general, a CFS would help strengthen commerce, help manage living marine resources, help protect life and property (in the event of storms), and help to monitor, predict, and improve environmental quality. In terms of developing a CFS, the long-range goal is to create an operational coastal ocean nowcast/forecast system for U.S continental margin waters that will provide continuous information on wind, surface elevations, temperatures, salinities, currents, and waves. Short-term goals include determining the feasibility of providing useful coastal ocean information by implementation of an operational system, assessing system skill using available data, testing sensitivity to boundary conditions, and assessing the impacts of different data types on the 4-dimensional data assimilation.

Initial modeling will focus on the East Coast, where resources are more extensive. Collaborators include the NOAA's National Ocean Service (NOS), NOAA's National Meteorological Center (NMC), NOAA's Coastal Ocean Program Office, NOAA's Geophysical Fluid Dynamics Laboratory (GFDL), and Princeton University. A CFS does not exist in the United States today, although several European countries including Norway, the United Kingdom, the Netherlands, and Germany currently use CFSs. Components of a CFS are present or being developed in the United States, but serious deficiencies exist with respect to observations (data), modeling, and general knowledge. The CFS as envisioned currently by NOAA (**Fig. 1**) will incorporate 1) an expansion of the network of operational coastal marine and atmospheric observations, which currently is inadequate; 2) operational and coupled ocean and atmosphere models; 3) a research and development component to advance coastal ocean and atmosphere forecast science; and 4) an attention to developing needed and useful products, information, and services.

NOAA's strategy is to begin with whole-coast feasibility studies that will identify observational weaknesses and assess predictability (i.e., for the East Coast, West Coast, Gulf Coast, Gulf of Alaska, and Hawaii), followed by regional demonstrations that will employ nested or imbedded models and use the whole-coast domain for boundary conditions.

Rudiments of the CFS Observations

The types of real-time data needed for the CFS include meteorology, water level, and currents. NOAA currently deploys a network of about 60 coastal meteorological buoys

(operated by NMC's National Data Buoy Center (NDBC)) and 60 C-MAN (Coastal Marine Automated Record) meteorological stations, a tidal gauge network with approximately 200 stations (over half of which provide telemetered real-time observations), and one physical oceanographic real-time system (PORTS) of water level, currents, and meteorological data in Tampa Bay, Florida. Additional PORTS are planned for estuaries/harbors such as New York Harbor and San Francisco Bay. NMC modernization includes establishment of 42 regional meteorological offices linked to NEXRAD (Next Generation Weather Radar) coverage. Satellite-borne sensors also contribute to CFS observations.

Forecasts/Warnings (Figure 2)

Current NOS marine forecast models and products include routine global and regional forecasts of weather out to 2-3 days, 2-day coastal winds at selected locations, 2-day East Coast fog and visibility, and global surface waves from NMC. Current NOS predictions include tidal height and tidal current tables produced annually for U.S navigable and coastal water. "As-needed" predictions by NOS include storm surge associated with extratropical storms (this is a new model that currently is not operational) and hurricane and associated storm surge forecasts.

Services

The CoastWatch program delivers satellite-derived sea surface temperature (SST) products through several regional nodes.

Development of the CFS

A prototype CFS exists as the Great Lakes Forecast System at Ohio Sate University and the Great Lakes Environmental Research Laboratory (GLERL). This system is in the process of testing operational procedures. A joint effort between NMC, NOS, GFDL, and Princeton University is underway to evaluate the feasibility of making predictions in the coastal ocean for the East Coast of the United States using a "one-way" coupled model. The Princeton hydrodynamic model (using a sigma vertical coordinate system and a curvilinear orthogonal horizontal coordinate system) runs operationally at NMC and is being tested by coupling it to surface fluxes from NMC's Eta model (a mesoscale atmospheric model used operationally for weather forecasting). The system currently is being tested for skill and sensitivity to boundary conditions, and it is expected that this effort will indicate deficiencies in both numerical modeling capabilities and observation networks that currently are in place. Skill assessment currently is being done of model operational forecasts using real-time coastal sea level data along the entire East Coast. NOS anticipates developing the following predictive capabilities for the CFS: improving coastal marine weather forecasts; improving coastal fog and visibility forecasts; adding a new suite of predicted oceanic fields derived from operational hydrodynamic models, including 3-dimensional fields of currents, water level, temperature, salinity, and density; and eventually coupling physical models to biochemical, water quality, and ecosystem models.

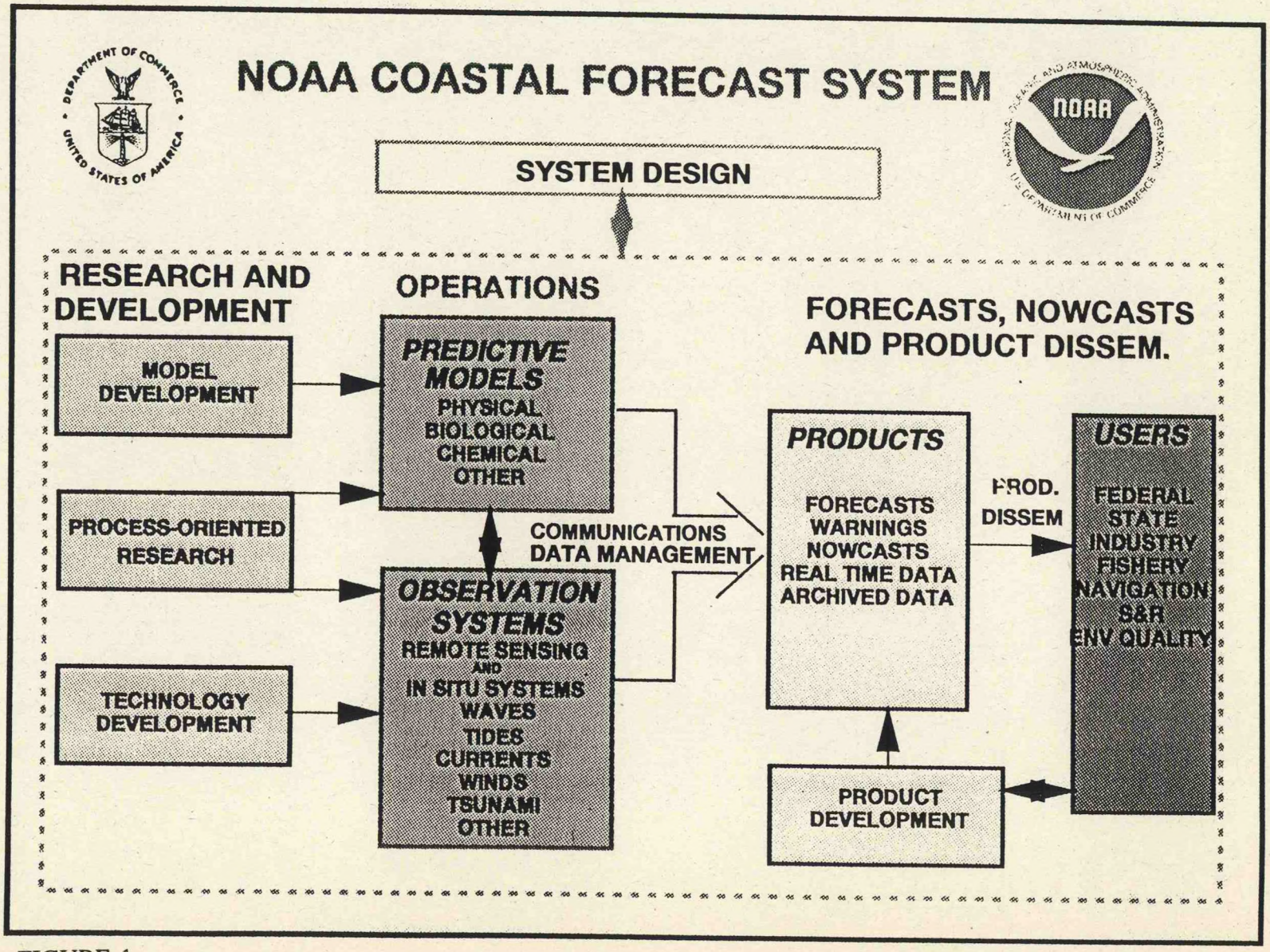
NOAA COASTAL FORECAST SYSTEM
SYSTEM DESIGN
RESEARCH AND DEVELOPMENT
OPERATIONS
FORECASTS, NOWCASTS AND PRODUCT DISSEM.
MODEL DEVELOPMENT
PROCESS-ORIENTED RESEARCH
TECHNOLOGY DEVELOPMENT
PREDICTIVE MODELS
PHYSICAL
BIOLOGICAL
CHEMICAL
OTHER
OBSERVATION SYSTEMS
REMOTE SENSING AND IN SITU SYSTEMS
WAVES
TIDES
CURRENTS
WINDS
TSUNAMI
OTHER
COMMUNICATIONS
DATA MANAGEMENT
PRODUCTS
FORECASTS
WARNINGS
NOWCASTS
REAL TIME DATA
ARCHIVED DATA
PROD. DISSEM
USERS
FEDERAL
STATE
INDUSTRY
FISHERY
NAVIGATION
S&R
ENV QUALITY
PRODUCT DEVELOPMENT

FIGURE 1

CURRENT MARINE FORECAST MODELS/PRODUCTS

Forecast Model	Horizontal Resolution	Cycles	Forecast Horizon	Lowest Layer Thickness
1. Global Aviation	~100 km	2/day	3 days	10 mb
(Surface Winds)		1/day	10 days	------
2. Regional (NGM)	~ 80 km	2/day	2 days	35 mb
(N. Hemisphere only)	(Coastal US)			
3. Hurricane	~ 40 km	As needed	3 days	20 mb
4. East Coast Fog/Vis.	~ 80 km	2/day	2 days	25 m
(Diagnostic)				
5. Coastal Winds	Selected	2/day	2 days	------
(Statistical)	Locations			
6. Global Waves	2.5° x 2.5°	2/day	2 days	------
(deep water - spectral)				
7. Gulf of Mexico Waves	~ 50 km	2/day	2 days	------
(shallow water - spectral)				
8. Sea Ice Edge Movement	-----	1/week	7 days	-----
(Arctic)				

9. Extratropical Storm Surge
   - Based on statistical analysis of historical storms;
   - used operationally at 11 East Coast stations;
   - uses NGM output.

10. SLOSH (Sea, Lakes, and Overland Surges from Hurricanes)
   - applied regionally, as needed, over about 200 miles of coastline;
   - as a planning tool and for forecasts.

11. Tide Height & Current Predictions
   - annual tables for all navigable US waters
   - tidal height based on measured tidal constituents
   - tidal current based on circulation surveys
   - global tables also produced

12. Tsunamis - time of arrival warnings in Pacific

FIGURE 2

Wave Interaction with Coastal Structures and Shorelines

Lecturer: John Ahrens
Date: June 17, 1994
Notes by: Cheng-Hsuan Lu
Xiaofeng Li

Problems and Motivation

The most pervasive erosional force exerted on the coastal zone is due to the sea-level rise (Dean, 1988). How the sea level rise pose influence on coastal zone and shorelines will be discussed in section 2. In an era of rising sea level and high coastal population, it is important to study the response of the shoreline and structures on the shorelines to waves. Greatly increasing coastal population and the associated infrastructure and economic activity make this topic urgent to deal with. Another problem associated with sea level rise is that as the sea level rises the water levels in the Great Lakes fluctuate in unpredictable ways.

There are two possible solutions for it. The first one is to abandon and retreat the coast, which is reluctant by most residents (at least in the U.S.). The second choice is to defend the coast, which will be discussed in section 3.

Sea level rise

It is easy to underestimate the influence of sea level rise on coastal problems because sea level rise is measured in the order of mm/year. However, it is a highly leveraged process, e.g.,

a). beaches - sandy ocean beaches would be expected to erode about 1 m for every cm of sea level rise.
b). dunes - dune erosion is very sensitive to water levels.
c). wetlands - wetlands are very sensitive to water levels, Louisiana loses about 1%, about 100 km^2, of wetlands for every 1 cm sea level rise.
d). saline wedge - wedge of saline water through estuaries and tidal rivers may advance about 1 km for a 10 cm rise, which will threaten municipal drinking water supplies, especially during periods of drought.
e). salinity intrusion - salinity intrusion into coastal aquifers has a very large amplification factor.
f). seawalls - seawall overtopping is very sensitive to sea levels, Ahrens (1991).

Shoreline protection

Since it is not feasible to retreat and abandon the coast, defending the coast becomes the only way to handle the sea level rising. The problem of high coastal population densities and rising sea level is not unique to the U.S. Some other countries, such as Dutch, have a lot of experience in defending the coast and intend to maintain the 1990 shoreline.

Table 1 lists the categories of protection:

a) hard - seawalls, revetments, bulkheads.
b) transitional - offshore breakwaters, groins, perched beach.
c) soft - vegetation, beach nourishment, dunes, submerged mounds, dynamic

revetments.

d) hybrids - beach nourishment with offshore breakwaters or groins or both.

Beach nourishment, sometimes in conjunction with other types of protection, is going to be the preferred type of defense in the future. Recreation and esthetics are important additional benefits for this type of protection. To date about 640 km of U.S. coast have been nourished at a cost about $8 billion. The first beach nourishment project in the U.S. was at Coney Island, New York in 1992. Beach nourishment is not a simple one dimensional category of protection and it must be considered in conjunction with a number of other items, which include:

a). cost
b). sources of sand - offshore, land, bypassing, dredging
c). dune building/grass planting
d). offshore breakwaters
e). offshore dredged mounds
f). new dredging and navigation technology
g). inlet dynamics, sand bypassing, and ebb-tidal shoals
h). gravel alternatives

How to determine the strategy to defend the coastal zone is a complicated issue. Several items (eg. cost, protection of wetlands, recreation value, ...etc.) need to be considered in order to find an optimal approach.

References

Ahrens, J.P., and Bender, T., 1991: Evaluating the Performance of Seawalls. *Proceedings of the Conference on Coastal Structures and Breakwaters '91*, Institution of Civil Engineering, London, Nov. 1991.

Dean, R.G., 1988: Managing Sand and Preserving Shorelines. *Oceanus*, **31**, No. 3.

TABLE 1

Type of Coast	Categories of Shoreline Protection		
	Hard		Soft
Exposed	Seawalls		Beach Nourishment Dunes
			Submerged Mounds
		Offshore Breakwaters	
	Riprap Revetment	Sand	Vegetation with Low-Cost Structures
	Other Revetments	Plants	Vegetation
			No Structure
Sheltered	Bulkheads		

Marine Forecasts for the Great Lakes

Lecturer: David Schwab
Date: June 17, 1994
Notes by: Alec Richardson
Axayacatl Rocha-Olivares

Great Lakes Marine Forecasting

The most advanced coastal modeling system presently operated by NOAA is the Great Lakes Marine Forecasting (GLMF) program. Dynamic water-atmosphere interactions observed in the Great Lakes can be considered a smaller scale analog of oceanic coastal phenomena. Of particular relevance among NOAA's responsibilities involved in the GLMF program, is the prediction of hazardous marine conditions, in particular storm surges and seiches, also known as standing waves.

Storm Surges and Seiches

Storm surges and seiches are wind-forced surface generated phenomena which involve drastic changes in water level at different time scales. Storm surges are the immediate result of wind-forcing on the lake surface; they intensify as turbulence escalates to larger spatial scales; and they are limited to the duration of the generating storm. In contrast, seiches can be experienced by the shoreline posteriorly to the abatement of storm activity. A seiche is a periodic oscillation of the water level as it returns to equilibrium after an initial disturbance. Because of the time lag between high winds and seiches, they can be more dangerous than surges for they may strike the coastline without warning some period after a storm.

The storm surge height is directly proportional to the windspeed squared and water basin length, and it is inversely proportional to channel depth. Because Lake Erie is relatively long (400 km) and shallow (20 m), compared to the other Great Lakes and basins, it can generate a larger storm surge height for a given wind speed. Automated storm surge forecasts are regularly conducted at 4 locations: Essexville, Lakeport, Toledo, and Buffalo. Storm surge records from Buffalo and Toledo, spanning the period 1940-1972, show that the most frequent surges are between 2 and 2.5 ft high and occur about 12 times per year.

Numerous 1-D and 2-D storm surge prediction models have been developed in order to predict the occurrence and magnitude of storm surges along the coasts of the Great Lakes. The surface winds from the weather forecast of a regional atmospheric model is used as the forcing function to drive the marine forecasting model (MFM). Thus, the accuracy of the marine forecasting model is directly dependent of the accuracy of the weather forecast.

A high resolution rectangular grid is typically used in the execution of the MFM model. The output includes hourly predictions of water level fluctuations out to 36 hours. Excellent agreement is generally obtained between the MFM's prediction data and the observed data of storm surges in the Great Lakes.

Wind-Generated Waves

The goal of 2-D wave models is to predict wave properties at all points in the water basin synoptically, and they differ from 1-D models in that the results for a given subregion

depend on the results of neighboring subregions, in addition to the local windspeed and fetch. Generally, wave height is a highly nonlinear function of windspeed and fetch.

The more sophisticated spectral models calculate a wave energy budget in each subregion for a complete set of directional and frequency bands covering the entire wave energy spectrum. The spectral wave model involves the solution of a substantial time derivative of the total wave energy as a function of group velocity, energy input from the wind, energy dissipation due to wave breaking and shoaling, a nonlinear interaction term between components of the wave spectrum, and an additional term including shallow water effects such as shoaling.

The JONSWAP (Joint North Sea Wave Program) 2-D wave prediction model fully characterizes the spectral wave energy as a function of 3 parameters: total energy in the wave spectrum, peak energy frequency, and a single average propagation direction. The forcing function for the model is the observed wind profile over the water surface. An empirical equation is used which relates wind stress at the sea surface to wind speed, phase speed, and a drag coefficient.

One of NOAA's advanced operational Great Lakes wave forecast model is the GLERL/Donelan wave model, which is a 2-D, time-dependent, parametric model which solves the local momentum balance equations in a grid of a given horizontal resolution. These momentum balance equations are solved for 3 parameters: wave height, period, and direction. The model is run forward in time using a finite differencing scheme. Wave height predicted with the GLERL model show a high degree of similitude with the observed data.

Comparisons of predictions of wave height and wave period as a function of fetch, made by numerous 1-D wave prediction models (SMB, JONSWAP, and Donelan) and a 2-D model show that all the models are within 10% of each other (**Fig. 1**). The 2-D model's predictions are intermediate between those of the 1-D models. Comparisons of observed and predicted wave heights (**Fig. 2**) have shown a strong agreement which gives strong credibility to the model and demonstrates its strength in describing the highly complex nonlinear interactions between winds and wave generation mechanisms.

The Great Lakes Forecasting System (GLFS)

The purpose of the Great Lakes Forecasting System (GLFS) is to implement a prototype operational system for making short range forecasts of water currents, temperatures, wind-generated waves, and water level. Uses of the GLFS include hazard forecasting (e.g. storm surges and seiches); enhancement of commercial and recreational activities; scenario testing, design, and risk assessment; and activities involving preservation of resources. The input data driving the GLFS models include surface wind field observations and forecasts, surface water temperature (obtained from both in situ and satellite), surface heat flux, water levels, tributary inflows, and bathymetry (**Fig. 3**). The data acquisition is based on the Great Lakes Marine Observation Network (GLMON) which has onshore and offshore stations located throughout the 5 Great Lakes.

Because the observational data may not coincide with the spatial and temporal resolutions utilized by the models, a series of interpolations are required to initialize them. The initialization involves calculations of surface wind stress and sensible heat flux, in addition to model evaluation and skill tests. Wind stress is the most important short term forcing function, whereas heat flux is the most important at longer time time scales. The

calculated output from these models includes a 3-D water current circulation and temperature fields, thermal structure, surface water level field, wind field (windspeed and direction), wave field (wave height and direction), a 3-D sediment field, coastal erosion potential, and water level (hydrologic) changes over time.

The GLFS model output is supported by in situ (e.g. buoy and ship observations) and remote (e.g. satellite) observational data. In the future, it is planned to couple this model with a regional atmospheric circulation model (Eta) to incorporate more realistic physics into the water-atmosphere interface and improve its forecasting performance.

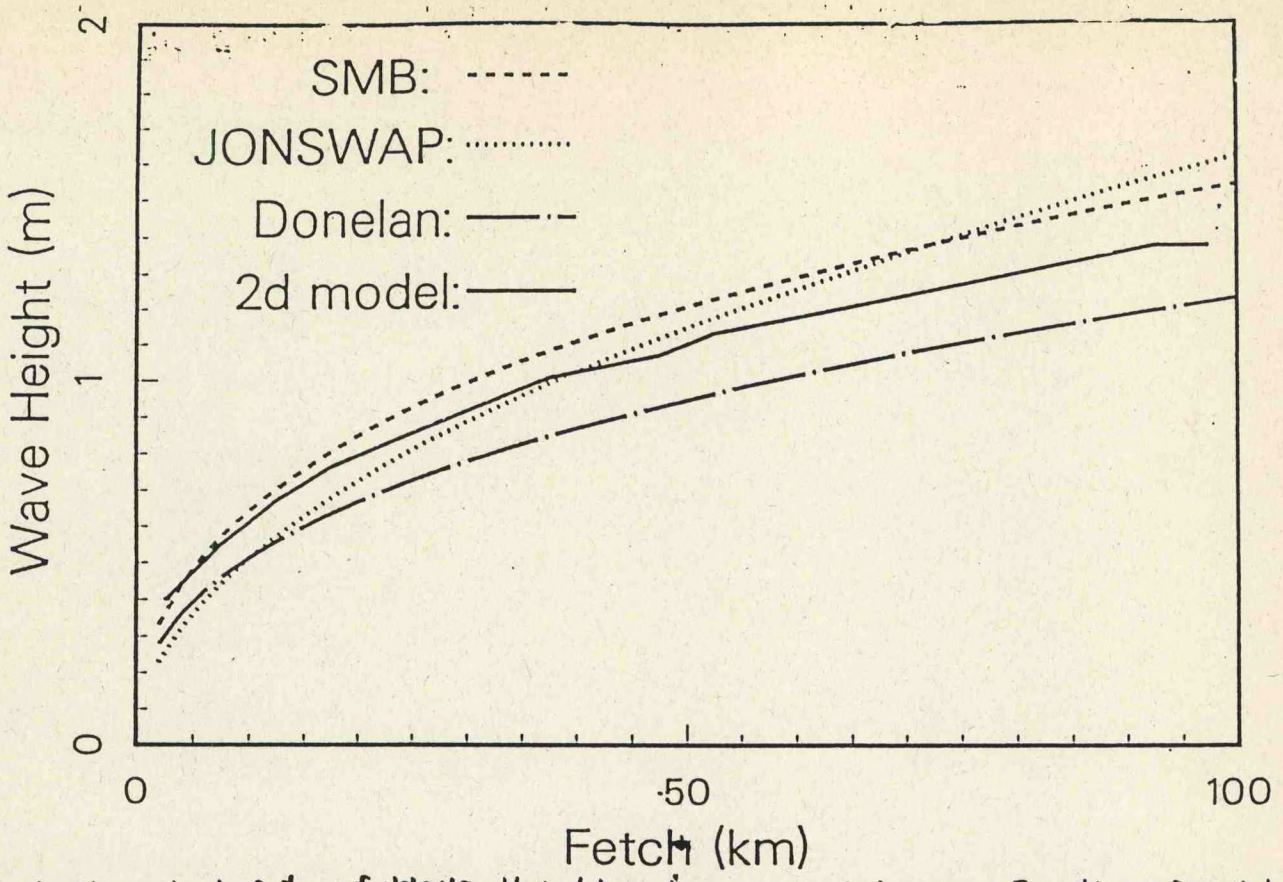

Fig. 1: Numerical Data of Wave Height and Wave Period as a Function of Fetch, Generated by Several 1-D Models (SMB, JONSWAP, Donelan) and a 2-D Model.

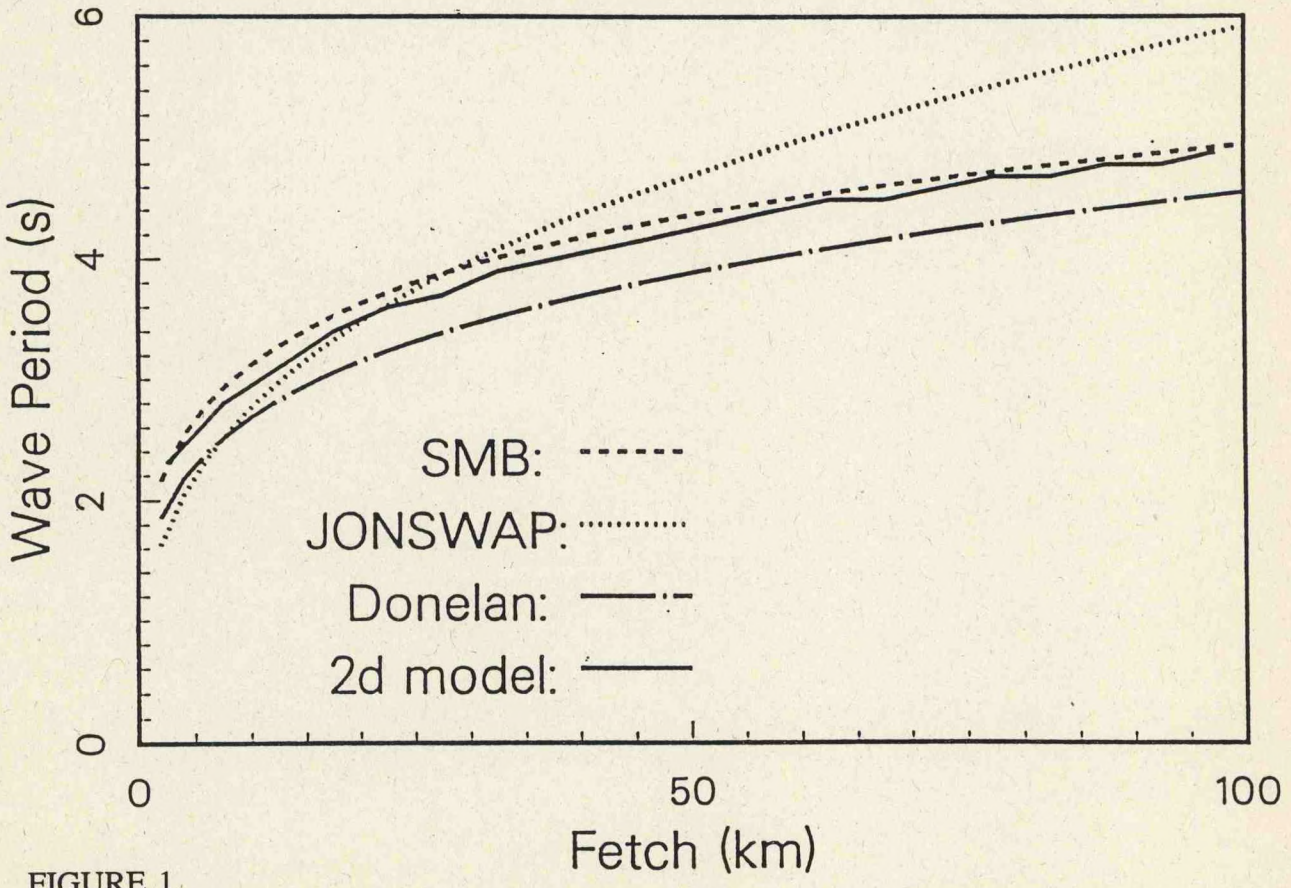

FIGURE 1

FIGURE 2 Comparison of Wave Height Data Generated from the Marine Forecast Model (MFM) with Observed Data for Lake Michigan (Nov. 1977).

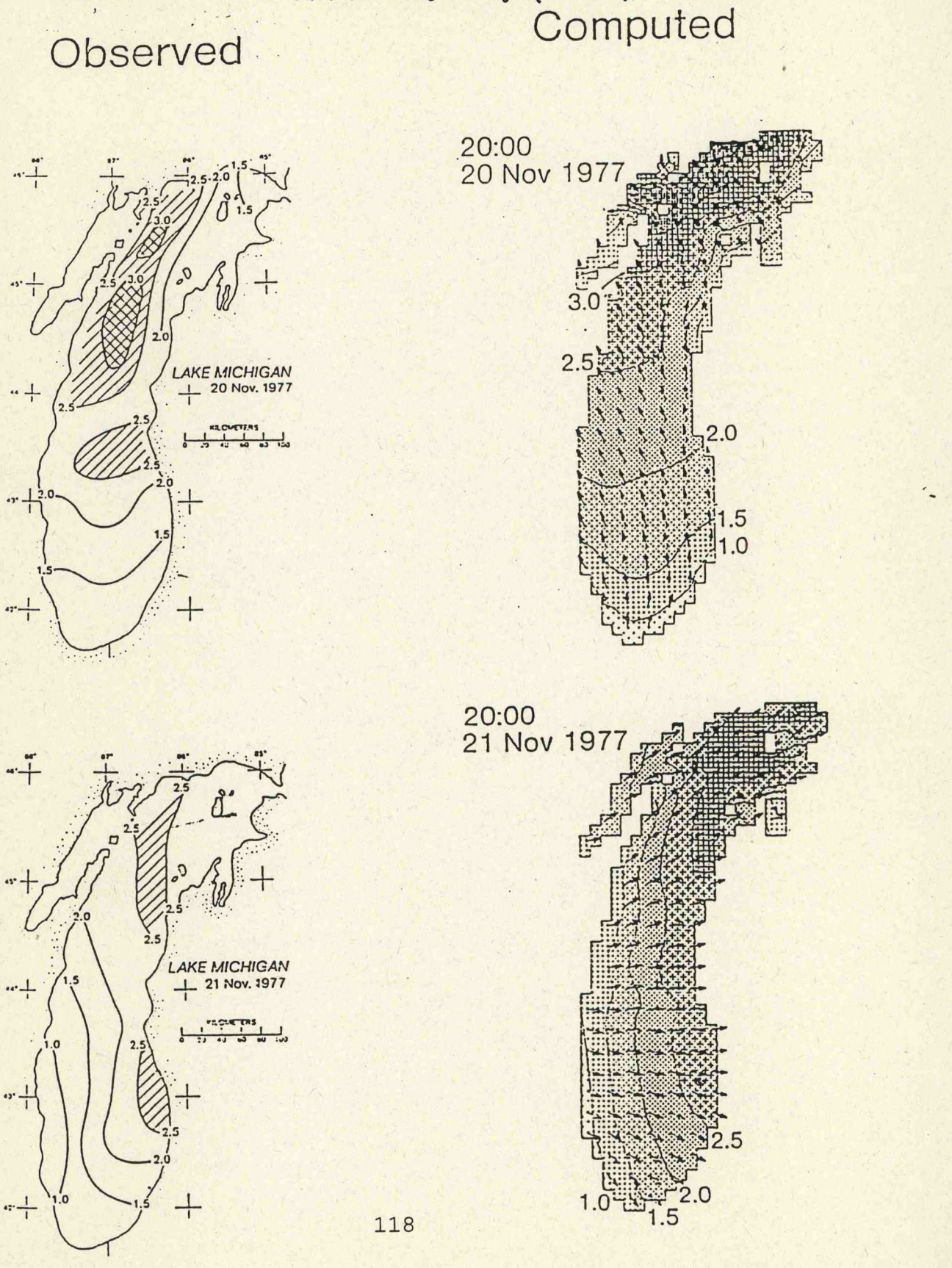

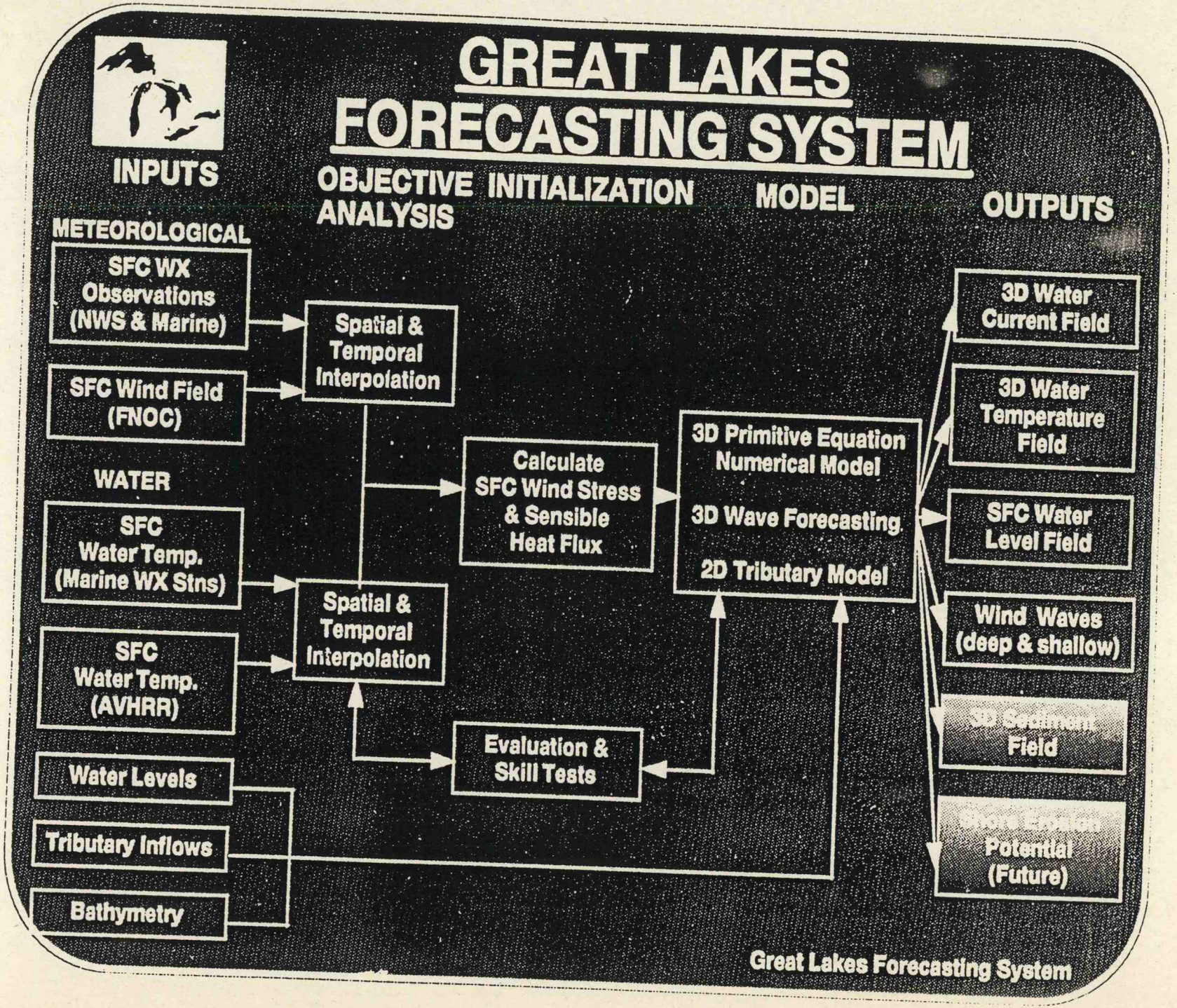

FIGURE 3 Schematic outline of the Great Lakes Forecasting System (GLFS), Illustrating Inputs, Objective Analysis, Initialization, Model and Outputs.

Nutrient-Enhanced Coastal Ocean Productivity (NECOP): Predicting Hypoxia and Effects on Benthic Populations

Lecturer: Nancy Rabalais
Notes by: Nan Schmidt
Axayacatl Rocha-Olivares
Date: June 20, 1994

Introduction

Close linkages exist between freshwater inflow (and subsequent nutrient flux), net surface water production, and bottom water oxygen deficiency on the Louisiana continental shelf adjacent to the Mississippi and Atchafalaya River deltas. Long-term trends in and the responses of the various components of the ecosystem to changes in nutrient structure (riverine and continental shelf) document these linkages.

Oxygen-depleted bottom waters are seasonally dominant features of this portion of the Louisiana continental shelf. The aerial extent of bottom-water hypoxia (< 2 mg/l dissolved oxygen) in mid-summer may be up to 9,500 sq. km. Sampling transects and time series data document hypoxic bottom waters as early as February and as late as October, with widespread, persistent and severe hypoxia/anoxia from mid-May to mid-September. Spatial and temporal variability in the distribution of hypoxia is, at least partially, related to the amplitude and phasing of Mississippi River discharge and, consequently, to nutrient flux to coastal waters and subsequent carbon flux from surface waters to the lower water column and seabed. Physical features of the system (large-scale circulation patterns, strong and persistent density stratification, and destratification due to wind-mixing events) also control the dynamics of hypoxia. The influence of Mississippi outflow was particularly notable during the later spring and summer of 1993, because sustained freshwater inputs and nutrient flux occurred when flows are usually lowest.

The seasonal dynamics of net productivity in the northern Gulf of Mexico are coherent with the dynamics of freshwater discharge. The surface layer in the Gulf shows an oxygen surplus during February-July; the maximum occurs during April and May and coincides with the maximum flow of the Mississippi River. The bottom layer, however, exhibits an oxygen deficit throughout the year but reaches its highest value in July, when surface-to-bottom density differences are greatest. There is a one-month time-lag between Mississippi River flow and surface oxygen surplus peaks and a two-month time-lag between river flow and bottom oxygen deficiency. This suggests that the oxygen surplus in the surface layer depends on nutrients from the river rather than regenerated nutrients from the water column or sediments. The oxygen surplus also means that there is excess organic matter derived from primary production that may be redistributed within the system, some of which will eventually reach the lower water column and sediments. The development of summer hypoxia is associated with the decay of organic matter accumulated during spring phytoplankton blooms. These findings demonstrate the close coupling between riverborne nutrients, net productivity, and hypoxia, as well as the implications that anthropogenic nutrient loads can alter a coastal marine ecosystem.

Characteristics of hypoxia: 1993 vs. long-term averages

Above normal freshwater inflow and nutrient flux from the Mississippi and Atchafalaya Rivers from late spring well into mid-summer, when flows are usually lowest, clearly were related in time and space to hypoxic water formation and maintenance on the Louisiana-Texas shelf through October 1993. A series of frontal passages with high winds and seas, thermal cooling of the surface water,and subsequent breakdown in the strength of water-column stratification lead to the dissipation of hypoxic conditions. Nitrate, silicate, phosphate, and surface water chlorophyll a concentrations in surface waters are normally elevated in the spring but in 1993 continued at higher than normal levels through the summer. Bottom water dissolved oxygen values were similar to normal levels in spring 1993 but extensive areas remained anoxic for extended periods in August and September. On a shelfwide scale, surface water signatures of less saline, nutrient-rich, and high chlorophyll a biomass waters paralleled the sustained and high freshwater outflow of the flooded Mississippi River. During late July 1993 surface water nutrient concentrations were especially elevated on the southeastern shelf, as was chlorophyll a biomass.

Effects on benthic and demersal communities

The response of benthic organisms and communities to a reduction in near-bottom water dissolved oxygen levels depends on the duration and severity of the event. Benthic macroinfaunal populations are drastically reduced in species richness and abundance of individuals, especially when dissolved oxygen levels fall below 0.5 mg/l. High percentages of juveniles in the population and reduced biomass indicate that the macroinfaunal populations are maintained in an early successional state by the annually recurring hypoxia.

Water quality changes in the lower Mississippi River

The mean annual concentration of nitrate was approximately the same in 1905-1906 and 1933-1934 as in the 1950s but doubled in the past 35 years. The mean annual silicate concentration was approximately the same in 1905-1906 as in the 1950s but declined by 50 percent in the past 35 years. Although the concentration of phosphorus appears to have increased since 1972, variations between years are large. The proportions of dissolved Si, N, and P in the lower Mississippi River have changed historically in such a way that they now closely approximate the Redfield ratio (Si:N:P=~16:16:1), suggesting a balanced nutrient structure.

The seasonal pattern in nitrate concentration has changed in a manner presumably related to seasonal agricultural activities (i.e., fertilizer application) timed with long-term peak river flow such that there is a spring peak.. A seasonal summer-fall maximum in Si concentration, in contrast, is no longer evident. The seasonal shifts in nutrient concentrations and ratios become increasingly relevant in light of the close temporal coupling of river flow to surface water net productivity and subsequent bottom water oxygen deficiency.

Nutrient structure of adjacent continental shelf

Comparisons of measured Si, N, and P concentrations with reconstructed and validated data from the Northern Gulf of Mexico revealed long-term changes in the proportions of surface water nutrients. The trends observed pointed towards a decrease in P and N deficiency and an increase in Si limitation. Recent nutrient concentrations were found to be scattered very close to the Redfield ratio, suggesting a close-to-balance nutrient structure. By comparing the ambient nutrient concentrations with parameters relevant to the nutrient-uptake dynamics by primary producers, a probable limitation was assessed. Results for the period 1985-1992 indicated that 13%, 17%, and 25% of the cases were below 1 mM, 0.1 mM, and 2 mM for dissolved N, reactive P and reactive Si concentrations, respectively.

Changes in phytoplankton species composition

A qualitative comparison of published reports of phytoplankton species composition (1955-57, 1972-73) with recent data indicates that (1) changes have occurred in the phytoplankton species composition in the three data sets with the observed trend being a reduction in the abundance or absence of heavily silicified diatoms; (2) more lightly silicified diatoms, especially at higher salinities, were found in the 1970s and present only; and (3) due to methodological limitations, the non-diatom fraction of the phytoplankton community could not be compared with the historical records. However, the numerical importance of flagellates and cyanobacteria (blue-green algae) in some recent samples and the increasing occurrence of species that threaten human health, together with the above comparisons, support the hypothesis that changes in the riverine and coastal nutrient concentrations and ratios may be having an effect in the phytoplankton community.

Silicate-based phytoplankton community response

Statistical modeling of Si uptake in the Mississippi River plume, involving the quantification of the departure from conservative mixing of two water end-members (riverine and marine) in a mixing diagram, indicates that the concentration of Si at the 20 ppt mixing point declined in the last several decades during the winter-spring and summer months. However, there was no discernible change during the fall and winter. Normalization for the effects of varying concentrations in the riverine end-member allows comparison of Si uptake as a function of Si end-member concentration. This results show that although Si concentrations have declined in the past few decades, the net uptake by phytoplankton has not changed or has even increased.

Biologically bound Si and C accumulation

Surficial sediments directly downstream and beneath the surface riverine/estuarine dilution plume were found to reflect the in situ primary production and subsequent sedimentation of organic matter within the Mississippi River bight. A time series of the percentage of biologically bound Si (BSi) obtained from dated sediment cores of this region showed an equilibrium accumulation throughout the last century, followed by a slow rise and a steeper increase in the past two decades. During this period, a parallel increase in N loading

in the river has been recorded simultaneously with the decrease in Si concentrations. Assuming a constant BSi:C ratio, it can be concluded that the sinking organic flux of diatoms to the sediments beneath the Mississippi River plume has increased. Up to 43% higher C deposition rates were found in cores dated after 1980 than in those dated between 1900 to 1960.

Consequences of hypoxic bottom water formation and severity

Shifts in species abundance of some benthic unicellular organisms (foraminifera) were interpreted as responses to increasing oxygen stress. In the context of modern hypoxia, species distribution in dated sediment cores indicated an overall increase in oxygen stress, whether in intensity or duration, in the last 100 years. This stress has been more severe since the 1950s. The use of these organisms as biological indicators points to an increase in hypoxia-related stress as nutrient loads and C flux to the sea bed have increased.

Predictions

The amount of dissolved nutrients in the Mississippi River may be influenced by management and economic decisions with consequences to the Mississippi River delta ecosystem. If riverine P is reduced, it is predicted that the rate of sequestering of BSi in freshwater sediments will decrease so that the release of dissolved Si from the sediments will return to exceeding the decrease of dissolved Si from the overlying water column. This would result in a decrease in diatom production and an increase of Si runoff onto the adjacent continental shelf. At the same time, controls on N use and loading within the watershed may or may not be affected. Several scenarios can be envisaged based on the biological consequences of documented historical riverine changes. If N concentration remains unchanged, there would be an increase in BSi and C accumulation in the sediments, increasing the severity of the hypoxia. If N concentration increases, the above prediction would be accentuated. If N loading is reduced, however, (e.g. to 1950s values) N would return to a limited status restricting the sequestering of Si and the hypoxia levels.

Because of the close coupling between riverine nutrient loading and phytoplankton production, reversal of the current effects of eutrophication and nutrient ratio changes depends on the degree to which effluent water quality may be modified. However, the efficiency of the management of any one nutrient (Si or N) may be compromised by eventual compensatory changes in the phytoplankton community, included those related to noxious or toxic species.

References

Justic', D., N. N. Rabalais, R. E. Turner, and W. J. Wiseman, Jr. 1993: Seasonal coupling between riverborne nutrients, net productivity, and hypoxia. *Marine Pollution Bulletin*, **26**, 184-189.

Justic', D., N. N. Rabalais, and R. E. Turner, 1994. Riverborne nutrients, hypoxia, and coastal ecosystem evolution: biological responses to long-term changes in nutrient loads carried by the Po and the Mississippi Rivers. In K. Dyer, ed., *Changes in Fluxes in Estuaries: Implications from Science to management.* Proceedings, ECSA22 Symposium, Joint ECSA/ERF Conference. International Symposium Series, Olsen & Olsen, Fredenberg, Denmark.

Justic', D., N. N. Rabalais, R. E. Turner, and Q. Dortch, 1994: Changes in nutrient structure of river-dominated coastal waters: Stoichiometric nutrient balance and its consequences. *Estuary and Coastal Shelf Science* (in press).

Predicting Nutrient and Productivity Processes in Outflow Regions of the Mississippi River

Lecturer: Steve Lohrenz
Date: June 20, 1994
Notes by: Alec Richardson
Axayacatl Rocha-Olivares

Nutrient Processes

The prediction and modeling of nutrients and primary productivity in aquatic ecosystems may be approached as a mass balance problem. This balance must include all relevant inputs and losses of a particular nutrient. Sources into the water column can be categorized as *autochthonous* (generated in the zone of their consumption) or *allochthonous* (generated elsewhere). Nutrient inputs to the marine environment include: fluvial runoff, water circulation (advection and diffusion), atmospheric sources (deposition and biogenic fixation), and regeneration processes (pelagic and benthic). Loss terms include ocean circulation processes (generally difficult to measure) and biological uptake and consumption. Of the above, only regeneration (source) and consumption (loss) have a potential for predictive purposes. Primary production appears to be the dominant mechanism of biological nutrient consumption (**Fig. 1**).

Time series analysis of river discharge and nutrient concentrations (NO_3) show that their variations are out of phase. While discharge may be easy to predict, nutrient concentrations are not, therefore nutrient flux into the marine environment is difficult to forecast. A factor contributing to this complexity is the presence of many processes having to be quantified in order to fully describe the dynamics of nutrient uptake and utilization. Direct atmospheric input is a negligible source of nutrients in coastal zones but regeneration from particles sinking on the continental shelf is significant in both the water column and sediments, where oxidative remineralization of particles may generate conditions of oxygen deficiency (hypoxia).

Biological Consequences of Nutrient Enrichment

Important biological consequences of nutrient enrichment of the surface waters include: (1) *Enhanced primary production and phytoplankton biomass*, caused by the release of nutrient limitation, to which phytoplankton is usually subjected in the marine environment. (2) *Enhanced secondary production*, produced by a higher availability of phytoplankton to the higher trophic levels. (3) *Enhanced sedimentation of particulate organic matter*, resultant from the increased production of organic matter at all trophic levels. (4) *Increased consumption of dissolved oxygen in the deep waters*, resulting from the larger rainfall of particulate organic matter settling to the bottom and being remineralized by oxidative bacteria.

Assessment and Prediction of Primary Production

Primary production, the process by which inorganic nutrients and carbon are converted into organic matter, is a fundamental biological characteristic of marine ecosystems. Accurate

and reliable measurements of primary production are required because: (1) it has a direct relationship with the metabolic photosynthetic assimilation of nutrients; (2) it has direct implications for the production of organic matter, eutrophication, and oxygen demand; (3) of its relevance as the base of the trophic pyramid and its subsequent influence to fisheries; (4) of the role of highly productive coastal ecosystems in the global carbon balance.

Primary production is measured using different techniques including: (1) Incubations which measure either the photosynthetic uptake or release of radiolabeled CO_2 or O_2, respectively. This method is labor intensive and discrete in time and space, it has limited predictive utility but is useful for process studies. (2) Geochemical tracers such as oxygen, argon, and dissolved inorganic carbon species of the system.

In addition to direct measurements, primary production has been modeled using bio-optical algorithms. Incorporated in these algorithms are adjustable parameters which govern the physical and biological mechanisms involved in the photosynthetic process. The variables include: irradiance, photosynthetic pigments, nutrients, phytoplankton species composition, and water temperature and salinity. A photosynthesis-irradiance model revealed seasonal variability in the coupling between riverine nutrient inputs and primary production, providing evidence that biological consumption was more efficient during late spring and summer. Observed data may be collected by in situ (e.g. ship observations and buoys) or remote sensing methods (e.g. Coastal Zone Color Scanner -CZCS- observations of ocean color from which surface chlorophyll concentration can be determined).

Predicted primary productivity values obtained from numerical simulations show a good agreement with the in situ/simulated in situ (IS/SIS) data collected over numerous cruises (**Fig. 2**). This illustrates the flexibility of the model and also the accuracy of the physics incorporated in it. In addition to bio-optical modeling, an associated remote sensing algorithm has been developed to predict primary productivity in the Gulf of Mexico (**Fig. 3**). Bio-optical provinces, defined in terms of water properties relevant to primary production, are characterized by assigning values to adjustable parameters that best describe quantitatively the observed data. Surface water primary production is closely related with the magnitude of sedimentation of particulate organic matter and hypoxic/anoxic events. A model designed to describe the processes associated with primary production in the Gulf of Mexico accurately predicts the decreasing onshore-offshore gradient in dissolved organic carbon. The sedimentation of particulate organic matter is not closely correlated with surface primary production. However, the sedimentation of these particles is generally associated with riverine nutrient inputs.

The above efforts have shown that coupled numerical physical-biological models must be continuously improved in order to better address the relationships between the physical forcing functions and the biological responses, particularly at continental margins.

References

Muller-Karger, F. E. et. al., 1991: On the Seasonal Phytoplankton Concentration and Sea Surface Temperature Cycles of the Gulf of Mexico as Determined by Satellites. *J. Geophys. Res.*, **96**, 12,645-12,665.

Walsh, J. J. et. al., 1989: Nitrogen Exchange at the Continental Margin: A Numerical Study of the Gulf of Mexico. *Prog. Oceanogr.*, **23**, 245-301.

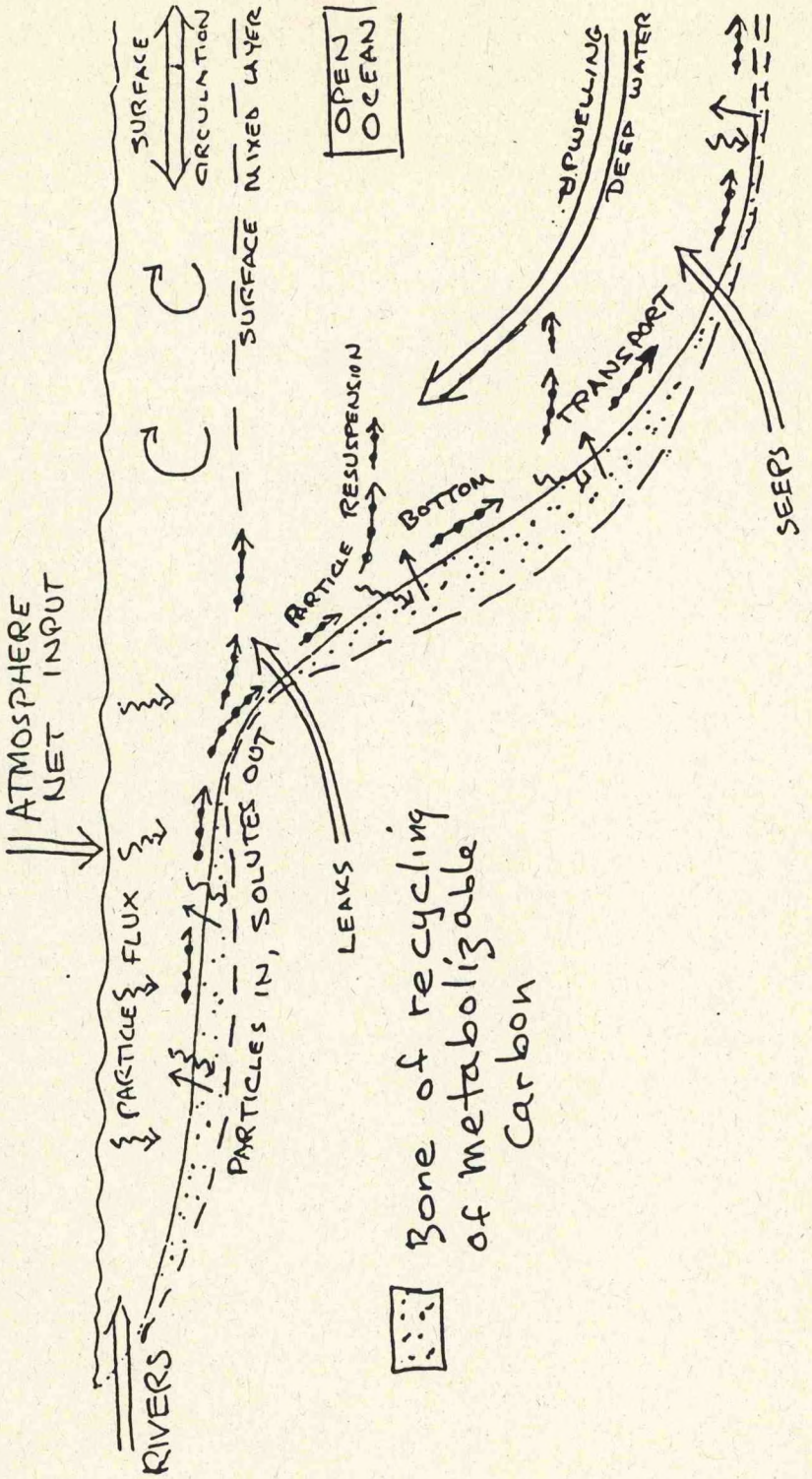

Figure 1. Margin Schematic Model

FIGURE 1

From "Ocean margins in GOFS", U.S. Global Ocean Flux Study Planning Report Number 6, Woods Hole Oceanographic Institution, Woods Hole, MA.

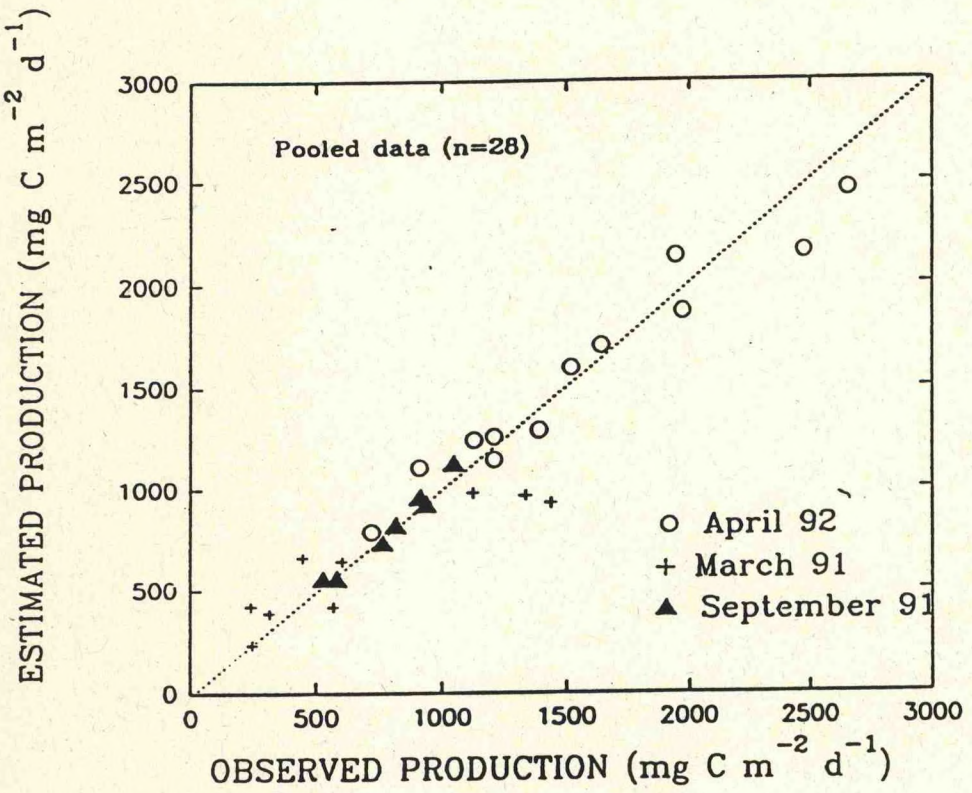

FIGURE 2

Comparison of production estimated using a satellite algorithm (estimated) with that determined by the input of in situ observations into a photosynthesis-irradiance model (observed). From Prasad, K. S., S. E. Lohrenz, D.G. Redalje and G.L. Fahnenstiel, in press. Primary production in the Gulf of Mexico coastal waters using "remotely-sensed" trophic category approach. Cont. Shelf Res.

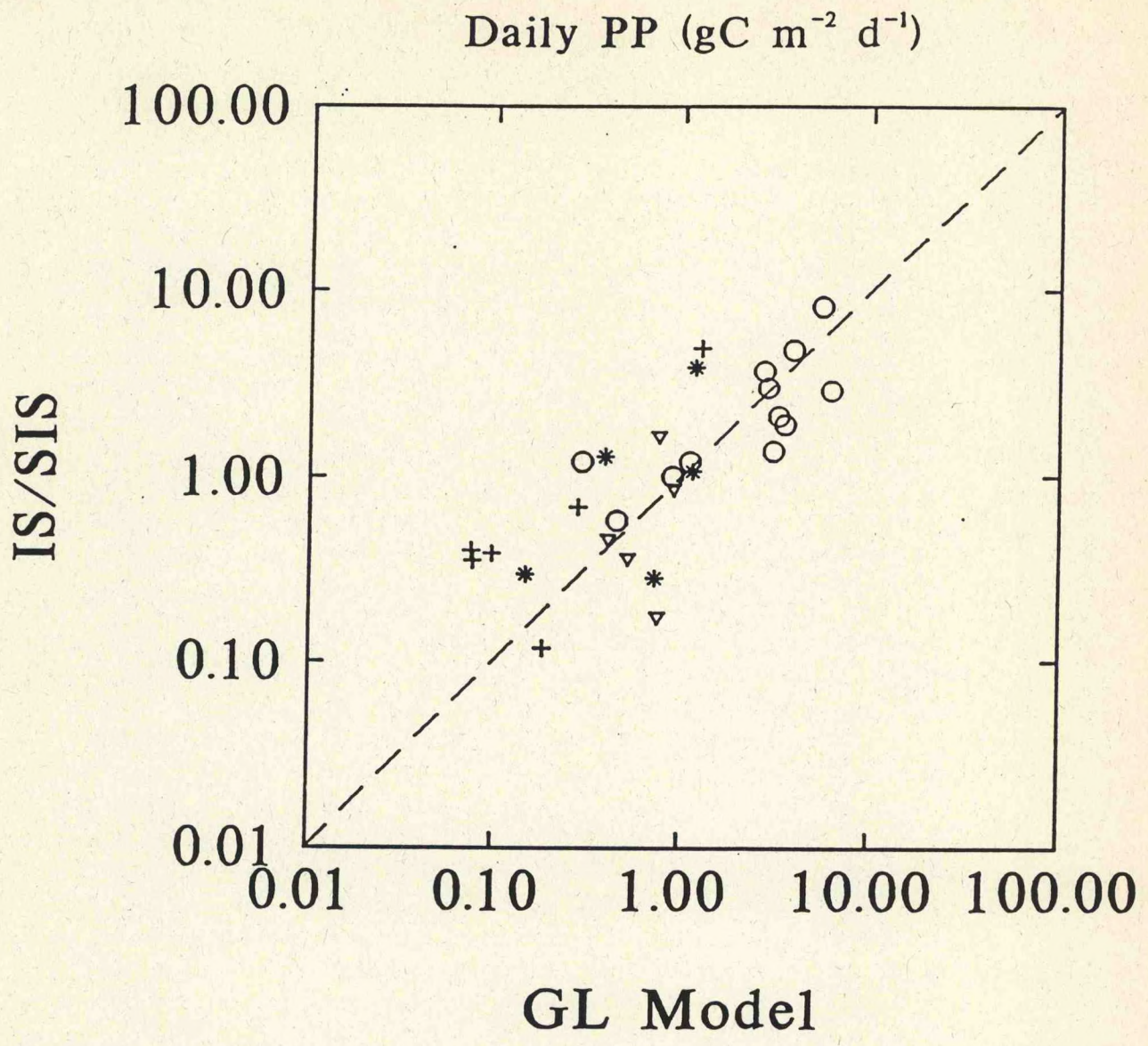

FIGURE 3

Comparison between primary production estimated by in situ or simulated in situ (IS/SIS) bottle incubations and the Great Lakes Model (GL Model). Symbols represent different cruises. From Lohrenz, S. E., G. L. Fahnenstiel, D. G. Redalje and G. A. Lang, in prep. Seasonal variability in coupling between primary production and outflow of the Mississippi River on the Louisiana continental shelf.

Overview of Ocean Observing and Predictions: A Look Ahead at Operational Programs, Global Scale to Coastal Scale

Lecturer: William E. Woodward
Date: June 20, 1994
Notes by: Jim Hansen
Christelle Escoffier

The purpose of this lecture is to present an overview of the way the ocean is observed and the ways those observations are used. Three questions must be raised:

1-Why the ocean has to be observed?
2-How the ocean is observed?
3-How to predict ocean behavior?

The Purpose of Ocean Observing

The ocean is one of the three major components of the earth system, the atmosphere and the land are the other two. They are linked to each other by several cycles and forces.

At shorter time scale (days), the atmosphere forces the ocean, but the knowledge of the ocean itself is also needed to predict the weather. However, nature and the dynamic coupling of the ocean and atmosphere is not well-known. The impact of the variability of the ocean at longer time scales is similarly poorly understood. It would be important to understand the exact role of the interaction and how it takes place.

The observing system of the ocean, through a data system is used to describe, understand, and then predict the climate variability. The US Global Change Research Program System gets back data observations for diagnostics, for initialization and validation of the models, for dynamical studies, and also for space based calibration and validation.

The interpretation of the observations to describe the ocean and for use in prediction are tricky. For example, in the simulation of global warming, if the curve of concentration in CO_2 continues to increase markedly in the years to follow, the interaction with the ocean may have not been fully considered. In the same way, a curve of SST versus time on a long period with gap in the data or a short period of this curve are difficult to interpret. Other considerations like the trend (% per decade) of SST are needed to interpret the general trend of the curve. The interpretation can easily be subjective and far from reality without enough observations. Forecasting Models are very sensitive to data observations (which must be calibrated and validated). If some data are incorrect in the assimilation (only few observations like 9/70), the run given can be very far from reality, once those wrong data are re-evaluate, the new pattern is tremendously different and closer to the observed pattern.

Means to Observe the Ocean.

The observing system is used mainly in the Research Community. This amount of observation has long-term value for Climate and Monitoring Systems. They should be used for operational prediction.

The observing system is composed of:

-Multi-platform (ship -drift buoys -anchored buoys)
-Multi-Source/ Multi-Objective Components
-Research and Operational Components
-Blended Fields
-XBT, drifter tracks, Moored buoys, tides stations, remote-sensing data with satellite.

We focus on particular observations like wind and SST (sea surface temperature), since they are more important in the models and need better coverage in space and time.

Transition from Research to Prediction.

Different research programs are in charge of collecting observations like TOGA in the Pacific ocean. Those programs were introduced to observe the ocean in the previous years. These programs have to be maintained periodically to keep on collecting observations for forecasting models.

Three international programs are set up to give observations on all the system: GTOS (for the land), GCOS (for the atmosphere and climate), GOOS (for the ocean). Together these programs interact to give global coverage.

In oceanography, observations of the upper ocean like SST, momentum, heat flux must be increased. So, an integrated, scientifically-based system for the coordinated monitoring and subsequent prediction have to be set up. With the global drifter project (1978-1994) which includes WOCE program, TOGA/NORPAX, TOGA/CONSORTIUM, etc., nearly all the ocean is covered by an observing system, except for a gap in the South Atlantic Ocean and in some other small areas around Antarctica.

All the observations are collected to be used in the prediction of weather for one to five days, in seasonal forecast, in interannual prediction or decadal to centennial prediction (climate). Previously, they had to be adjusted to different systems of data assimilation.

In conclusion, the challenge for the further years is :

-to seek best balance between Research and Operational System. The way to interact must be found.
-to insure continuing research role (Scientific Use of data, technology innovations, Market programs)
-to carefully define operational data in terms of their accuracy and quality, and to insure the continuity and integrity of the data set.

Precipitation Estimation for Climate

Lecturer: Phillip A. Arkin
Date: June 21, 1994
Notes by: Lihang Zhou
Cheng-Hsuan Lu

Background and Motivation

Observations and analyses of time-averaged large scale precipitation are needed for the following applications. First, for practical reason, this is an important factor to monitor drought and flood events, particularly in the tropical area. Second, reasonable estimates can be used to initialize, validate, and tune the current forecast and climate models. Finally, from scientific challenging prospect, they are useful in further research work to understand the earth system.

Global Precipitation Climatology Project (GPCP)

The objective of GPCP is to produce a 10-year record (1986-1995) of monthly global precipitation with resolution 2.5 degree latitude/longitude. It uses satellite estimates based on IR and microwave data, together with station observations. The primary data sources for the satellites are the GOES (US), GMS (Japan), and METEOSAT (Europe) geostationary satellites, the NOAA polar orbiting satellites and the Special Sensor Microwave/Imager (SSM/I) observations from the Defense Meteorological Satellite Program (DMSP) polar orbit satellites. The GPCP includes several principle centers shown in **Fig. 1**, each of which currently used exiting observations and techniques to produce rainfall estimates and analyses.

Satellite Techniques

a. IR techniques

IR refers to the 11 micron window. Categories include single-point (space & time), single-point space/extended time (examine the rate of change with time), single time/extended space (examine the gradient over extended space), and extended space & time (examine the rate of change and the gradient). GPI (GOES Precipitation Index, Arkin and Richards 1981) estimates area-averaged rainfall by multiplying the fractional coverage of an area by IR temperature colder than 235K by a coefficient of 3.0 mm h^{-1}. CST (Convective Stratiform Technique, Adler and Negri, 1988) identifies thunderstorm cores using geosynchronous IR data and eliminating thin cirrus. It assigns convective rainrate and area to thunderstorms based on cloud model-based relations. A comparison between GPI and CST is shown in **Fig. 2**.

b. Microwave algorithms

Microwave observations are currently available only from polar orbiting satellites. However, methods using microwave data derive rainfall from the effects of large liquid and solid hydrometeors on upwelling terrestrial radiation through well-founded physical relationships, while methods using IR data estimating rainfall indirectly by using empirical

relationships between rainfall and cloud features.

Generally, microwave rainfall estimation techniques can be divided into three categories. Emission-based techniques measure Tb elevation at frequencies below ~30GHZ due to emission from raindrops over cold (low emissivity) background; only ocean can be covered, with the poor spatial resolution; can detect non-ice related rain only. Algorithms using scattering information measure Tb depression at frequencies above ~60 GHz due to scattering of upwelling radiation by large ice particles; can cover both land and ocean with better spatial resolution; and principally for convective rain. The predictive approaches adjust precipitation parameters of radiative transfer model to match observed spectra; both land and ocean are being covered; can be used for all precipitation theoretically; but they are very expensive and with risks of non-unique solution.

Global Precipitation

There are five different sources can provide estimate of precipitation but none of these sources can provide complete global coverage of monthly precipitation with reasonable quality. The existing sources and their characteristics are summarized in the following :

(1) gauge observation: cover global land, function of gauge density, poor spatial resolution (only half 2.5 degree grids with any gauge)

(2) IR measurement: cover 40°S to 40°N, good for tropical and warm season sub-tropical rainfall

(3) scattering component: cover global land and ocean, good for convective but poor for stratiform rainfall

(4) emission component: cover global ocean, good for both convective and stratiform rainfall over ocean

(5) model forecast: cover global land and ocean, good for extra-tropical but poor for tropical rainfall.

Xie and Arkin (1994) merge gauge observations, satellite estimates and numerical model prediction to estimate global monthly precipitation. The data they used include GPCC gauge precipitation analysis (gauge observation), GOES precipitation Index (GPI, IR estimates), Grody estimates from SSM/I MW observation (MW scattering estimates), Chang estimates from SSM/I MW observation (MW emission estimates) and ECMWF 12-36 hr precipitation prediction (model prediction). The period is July 1987 - December 1988 monthly data, with global land/ocean coverage and 2.5 degree lat/lon grids resolution. They combine the three kinds of satellite estimates and the model prediction linearly to reduce the random errors. Then the combined analysis (CA) is blended with the gauge observations to reduce the systematic error (bias). This merged analysis is successful in depicting major features in global precipitation distribution and the quality of the merged analysis is reasonable everywhere (**Fig. 3**).

References

Richards, F., and P. A. Arkin, 1981: On the relationship between satellite-observed cloud cover and precipitation. *Mon. Wea. Rev.*, **109**, 1081-1093

Negri, A. J., and F. Adler, 1988: Infrared and visible satellite rain estimation. Part 1: A grid cell approach. *J. Appl. Meteor.*, **26**, 1553-1564

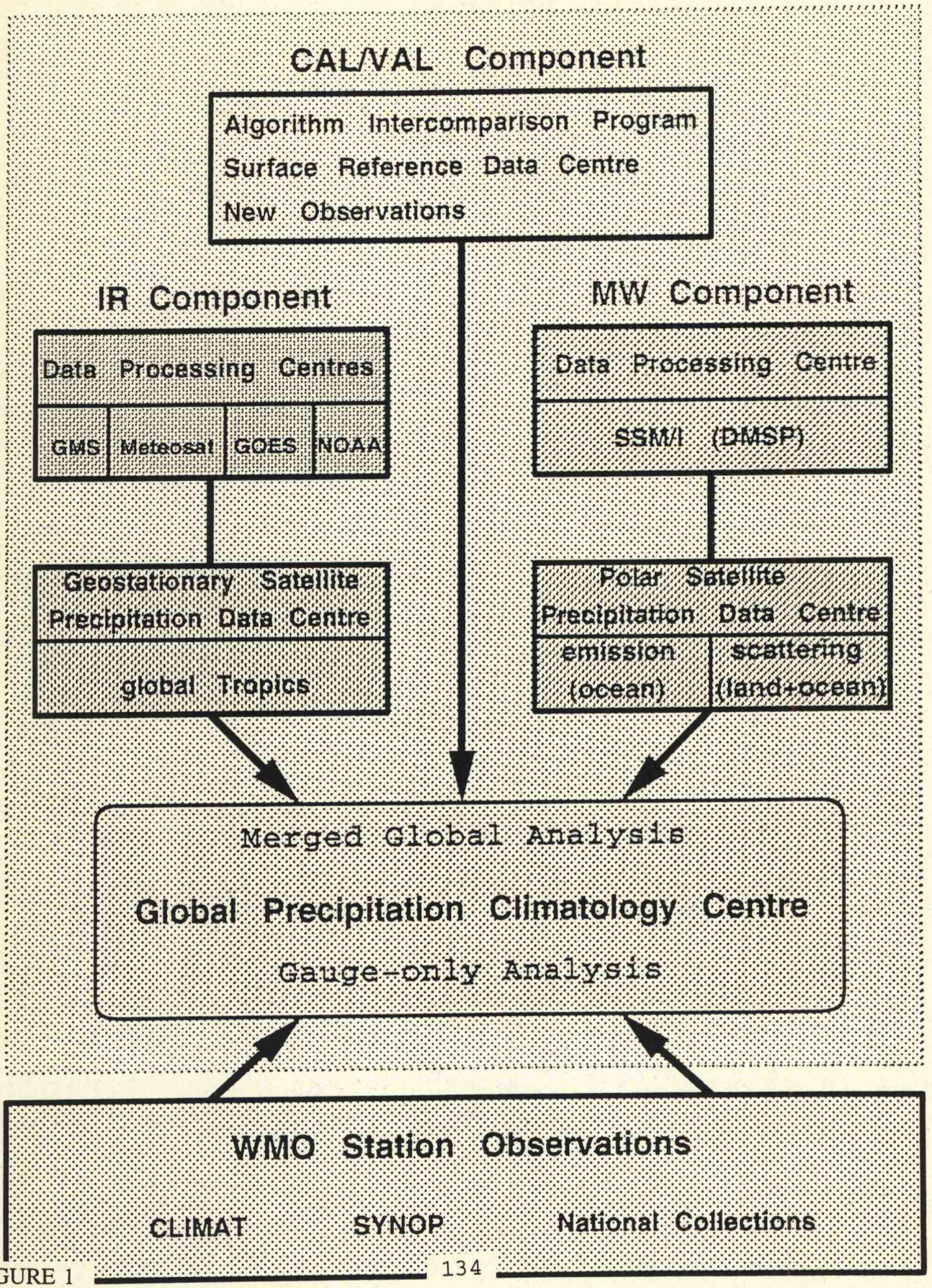
G P C P
CAL/VAL Component
Algorithm Intercomparison Program
Surface Reference Data Centre
New Observations
IR Component
Data Processing Centres
GMS
Meteosat
GOES
NOAA
MW Component
Data Processing Centre
SSM/I (DMSP)
Geostationary Satellite Precipitation Data Centre
global Tropics
Polar Satellite Precipitation Data Centre
emission (ocean)
scattering (land+ocean)
Merged Global Analysis
Global Precipitation Climatology Centre
Gauge-only Analysis
WMO Station Observations
CLIMAT
SYNOP
National Collections

FIGURE 1

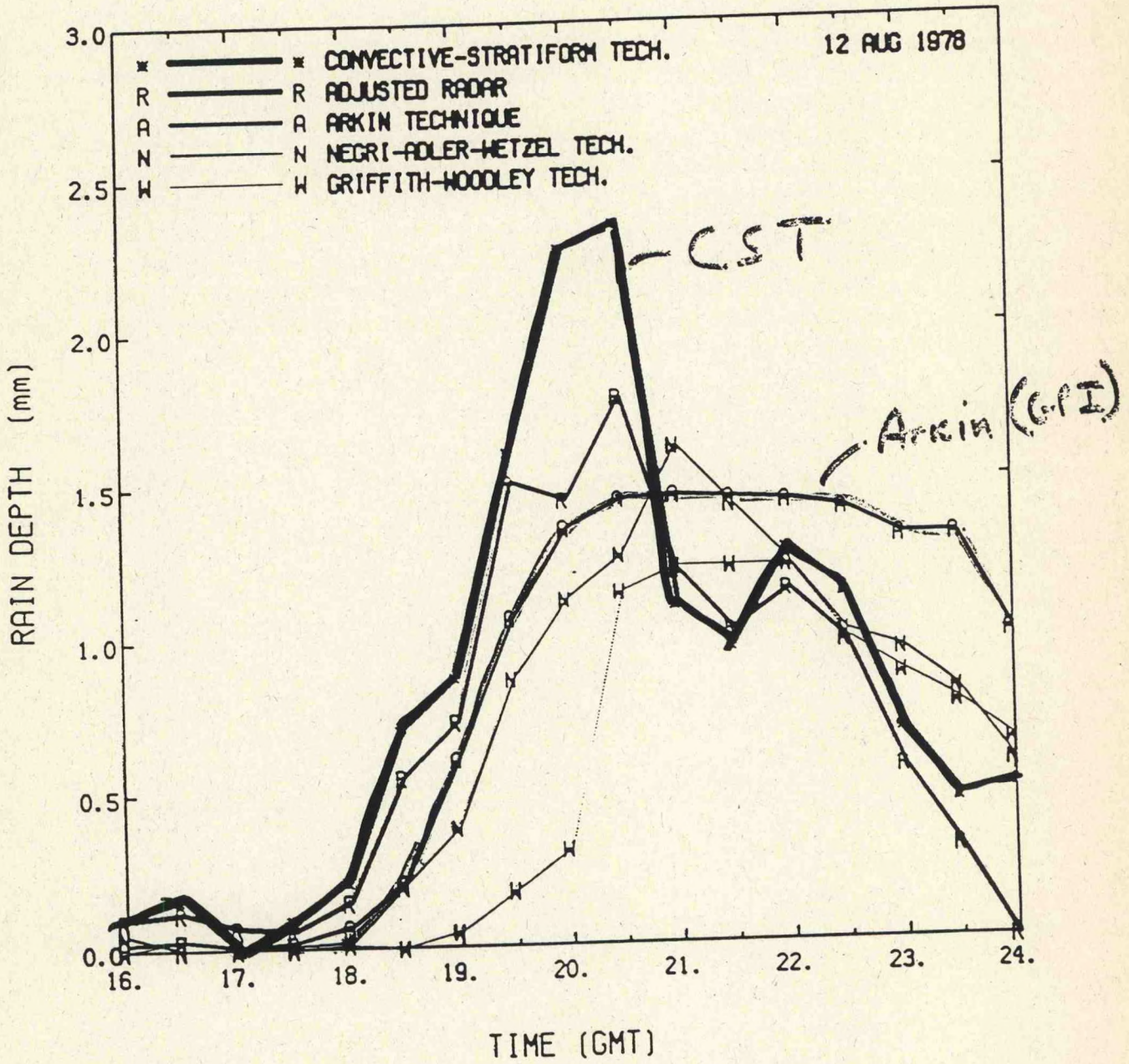
12 AUG 1978
* CONVECTIVE-STRATIFORM TECH.
R ADJUSTED RADAR
A ARKIN TECHNIQUE
N NEGRI-ADLER-WETZEL TECH.
W GRIFFITH-WOODLEY TECH.
CST
Arkin (CPI)
RAIN DEPTH (mm)
TIME (GMT)
3.0
2.5
2.0
1.5
1.0
0.5
0.0
16.
17.
18.
19.
20.
21.
22.
23.
24.

FIGURE 2

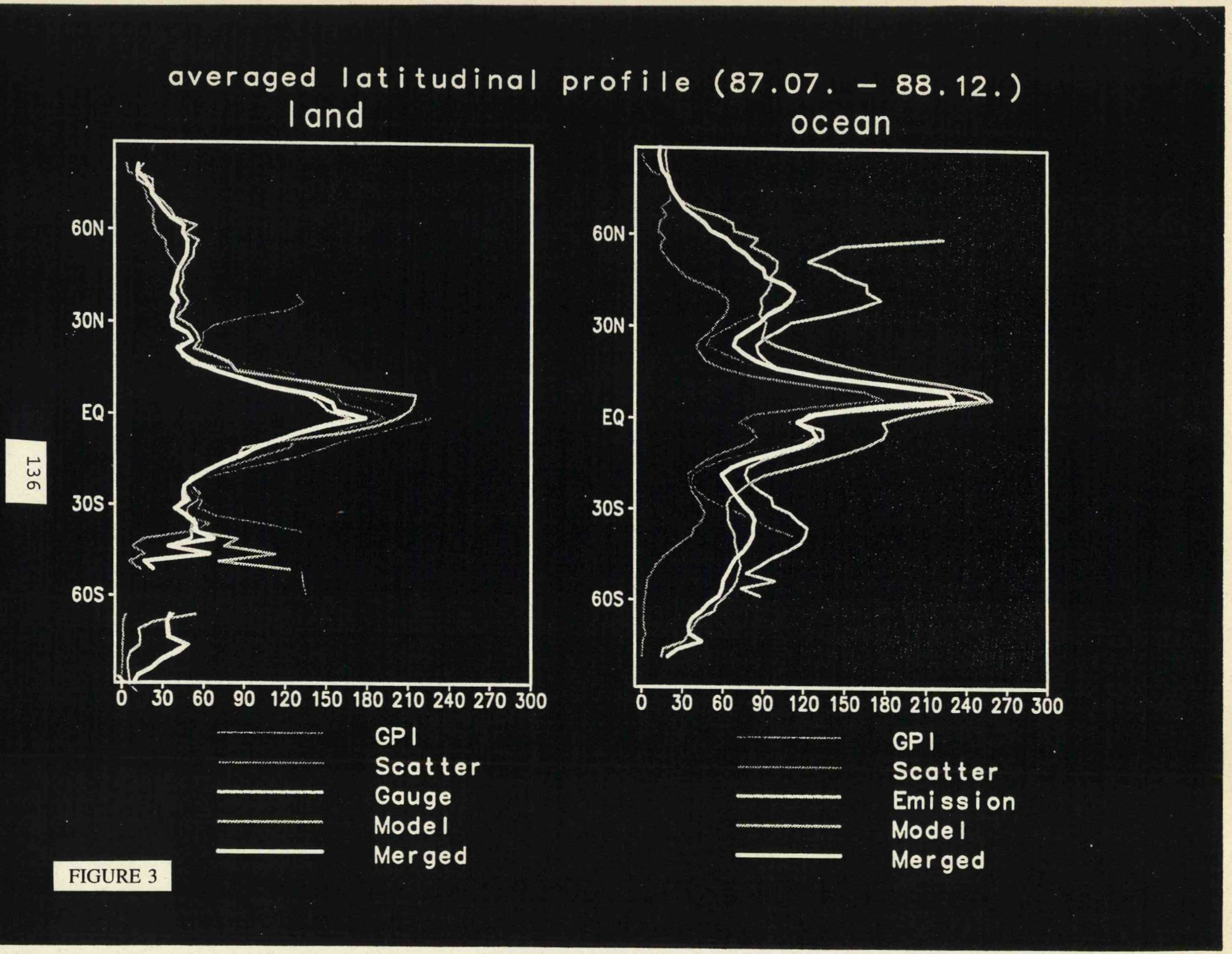
averaged latitudinal profile (87.07. – 88.12.)
land
ocean
60N
30N
EQ
30S
60S
0 30 60 90 120 150 180 210 240 270 300
GPI
Scatter
Gauge
Model
Merged
GPI
Scatter
Emission
Model
Merged

FIGURE 3

Review of 1993 Extreme Weather Events

Lecturer: Joe Golden
Notes by: Xiaofeng Li
Jim Hansen
Date: June 21, 1994

Severe weather in 1993 caused on the order of $14 billion worth of damage in the United States. The most costly events were the $7 billion lost to flood, and the $3 billion lost to heavy rain. The cost of this severe weather transcended property damage as 351 people lost their lives and 2800 were injured. Flash flooding killed 85 individuals, while blizzard events took the lives of 65 more. The 1173 tornadoes reported in the US last year killed 34. For a more complete list of weather events, deaths, injuries and damage costs, see **Table 1**.

Weather Event	Deaths	Injuries	Est. Cost (millions)
Lightning	43	279	29.7
Tornado	34	964	307.7
Tstm-Winds	23	393	250.6
Hail	0	20	273.8
Extreme Cold	16	1	323.2
Extreme Heat	13	66	70.4
Flash Flood	49	45	295.3
River Flood	36	28	6936.7
Coastal Storm	0	0	0.2
TS/Hurricanes	1	1	12.6
Snow/Blizzard	65	518	631.3
Ice Storm	8	92	18.2
Avalanche	1	0	0.0
Drought	1	0	514.0
Dust Storm	0	1	0.0
Fire Weather	3	239	950.0
Rain	1	14	2931.5
Fog	5	9	0.4
High Winds	38	112	226.5
Water Spouts	1	0	0.4
Mud Slide	2	0	0.0
Other	11	1	25.5
TOTAL	351	2783	$13798.0

Superstorm

The so-called "Superstorm" or "Storm of the Century" that hit the east coast of the US on March 12th of 1993, caused the majority of damage and casualties under the blizzard category of **Table 1**. Associated with the storm was a killer storm surge in northern Florida, and a series of at least a dozen tornadoes. Although the National Meteorological Center (NMC) was able to accurately predict the cold temperatures and heavy snowfall from the storm over the east coast, it unfortunately missed the early morning storm surge of up to 12 feet in northern Florida that killed many people in their beds, as well as the tornadoes.

For clues as to what caused this storm surge and tornado outbreak, one must turn to the reconstruction of the event from real-time satellite and radar observation. The dominating feature of the analysis is the major squall line that moved through the eastern part of the Gulf of Mexico and over the state of Florida. However, this squall line preceded the surge and tornado outbreaks by a couple of hours. It appears as though the real culprit was a cold front moving in behind the squall line with wind speeds of 30-40 kts in front of it, and 50-60 kts behind. **Figure 1** shows evidence of the cold front in the small lines of clouds just making landfall behind the well developed squall line. This strong velocity gradient would have piled water up along the front that would cause the type of damage observed. Atmospherically, the front could have easily initiated the microbursts, tornadoes, and other severe weather assailing panhandle. Of the tornadoes reported, damage investigation has classified two of them as F2 (Fugita scale) and one of them F3.

Great Flood

Much has already and will be said in these proceedings about the Great Flood of 1993. Basically, an anomaly in the jetstream flow over the midwest U.S. created lasting conditions that were favorable for heavy rains over the area. Instead of the Bermuda high taking up residence in the eastern U.S. and driving the jet stream up over the northern U.S., it sat well off the coast of southeastern U.S. and allowed the jet stream to take a more zonal path across the middle of the country. Associated with this was cool air being pulled down from Canada, and plenty of warm, moist air from the Gulf of Mexico. The combination of these two air masses meeting in the midwest was a steady pattern of strong convection and heavy rain (see **Fig. 2**). No cause was given this unusually high-level flow, but it was stated that leading up to the flood, the soil moisture content in the midwest was much higher than normal.

The Midwest, although the most severely affected, was not the only part of the United States impacted by this anomalous jet stream pattern. The northwest experienced unusually cool summer temperatures, while the southeast suffered from extreme heat.

Water Spouts

Golden has spent a significant amount of time studying the behavior of water spouts off of the Florida Keys. National Geographic recently enlisted his help to document these common, yet not well understood phenomena. With a core diameter of 5-15 meters, and tangential velocities that can approach 50 m/s, these frequent visitors to the popular waters of the Keys have a significant potential for damage. This area is such a prolific breeding

ground of these events as a result of the significant convection produced by the string of islands stretching south and west from the southern tip of Florida. Couple this strong convection with moist air and a reliable sea breeze and you have the conditions necessary to produce strong, stable atmospheric vortices.

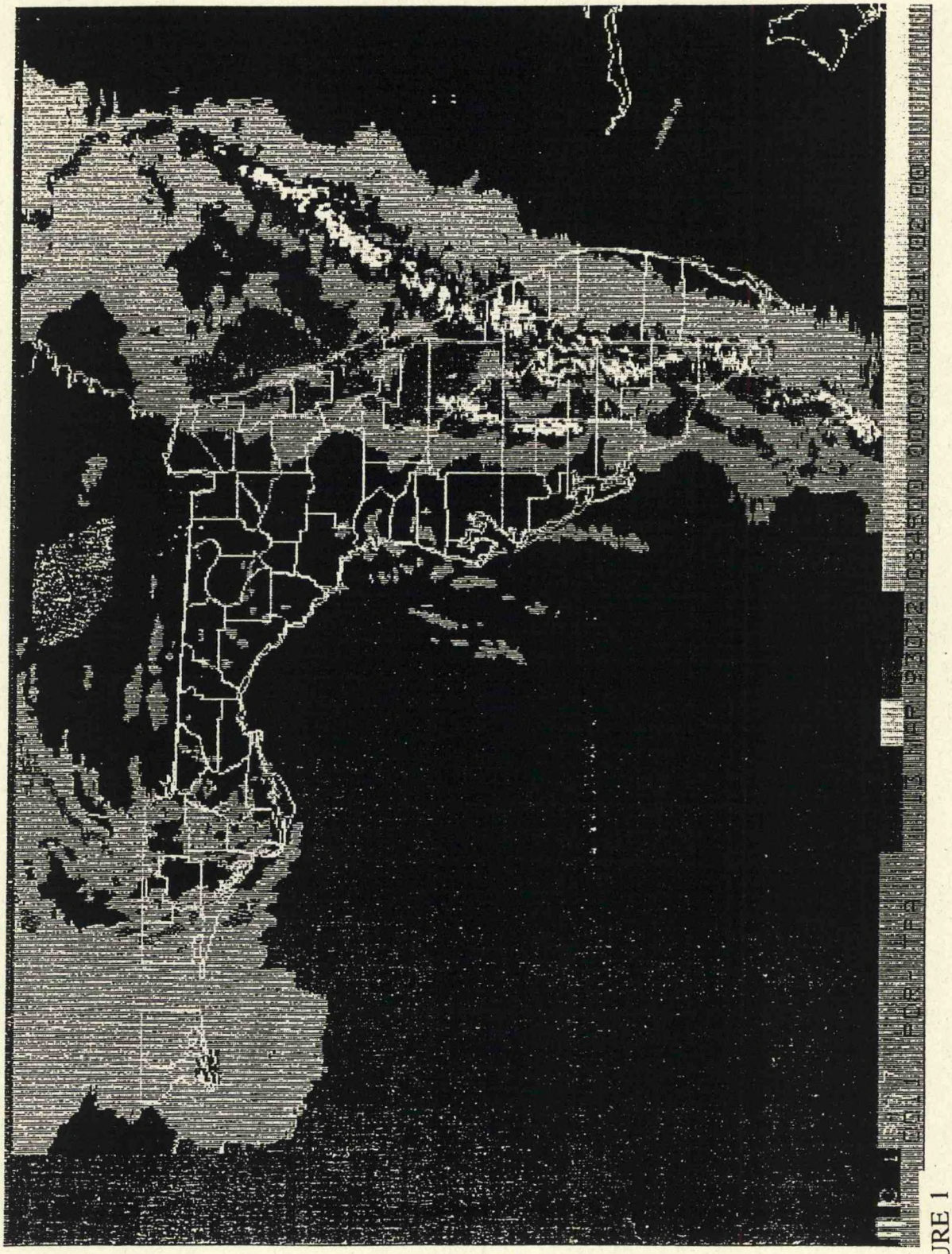

FIGURE 1

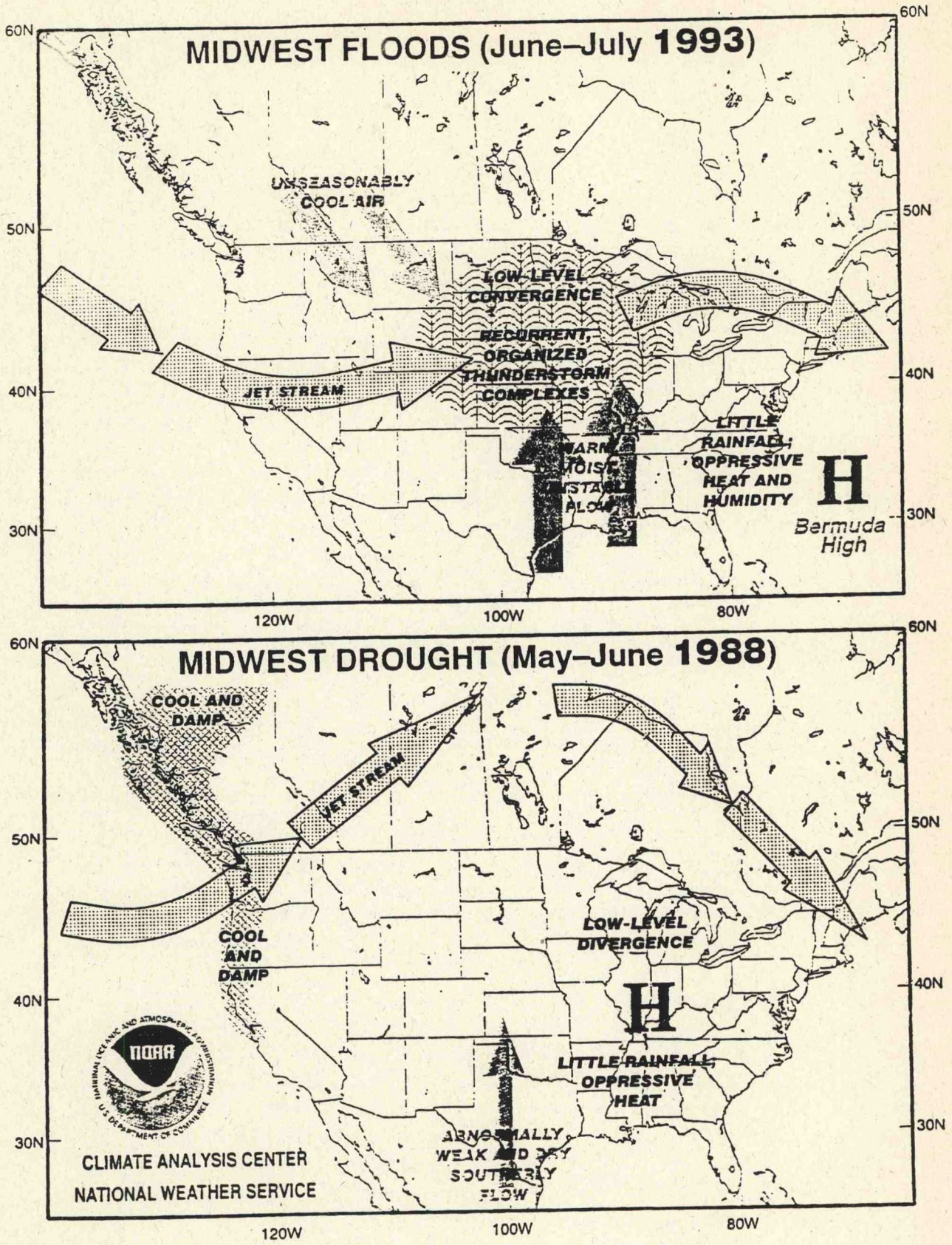
MIDWEST FLOODS (June–July 1993)
UNSEASONABLY COOL AIR
LOW-LEVEL CONVERGENCE
RECURRENT, ORGANIZED THUNDERSTORM COMPLEXES
JET STREAM
LITTLE RAINFALL; OPPRESSIVE HEAT AND HUMIDITY
H
Bermuda High
60N
50N
40N
30N
120W
100W
80W
MIDWEST DROUGHT (May–June 1988)
COOL AND DAMP
JET STREAM
COOL AND DAMP
LOW-LEVEL DIVERGENCE
H
LITTLE RAINFALL; OPPRESSIVE HEAT
ABNORMALLY WEAK AND DRY SOUTHERLY FLOW
CLIMATE ANALYSIS CENTER
NATIONAL WEATHER SERVICE
NOAA

FIGURE 2

Predicting Heavy Precipitation and Flash Flooding

Lecturer: Roderick Scofield
Date: June 21, 1994
Notes by: Lihang Zhou
Alan Zeigler

NMC uses many visual aides, particularly those created from satellite data (GOES geostationary satellites, NOAA and DMSP polar orbiting satellites) to identify weather patterns that produce heavy rainfall and associated flash flooding. Satellite observations provide simultaneous coverage of all weather scales (global, synoptic, mesoscale, and storm), allowing forecasters to study the evolution of heavy rainfall systems through several multiscale stages: preparation, development, focus and maintaining, and storm intensification and movement.

Satellite Data

GOES satellite data, available about every 30 minutes, are utilized extensively for forecasting heavy precipitation. Data from polar orbiting satellites (NOAA, DMSP) are perhaps more physically linked to precipitation than GOES data, but are recorded too infrequently for heavy rainfall analysis (only two paths a day).

IR (infra-red) data from GOES satellites are available both day and night. Enhancement curves created from IR images show contours of top-of-cloud temperature, allowing forecasters to track the coldest clouds, which are usually associated with severe weather and heavy rainfall.

VIS (visible) data, showing day time cloud patterns and movement complement IR data.

WV (water vapor) imageries (6.7 micron) provide synoptic scale moisture information in the middle and upper atmosphere (700 mb - 200 mb), but can not sense the moisture near the surface.

MW (microwave) data from Special Sensor Microwave Imager (SSM/I) on the Defense and Military Satellite Program (DMSP) satellite provide information about global vegetation and snow cover. MW data are a primary source for the Soil Wetness Index..

Data from new GOES (GOES-8) should be more useful in observing cloud features than previous GOES images because the resolution is. (GOES 8 will become operational 10/94)

Flash Flood Forecasting and Analysis

Forecasting heavy rainfall involves identifying three critical ingredients: instability of the atmosphere, moisture, and upward vertical motion. Instability can be estimated from the equivalent potential temperature ('theta-e') ridge axis (maximum potential energy for convective development) derived from temperature and dew point sounding. Moisture information can be derived from GOES/VAS and SSM/I.

Jet streaks, visible in cloud data of satellite images, are good indicators of strong upward motion. Animations visualizing movement of cyclonic circulations, tropical water vapor intrusions, and jet streaks are important tools for predicting heavy rainfall. Cyclonic

circulations are low pressure systems usually moving from the west to the east that produce most of the severe weather in the spring in North America (in the fall in Europe). Tropical water vapor intrusions are pseudo-monsoon systems coming north from the ITCZ producing heavy rainfall when coming in contact with a lifting mechanism such as a jet streak. Jet streaks are strong cyclonic or anticyclonic winds that usually appear as max winds in conventional upper level data, or as dark areas (cyclonic jet streak) or a cirrus areas (anticyclonic jet streak) on water vapor imagery. Jet streaks produce heavy summer rainfall over the USA, China, and many other parts of the world (i.e. the 1993 Midwest flood maintained a permanent area of tropical moisture intrusion colliding with jet streaks).

Thickness patterns showing the vertical distance between two constant pressure surfaces are useful in showing Multiple Convective Systems (MCSs) movement that tends to be along the thickest isopleths. Backward moving and stationary MCSs, which often produce great rainfall in one area, occur where isopleth lines diverge.

The interactive flash flood analysis (IFFA) estimates rainfall rates from weather features appearing on satellite images (mergers, cloud top temperature, cloud growth, overshooting tops, and stationary storms). Moisture availability parameters are used to adjust rainfall estimates. Satellite-derived rainfall estimates and those from ground observations are similar, although both tend to be lower than Doppler radar estimates.

Rainfall Estimation Using Radar

Lecturer: David H. Kitzmiller
Date: June 22, 1994
Notes by: Elvira Brankov
David C. Burwell

Importance of Remote-Sensor Estimation of Rainfall

a) High spatial variability of rainfall makes continuous observations from radar necessary in time-critical forecasting applications.
b) General hydrological applications:
    1. Refine estimates of rainfall based only on gage networks
    2. Used in forecasts of mainstream river levels.
c) Short-range forecasting applications:
    1. Determine intensity of rainfall over remote areas (particularly mountains) subject to flash flooding
    2. Subjective and objective interpretation methods used to forecast future rainfall to 1-2 hours.

Physical Principles

Radio waves striking water droplets excite surface molecules to produce return radio energy (backscatter). Sensitive radio receiver detects the returned energy. The distance to target can be estimated from time between transmitted and returned pulse, and the strength of return (magnitude of radio wave flux) is used to estimate density of backscatters. Since the electrical properties of water drops are known, and a common distribution of drop sizes can be assumed, it is possible to use radar return to estimate raindrop sizes and mixing ratio. In microwave spectrum, backscattered return flux is proportional to the sum of the 6th powers of droplet radii.

In meteorological radar applications, reflectivity is usually expressed in terms of drop-size distribution that would produce the observed radio return strength (DBZ). Meteorological radars typically use microwaves of 5 or 10 cm wavelengths.

History of Radar Rainfall Estimation

Echoes from rainfall were first noted by researchers in 1940's. The operational use of radars for detection of precipitation started in 1950's in U.S., Britain and Canada. In 1960's automated reflectivity processing was made possible through use of Digital Video Integrator and Processor.

Commonly Used Reflectivity-Rainfall Relationships

* Marshall-Palmer: $Z = 200\ R^{1.6}$
* WSR-88D (NEXRAD): $Z = 300\ R^{1.4}$
* Convective: $Z = 200\ R^{1.5}$

Here Z is the reflectivity factor in units mm^6 per m^3, and R is rainrate in mm per hour.

Common Problems/Solutions with Radar Rainfall Estimation

* Drop-size distributions improperly modeled. This can be partially corrected by comparing coincident gage and radar estimates.
* Returns from precipitation other than rainfall (snow, melting snow, hail),
* anomalous propagation, which can be minimized by checking for near zero doppler velocities, and then using a higher radar beam angle.
* Ground clutter regions, can be detected with a clutter map or by comparing current radar/satellite IR images.
* Radar beam blockage, which is minimized by using higher radar beam angles, or they can be interpolated away using nearby unblocked radials.
* Gage/radar sampling inconsistencies.

Sources of Gage/Radar Measurement Inconsistencies

One of the inconsistencies between gages and radar measurements comes from the difference in their sampling frequency: radar samples rainrate every 5-6 minutes, while gage measures continuously. Also they differ by their horizontal measurement area: for radar it is typically 1 square mile whereas for gage this area is 50 square inches.

Solution for these problems is in estimating the current gage/radar bias by comparing coincident gage and radar estimates.

Future Refinements to Radar Rainfall Estimation

a. Dual-polarization radar

This radar relies on polarized radio waves (vertical and horizontal) considered separately. Since large raindrops are more oblate than spherical, they return horizontally-polarized waves more strongly than vertically-polarized. Hence, the drop-size distribution can be estimated more directly. Hailstones, which tend to appear spherical to radar do not affect dual-polarization measurements.

a. Differential doppler phase measurements

Oblate (large) drops return a signal with phase shift different from return by spherical drops. This phase shift can be systematically separated from the phase shift due to horizontal motion.

Some references for further reading can be found following the Fulton and Smith review that follows.

Quantitative Precipitation Forecasting

Lecturer: Wes Junker
Date: June 22, 1994
Notes by: Cheng-Hsuan Lu
Yuval Shay-El

Quantitative Precipitation Forecasting (QPF) is needed for two main reasons: to anticipate floods and flash floods, and for hydrological planning and water management. QPF forecasting involves two problems; the first is to interpret the numerical guidance, and the second is to know a big rainfall event from a small one (in terms of scale and intensity). Current numerical models have the following problems in forecasting QPF: 1) initialization and quality control tend to smooth the fields, 2) lack of data over oceans and Mexico, 3) inadequate physics, due to parameterization of convective processes, radiation and evaporation, and 4) atmospheric processes are non-linear.

Too few soundings and smoothing of data can lead to underestimating or missing upper-level features such as jet streaks and tropospheric folds, as well as inadequately representing the structure of the atmosphere especially in the boundary layer. These factors are very important in determining where the heaviest snow falls. Non linearity, introduced first by Edward Lorenz, and exemplified by the famous "butterfly effect", leads to strong dependence of models on initial conditions, and to divergence of solutions starting with similar initial conditions. "Linear thinking" of the human forecaster is a related problem, since most big storms are non-linear.

Numerical models are used to identify: 1) synoptic patterns conducive to heavy rain; 2) possible triggering mechanisms; 3) the strength of the low-level jet; 4) available moisture and instability. They usually forecast well the synoptic patterns, however the smaller scale may be wrong. **Figure 1**, for example, shows a 24-h precipitation forecast. The associated synoptic pattern, not shown here, was forecasted well. The model, however, overestimated the inland precipitation, and underestimated the precipitation along the Louisiana coast. This event exemplifies the high importance of pattern recognition. Our minds are very good at distinguishing between complex patterns. The forecaster should, therefore, use the model mainly for identification of the synoptic pattern, and then use his knowledge for estimation of the precipitation related to the pattern.

The questions to ask when preparing a quantitative precipitation forecast include: 1) how much moisture will be available? 2) will there be lifting? 3) will precipitation be stratiform or convective? and 4) how long will the precipitation last?

In assessing moisture, the forecaster should remember the moisture can change rapidly. He should examine carefully the dewpoints, temperatures, and winds, at the surface, 850, 700 mb. He should be alert when precipitable water values are above 1.60 inches if a focusing mechanism is present. Most heavy rains are associated with convection. Various stability indices should therefore be examined to see if instability exists. Boundaries, cold pools, moisture and jet streaks should be examined as well. For this the forecaster should analyze heights or pressures at sea level, 850, 700, 300, 250 mb. He should also analyze winds, temperatures, dewpoints, and theta-e, and **not** trust machine analyses.

In assessing lifting, the forecaster should examine the presence of low-level convergence, upper-level divergence, differential warm advection, and differential vorticity advection. The low-level jet is an important factor. Other ones are diffluent flow, jet streaks,

and curvature. Some environments favor the training or regeneration of convection. These include slow moving front or boundaries, a quasi-stationary low-level jet, front parallel to the mean upper flow, quasi-stationary area of upper divergence, and the lack of strong vertical shear.

Patterns vary by season, geographic region, and scale. They are identified using conventional data, model output, satellite imagery and radar. The duration of an event depends on the size and movement of the area of precipitation. In general, small and fast moving systems produce less rain and slow moving systems produce more rain.

The floods of 1993 can be used as an example for the process of QPF. Forty three events with precipitation above 5 inches occurred during the period 1 April - 25 July 1993. The mean synoptic pattern was characterized by an upper-level trough over the West, stronger than normal upper-level jet, stronger than normal 850-mb winds, and lower than normal pressure across the westerns plains. Mesoscale Convective Complexes (MCCs) east of the Rockies caused flash floods. These convective systems are not easy to forecast based solely on the numerical models, since their scale is only few hundred kilometers, while the model resolution is 80 kilometers at the most (Eta model at 1993), not good enough for presentation of the MCCs' development. Studying their characteristics can therefore help the forecaster to predict the small-scale dynamics which cause floods. Some of the characteristics are: moisture is deep, and Precipitable Water (PW) average is about 1.60 inches; surface dewpoints are high; vertical shear is weak to moderate; MCCs occur near the 500-mb ridge position; and they usually occur at night.

In order to better understand the pattern characteristics of MCCs, Wes Junker composed twelve MCCs that caused the worst rain events during 1993. The atmospheric fields of these events were averaged with relation to a common central point. **Figure 2**, for example, depicts the composite of theta-e. The central point is where most precipitation occurred. Based on this analysis, the best indicator of location of the maximum rainfall was near the juxtaposition of the theta-e ridge, positive theta-e advection, axis of strongest 850-mb moisture flux, axis of highest PWS and instability. Other findings for flood cases during June and July 1993 are: about 50% occurred near 500-mb ridge axis; 60% in area of thickness diffluence; about 50% near southern edge of westerlies; most were associated with right rear quadrant of jet streak; more than half were associated with positive vorticity advection (PVA).

In short, MCCs are characterized by sub-grid details. Numerical models don't predict these details well. A cautious forecaster is therefore needed for better quantitative precipitation forecast.

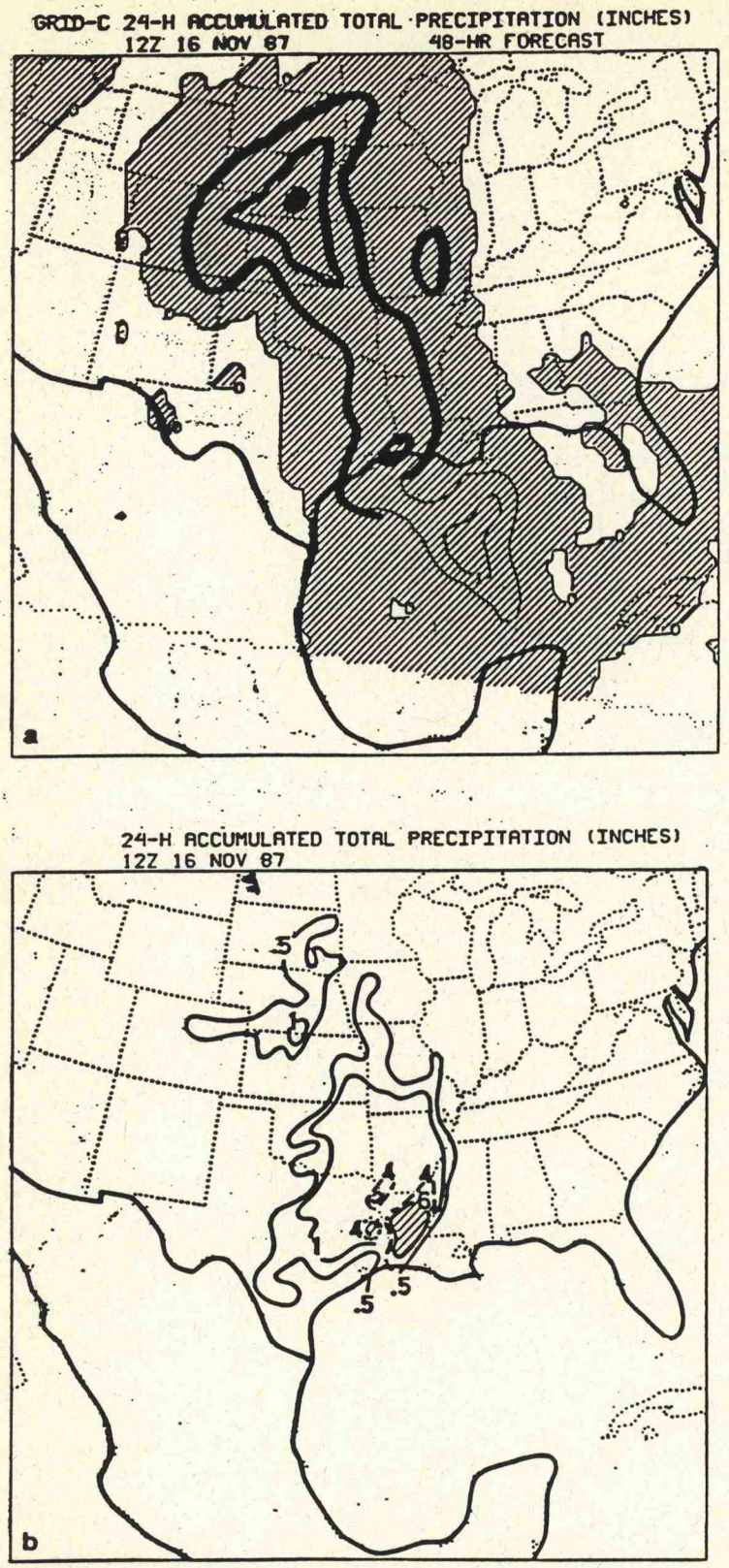

FIGURE 1 24-h precipitation ending 1200 UTC 16 November 1987 of (a) the NGM from 24 to 48 hours and (b) the observed amounts. In Panel a, areas of precipitation are shaded and the contour interval is 0.50 in., whereas in Panel b the contours are 0.50 in., 1 in., 4 in., and 6 in.

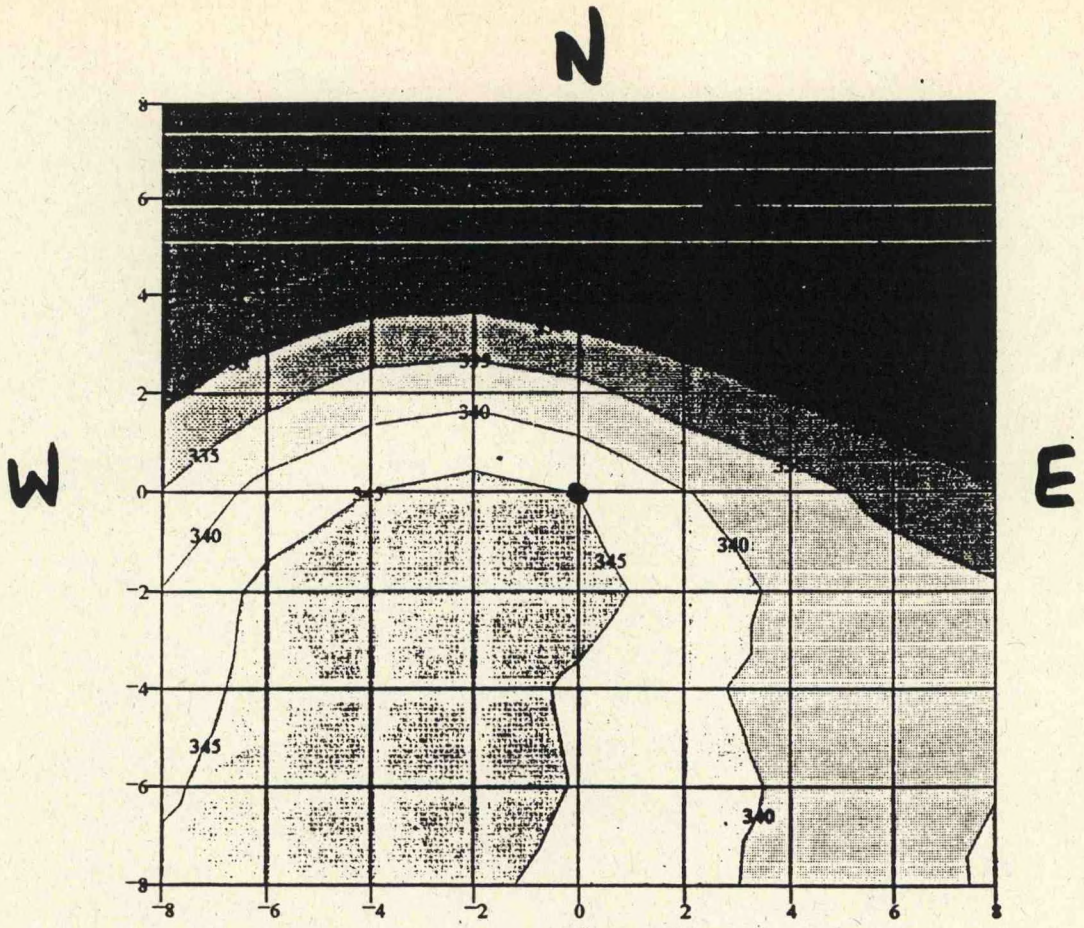

346.5	344.1	341.8	340.2	335.3	32[illegible]	324.3	321.5	318.1
347.6	347.8	347	346.4	341.9	333.6	325.5	321.4	317.6
346.7	348.1	349.5	348.8	345.1	337.6	328	320.7	317
345.8	347.2	347.4	349.2	346.8	338.7	328.5	320.8	316.3
343.8	344.8	344.2	347.1	344.9	336.6	326.5	320.5	314.6
342.1	341.3	340.7	342.8	340.3	332.6	325.2	319.7	314.1
338.2	339.6	339	339.1	337.2	329.7	323.4	319.6	315.2
338.6	339.5	338.6	337.7	333.4	326.9	321.1	318.8	316
340.5	339.9	336.3	335.6	330.6	324.5	319.5	317.6	315.3

COMPOSITE OF THETAE

FIGURE 2

Rainfall Estimates from NEXRAD

Lecturers: Richard Fulton and James Smith
Notes by: David C. Burwell
Paul Gaertner
Date: June 22, 1994

Rainfall rates and total quantities are important in scales that range in size from sub-mesoscale downpours, that occur over hourly time intervals for flash flood prediction, to world averages over decadal time scales, that are useful in driving climate models. NEXRAD, the WSR-88D system, has many advantages in determining precipitation patterns at all scales. As this system has 4 km resolution and products can be "mosaic-ed" into fields of any size, it is the best tool available for measuring precipitation. Satellites don't have the spatial or temporal resolution; numerical models are dependent on parameterizations from some independent source; and rain gauges are too sparse and unreliable. Applications of the NEXRAD system include heavy precipitation (real-time and anytime products), low precipitation (monthly and seasonal data), total precipitation (storm, day, week, month or seasonal data) and serve precipitation (hail and freezing rain). The system obtains these products utilizing a precipitation processing data flow (**Fig. 1**).

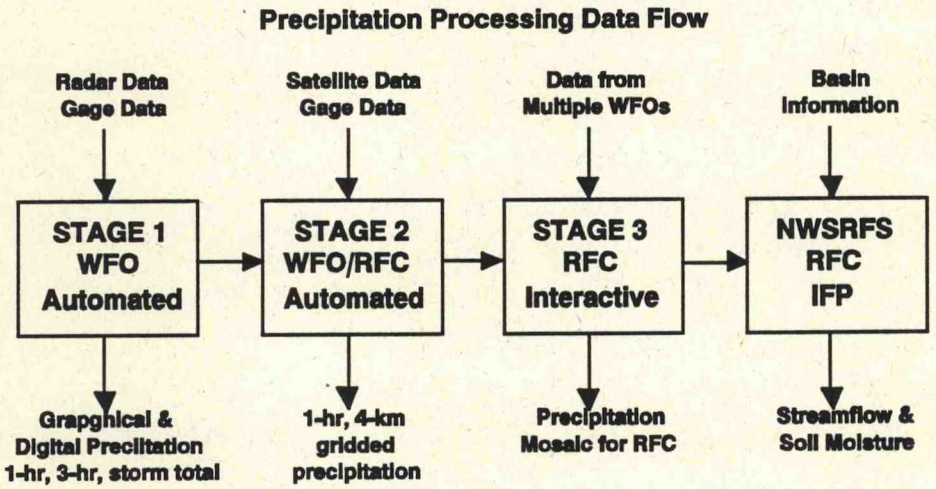

Figure 1

Stage one starts by collecting data and running a precipitation processing algorithm to produce precipitation products. This algorithm is used as a quality control mechanism to minimize both the radar estimates of precipitation, and the rain gauge representation of precipitation. The algorithm corrects for physical radar beam blockage, spurious noise, reflectivity outliers, normal and abnormal ground return, and beam height with range. Output from this first stage includes reflectivity data from sectorized hybrid scans (1 degree by 0.54 nm sample volumes). These are most accurate for large-scale precipitation systems. Stage one provides good spatial and temporal resolution for the mesoscale details of precipitation systems. The PPS provides some flexibility for different locations and climate regimes and can evolve into a better algorithm able to effectively account for variability on a geographic, seasonal and even hourly basis. However, the PPS can not adequately account for hail or

mixed state hydrometeors, snow or frozen precipitation with different Z-R relationships, errors in signal processing, rain gauge inaccuracies and sampling errors.

Stage two, takes the first stage as input in an hourly digital precipitation array together with additional gauge and satellite data and produces hourly multisensor rainfall field and also incorporates gages reading from under the radar umbrella to give either gauge only rainfall field or rain gauge radar table. Stage two is geared towards small scale systems.

Stage three is an interactive x-window system that allow the forecaster to use her best judgement to remove anomalies or any inconsistent data remaining after stage two. At this stage mosaics are made and adjusted to be consistent over a wide spatial scale. Hourly rainfall data from each NEXRAD in the system can be used to produce a quantitative hydrologic product. This allows radar data to give a good rain climatology on a nationwide scale at high resolution . Even with the older WSR-57 system, its long history provides the best multi-year climatology although at lower resolution than the NEXRAD system. These types of products can also give a good idea of the temporal cycles that occur in precipitation patterns for example, the diurnal cycle near the coast.

The challenge with the NEXRAD system is not so much as to attain a more detailed look at thunderstorm severe weather development so much as to get a better understanding of the hydrologic/meteorologic effects of precipitation. For further information see the following references:

References

Klazura, G.E., T.D. Crum and R.L. Alberty, 1992: The WSR-88D and its Applicability to Water Resources Data Collection. 28th Symp. of Amer. Water Resources Assoc., Reno, NV, pp. 14.

Shedd, R and R. Fulton, 1993: WSR-88D Precipitation Processing and its use in National Weather Service Hydrologic Forecasting, pp. 6.

Smith, J.A., R.C. Shedd and M.L. Walton, 1989: Parameter Estimation for the NEXRAD Hydrology Sequence. 24th Conf. on Radar Meteor., Tallahassee, FL, pp. 259-263.

Large-Scale Applications with an Emphasis on the 1993 Floods

Lecturer: Lee Larson
Date: June 22, 1994
Notes by: Suzanne Hartley
Nan Schmidt

Introduction

The National Weather Service (NWS) is responsible for the monitoring and prediction of not only meteorological events, but also hydrologic events. Its mission is to provide river and flood forecasts and warnings for the protection of life and property and to provide basic hydrologic forecast information for the nation's economic and environmental well being.

Thirteen River Forecast Centers (RFCs), each covering a major drainage region of the country, provide the hydrologic expertise for the NWS. The RFCs develop the forecast procedures, new technologies (both hardware and software) and new data techniques. The RFCs deal with the Weather Forecast Offices (WFOs) rather than the public directly. Incoming data (precipitation forecasts, river stages, snowpack measurements etc.) are input to hydrologic models. The outcome is a forecast that is then forwarded to a WFO. The WFO then conveys information such as the following to the public via the broadcast media.

Forecasts - floods, minor rises, daily mainstem conditions, reservoir inflows
Outlooks - water supply, spring flood potential, navigation
Advisories - headwater/flash floods, ice conditions (i.e. threats of jamming)

River Forecasting

There are three steps to producing a forecast:

1. Estimate runoff that will result from precipitation
2. Forecast distribution of runoff as it passes a forecast point, i.e. construct hydrograph
3. Forecast change in shape of hydrograph as it moves downstream - routing.

These steps will be discussed in turn.

1. A number of methods exist for translating rainfall into runoff. Two methods are presented here: an empirical method and the use of a conceptual model. Nomograms have been developed that estimate runoff from: the time of year (accounts for seasonal variation in runoff); total storm precipitation; storm duration; and the antecedent precipitation index (API).

The amount of precipitation that actually becomes runoff depends on the antecedent wetness or dryness of the watershed. The relative wetness or dryness of the watershed can be represented by the API . Suppose on day 1 that the API is equal to 3. On day 2, the value of the API will be the sum of some fraction (e.g., 0.9) of the API on day 1 and the depth of rain that fell on day 1. If day 1 was dry, then the new API is simply 0.9*3 = 2.7. This lower values indicates the watershed is drying. If, on the other hand, there was 2 inches of rain on day 1, then the new API would be 0.9*3 + 2 = 4.7, i.e., the watershed is becoming wetter.

The nomograms are derived empirically and are thus only valid for the regions for

which they were developed. A more generalized approach is the use of a conceptual model that attempts to model the various processes which determine how much of the incident precipitation will actually runoff into the river channel. The model used by the NWS is the NWS River Forecasting System (NWSRFS) catchment model (also known as the Sacramento model). The model includes a number of parameters than can be varied to suit specific local conditions. The values of these parameters are usually determined by calibration. Historical data are run through the model, and values of parameters found such that the modeled hydrograph duplicates the observed hydrograph.

2. The concept of the unit hydrograph is used to determine the shape of the hydrograph. Application of the unit hydrograph approach is based on the assumption that hydrographs (at a given point) from similar storms will be similar in shape and length. The unit hydrograph is also based on a runoff volume equivalent to a depth of one inch over the entire area. For a runoff volume equivalent to N inches, the hydrograph can be constructed by simply multiplying the value of each ordinate by N.

The unit hydrograph approach also assumes that the rainfall is uniform across the area, and so tends to be computed for small hydrologic units. The hydrograph at a point near the bottom of a large drainage is actually the sum of the many small unit hydrographs within the drainage.

3. Once the hydrograph is computed at one forecast point, it then has to be routed downstream. As the flood wave moves downstream, the flood crest becomes reduced in height and occurs relatively later (the rising limb of the hydrograph is longer in time). Hydrographs for forecast points downstream can be determined by a number of procedures that will not be discussed here, but are described in most hydrology texts.

Discharge-Stage Relationships

Most computational procedures produce river forecasts in terms of discharges e.g., in cubic feet per second (cfs). This is meaningless to most of the general public - what is most important is the corresponding depth, or stage, of the flow as this will determine whether the river will flow overbank, i.e., flood.

Stage-discharge relationships convert river discharge to river stage. These relationships are determined from measurements made by the U.S. Geological Survey (USGS). There is a lot of scatter in the curves - a good one may be accurate to within 5-10%, but this may amount to a stage difference of 2 feet. The other problem with stage-discharge relationships is that they are based on measure historic river flow and so have to be extrapolated (often considerably!) for floods of record.

1993 Floods

The 1993 floods in the Midwest provide a good example of large-scale hydrologic predictions of precipitation, flooding, impacts, and verification. In a nutshell, too much rain caused the 1993 floods, especially three episodes in July. Other factors identified by NWS include wet soils in the Fall, high base flows in rivers, and significant spring snow cover. NWS spring flood predictions take snowcover, soil moisture, and streamflows into account.

Model forecasting melts snow based on historical temperature patterns, which can be modified based on temperature forecasts. Future precipitation is added during the model runs based on historical patters (or can be modified based on quantitative predictive forecasting (QPF)). Outlooks provide crest and date information for selected locations throughout the Midwest (approximately 1,000 locations are available).

By July 1993, much of the Midwest had received at least 10 extra inches of annual rain (**Fig. 1**). The flooding caused by this rain caused rivers such as the Missouri and the Mississippi to exceed flood stage (the level past which the river spills over its banks or levees) by July. Peak flood levels on the Missouri River at Kansas City, MO, were almost 47 ft and were almost 50 feet at St. Louis, MO. This unprecedented flooding caused many nonfederal levees to fail (1043 out of 1345) but most federal levees held (40 out of 226 failed). Flooding on the Missouri River lasted 62-94 days, whereas Mississippi River flooding lasted as long as 195 days in some areas. Construction of hydrographs along the affected river stretches allowed hydrologic predictions of peak flooding; important information for planning evacuations as levees threatened to fail.

As a result of the 1993 Midwest floods, debate is still ongoing about whether or not the breached levees should be rebuilt. Arguments against rebuilding include minimizing future risks by discouraging new construction in floodplains and benefits to wetlands and wetland species.

Damages associated with the 93 floods will probably reach $15 billion; between 45-50 people died as a result of the floods, and 75 towns were inundated. Barge traffic on the Mississippi and Missouri Rivers was halted, as was railroad traffic in the Midwest. Damage savings due to NWS hydrologic services during the 1993 Midwest flood are estimated at 10% of $15 billion=$1.5 billion. This is in contrast to the approximately $2 million annual cost of the services provided.

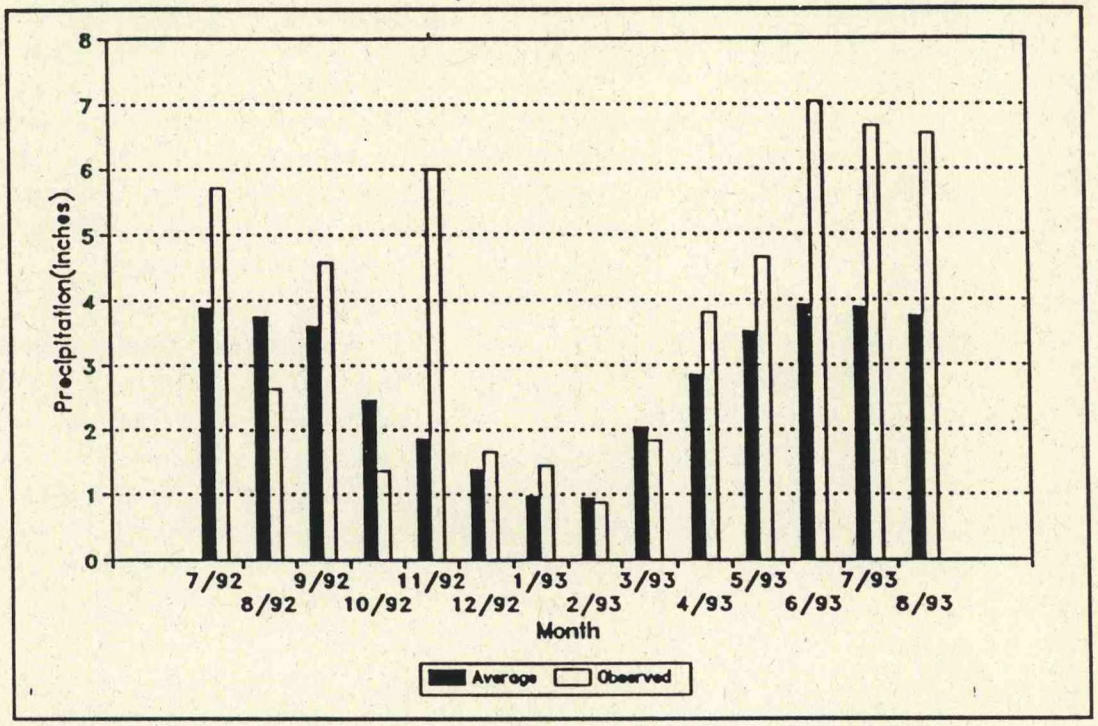

FIGURE 1 *Comparison of average and observed monthly precipitation totals for the upper Mississippi River basin.*

Snow Data

Lecturer: Tom Carroll
Date: June 23, 1994
Notes by: Greg Poulos
Nan Schmidt

Along with its normal duties as a River Forecasting Center (RFC), the NOAA hydrological office in Minneapolis operates an airborne snow survey program and a snow estimation and update system. These programs enable the NOHRSO to produce mean areal maps of snow water equivalent (SWE) with 1 km resolution. Primarily, snow information is generated from point, line and area measurements by snow core samples, aircraft flight measurements and satellite sweeps, respectively. The gridded SWE information is available for general use on optical disk back to 1989 (for a fee) and is available over internet.

The airborne snow survey program is operated with 3 planes nationally, each equipped with gamma radiation detectors. Prior to the first snowfall in a region over which snow water equivalent is desired, measurements of the gamma radiation are made. This provides a background measurement to which later measurements can be compared. Gamma radiation is emitted from Uranium-238, Thorium-237 and Potassium-40 which exist in the Earth soils. The instruments that measure this radiation detect the rate of scintillation of gamma-sensitive sodium iodide crystals. Air pressure and temperature are also measured along the flight line. Flight lines are generally 100 miles long and multiple passes are made. This measurement is considered a line measurement although it actually represents a swath about 2-3 km wide along the flight path. Using established but empirical algorithms the SWE is then calculated. The algorithm is based on the difference between later and initially measured soil moisture and gamma radiation. Based on comparison with the average over 1000 snow cores (to represent SWE over the flight path 2-3 km wide) this method is accurate within 0.81 cm and 2.31 cm of the actual SWE for non-forested and forested areas, respectively. This method also produces reasonable SWE over mountainous areas despite the complex terrain features.

Since soil moisture and SWE measured by these flight surveys is limited in spatial extent, the generation of national maps is greatly improved by satellite data. Soil moisture can be estimated from the Landsat satellite with 90 meter resolution from its thematic mapper (TM) in the 1.6 micron radiation band. This very, very, very high resolution data is not available daily so that operationally the AVHRR (Advanced Very High Resolution Radiometer) satellite is used. A 1.6 micron channel is to be included on the AVHRR/2 satellite (launched in a couple years) so that SWE estimation will become much better. Using digitized land surface information from digital elevation models (DEM) and a GIS (Geographical Information System) the satellite data can be processed in 2 hours from its receipt. Because the AVHRR channels cannot see through clouds to detect snow cover a sister data set is generated from the SSM/I satellite (Special Sensor Microwave Instrument) whose channels can probe despite cloud cover. Unfortunately the resolution of the SSM/I is about 20 km. Combining the data from each satellite allows routine mapping of the SWE for the entire U.S..

The entire snow estimation and update system is comprised of three parts. First, the above described techniques are calibrated to ground truth. Melting of snow cover is estimated by classifying the ground surface into melt zones. This melt zone classification is based on

location, elevation, slope, forest cover and aspect. The second part is the operational portion, and it uses the algorithms as data is ingested to create the various data sets from point, line and area observations. Then the third step, SWE updating, is completed through an optimal interpolation procedure which combines the strengths and weaknesses of the various data types in a systematic fashion to produce the best possible SWE map. Over time these maps have been used to create mean monthly areal SWE maps (climatic norms). This then allows the daily output of SWE deviation from the norm maps at 1 km resolution. In combination with mean monthly temperature and precipitation maps, the SWE maps can alert those at the RFC of developing potential flooding situations.

Runoff Modeling

Lecturer: Eric Anderson
Date: June 23, 1994
Notes by: Alan Zeigler
Sam Levis

Runoff is estimated from coupled models of snow accumulation, snow ablation, and soil water transport. The four basic categories of runoff models are:

1) Black box - purely statistical, no physical basis
2) Empirical - based on experiments and observations, no physical basis
3) Conceptual - simplified representations of the most important physical processes
4) Physically Based - parameterization of non-linear physical processes

Runoff models can be applied to entire watersheds (lumped, e.g. black box) or elements of watersheds (distributed, e.g. physically based).

The National Weather Service (NWS) has three forecasting applications for runoff models (usually empirical and conceptual):

1) Short term forecasts of river conditions (hours to days)
2) Extended Predictions of streamflow (weeks to months)
3) Flash flood forecasts (less than 12 hours)

The objectives of these forecasts are flood forecasting, reservoir control, and navigational and recreational safety.

Models used by NWS

The NWS is making a transition from empirical to conceptual models. Empirical models are event-based; they compute runoff from precipitation, an antecedent precipitation index (API), storm duration, and time of year.

The snow model used by most NWS RFCs is conceptualized by **Fig. 1.**

NWS uses the Sacramento model to account for soil moisture conditions and water flow within a stream network. The model breaks down the flow into several subprocesses, which operate at variable time scales: direct runoff, surface runoff, infiltration, interflow, percolation, baseflow, subsurface outflow, and evapotranspiration (see **Fig. 2**). The Sacramento model simulates runoff well with reasonably accurate mean areal estimates of precipitation. Some RFCs use API type models because they are simpler and easier to adjust in real time, however, the Sacramento model performs better overall--specifically after dry periods. To produce extended stream flow predictions only the Sacramento model or a continuous form of the API can be used.

Runoff models must be calibrated to individual watersheds because they are simplifications of physical processes. NWS uses a 3 phase approach to model calibration:

Phase 1: Determination of initial parameters from physiographic factors, hydrograph analysis, or similar nearby calibrated watersheds.

Phase 2: Manual adjustment of parameter values based on knowledge of the model versus historical trends (trial and error).

Phase 3: Automatic optimization of selected parameters (sometimes done to facilitate the trial and error procedure).

Future Developments

NWS is developing distributed (sub-watershed scale) models using gridded rainfall data derived from NEXRAD.

Where to Look

Contact Eric Anderson by e-mail if you want documentation and subroutine code for the runoff models used by NWS.

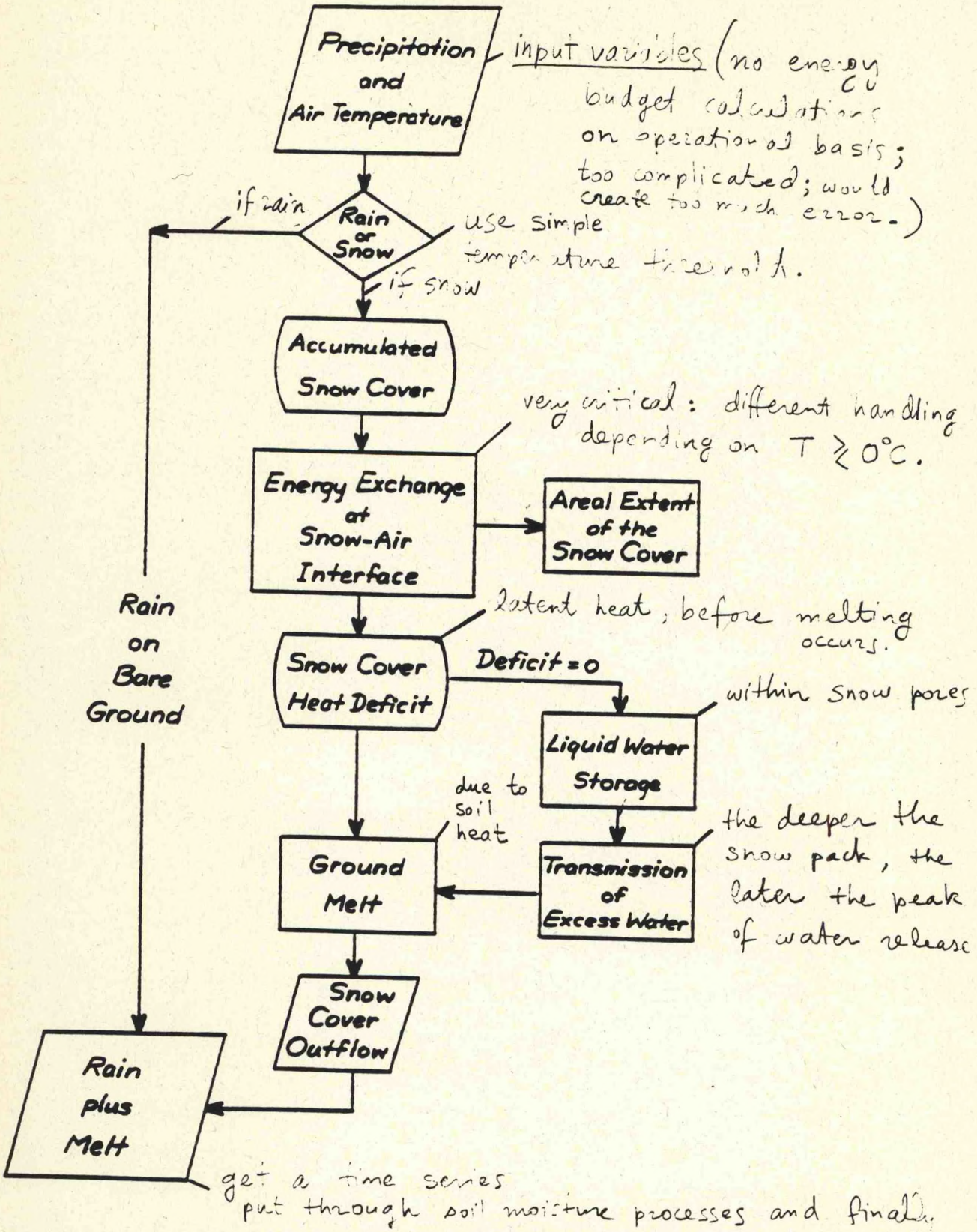

Figure 1. Flowchart of the snow accumulation and ablation model

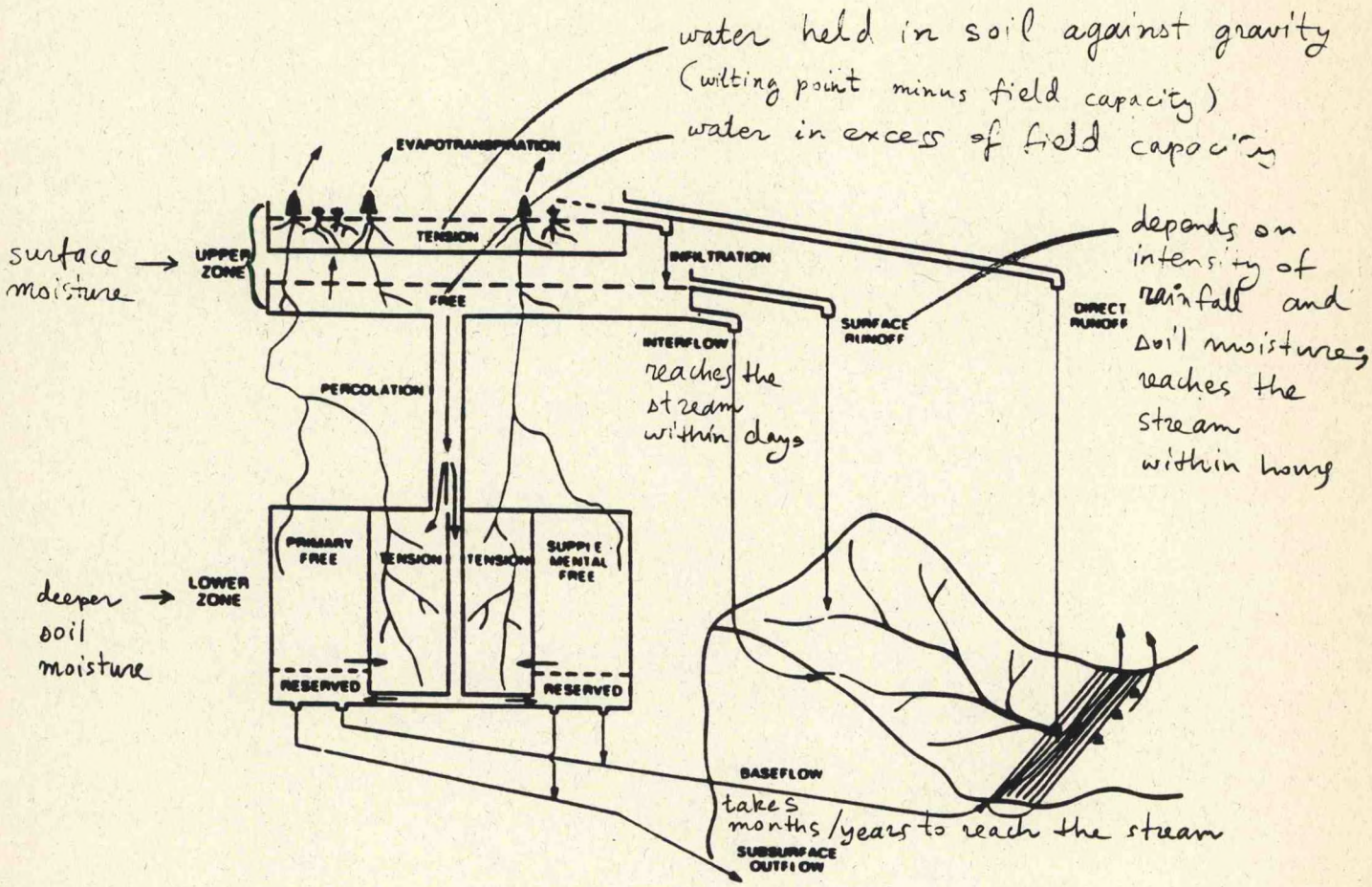

FIGURE 2 Schematic representation of the Sacramento model

Interactive Forecast Program

Lecturer: George Smith
Date: June 23, 1994
Notes by: Yimin Ji
Suzanne Hartley

Overview

The NWSRFS (National Weather Service River Forecasting System) Interactive Forecast Program (IFP) is a "front-end" program in which the NWSRFS Operation Forecast System (OFS) is linked to a Graphical User Interface (GUI).

The fundamental aims are:

1. To provide river forecasters with the information needed to make decisions about the quality of data or model results, and
2. To provide them the capability to easily and quickly put those decisions into action and produce a forecast reflecting the best estimates of current and future meteorological conditions.

There are two main applications which make up the NWSRFS/IFP:

1. NWSRFS itself, which performs the hydrologic computations. The hydrologic models used are identical to those run on other computers of the OFS.
2. A GUI which provides a geographic display of the River Forecast Center area, displays the results of model runs, and allows the forecaster to interactively make adjustments to model parameters, including the unit hydrograph.

The IFP uses the forecast group as the basic unit for modeling the rainfall-runoff process. A forecast group is a drainage basin that is comprised of contiguous, topologically-connected sub-basins (forecast points or segments). It is at the sub-basin scale that the hydrologic models within NWSRFS are applied. The system forecasts all points daily or twice daily.

Graphical User Interface

The principal intent of the IFP is to make the use of NWSRFS as simple as possible such that forecasters can concentrate on the process of issuing hydrologic forecasts without having to struggle through compute and operating system gymnastics!

The IFP/GUI, which is written within the X-Window system using the C programming language and Motif Toolkit, provides a graphical means by which the user interacts with the computer and NWSRFS. The IFP runs on a workstation in a UNIX environment.

Initial Display

After initial data such as model parameters, rating curves, segment connectivity and other operational values have been selected, the application creates a geographic display and

a schematic of the forecast group (**Fig. 1**, bottom left). The small boxes with forecast names in them represent the individual segments of the forecast group. The lines connecting the boxes show stream connectivity. The color of each box represents the current flow conditions: green indicates a normal flow condition; yellow, near to bankfull or alert conditions; and red, flood conditions. Gray indicates that the flow condition can not be determined. The same color scheme is used in the display for the sub-basin outlines (**Fig. 1**, upper left).

Interactive Forecasts

After selecting the forecast group, the carryover date (the date from which the forecast will be matched with observations) and the start date in the initial window, the forecaster can run the hydrologic models. The forecaster can select from a number of operational options and direct the flow of the program to model an area by a particular process, e.g., if parts of the forecast group are snow-covered, then the snow accumulation and melt routines of HYDRO-17 can be applied. The system begins the model run with the most upstream forecast point in the forecast group and proceeds downstream. Results can be displayed for any selected segment or forecast point. Results are displayed in 3 main plot areas (**Fig. 2**). A hyetograph of the precipitation time series is shown at the top. The middle plot shows observed runoff (for the carryover period). The bottom plot shows observed (circle plot) and forecast hydrographs. Flood or flood-warning stages are also shown in the display.

At this point, the user can interactively make changes to certain input data and parameters (including the form of the unit hydrograph) and rerun the current forecast point, or continue with another downstream forecast point. The process is repeated until the forecaster is satisfied with the forecasts for all the points in the forecast group.

Interactive modifications results in improved forecasts for several reasons. For example, inaccuracies in the calibration process may make some adjustments necessary. Application of the unit hydrograph assumes a uniform distribution of rainfall over the basin. If the distribution of rainfall is non-uniform, then a different hydrograph shape may be required to better reflect how the basin is responding to the rainfall event. The actual shape of the unit hydrograph can be modified graphically in the IFP.

Modifications do not apply to the basic calibrated model parameters, but only apply to the current forecast. However, while the forecast is being prepared, any modifications made are saved in a mod. file. The changes can be saved and carried over to the next forecast, but they will only be applied to the carryover period. Hopefully, as distributed models come on line, and further advantage is taken of improvements such as NEXRAD, such adjustments will become less necessary.

Reference

Office of Hydrology, 1994: *NWSRFS Interactive Forecast Program, User's Guide.*

NWSRFS
Interactive Forecast Program

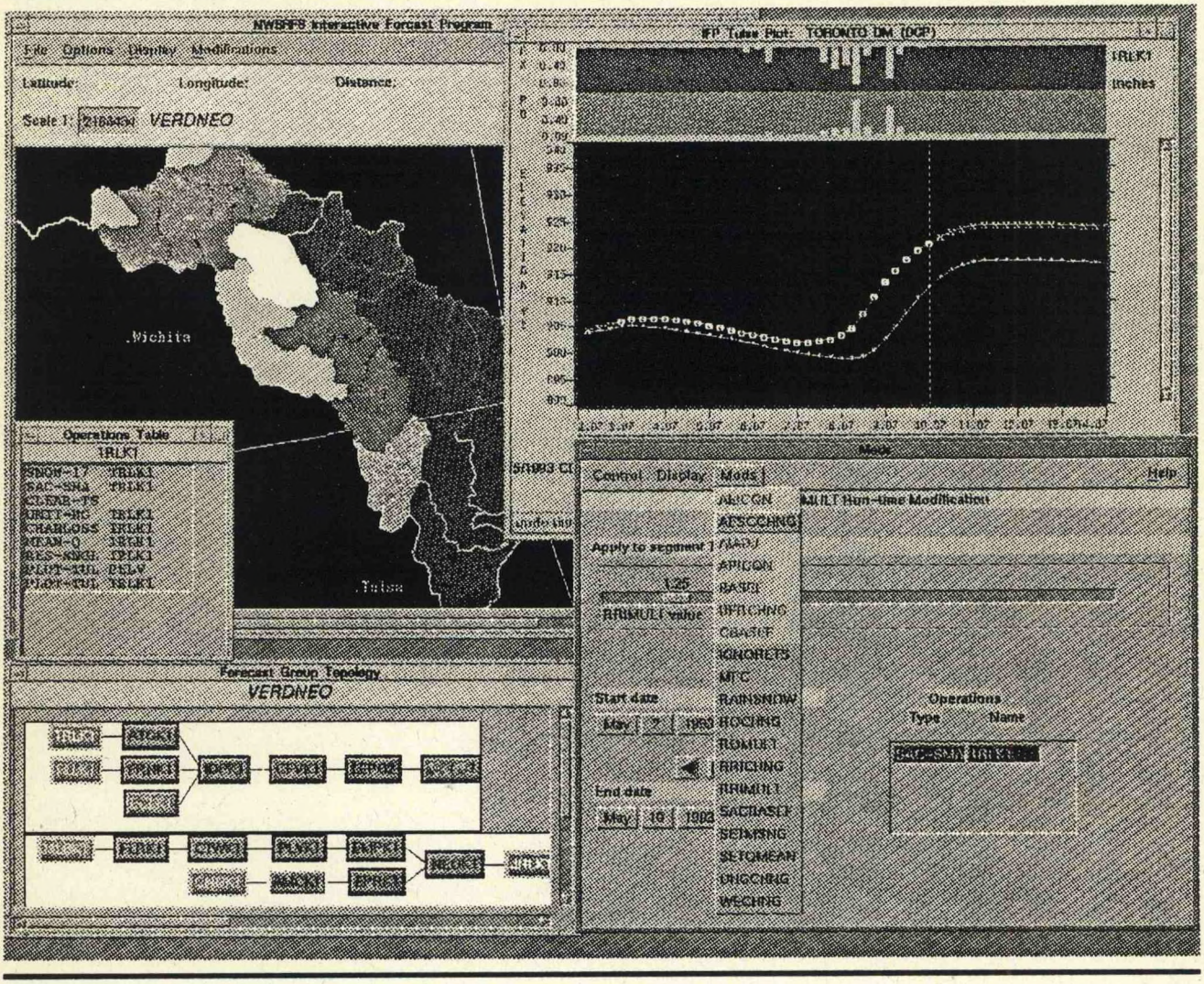

User's Guide

FIGURE 1

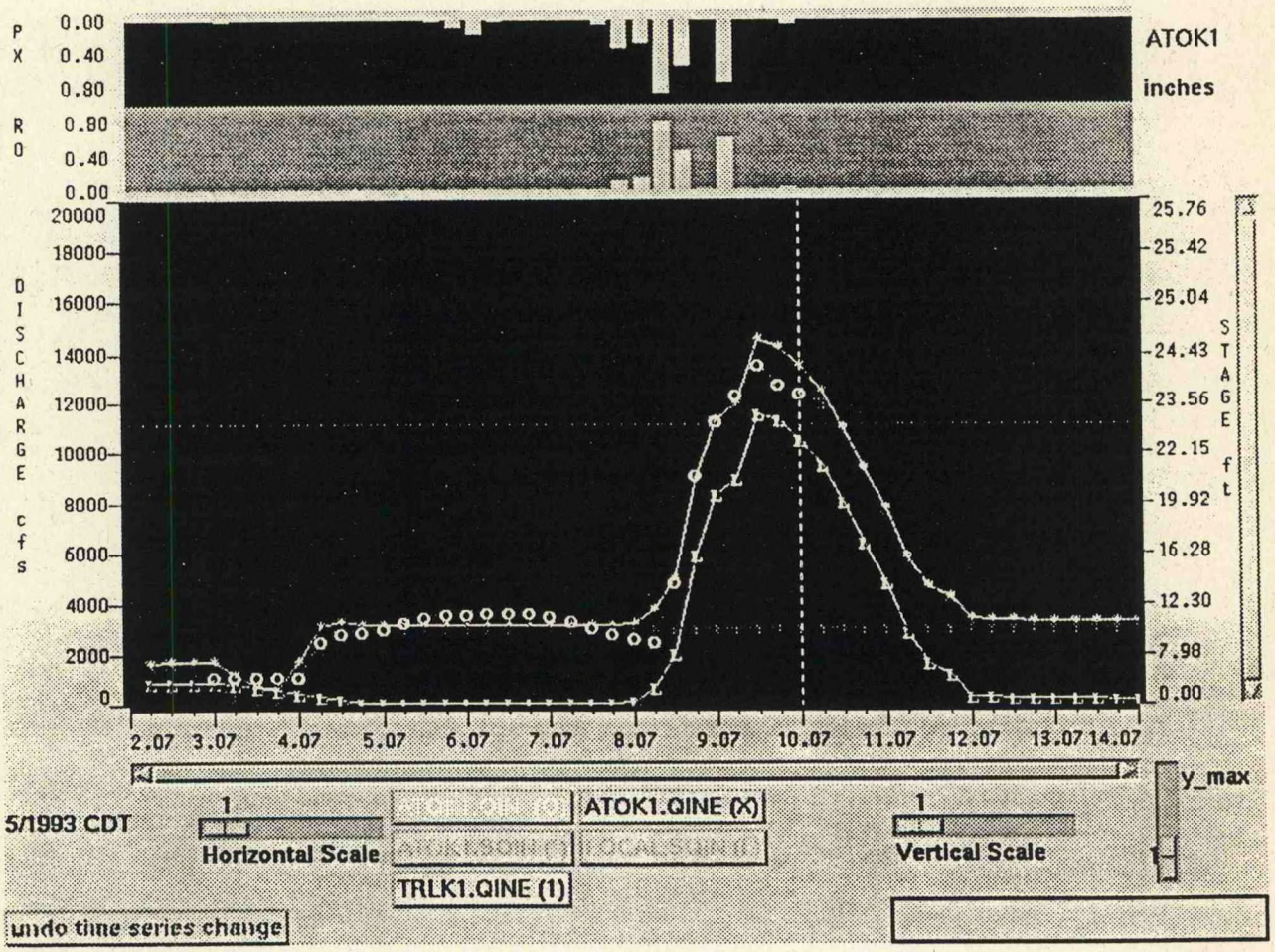
P
X
0.00
0.40
0.80
ATOK1
inches
R
O
0.80
0.40
0.00
DISCHARGE cfs
20000
18000
16000
14000
12000
10000
8000
6000
4000
2000
0
25.76
25.42
25.04
24.43
23.56
22.15
19.92
16.28
12.30
7.98
0.00
STAGE ft
2.07
3.07
4.07
5.07
6.07
7.07
8.07
9.07
10.07
11.07
12.07
13.07
14.07
y_max
5/1993 CDT
1
Horizontal Scale
ATOK1.QINE (X)
TRLK1.QINE (1)
1
Vertical Scale
undo time series change

FIGURE 2

Hydrologic Forecasting in the NWS

Lecturer: Michael D. Hudlow
Date: June 23, 1994
Notes by: Suzanne Hartley
Lihang Zhou

Introduction

The Hydrologic Services Program of the NWS has a two-part mission: to provide river and flood forecasts and warnings for protection of life and property; and, to provide basic hydrologic forecast information for the nation's economic and environmental well being. Although the first part of the mission was originally the primary purpose of the program, the increasing importance of water resources has now made the provision of hydrologic forecasts for economic purposes a priority.

The importance of the program is reflected by the fact that over 75% of presidential disaster declarations are a result of flooding. Average annual flood losses total more than $2 billion, a number that is growing due to continuing development of floodplains and growth in parts of the economy that depend on rivers.

Organization

The organizational structure of the current NWS Hydrological Program is shown in **Fig. 1**. The Office of Hydrology oversees the Hydrologic Research Laboratory, the Hydrologic Operations Division, and the Water Management Information Division. Field offices include the thirteen River Forecast Centers (RFCs), the Weather Forecast Offices (WFOs), and the Regional Directors' Offices. The RFCs are responsible for hydrologic modeling and forecasting. The forecasts are forwarded to the WFOs which have the responsibility of alerting the public of flood watches and warnings. The RFCs also provide hydrologic information for agencies such as the Bureau of Reclamation and the Tennessee Valley Authority (TVA), which need to plan reservoir releases, turbine operations, etc. The RFCs and WFOs coordinate with the Regional Directors' Offices, and all parts of the program interface with other agencies and universities.

The thirteen RFCs provide forecasts for around 3000 forecast locations in the United States. In addition to providing warnings of potential for either flash flooding or local flooding, the forecasts are used to determine water availability for navigation, irrigation, recreation, power generation etc.

River Forecast System

The river forecast system consists of four components:

DATA => PROCESSING => MODELS => OUTPUT

The data are acquired from multiple sources, such as rain gages, stream gages, weather radar, satellites, and snow surveys. Around 5500 hydrometeorological automated data systems are located throughout the country and river discharges are measured at over 7000 stations.

Consequently, good data management and analysis capabilities are required. The NOAA hydrologic data system strives to ensure that appropriate data are acquired and managed for the purposes of forecasts and precipitation. The data itself is often the weakest component in the system. Inadequate data (with regard to both quality and quantity) can make calibration of models more difficult. Increasing use of NEXRAD for precipitation estimates combined with improved processing capabilities has resulted in considerable improvements where the facilities are already installed. By 1996, virtually all of the conterminous United States will be covered by NEXRAD.

Data are also obtained from many local flood warning systems throughout the country. These are positioned to capture small, rapidly responding basins which are susceptible to flash flooding. Most are automated, relaying precipitation and streamgage data to a processing station where the potential for flash flooding can be evaluated. Many have been installed by local communities in response to a damaging flash-flood event. They are located primarily in mountainous regions or in flatter areas where surface ponding tends to occur.

Advances in River Forecasting

Advancements in the hydrologic prediction system are in the pipeline and will improve these forecasts. The four main components of the Advanced Hydrologic Prediction System are shown in **Fig. 2**. The system is set to be able to take advantage of NOAA's science and operations infrastructure, NWS modernization (e.g. the installations of NEXRAD), a new water resources forecasting system (WARFS), and partnerships with various agencies. As the Office of Hydrology is not large, the partnerships with other agencies are very important. WARF Cooperators include federal agencies (e.g., US Geological Survey, Corps of Engineers), regional commissions (e.g., Salt River Project, Denver Water Department), state/local agencies, universities, and some private sector companies (e.g., Westinghouse Savannah River Company). WARFS was recently approved by Congress and will be operational shortly, enabling the NWS to do a much more complete job with the second part of the mission, i.e. the provision of hydrologic forecast information for the nation's economic and environmental well being. Solutions for more complex river systems will be possible owing to advancements in data collection, data analysis and modeling. Predictions which are more accurate and available further in advance will provide opportunities for improved management of the nation's water resources.

The Advanced NOAA River Forecast System combines the most advanced modeling with the best data available. Nonetheless, deterministic forecasts cannot typically be carried out further than 7 days. It is not reasonable to carry the forecast any further without taking into account future rainfall events. Thus, an approach somewhat akin to ensemble forecasting in meteorological models is adopted (**Fig. 3**). Possible future conditions for the time period in question are taken from the historical record. For example, if 40 years of record are available then up to 40 possible scenarios or traces of river flows can be obtained and used in an extended streamflow prediction (ESP) analysis. A specified window at any time into the forecast (up to one year) can be selected and the 40 traces treated in a probabilistic manner (weights can be applied to the traces in the ensemble if the forecaster has reason to be believe that some scenarios are more likely to occur than others). For example, one may estimate the probability of the total cumulative river discharge during the specified window exceeding a specified volume. Estimates of a range of probabilities provide managers with

a basis for risk assessment analysis for reservoir operations, navigation, etc.

In the future, it is hoped that the ESP analysis will be linked with GCMs. However, this is not yet a viable option for real-time applications.

References

Hudlow, M. D., 1988: Technological Developments in Real-Time Operational Hydrologic Forecasting in the United States. *Journal of Hydrology*, **102**, 69-92.

Day, G. N., 1985: Extended Streamflow Forecasting Using NWSRFS. *Journal of Water Resources Planning and Management*, **111**, 157-170.

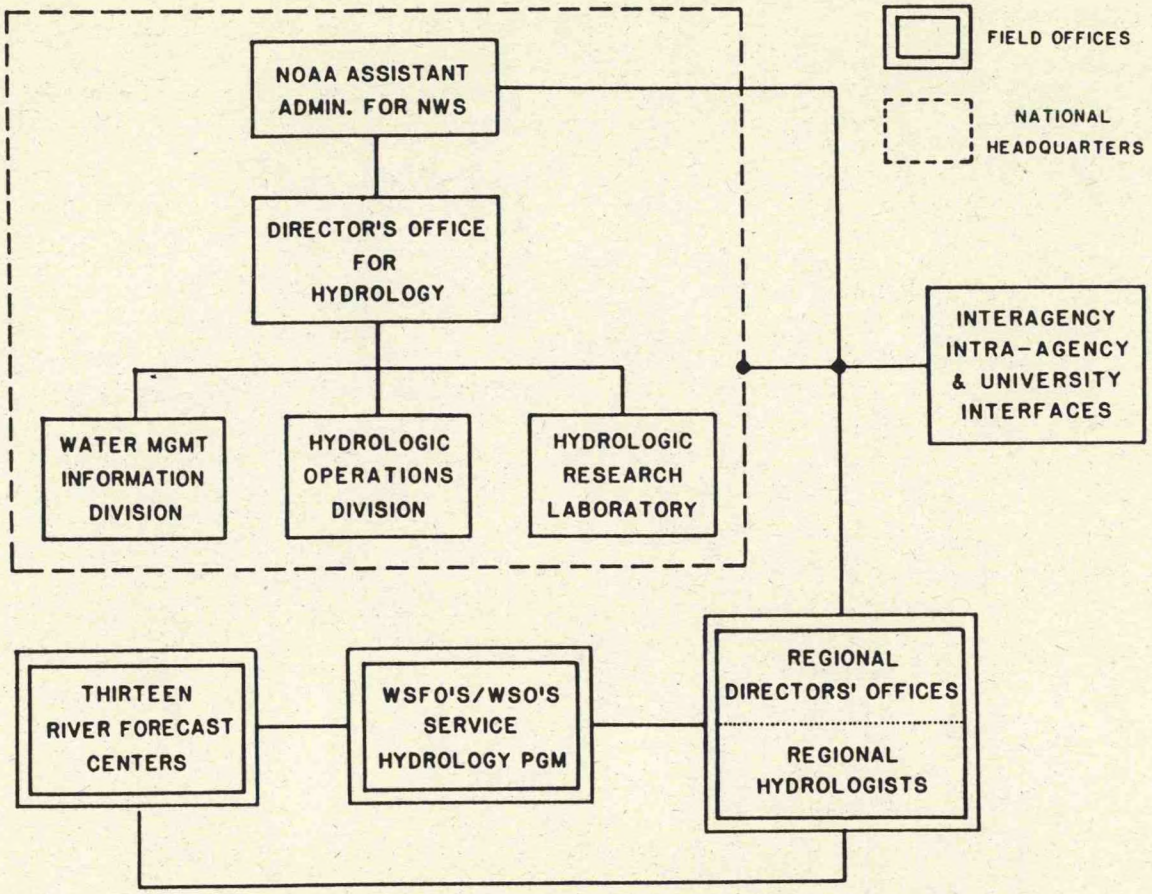

Fig. 1. Basic organizational structure of the current NWS hydrologic program.

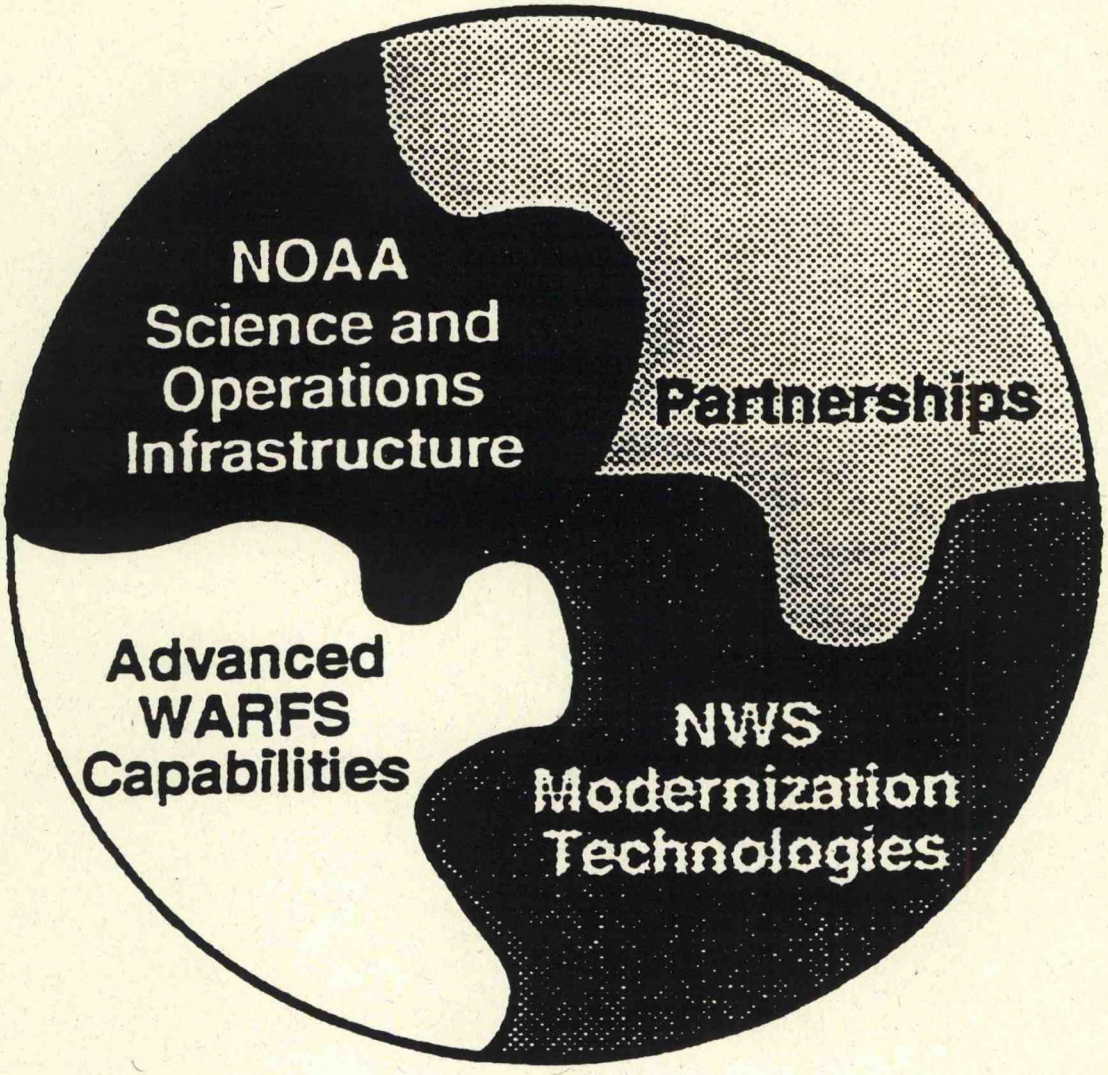

Figure 2: Major programmatic components of the Advanced Hydrologic Prediction System (AHPS).

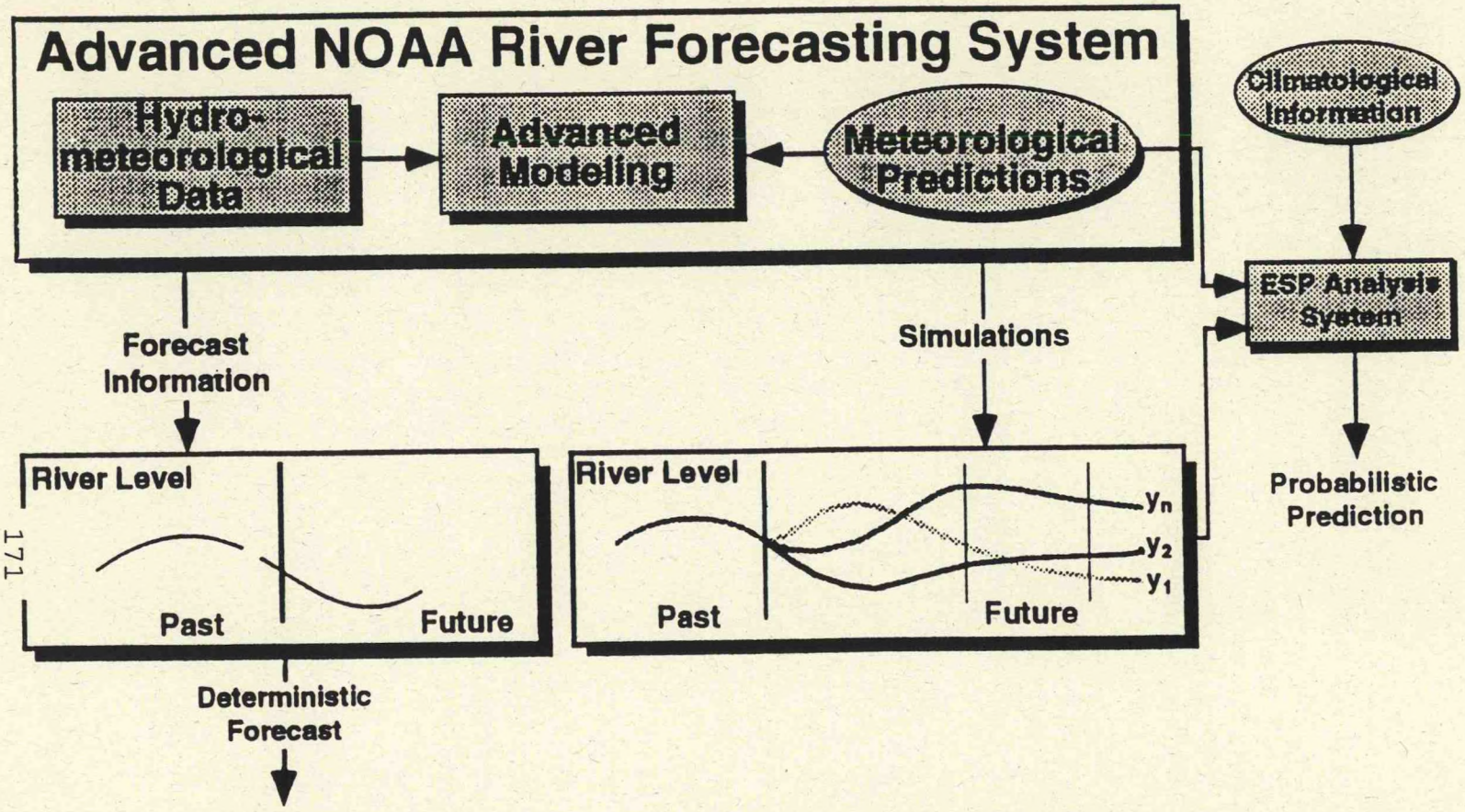

Figure 3: Illustration of the major data, modeling, and prediction functions of the AHPS, embodying WARFS scientific applications; y_1, y_2 ... y_n are ESP simulations for *n* years of historical records.

Hydrodynamic Modeling of Rivers, Reservoirs, and Estuaries

Lecturers: Danny L. Fread and Janice Lewis Notes by: Scott Stanley
Date: June 24, 1994 Zhaoqing Yang

The technique of mathematically modeling the unsteady flow through a waterway is called flow routing. The primary parameters which are calculated using this procedure are the variation of the magnitude, speed, and shape of the flood wave with time. The types of waterways which can normally be modeled using the flow routing techniques include rivers, streams, reservoirs, estuaries (intersection of a river and an ocean), canals, drainage ditches, and storm sewers. Likewise, the flows can be caused by a number of phenomena including precipitation runoff, planned reservoir releases, dam failures, landslide and earthquake generated waves, volcanic mud flow, hurricane generated storm surges, and many others.

The most common, and most feasible, methods of flow routing is a one-dimensional approach. Fread discusses a variety of models of this type in chapter ten of the book *A Handbook of Hydrology*. The governing equations for this one-dimensional approach are the Saint-Venant equations which are discussed by Fread. One-dimensional flow routing models can be divided into two types, lumped routing (storage routing) and distributed routing (hydraulic routing). In lumped flow routing models the flow variation with time is calculated at one location along the waterway at a time. This one location represents a large section of the waterway. In distributed flow routing models, on the other hand, the flow variation with time is calculated simultaneously for a number of locations down the waterway. A graphic representation of these two types of models can be seen in **Fig. 1**.

In the depiction of a lumped process in **Fig. 1**, the inflow, $I(t)$, and outflow, $Q(t)$, from the lumped portion of the waterway are both functions of time. The principle of mass conservation then leads to a simple equation:

$$I(t) - Q(t) = dS/dt$$

where $S(t)$ is the storage of water in the lumped portion of the waterway. The most simple forms of the storage function are single-valued functions of either outflow, Q, or flow height, h. This implies that the fluid height is uniform throughout the lumped portion of the waterway. The advantage of lumped models is their relative simplicity. However, they neglect backwater effects, and do not work well for rapidly rising waters in mild to flat sloping rivers, or in reservoirs.

Distributed models do a much better job of modeling the unsteady flow in waterways due to the fact that they allow the flow rate, velocity, and depth of the fluid to vary in space as well as in time. As discussed above, lumped models assume the fluid height is constant through the lumped region. Distributed models are governed by the full one-dimensional Saint-Venant equations,

Conservation of Mass;

$$\partial Q/\partial x + \partial s(A + A_o)/\partial t = 0$$

Conservation of Momentum;

$$\_Q/\_t + \_(Q^2/A)/\_x + gA\ (\_y/\_x - S_o + S_f) = 0$$

where,

$$S_f = S_o - \_y/\_x - 1/(gA)\ \_(Q^2/A)/\_x - 1/(gA)\ \_Q/\_t$$

In these equations, A is the wetted cross sectional area of active flow, A_o is the cross sectional area of inactive flow, and g is the acceleration of gravity. The first term on the right hand side of the equation for S_f is the kinematic term, the second term is the diffusion term, and the remaining terms are the inertia terms. Depending on the problem being solved, the importance of these terms varies. These one-dimensional equations are typically solved using an implicit/explicit finite difference technique.

The National Weather Service uses two models based on the distributed flow routing technique. The first and most general of these models is FLDWAV. This model is described in the books by Chow et. al. (1988), and Fread (1985), and the paper by Fread and Lewis (1988). The second model, DAMBRK, is geared toward floods due to dam breaks and is described in the book by Chow et. al. (1988), and the papers by Fread (1977, 1988, 1989). Efforts are currently underway at the National Weather Service to incorporate these two models into one more general unified model.

References

Chow, V. T., D. R. Maidment, and L. W. Mays 1988: *Applied Hydrology*, McGraw-Hill, New York.

Fread, D. L., 1992: Flow Routing. *Handbook of Hydrology*, (Ed. R. Maidment), McGraw-Hill, New York, Chapter 10.

Fread, D. L., 1977: The Development and Testing of a Dam Break Flood Forecasting Model. *Proc. of Dam-Break Flood Modeling Workshop*, U.S. Water Resources Council, Washington, D.C., pp. 164-197.

Fread, D. L. 1985: Channel Routing. *Hydrological Forecasting*, (Eds. M. G. Anderson and T. P. Burt), John Wiley and Sons, New York, Chapter 14, pp. 437-503.

Fread, D. L., 1988: *The NWS DAMBRK Model: Theoretical Background/User Documentation*, HRL-256, Hydrologic Research Laboratory, National Weather Service, Silver Springs, MD, 315 pp.

Fread, D. L., 1989: National Weather Service Models to Forecast Dam-Breach Floods. *Hydrology of Disasters* (Eds. O. Starosolszky and O. M. Melder), Proc. of the World Meteor. Org. Tech. Conf., Nov. 1988, Geneva, Switzerland, pp. 192-211.

Fread, D. L., and J. M. Lewis, 1988: FLDWAV: A Generalized Flood Routing Model. *Proc. of Nat. Conf. on Hydr. Engr.*, ASCE, Colorado Springs, CO, pp. 668-673.

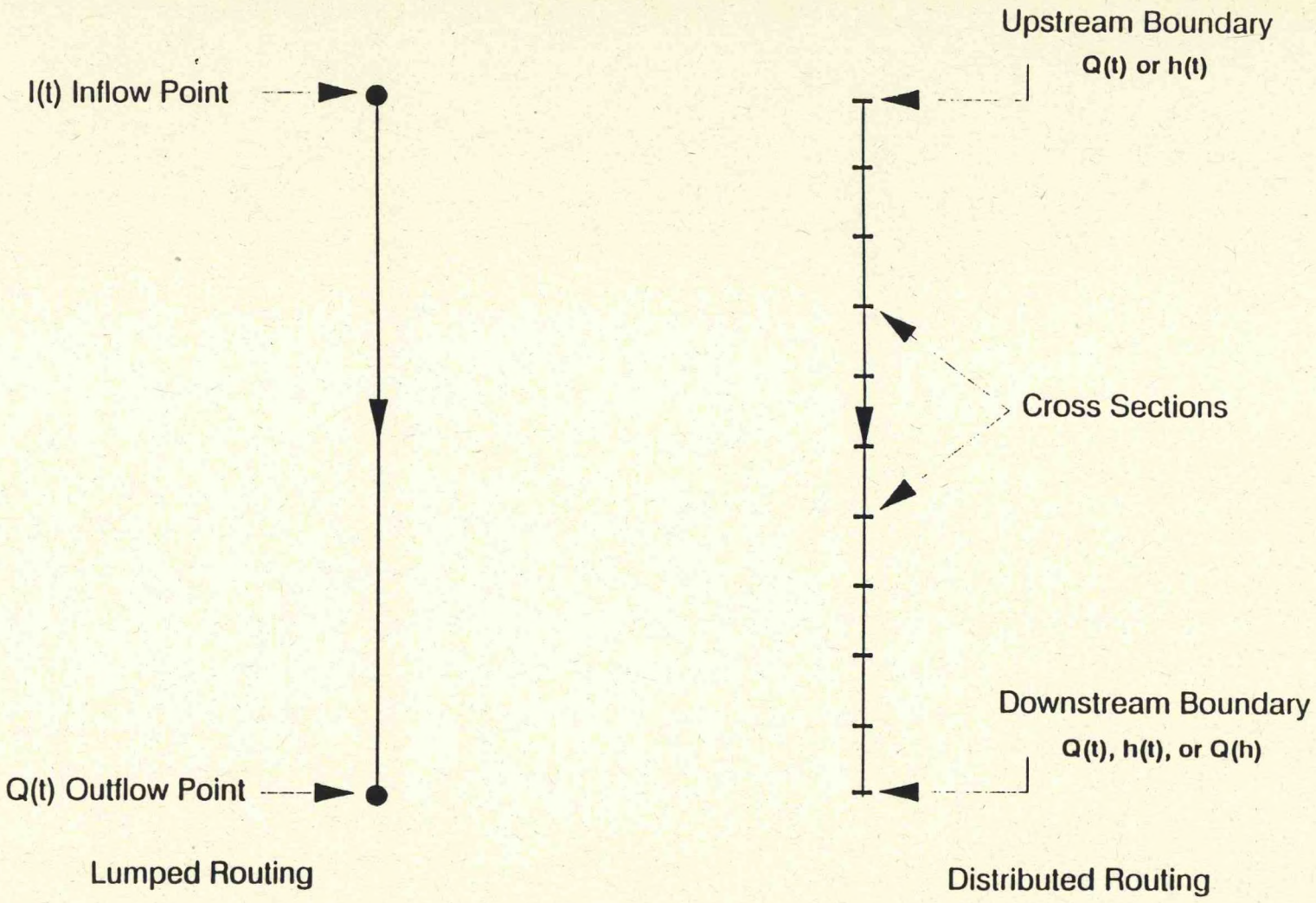

FIGURE 1 Schematic showing lumped and distributed flow routing systems, where Q is discharge or flow rate, and h is water surface elevation or stage.

Hydrodynamic Modeling Demonstration

Lecturer: Danny Fread and Janice Lewis
Notes by: Zhaoqing Yang
Axayacatl Rocha-Olivares
Date: June 24, 1994

A new comprehensive flood routing model FLDWAV (Flood Wave) has been developed in NWS. FLDWAV combines the capabilities of the popular DWOPER (Dynamic Wave Operational) and DAMBRK (Dam Break) models, as well as provides features not contained in these models. The FLDWAV model is based on an implicit finite-difference solution of the complete one-dimensional Saint-Venant equations of unsteady flow coupled with an assortment of internal conditions for simulating unsteady flows controlled by a wide spectrum of hydraulic structures. The FLDWAV model can be used on micro-, mini-, or mainframe computers to simulate a wide range of unsteady flow applications such as real-time flood forecast, dam-break analysis, levee over topping, design of waterway improvement structures, floodplain mapping,and analysis of irrigation system with gate controlled flows. FLDWAVE can be automatically calibrated for a single channel or dendritic system of channels through an efficient automatic adjustment of the Manning coefficient (n) that varies with location and flow depth.

Applications of FLDWAV model on five different river and estuary systems are demonstrated: (1) a dendritic river system consisting of 393 mile of the Mississippi-Ohio-Cumberland-Tennessee rivers; (2) a 292 mile reach of the Lower Mississippi which was calibrated for a 1966 flood and for 1969 Hurricane Camille; (3) a 131 mile reach of the tidal affected lower Columbia River including a 25 mile tributary reach of the Williamette; one single discharge value at a fixed location; (4) a 60 mile reach of the Teton-Snake rivers located downstream of 262 ft high Teton dam which failed in 1976; (5) tidal waves in the Bay of Fundy.

The Mississippi-Ohio-Cumberland-Tennessee River System

A schematic of the river system with 16 gauges stations is shown in **Fig. 1** The main-stem river of the system is considered to be the Ohio-Lower Mississippi considered as first-order tributaries. The Saline River and Tradewater River are considered as lateral inflow into the main stem. The boundary conditions are specified using gauge observations on the boundaries. The gauge observations within the modeling domain are used to calibrate the model. **Figure 2** shows that the simulated water surface elevations agree very well with the observed data for the 1970 flood at Cairo of the system. Five increasing stages of peaks of surface elevation along the main-stem due to three first-order tributaries and two lateral inflows are also well simulated. The loop rating plat also shows that one single discharge value may correspond to more than one water surface elevation at a fixed location. This is due to the non linearity of the system.

The Lower Mississippi River

The Lower Mississippi River is a relatively flat channel and sensitive to the initial

pressure conditions. The river is considered as a single channel river with outflow at Morganza Diversion and Bonnet Carre Diversion. The model is calibrated for the 1966 flood and 1969 Hurricane Camille event at six gauges along the river. Comparison of the simulated and observed water surface elevations shows a good agreement in terms of peak magnitude of phase for both 1966 and 1969 cases. The attenuation of the Hurricane as it moves upstream can be also well simulated. The loop rating shows that the elevation increases in the back loop due to the increase of the elevation in the initial condition.

The Lower-Columbia-Williamette River System

The Lower-Columbia River is considered as the main-stem with the Williamette tributary in the model. The downstream of the Lower Columbia River is forced by mixed semi-diurnal diurnal tides from the Pacific Ocean and the upstream boundary condition is controlled by fresh water discharge. Since the river is strongly mixed by tidal currents, the water density is treated as constant in the whole domain and only barotropic motion is considered. The model is calibrated at six gauge stations. **Figure 3** shows that the model can simulate mixed semi-diurnal tidal waves very well when compared with the observed data.

Teton-Snake Rivers

This experiment is aimed to simulate the flood due to the failure of the Teton dam which produced a peak discharge in excess of 2 million cfs. The calibration of the Manning coefficient in this problem is difficult due to the lack of historical data for such an extreme flood event. However this dam-breach problem is not so sensitive to the Manning coefficient as river problems. **Figure 4** shows that the model can well reproduce the peak flood elevation downstream of the Teton dam.

The Bay of Fundy

The Bay of Fundy is a tidally dominated estuary, and has the largest tidal amplitude of the world. The open boundaries are controlled by strong diurnal tides. The simulated results show that semi-diurnal tide is generated within the Bay as the result of tidal forcing.

The demonstration of five diverse applications of FLDWAV model, showed that FLDWAV has the capability to deal with a wide range of problems in different types of river systems.

References:

Fread, D. L., and G. F. Smith, 1978: Calibration technique for 1-D unsteady flow models. *J. Hydraul. Div., ASCE*, **104**, 1027-1044.

Fread, D. L., 1978: NWS operational dynamic wave model. Verification of Mathematical and Physical model. *Proceedings of 26th annual Hydr. Div. special Conf., ASCE,* College Park, MD: 455-465.

Fread, D. L., and G. M. Lewis, 1988: FLDWAV: Generalized flood routing model. *Proceeding of National Conference on Hydraulic Engineering, ASCE*, Colorado Springs, Colorado, 668-673.

Fread, D. L., 1989: National Weather Service models to forecast dam breach floods. *Hydrology of disasters*, Eds. O. Starosolszky and O.M. Melder, Proceedings of the World Meteorological Organization Technical Conference, November 1988, Geneva, Switzerland: 192-211.

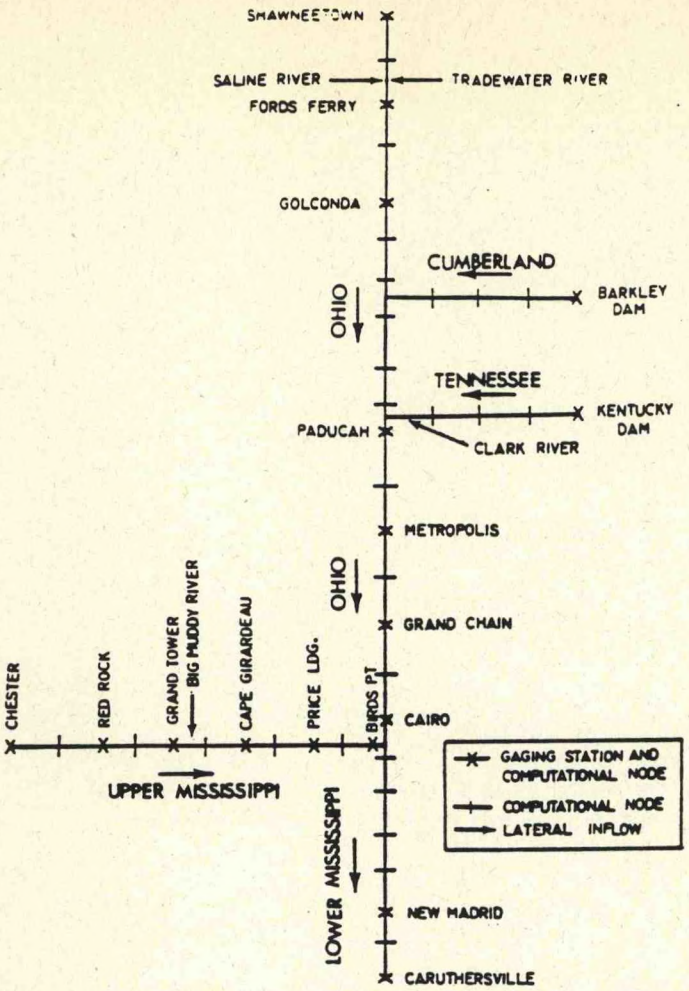

FIGURE 1 Schematic of Mississippi-Ohio-Cumberland-Tennessee River System

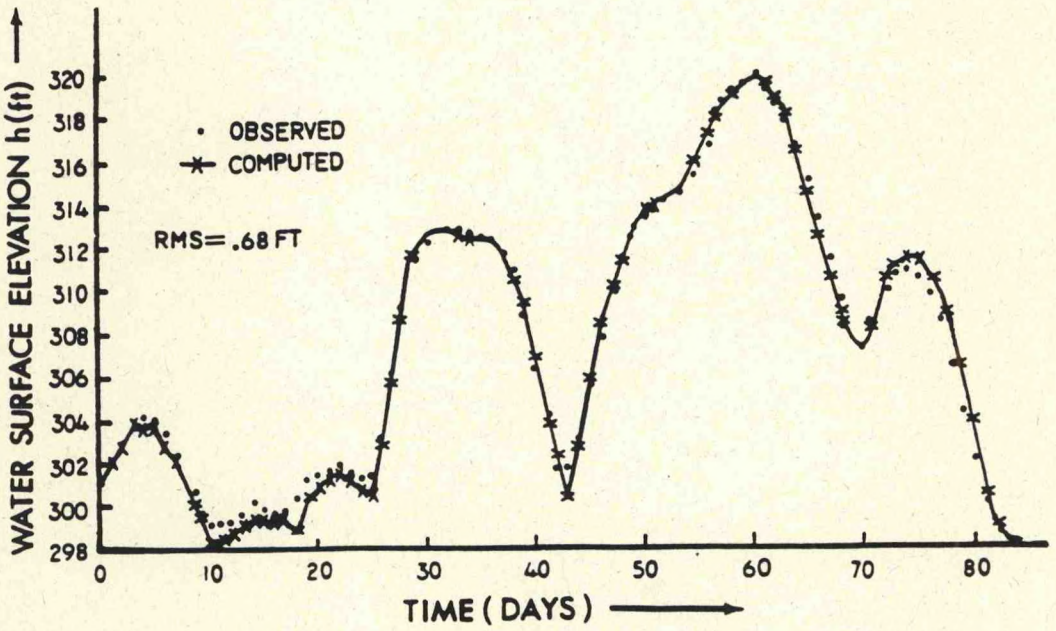

FIGURE 2 Computed and Observed Stages for Cairo at Junction of Mississippi and Ohio Rivers

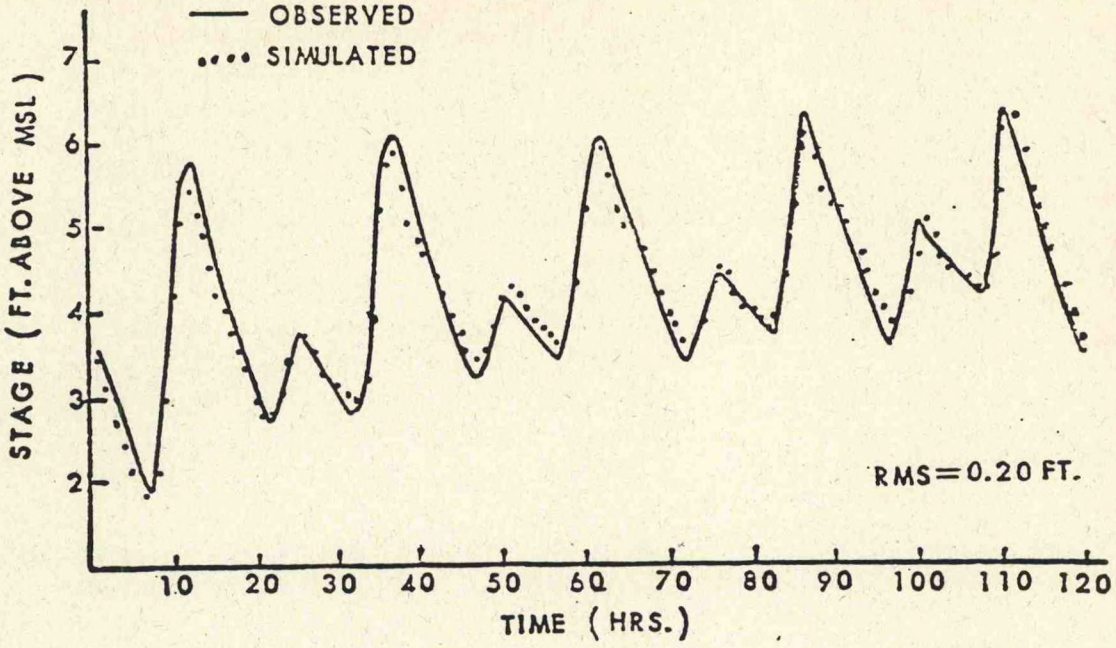

OBSERVED VS. SIMULATED STAGES AT PORTLAND

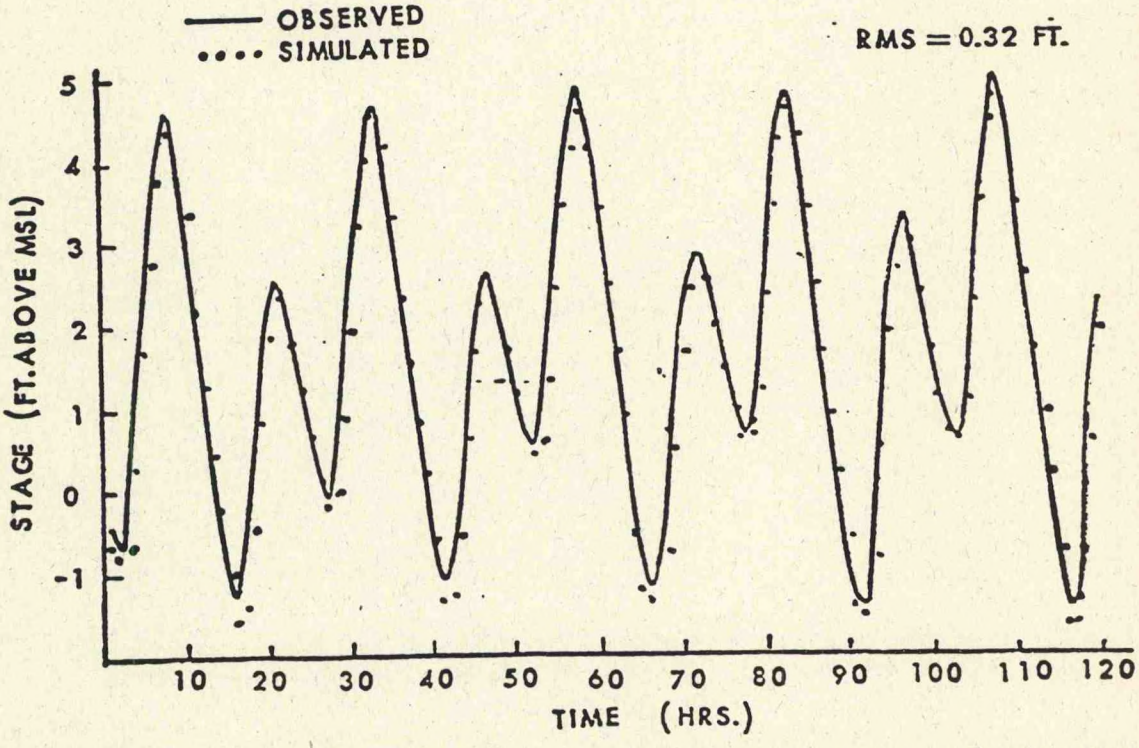

FIGURE 3 - OBSERVED VS. SIMULATED STAGES AT WAUNA

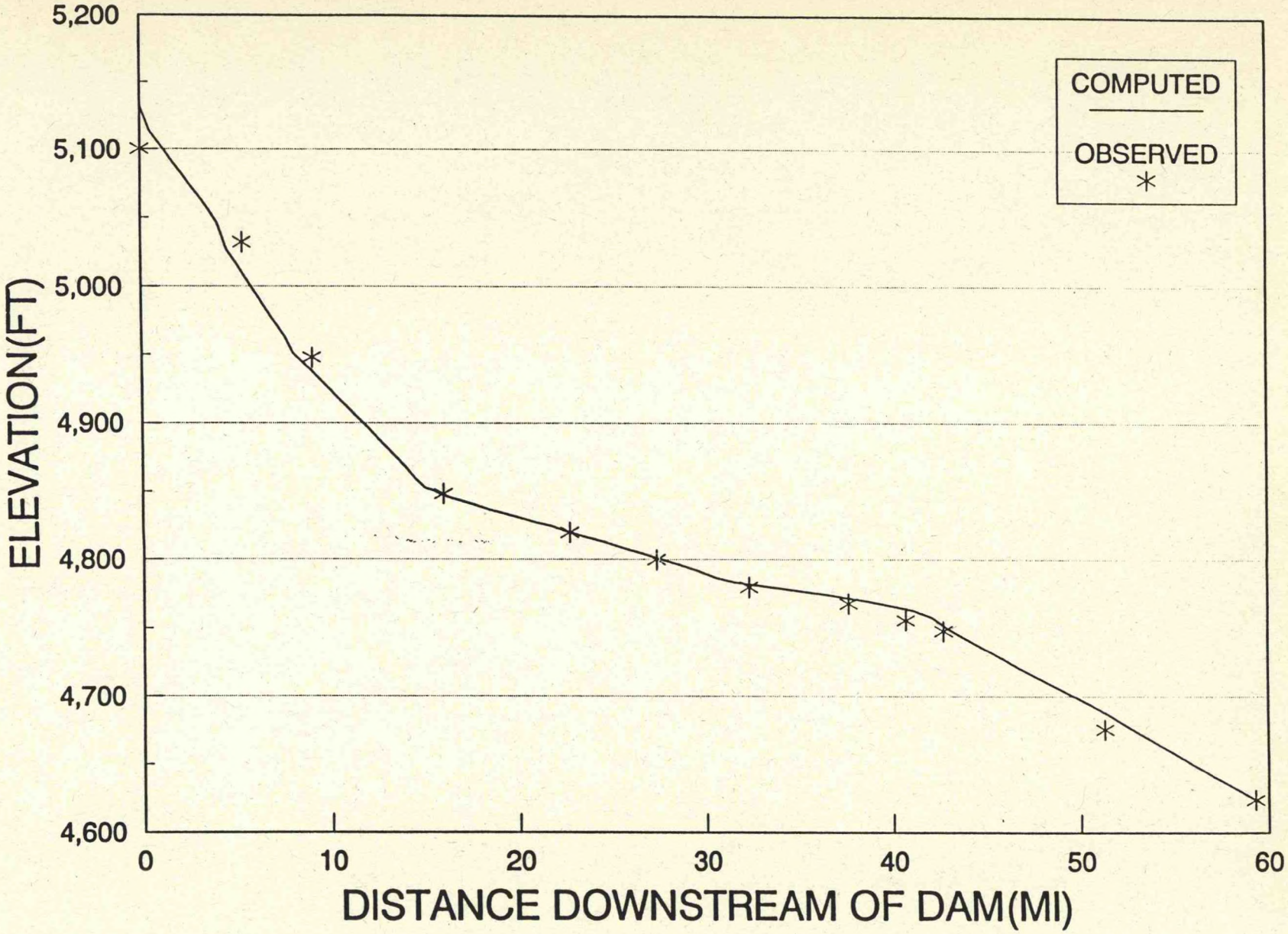

FIGURE 4

PROFILE OF PEAK FLOOD ELEVATION FROM TETON DAM FAILURE

Long Range Hydrologic Forecasting

Lecturers: Gerald N. Day and Ann McManamon
Notes by: Sam Levis
Yimin Ji
Date: June 24, 1994

Introduction

The lecture began with a hypothetical example in which we, as specialists, are requested to estimate the availability of water for a few villages in a third world country. The villages rely on a lake at the bottom of a river for their supply. What type of information must we have available to give a reasonable estimate?

-Precipitation data (snow, rain)
-Temperature (estimate evaporation, ablation, etc)
-Soil moisture
-Topographic map
-Land use (=> runoff amount, timing, demand for agriculture, etc)
-Discharge measurements (lake inflow). Long-term data allows us to forecast a mean.
Current data helps us predict drier or wetter year, but with caution.
-Interannual variability (related climatology to El Niño, SSTs, ...)

A long term forecast in hydrology refers to any forecast for a time scale greater than a week into the future. The reason is that in general we know what weather to expect for about a week. We can, therefore, make a hydrologic forecast, as long as we know the state of the watershed and the future meteorology.

Types of forecasts:
-Short term => deterministic (the use of QPF has improved results markedly.)
-Long term => probabilistic (based on historical data)

Nevertheless, the same models are used for both short and long term forecasting.

Types of models: (see definitions in Eric Anderson's talk)
* physical; *physically based or conceptual models; * stochastic; * Lumped;
* Distributed

Types of data:
*spatially averaged (used in lumped modeling [defined in Anderson's talk])
*gridded (used in distributed modeling)

Applications: in operations, planning and research.

Issues

What kind of forecasting information do user need?
* Accuracy and uncertainty; * Frequency and timeliness
Quick .vs. accuracy.

How easily can system be updated to represent current conditions accurately?

* Source information (mentioned above)
* other source information (atmosphere, ocean)

What are the investment considerations?

* Better forecast model; * better operational model; * Interface; *Resources to calibrate
* Long term maintenance; * Training and support; * Better data

The most important investment for the future of forecast models lies in improving our data sets. Of the methods used in long-term hydrologic forecasting, this lecture focused on the conceptual simulation of Extended Streamflow Prediction (ESP).

Extended Streamflow Prediction

Because of the limited skill presently available in forecasting future meteorological conditions, it is not possible to develop quantitative estimates of future precipitation and temperature more than few days into the future. EPS uses historical meteorological data and assumes that each year of historical data is a possible representation of the future. Separate streamflow time series are simulated for each year's historical data using the current watershed conditions as the starting point from each simulation. A statistical analysis is performed using the results from each year's simulation to produce a probabilistic forecast for the streamflow variability.

Figure 1 describes in a schematic the ESP procedure. It shows the type of information required as input and briefly describes the output.

ESP has the following capabilities:

-can use any of the different existing forecast models
-can incorporate forecast meteorological data into the procedure
-can produce output useful for navigation, water quality prediction and many other hydrologic applications
-can forecast for different time frames, both short and long time periods
-can assess forecast uncertainty

ESP applications include:

Water supply forecasts; Spring flood outlooks; flood control planning; Drought analysis; Hydropower planning; Navigation forecast; Recreation Multi-purpose reservoir operation

Future Research at the NWS

-improved models: hydrologic cycle (moving from lumped to distributed models) * reservoirs; * diversions
-model calibration procedures (autocalibration techniques and manual intervention => interactive calibration)
-updating model states, ie. adjusting model states to be consistent with observations
-integrating hydrologic and meteorologic forecasts
-other sources of uncertainty
-verification of probabilistic forecasts

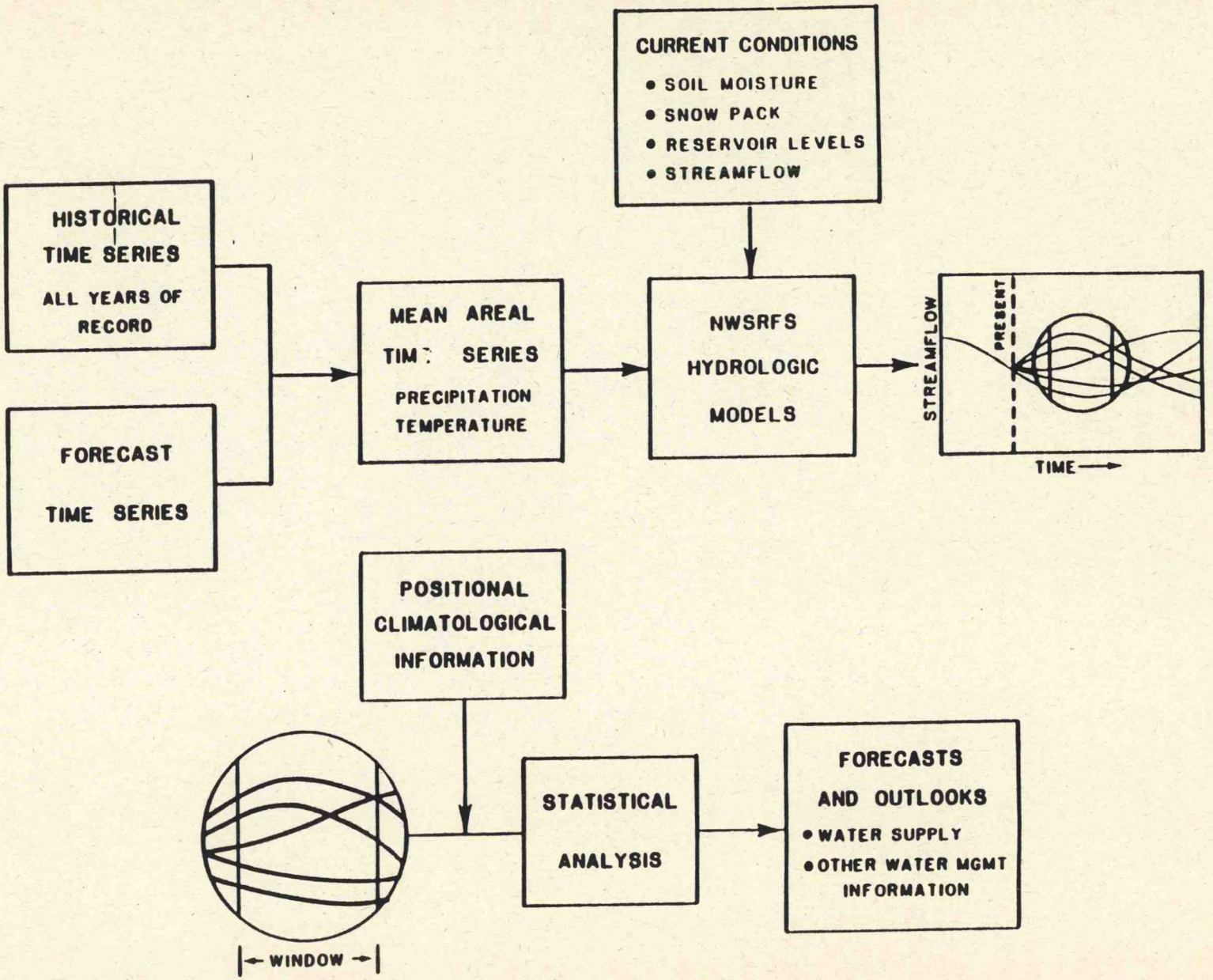

FIGURE 1

The ESP Procedure.

Appendix 1: 1994 NOAA Colloquium Speakers List

Diana Josephson
Deputy Undersecretary
NOAA
14th & Contitution Ave. NW
Room 5810 Hoover Building
Washington, DC
Tel: (202) 482-4569

Weather Analysis and Prediction

John Stackpole W/NMC42
NOAA/NWS National Meteorological Center
NOAA Science Center, Room 307
5200 Auth Road
Camp Springs, MD 20746
Tel: (301) 763-8115

Eugenia Kalnay
NOAA/NWS National Meteorological Center
NOAA Science Center, Room 204
5200 Auth Road
Camp Springs, MD 20746
Tel: (301) 763-8005

Louis Uccellini
NOAA/NWS National Meteorological Center
NOAA Science Center, Room 410
5200 Auth Road
Camp Springs, MD 20746
Tel: (301) 763-8097

James S. Lynch E/SP23
NOAA NESDIS
NOAA Science Center, Room 401
5200 Auth Road
Camp Springs, MD 20746
Tel: (301) 763-8444

Thomas Schlatter R/E23
NOAA/ERL/PROFS
325 Broadway
Boulder, CO 80303
Tel: (303) 497-6803

John Gamache
NOAA/AOML
Rickenbacker Causeway
Miami, FL
Tel: (305) 361-4437
e-mail: gamache@ocean.aoml.erl.gov

Roger Wakimoto
UCLA Atmospheric Sciences Dept.
Math Sciences Building Rm 7127
405 Highland Ave.
Los Angeles, CA 90024-1565
Tel: (310) 825-1751

Joe Golden
NOAA/OAR/R-PDC
1315 East-West Highway, Room 11554
Silver Spring, MD 20910
Tel: (301) 713-2465
e-mail: jgolden@vines.erl.gov

Climate Monitoring and Prediction

Anthony Broccoli R/E/GFDL
Geophysical Fluid Dynamics Laboratory
P.O. Box 308
Princeton, NJ 08542
Tel: (609) 452-6671
Fax: (609) 987-5063

A. James Miller
NOAA/NWS National Meteorological Center
NOAA Science Center, Room 805
5200 Auth Road
Camp Springs, MD 20746
Tel: (301) 7634670

Walter Planet E/RA14
NOAA NESDIS Research Applications
NOAA Science Center, Room 810
5200 Auth Road
Camp Springs, MD 20746
Tel: (301) 763-8136

George Ohring E/RA1
NOAA/NESDIS
NOAA Science Center, Room 712
5200 Auth Road
Camp Springs, MD 20746
Tel: (301) 763-8078

Steven Tracton
NOAA/NWS National Meteorological Center
NOAA Science Center, Room 604
5200 Auth Road
Camp Springs, MD 20746
Tel: (301) 763-8155
Fax: (301) 763-8395

Kingste Mo
NOAA/NWS National Meteorological Center
NOAA Science Center, Room 605
5200 Auth Road
Camp Springs, MD 20746
Tel: (301) 763-8227
Fax: (301) 763-8395

Edward O'Lenic
NOAA/NWS National Meteorological Center
NOAA Science Center, Room 604
5200 Auth Road
Camp Springs, MD 20746
Tel: (301) 763-8155
Fax: (301) 763-8395

Chester Ropelewski
NOAA/NWS National Meteorological Center
NOAA Science Center, Room 605
5200 Auth Road
Camp Springs, MD 20746
Tel: (301) 763-8227
Fax: (301) 763-8395
e-mail: wd52cr@sun1.wwb.noaa.gov

John Derber
NOAA/NWS National Meteorological Center
NOAA Science Center, Room 204
5200 Auth Road
Camp Springs, MD 20746
Tel: (301) 763-8301

Mike McPhaden
NOAA/PMEL
Sand Point Way
Seattle, WA
Tel: (206) 526-6783
e-mail: mcphaden@pmel.noaa.gov

Ming Ji
NOAA/NWS National Meteorological Center
NOAA Science Center, Room 808
5200 Auth Road
Camp Springs, MD 20746
Tel: (301) 763-8396

Oceanographic Prediction

Richard W. Reynolds
NOAA/NWS/NMC
NOAA Science Center, Room 808
5200 Auth Road
Camp Springs, MD 20746
Tel: (301) 763-8396

Tal Ezer
P.O. Box CN710, Sayre Hall
Princeton University
Princeton, NJ 08544-0710
Tel: (609) 258-1318
Fax: (609) 258-2850
e-mail: ezer@splash.princeton.edu

Christopher Hayden
1225 W. Dayton Street FL2
Madison, WI 53706
Tel: (608) 264-5325

Frank Aikman N/OES333
NOAA/NOS SSMC4
1305 East-West Highway, Room 6543
Silver Spring, MD 20910
Tel: (301) 713-2809

John Ahrens R/OR1
NOAA/OAR SSMC3
1315 East-West Highway, Room 11829
Silver Spring, MD 20910
Tel: (301) 713-2435

David Schwab R/E/GLERL
Great Lakes Environmental Research Lab.
2205 Commonwealth Blvd.
Ann Arbor, MI 48105
Tel: (313) 741-2120
Fax: (313) 741-2055

Nancy Rabalais
Louisiana University Marine Consortium
824 Highway 56
Chauvin, LA 70344
Tel: (504) 851-2800
Fax: (504) 851-2874

Steve Lohrenz
Center for Marine Science
University of Southern Mississippi
Stennis, MS 39529

William E. Woodward
NOAA/NOS SSMC4
1305 East-West Highway, Room 6219
Silver Spring, MD 20910
Tel: (301) 713-2790

Hydrologic Prediction and Workshops

Michael Hudlow W/OH
NOAA/NWS Office of Hydrology
1325 East-West Highway, Room 8212
Silver Spring, MD 20910
Tel: (301) 713-1658

Roderick Scofield
NOAA/NWS National Meteorological Center
NOAA Science Center, Room 601
5200 Auth Road
Camp Springs, MD 20746
Tel: (301) 763-8251

Phillip Arkin
NOAA/NWS National Meteorological Center
NOAA Science Center, Room 101
5200 Auth Road
Camp Springs, MD 20746
Tel: (301) 763-8317

David H. Kitzmiller W/OSD23
NOAA/NWS
1325 East-West Highway, Room 10392
Silver Spring, MD 20910
Tel: (301) 713-1774

Norman Junker
NOAA/NWS National Meteorological Center
NOAA Science Center, Room 402
5200 Auth Road
Camp Springs, MD 20746
Tel: (301) 763-8201

Robert Shedd W/OH3
NOAA/NWS Office of Hydrology
1325 East-West Highway, Room 8392
Silver Spring, MD 20910
Tel: (301) 713-0640

James Smith
Department of Civil Engineering
Operations Research
Princeton University
Princeton, NJ 08544
Tel: (609) 258-4615

Lee Larson
NOAA/NWS Central Region
601 E. 12th Street, Room 1835A
Kansas City, MO 64106
Tel: (816) 426-3229

Tom Carroll W/OH23
NOAA/NWS Office of Hydrology
RMT Sensing Center
6301 34th Ave S.
Minneapolis, MN 55450-2985
Tel: (612) 725-3039

Eric Anderson
NOAA/NWS Office of Hydrology
1325 East-West Highway, Room 8384
Silver Spring, MD 20910-3233
Tel: (301) 713-0640

George F. Smith W/OH3
NOAA/NWS Office of Hydrology
1325 East-West Highway, Room 8376
Silver Spring, MD 20910-3233
Tel: (301) 713-0640

Danny Fread W/OH3
NOAA/NWS Office of Hydrology
1325 East-West Highway, Room 8348
Silver Spring, MD 20910-3233
Tel: (301) 713-0619

Janice Lewis W/OH3
NOAA/NWS Office of Hydrology
1325 East-West Highway, Room 8406
Silver Spring, MD 20910-3233
Tel: (301) 713-0640

Ann McManamon W/OH3
NOAA/NWS Office of Hydrology
1325 East-West Highway, Room 8392
Silver Spring, MD 20910-3233
Tel: (301) 713-0640

Gerald Day
Riverside Technology, Inc.
5840 Bannekar Road
Suite 170
Columbia, MD 21044
Tel: (410) 740-8220
Fax: (410) 715-0557

Appendix 2: Acronyms and Abreviations

AC - Anomaly Correlation
ACARS - Aircraft Automated Reporting System
ADCP - Acoustic Doppler Current Profiler
AFOS - Automation of Field Operations and Services
AGCM - Atmospheric General Circulation Model
AgRISTARS - Agriculture Resource and Inventory Survey Through Aerospace Remote Sensing
AHPS - Advanced Hydrologic Prediction System
AIRS - Atmospheric Infrared Sounder
ALERT - Automated Local Evaluation in Real-Time
AMSU - Advanced Microwave Sounding Unit
AOML - Atlantic Oceanography and Meteorology Laboratory
AP - Anomalous Precipitation
APE - Available Potential Energy
API - Antecedent Precipitation Index
APT - Automatic Picture Transmission
ASOS - Automated Surface Observing System
ATSR - Along Track Scanning Radiometer
AVE - Atmospheric Variability Experiments
AVHRR - Advanced Very High Resolution Radiometer
AVN - Aviation Model
AWIPS - Advanced Weather Interactive Processing System
BASEFLOW - Baseflow Generation Runoff Model
BGM - Breeding of Growing Modes
BOMEX - Barbados Meteorological Experiment
C-MAN - Coastal-Marine Automated Network
CAC - Climate Analysis Center
CADAS - Centralized Automatic Data Acquisition System
CAPE - Convection And Precipitation/electrification Experiment
CAT - Clear Air Turbulence
CCA - Canonical Correlation Analysis
CCM - Community Climate Model
CCOPE - Cooperative Convective Precipitation Experiment
CDA - Command and Data Acquisition
CDAS - Climate Data Assimilation System
CEOF - Complex Empirical Orthoganal Functions
CERES - Cloud and Earth Radiant Energy System
CFC - Chloroflourocarbon
CFS - Coastal Forecast System
CHANLOSS - Channel Loss Routing Model
CHQC - Comprehensive Hydrostatic Quality Control
CIAM - Cooperative Institute for Applied Meteorology

CIMSS - Cooperative Institute for Meteorological Satellite Studies
CINDE - Convection Initiation and Down Gust Experiment
CLIPER - Climatology and Persistence
CLIVAR - Climate Variability
CMDL - Climate Monitoring and Diagnostic Laboratory
CNRS - Centre National de Resherche Scientifique
COADS - Comprehensive Ocean-Atmosphere Data Set
COE - U.S.Army Corps of Engineers
COHMEX - Cooperative Huntsville Meteorological Experiment
COLA - Center for Ocean, Land, and Atmospheres
CONV - Contribution from Convection
CPR - Convective Precipitation Rate
CPU - Central Processing Unit
CQC - Complex Quality Control
CREW - Columbia River Entrance
CRT - Cathode Ray Tube
CST - Convective Stratiform Technique
CYC - Cyclone Hurricanes Model
CZCS - Coastal Zone Color Scanner
DAC - Disaster Application Centers
DCP - Data Collection Platforms
DEM - Digital Elevation Models
DERF - Dynamical Extended Range Forecasting
DIN - Dissolved Inorganic Nitrogen
DKE - Divergent Kinetic Energy
DLM - Deep Layer Mean Wind
DMA - Decision Making Algorithm
DMSP - Defense Meteorological Satellite Program
DOC - Department of Commerce
DOD - Department of Defense
DSB - Direct Sounder Broadcast
DWOPER - Operational Dynamic Wave Routing Model
ECMWF - European Center for Medium-Range Weather Forecasts
EDAS - Eta Data Assimilation System
EIR - Enhanced Infrared
EMA - Emergency Management Agency
ENSO - El Niño / Southern Oscillation
EOC - Emergency Operations Center
EOF - Empirical Orthoganal Functions
EOS - Earth Observing System
EPOCS - Equatorial Pacific Ocean Climate Study
EPS - Energetic Particle Sensor
ERB - Earth Radiation Budget
ERBE - ERB Experiment

ERICA - Experiment on Rapidly Intensifying Cyclones over the Atlantic
ERS - European Research Satellite
ESA - European Space Agency
ESMR - Electrically Scanned Microwave Radiometer
ESP - Extended Stream Prediction
FAA - Federal Aviation Administration
FEMA - Federal Emergency Management Agency
FFA - Flash Flood Advisory
FFP - Flash Flood Potential
FFS - Flash Flood Statement
FFW - Flash Flood Warning
FGGE - First Global GARP Experiment
FIFE - First ISLSCCP Field Experiment
FLS - Flood Statement
FLW - Flood Warning
FNOC - Fleet Numerical Oceanographic Center
FORTRAN - Formula Translation
FOV - Field of View
FTIR - Fourier Transform Infrared
GAC - Global Area Coverage
GARP - Global Atmospheric Research Program
GATE - GARP Atlantic Tropical Experiment
GCIP - GEWEX Continental-scale International Project
GCM - General Circulation Model
GCOS - Global Climate Observing System
GDAS - Global Data Assimilation System
GEOSAT - Geostationary Satellite
GEWEX - Global Energy and Water Experiment
GFDL - Geophysical Fluid Dynamics Laboratory
GIP - GOES Precipitation Index
GIS - Geographic Information System
GLA - Goddard Laboratory for Atmospheres
GLERL - Great Lakes Environmental Research Laboratory
GMMM - GFDL Multiply-nested Movable Mesh
GMT - Greenwich Mean Time
GNMP - Global Numerical Weather Predictor
GEO - Geosynchronous Earth Orbit
GHG - Greenhouse Gas
GOALS - Global Ocean Atmosphere Land System
GOES - Geostationary Operational Environmental Satellite
GOMR - Global Ozone Monitoring Radiometer
GOOS - Global Ocean Observing System
GOSSTCOMP - Global Operational Sea Surface Temperature COMPutation
GPCC - Global Precipitation Climatology Center

GPCP - Global Precipitation Climatology Project
GSFC - Goddard Space Flight Center
GSOWM - Global Spectral Ocean Wave Model
GTOS - Global Terrestrial Observing System
GTS - Global Telecommunications System
GVI - Global Vegetation Index
HADS - Hydrometeorological Automated Data System
HAS - Hydrometeorological Analysis and Support
HEPAD - High-Energy Proton and Alpha Detector
HIC - Hydrologist in Charge
HIPLEX - High Plains Experiment
HIRS - High Resolution Infrared Sounder
HRC - Hurricane Research Center
HRD - Hurricane Research Division
HRL - Hydrologic Research Laboratory
HRPT - High Resolution Picture Transmission
HSA - Hydrologic Service Area
IAXS - Image Axis
IBM - Individual Based Model
ICSU - International Council of Scientific Unions
IFFA - Interactive Flash Flood Analyzer
IFOV - Instantaneous FOV
IMSL - International Mathematics and Statistics Library
INR - Image Navigation and Registration
IOC - International Oceanographic Commission
IPCC - International Pannel on Climate Change
IPS - Interactive Processing System
IR - Infrared
IRICP - International Research Institute for Climate Prediction
ISCCP - International Satellite Cloud Climatology Project
ISLSCP - International Satellite Land Surface Climatology Project
ITCZ - Intertropical Convergence Zone
ITOS - Improved TIROS Operational Satellite
JIC - Joint Ice Center
JGOFS - Joint
JOI - Joint Oceanographic Institutions
JPL - Jet Propulsion Laboratory
JTWC - Joint Typhoon Warning Center
LAC - Local Area Coverage
LAF - Lagged - Average Forecasting
LAG/K - Lag and K Routing Model
LANDSAT - Land Satellite
LARC - Langley Air Force Research Center, or Limited Automatic Remote Collector
LAY/COEF - Layered Coefficient Routing Model

LEO - Low Earth Orbit
LFWS - Local Flood Warning System
LFM - Limited-area Fine-mesh Model
LFMR - Low Frequency Microwave Radiometer
LGSCL - Large Scale
LOP - Limit of Predictability
LRF - Long Range Forecasting
LSL - Lowest Sigma Layer
LUMCON - Louisiana Universities Marine Consortium
LW - Long Wave
MALLOC - Memory Allocation Errors
MAP - Mean Areal Precipitation
MAR - Modernization and Associated Restructuring
MARS - Marine Stations
MAT - mean Areal Temperature
MCC - Mesoscale Convective Complex
McIDAS - Man Computer Interactive Data Access System
MCS - Mesoscale Convective System
MCSST - MultiChannel Sea Surface Temperature
MEPED - Medium Energy Proton and Electron Detector
MFE - Mean Forecast Error
MIC - Meteorologist in Charge
MIMR - Multifrequency Imaging Microwave Radiometer
MOD - Meteorological Operations Division
MOS - Marine Optical System or Model Output Statistics
MPP - Modified Perfect Prognosis
MRF - Medium-Range Forecast
MSLP - Mean Sea Level Pressure
MSS - Multi-Spectral Scanner
MSU - Microwave Sounding Unit
MUSKROUT - Muskingum Routing Model
MW - Microwave
NAS - National Academy of Science
NASA - National Aeronautics and Space Administration
NCAR - National Center for Atmospheric Research
NCCF - NOAA Central Computer Facility
NCDC - National Climate Data Center
NCEP - New Centers for Environmental Prediction
NDBC - National Data Buoy Center
NDVI - Normalized Difference Vegetation Index
NECOP - Nutrient Enhanced Coastal Ocean Process
NEMS - Nimbus-E Microwave Spectrometer
NESDIS - National Environmental Satellite Data and Information Service
NEXRAD - Next-Generation Weather Radar

NGM - Nested Grid Model
NGWLMS - Next Generation Water Level Measurement System
NHC - National Hurricane Center
NIDS - NEXRAD Information Dissemination System
NIR - Near Infrared
NIST - National Institute for Standards and Technology
NLNMI - Nonlinear Normal Mode Initialization
NMC - National Meteorological Center
NMFS - National Marine Fisheries Service
NOAA - National Oceanic and Atmospheric Administration
NOHRSC - National Operational Hydrologic Remote Sensing Center
NORPAX - Northern Pacific Experiment
NOS - National Ocean Service
NOW - NOAA Ocean Wave Model
NPPU - National Precipitation Prediction Unit
NRC - National Research Council
NROSS - Navy Research Oceanographic Satellite System
NRSC - National Remote Sensing Center (England)
NSF - National Science Foundation
NSSFC - National Severe Storms Forecast Center
NURP - National Undersea Research Program
NWP - Numerical Weather Prediction
NWR - NOAA Weather Radio
NWS - National Weather Service
NWSRFS - NWS River Forecast System
NWWS - NOAA Weather Wire Service
ODAS - Ocean Data Acquisition Systems
ODW - Omega Dropwindsonde
OGCM - Oceanic GCM
OH - Office of Hydrology
OI - Optimal Interpolation
OM - Office of Meteorology
OIQC - OI Quality Control
OLR - Outgoing Longwave Radiation
ONR - Office of Naval Research
OPC - Ocean Products Center
ORA - Office of Research and Applications
OTIS - Optimal Thermal Interpolation System
OWS - Ocean Weather Stations
PAC - Pattern Anomaly Correlations
PBL - Planetary Boundary Layer
PC - Principal Components or Personal Computer
PCPN - Precipitation
PDI - Palmer Drought Index

PIXEL - Picture Element
PODS - Pilot Ocean Data System
POES - Polar Orbiting Environmental Satellite
POM - Princeton Ocean Model
PORTS - Physical Oceanography Real-Time System
PPS - Precipitation Processing System
PUP - Principle User Processor
QBO - Quasi-Biennial Oscillation
QLM - Quasi-Lagrangian Model
QPF - Quantitative Precipitation Forecast
RAFS - Regional Analysis and Forecast System
RCC - Regional Climate Center
RDAS - Regional Data Assimilation System
RES-SINGL - Single Reservoir Simulation Routing Model
RFC - River Forecast Center
RH - Relative Humidity
RJE - Remote Job Entry
RKE - Rotational Kinetic Energy
RMS - Root Mean Square
RMSE - RMS Error
ROI - Regional Optimum Interpolation
ROSA - Remote Observation System Automation
ROV - Remotely Operated Vehicle
RPS - Ranked Probability Score
RRSD - Research Rapid Scan Days
RTNEPH - (cloud retrieval)
RTE - Radiative Transfere Equation
RUC - Rapid Update Cycle
RVA - River Summary
RVS - River Statement
SAB - Synoptic Analysis Branch
SAC-SMA - Sacramento Soil Moisture Accounting Runoff Model
SAGE - Stratospheric Aerosol and Gas Experiment
SAR - Synthetic Aperture Radar
SARSAT - Search and Rescue Satellite Aided Tracking
SATEM - Satellite Temperature
SBUV - Solar Backscatter Ultraviolet
SCAMS - SCAnning Microwave Spectrometer
SCS - Soil Conservation Service
SEC - South Equatorial Current
SEM - Space Environment Monitor
SESAME - Severe Environmental Storm and Mesoscale Experiment
SFSS - Satellite Field Services Station
SGM - Spectral Global Model

SHEF - Standard Hydrometeorological Exchange Format
SHIFOR - Statistical Hurricane Intensity Forecasts
SHIMS - Service Hydrologist Information Management System
SHIPS - Statistical Hurricane Intensity Prediction System
SIM - Satellite Interpretation Message
SLAF - Scaled LAF
SLOSH - Sea,Lakes, and Overland Surges from Hurricanes
SLSI - Semi-Lagragian Semi-Implicit
SMMR - Scanning Multichannel Microwave Radiometer
SNOW-17 NWSRFS - Snow Accumulation and Melt Runoff Model
SO - Southern Oscillation
SPC - Satellite Planning Committee
SPCZ - South Pacific Convergence Zone
SPS - Special Weather Statement
SSA - Singular Spectrum Analysis
SSH - Sea Surface Height
SSI - Spectral Statistical Interpolation
SSM/I - Special Sensor Microwave Imager
SSM/T - Special Sensor Microwave Sounder
SST - Sea Surface Temperature
SSU - Stratospheric Sounding Unit
STAGE-Q - Stage-Discharge Conversion Model
SVR - Severe Thunderstorm Warning
SVS - Severe Weather Statement
SWE - Snow Water Equivalent
SWR - Short Wave Radiation
TAO - Tropical Atmosphere-Ocean
TATUM - Tatum Routing Model
TED - Total Energy Detector
TIN - Total Inorganic Nitrogen
TIP - TIROS Information Package
TIR - Thermal IR
TIROS - Television and Infrared Operational Satellite
TM - Thematic Mapper
TOA - Top-of-the- Atmosphere
TOGA - Tropical Ocean Global Atmosphere
TOMS - Total Ozone Mapping Spectrometer
TOR - Tornado Warning
TVOS - TIROS Operational Vertical Sounder
UARS - Upper Atmosphere Research Satellite
UPS - Uninterruptable Power Supply
USCG - United States Coast Guard
USDA - U.S.Department of Agriculture
USGS - U.S.Geological Survey

UTC - Universal Time Coordinated
VAS - VISSR Atmospheric Sounder
VDUC - VAS Data Utilization Center
VIS - Visable
VISSR - Visible-Infrared Spin Scan Radiometer
VLF - Very Low Frequency
VOS - Volunteer Observing Ships
VTPR - Vertical Temperature Profile Radiometer
WAM - Wave Model
WARFS - Water Resources Forecasting System
WCM - Warning and Coordination Meteorologist
WCRP - World Climate Research Program
WD - Westerly Dipole
WEFAX - Weather Facsimile
WFO - Weather Forecast Office
WGNE - Working Group on Numerical Experimentation
WMO - World Meteorological Organization
WOCE - World Ocean Circulation Experiment
WODC - World Ozone Data Center
WSFO - Weather Service Forecast Office
WSO - Weather Service Office
WSR-57 - Weather Surveillance Radar 1957
WSR-88D - Weather Surveillance Radar 1988 Doppler
XBT - Expendible Bathythermograph
XIN-SMA - Xinanjiang Soil Moisture Accounting Runoff Model
XRS - X-Ray Sensor